Complex saddles in stochastic path integrals

Daniel Baldwin

Supervisor: Professor Steve Fitzgerald

Department of Applied Mathematics
University of Leeds

This thesis is submitted for the degree of
Doctor of Philosophy

September 2025

Declaration

I undertook this thesis as a postgraduate researcher in the School of Mathematics at the University of Leeds from October 2021 to September 2025, under the supervision of Professor Steve Fitzgerald. The research was supported by the Leeds Doctoral Scholarship (LDS).

This work builds on contributions by Gerald V. Dunne and collaborators in quantum field theory, particularly the papers [12–14, 71], and develops their ideas within a novel stochastic framework. Except where explicit references are made to the work of others, the content of this thesis is original. Collaborative work is clearly acknowledged within the text and is cited in accordance with the University's academic guidelines.

Chapter 2 presents a review of work by A. J. McKane and H. C. Luckock, as described in [117]. Some of the results in Chapter 3 were developed in collaboration with Alan McKane and Steve Fitzgerald and are explicitly marked as such.

Lastly, I declare that this document is submitted solely in fulfilment of the requirements for the degree of Doctor of Philosophy at the University of Leeds and has not been submitted for any other degree or professional qualification. This thesis complies with the prescribed word limit set by the relevant Degree Committee.

Daniel Baldwin

September 2025

Acknowledgements

It has been an immense privilege to be supervised by Professor Steve Fitzgerald. Our first research collaboration dates back to my undergraduate years, when we studied the dynamics of crystal defects. That early project set the tone for future work and introduced me to the rich mathematical landscape of path integrals. I have become the mathematician and scientist I am today largely due to Steve's insight, encouragement, and prompting, all of which have been integral to my career. I treasure the many conceptual discussions we have had while navigating the cerebral labyrinth of research; these conversations have been, without doubt, the project's most valuable resource.

One particularly memorable moment occurred during a long-standing puzzle that involved a surprisingly persistent error factor. After considerable effort, we traced the discrepancy to a subtle but critical mistake: treating a non-Gaussian mode as if it were Gaussian. The correction involved a factor whose leading asymptotic form is none other than Stirling's formula. Ironically, and much to our amusement, this exact formula had been emblazoned across Steve's office window the entire time, printed in crisp and decorative font. It had been silently watching us each time we met, like a cosmic joke waiting to be revealed. Whether it was a coincidence or a quiet act of intergalactic mischief, it certainly made us laugh.

I am also deeply grateful to Professor Alan McKane for his incisive and generous guidance. Alan's sharp insights and constructive feedback were pivotal in shaping the research. The experience of working with both Steve and Alan has been intellectually formative and one I will always cherish.

I have had the privilege of sharing this journey with a wonderful group of friends, colleagues, and family who have offered encouragement, support, and humour along the way. To name a few: Alex, Aaron, Parisha, Abdul, Nikhil, Bethan, Jay, Jaber, Francis, Tat, Nils, Shraddha, Richard, Sam, Tommy, Kuba, Jake, Max, Jamie, Abdullah and Amrit. Thank you for all the pep talks and the high-spirited memories.

Finally, I owe my deepest gratitude to my mother, Sharon; my stepfather, John; and my wife and best friend, Vanshika, for their unwavering love and belief in me—and, in loving memory, to my grandmother, Bernadette. I dedicate this thesis to them.

...it came to appear that, between two truths of the real domain, the easiest and shortest path quite often passes through the complex domain.

—Paul Painlevé

Abstract

This thesis builds on the work of Dunne and collaborators [12–14], advocating for the use of Picard–Lefschetz (PL) theory to perform semiclassical expansions of path integrals in the context of quantum field theory. We demonstrate that the PL theory also provides a rigorous framework for evaluating stochastic path integrals in the weak-noise limit, $D \to 0$. In particular, it offers a natural resolution to long-standing issues associated with multi-instanton contributions, particularly the role of instanton-anti-instanton $[\mathcal{I}\bar{\mathcal{I}}]$ pairs in the thermal escape rate across a potential barrier.

Traditional approaches focus on real-valued $[\mathcal{I}\bar{\mathcal{I}}]$ configurations, but the integral over the quasi-zero mode (QZM) direction diverges due to the mutual attraction between instantons and anti-instantons. The standard analytic workaround continues the noise parameter as $D \to -D$, known as the Bogomolny–Zinn–Justin (BZJ) procedure. However, while operationally effective, the BZJ procedure lacks conceptual clarity and introduces ambiguity. Instead, we apply PL theory to uncover a complex saddle-point solution, which we call the stochastic complex bounce $[\mathcal{CB}]$. The $[\mathcal{CB}]$ dynamics takes place in a tilted effective potential. In the Markovian-stochastic setting, the tilt is a feature of the discretisation scheme, whereas in quantum field theory, the tilt arises from fermionic effects.

The $[\mathcal{CB}]$ offers a fresh perspective and emerges as a genuine saddle of the complexified action, connecting to a convergent integral defined over a special descent manifold known as a Lefschetz thimble. Embedded within the $[\mathcal{CB}]$ is a composite structure of the form of an instanton-anti-instanton $[\mathcal{I}\bar{\mathcal{I}}]$ pseudoparticle pair. A well-defined complex separation characterises the instantonic substructures. The PL framework refines the BZJ procedure with rigorous justification, and the QZM integral becomes both convergent and physically transparent when defined over the appropriate Lefschetz thimble.

We present an algorithm using PL theory to evaluate stochastic path integrals in the weak-noise limit, incorporating quadratic fluctuations around complex saddles. This method is applied to compute escape rates in two canonical systems: the stochastic cubic potential and the stochastic sine-Gordon potential.

The thesis concludes by highlighting the broader implications of complex stochastic saddles, including their applications in non-equilibrium stochastic systems and their potential role in the deeper theoretical framework of resurgence theory.

Contents

Perturbation theory's failure is not a bug—it's a signal.

— Inspired by Dyson (1952)

Chapter 1

Introduction

Chapter summary

This chapter outlines the thesis's scope and objectives. It outlines the originality of the work, summarises the main results, and situates them within the path integral formulation of classical Markovian stochastic dynamics.

We introduce the essential tools of stochastic calculus, ranging from the Langevin equation to the Fokker–Planck–Smoluchowski framework, with a focus on the path integral representation of transition probabilities. We work in the weak-noise limit $D \to 0$ and exploit the analogy with semiclassical expansions in quantum mechanics, where perturbation theory fails without incorporating complex saddles.

We then advocate a shift in viewpoint, extending classical stochastic trajectories into the complex domain so that new analytic structures emerge which encode both perturbative and non-perturbative information. Picard–Lefschetz theory provides the natural framework for organising this complexified landscape. We adopt a practical approach to resolving real-contour ambiguities and set the stage for a systematic study of complex saddles in a stochastic setting. The chapter closes with a concise roadmap and a preview of the escape-rate computations developed in later chapters.

Glossary of abbreviations and notation

OM (functional)	**Onsager–Machlup functional.** For additive, overdamped Langevin dynamics, the path weight is proportional to $\exp(-\mathcal{S}[x]/(4D))$, where $\mathcal{S}[x] = \int_{-\mathcal{T}/2}^{+\mathcal{T}/2} (\dot{x} + V'(x))^2 \, \mathrm{d}t$ denotes the Onsager–Machlup functional. This formulation expresses transition probabilities as a path integral and is derived in § 2.1.4.
MOSD	**Method of steepest descents.** An asymptotic method for integrals of the form $\int \exp(\lambda f)$ with $\lambda \gg 1$, obtained by deforming the integration contour onto paths of steepest decrease through critical points of f. Reviewed in § 1.2.3.
PL **(theory)**	**Picard–Lefschetz theory.** A framework for deforming integration contours in complexified path space so that oscillatory integrals become sums of steepest descent contour contributions associated with critical points. Introduced in § 3.6; the main application of the theory is reiterated in § 1.2.7.
Thimble	**Lefschetz thimble.** The steepest descent manifold for $h = \mathrm{Re}(\mathcal{S}/(4D))$ through a saddle, along which $\mathrm{Im}\,\mathcal{S}$ is constant. Defined (together with dual thimbles) in § 3.6.
EZM	**Exact zero mode.** A symmetry direction of the quadratic fluctuation operator (e.g. time translation), yielding a zero eigenvalue in the $\mathcal{T} \to \infty$ limit and treated by collective coordinates; see § 2.1.9.
$[\mathcal{I}]$, $[\bar{\mathcal{I}}]$	**Instanton / anti-instanton.** Distinguished classical solutions related by time reversal; defined in § 1.2.4.
QZM	**Quasi-zero mode.** A near-flat direction in a multi-saddle problem (typically the separation parameter in a multi-instanton configuration). Introduced in § 2.3 and developed in § 3.5.
$[\mathcal{I}\bar{\mathcal{I}}]$	**Instanton-anti-instanton sector.** Two-event configuration whose separation integral is the QZM integral studied extensively in this thesis; see § 2.3.2.
$[\mathcal{I}\mathcal{I}]$	**Instanton-instanton sector.** Two-event configuration with a QZM whose correct thimble contour is the full real line; see § 2.3.1.
BZJ	**Bogomolny–Zinn–Justin** (BZJ) continuation. A prescription for the attractive instanton-anti-instanton QZM integral in which one analytically continues to the repulsive sheet (equivalently $D \mapsto \mathrm{e}^{\pm i\pi} D$), evaluates the now well-defined separation integral, and then returns to $D > 0$ across the logarithmic branch cut. See § 1.2.8 for a practical overview.

1.1 Novelty and the aim of the thesis

This thesis presents, to our knowledge, the first systematic study of complex saddles via Picard–Lefschetz theory [7] for weak-noise asymptotics in Markovian stochastic dynamics. We show that complex saddles and their Lefschetz thimbles resolve the instanton-anti-instanton ambiguity along the real contour and render ad hoc sign-flip prescriptions such as $D \to -D$ unnecessary, replacing them with a geometrically correct contour. The Itô discretisation choice qualitatively alters the extremising solutions by inducing an $\mathcal{O}(D)$ curvature term; together with complexification, this furnishes the geometric setting in which exact complex stochastic bounce trajectories solve the complexified Euler–Lagrange equation associated with the Onsager–Machlup functional [118, 135].

Although complex saddles and thimbles are well established for quantum path integrals in quantum mechanics (see Witten [184]) and quantum field theory (see, e.g., Dunne et al. [13, 71]), and have been contrasted with complex Langevin methods [1], they have not, to our knowledge, been applied to the Onsager–Machlup formulation of Markovian stochastic dynamics in order to resolve $[\mathcal{I}\bar{\mathcal{I}}]$ ambiguities and compute escape rates via thimble contours. Unlike quantum path integrals, the stochastic path integral is inherently real, so the necessity of complexification here is a mathematically substantive outcome.

Our main contribution is to import and operationalise standard thimble geometry associated with complex saddles in this stochastic setting. Within the PL framework, the QZM reduces to a *bona fide* one-dimensional integral along its thimble (e.g., [15, 71, 184]), providing a robust, contour-fixed treatment of instanton-anti-instanton configurations in the stochastic setting. We demonstrate the method in the escape-rate computation for Brownian motion in cubic and sine–Gordon potentials, where complex saddles cleanly recover *Kramers' rate* [85] and clarify the limitations of real-contour approaches.

We next review the stochastic foundations and give the full Itô variational derivation, contrasting Itô and Stratonovich (§ 1.2.2). We then develop steepest descents for the Onsager–Machlup functional (§ 1.2.3) and give a background on instantons and on bounce solutions (used later in the escape-rate

analysis), see § 1.2.4 and § 1.2.5. Then, we introduce complexification and Picard–Lefschetz theory (§ 1.2.7), which leads to the local EZM $\times$ QZM$\times$ Gaussian factorisation and a thimble-fixed QZM contour. A minimal toy model (§ 1.2.8) illustrates how thimbles fix the $[\mathcal{I}\bar{\mathcal{I}}]$ phase unambiguously (BZJ vs thimble). We conclude with a brief validation on cubic and sine–Gordon escapes (Kramers' problem; § 1.3) and thesis roadmap, § 1.4.

In the following text, we summarise the thesis and the concepts and techniques we use; some full derivations are deferred to subsequent chapters and will be appropriately signposted. What follows serves as a high-level overview.

1.2 Preliminaries

1.2.1 Stochastic foundations

1.2.1.1 Brownian motion, Langevin equation, and the Fokker–Planck–Smoluchowski equation

Brownian motion was first recorded in 1827 by the Scottish botanist Robert Brown, who observed the incessant jitter of pollen granules suspended in water [29, 30, 141] (see Fig. 1.1). In 1905, Einstein [58, 59, 142] and, independently, in 1906, Smoluchowski [164] provided quantitative theories of Brownian motion. Their explanation is that a visible grain is buffeted by countless, rapid and uncorrelated molecular impacts, leading to diffusive spreading with mean-square displacement,

$$\left\langle [x(t) - x(0)]^2 \right\rangle \;=\; 2\,D\,t, \tag{1.1}$$

where D is the diffusion constant (which we call the noise strength in our setting) and t is the time [36, 58, 74, 151, 172]. Crucially, Einstein linked D to dissipative transport through the Einstein relation $D = \mu\, k_{\mathrm{B}} T$ [36, 58], where k_{B} is the Boltzmann constant [32, 144], μ is a mobility coefficient and T is the system temperature. This relation is an early form of the fluctuation-dissipation principle: the same

microscopic collisions that produce viscous drag also generate thermal fluctuations, and in equilibrium these balance [34, 80, 86, 104, 105].

Langevin (1908) recast this picture as a stochastic differential equation (SDE) driven by Gaussian white noise, which takes the heuristic form [37, 114, 140, 172]

$$m\,\ddot{x} \;=\; -\,\zeta\,\dot{x} \;+\; F(x,t) \;+\; \xi(t), \tag{1.2}$$

where m is the mass of the Brownian particle, ζ is the friction coefficient, $F(x,t)$ is a mechanical force, and $\xi(t)$ encodes the stochastic data. Assuming a viscous bath, rescaling units to set $\zeta = 1$ (so the mobility $\mu = 1/\zeta = 1$, whence $D = k_{\mathrm{B}}T$ in these units), and neglecting inertia ($|m\ddot{x}| \ll |\zeta\dot{x}|$), one obtains the *overdamped* (small mass $m \to 0$) Langevin equation with conservative drift [56, 74, 82, 140, 154]:

$$\dot{x}(t) \;=\; -\,V'\big(x(t)\big) \;+\; \xi(t), \qquad \langle \xi(t) \rangle = 0, \quad \langle \xi(t)\xi(t') \rangle = 2D\,\delta(t-t'), \tag{1.3}$$

where $F = -V'(x)$ and $\xi(t)$ models the random kicks and is idealised as Gaussian white noise. In stochastic calculus notation, writing X_t for the random position, this may be expressed as [96, 155]

$$\mathrm{d}X_t \;=\; -\,V'(X_t)\,\mathrm{d}t \;+\; \sqrt{2D}\,\mathrm{d}W_t, \tag{1.4}$$

where $W = (W_t)_{t \geq 0}$ is a standard Brownian motion (Wiener process) [73, 96, 130, 150, 156]. Here $\langle \cdot \rangle$ denotes ensemble averaging over realisations of the noise, and Brownian motion is characterised by $W_0 = 0$, almost surely continuous sample paths, and independent stationary Gaussian increments

$$W_t - W_s \sim \mathcal{N}(0, t-s) \qquad (0 \leq s < t), \tag{1.5}$$

where $\mathcal{N}(\mu, \sigma^2)$ denotes the normal distribution with mean μ and variance σ^2. Equivalently, $\langle W_t \rangle = 0$

and

$$\langle W_t W_s \rangle \;=\; \min\{t, s\}. \tag{1.6}$$

[1] The differential notation $\mathrm{d}W_t$ is the shorthand for these increments, and (1.4) is understood through the integrated form

$$X_t \;=\; X_0 \;-\; \int_0^t V'(X_s)\,\mathrm{d}s \;+\; \sqrt{2D}\,W_t. \tag{1.7}$$

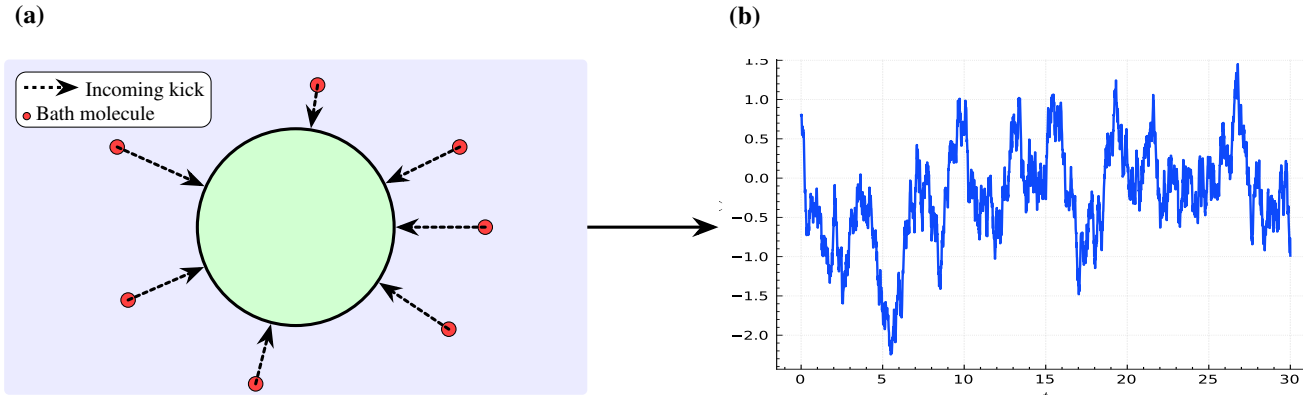

Figure 1.1: Microscopic origin of thermal noise and its impact on a Brownian particle. **(a)** A mesoscopic tracer (green disc) is incessantly bombarded by fast bath molecules (red); dashed arrows indicate instantaneous momentum transfers. **(b)** A numerically generated sample path of the Ornstein–Uhlenbeck process (the overdamped Langevin dynamics in a harmonic potential), $\mathrm{d}X_t = -X_t\,\mathrm{d}t + \sqrt{2D}\,\mathrm{d}W_t$.

The overdamped Langevin model has an equivalent ensemble description: if X_t follows (1.4) with initial law P_0, then its probability density $P(x,t)$ satisfies the Fokker–Planck–Smoluchowski equation [62, 63, 74, 100, 151]

$$\frac{\partial P(x,t)}{\partial t} \;=\; \frac{\partial}{\partial x}\big[V'(x)\,P(x,t)\big] \;+\; D\,\frac{\partial^2 P(x,t)}{\partial x^2}, \qquad P(x,0) = P_0(x). \tag{1.8}$$

We consider a point start at x_0, enforced by the delta-function condition $P_0(x) = \delta(x - x_0)$. On a bounded interval, *reflecting boundaries* mean that no probability flux crosses the endpoints. Equiva-

[1] For $t \geq s$, write $W_t = W_s + (W_t - W_s)$ and use independence plus $\langle W_t - W_s \rangle = 0$ and $\langle W_s^2 \rangle = s$.

lently, the probability current

$$J(x,t) \;=\; -\,V'(x)\,P(x,t) \;-\; D\,\partial_x P(x,t) \tag{1.9}$$

satisfies $J = 0$ at the boundary. With reflecting boundaries (or for confining V), the stationary *zero-current* solution is the equilibrium density obtained by imposing $J(x) \equiv 0$, namely $P_{\mathrm{eq}}(x) \propto \exp\!\big(-V(x)/D\big)$, i.e. the Boltzmann distribution. Finding an analytical solution of this PDE is difficult and, except for special choices of V (e.g. harmonic), (1.8) is rarely solvable in closed form. In the *weak-noise* regime $D \to 0^+$ (equivalently, D small compared with a characteristic potential scale, for instance a barrier height ΔV when present; see § 2.1.6, § 2.1.7), it is convenient to use the Onsager–Machlup path integral formulation [118, 135]

$$P \;\propto\; \int \mathcal{D}x\; \exp\!\Big(-\frac{1}{4D}\,\mathcal{S}[x]\Big), \qquad \mathcal{S}[x] = \int_{-\mathcal{T}/2}^{+\mathcal{T}/2} \big(\dot{x} + V'(x)\big)^2\,\mathrm{d}t. \tag{1.10}$$

Here $\int \mathcal{D}x$ denotes an integral over trajectories $x(\cdot)$ on $[-\mathcal{T}/2, \mathcal{T}/2]$ (with the appropriate endpoint constraints for the transition probability), defined as the continuum limit of a time sliced integral. Concretely, for a partition $t_n = -\mathcal{T}/2 + n\Delta t$ with $\Delta t = \mathcal{T}/N$ and $x_n = x(t_n)$, one may read

$$\int \mathcal{D}x\;(\cdots) \;\equiv\; \lim_{N\to\infty} \int_{\mathbb{R}^{N-1}} \Big(\prod_{n=1}^{N-1} \mathrm{d}x_n\Big)\,(\cdots), \tag{1.11}$$

with any overall normalisation absorbed into the proportionality constant in (1.10). A complete derivation of the stochastic path integral is given in § 2.1.4. It is possible to show that (1.10) solves (1.8), so solving the Fokker–Planck (FP) equation is equivalent to evaluating the stochastic path integral. The large parameter $1/(4D)$ multiplies a functional $\mathcal{S}$, and we apply the method of steepest descents (MOSD) to evaluate the integral asymptotically [23, 43, 128, 134, 138, 185]. A brief recap of MOSD and its use in (1.10) appears in § 1.2.3. This asymptotic evaluation of the stochastic path integral in the weak-noise limit is the focus of this thesis.

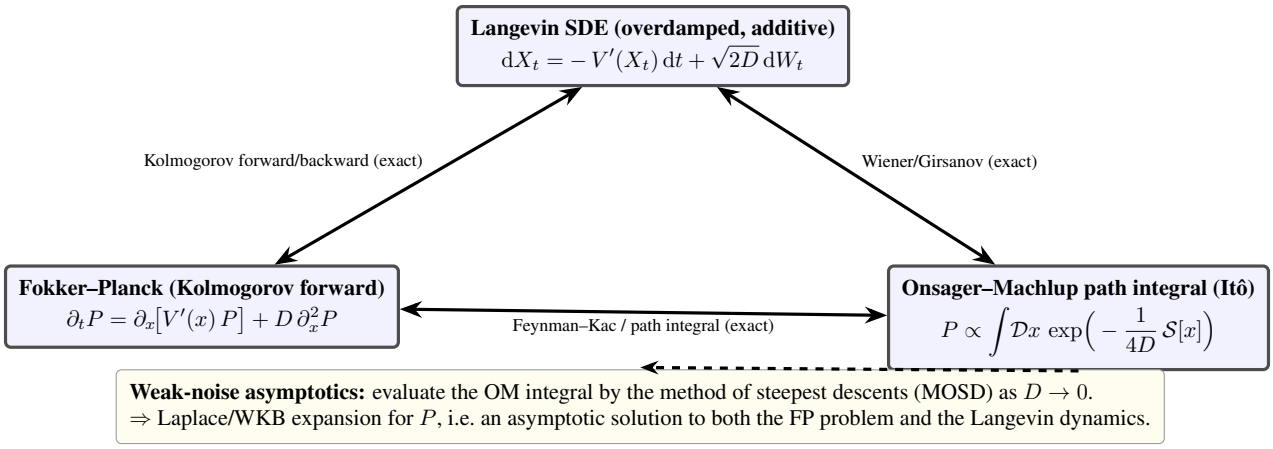

Figure 1.2: ***Equivalence triangle.*** *A schematic illustration depicting the equivalence among the three formulations, valid under identical initial and boundary conditions. The diagram considers additive noise; in contrast, multiplicative noise introduces additional drift terms and path integral corrections. It is essential to maintain consistency in the discretisation scheme (Itô versus Stratonovich) throughout the analysis.*

The overdamped Langevin SDE, its Fokker–Planck (Kolmogorov forward) equation, and the Onsager–Machlup path integral are different representations of the same Markov diffusion (for fixed initial/boundary data and a fixed discretisation convention). The arrows in Fig. 1.2 indicate exact correspondences. The only approximation enters when we evaluate the path integral in the weak-noise limit by the method of steepest descents (MOSD): this yields a Laplace/WKB asymptotic for P, see historically [102, 181] and for a modern tutorial [16], which is therefore an asymptotic solution to the FP equation.

We conclude by summarising the equivalence triangle (SDE, FP, OM; additive noise). The SDE $\leftrightarrow$ FP correspondence follows directly from Itô's formula and integration by parts (forward/backward Kolmogorov theory) [62, 74, 96, 100, 133, 140, 151, 153, 165]. The SDE $\leftrightarrow$ OM connection comes from the Onsager–Machlup construction of path weights together with Girsanov's change of measure [77, 96, 109, 116, 118, 135]. The FP $\leftrightarrow$ OM link is the Feynman–Kac representation of parabolic solutions as Wiener expectations/path integrals [22, 44, 92, 96, 130, 133].

1.2.2 Itô vs Stratonovich primer and variational overview

This section contrasts the Itô and Stratonovich calculi (see, e.g. [145], [133] and [107] for practical texts). The methodological choice in this thesis is to work in the Itô convention, which produces a D-dependent tilt term in the equations of motion and naturally accommodates complex saddles. The full Itô variational derivation is given in the next subsection, while this subsection gives a fast but sufficient overview of stochastic calculus at the level required for this thesis. We refer the reader to Itô 's book for additional background [90].

Acknowledgement. I thank A. J. McKane for discussions on the Itô variational problem.

1.2.2.1 Stochastic calculus primer

We consider the general one-dimensional SDE

$$\mathrm{d}X_t \;=\; F(X_t)\,\mathrm{d}t \;+\; \sqrt{2D}\,G(X_t)\,\mathrm{d}W_t, \tag{1.12}$$

where X_t is the state, W_t a standard Wiener process, F the drift, G the noise amplitude ("multiplicative" if G depends on x), and $D > 0$ the noise strength. Let $f \in C^2$ be a test function; the primes denote x-derivatives.

Let us begin with the Itô discretisation scheme. We define the Itô integral and Itô's lemma [87,90,103]. Fix $t > 0$ and let $\Pi = \{0 = t_0 < t_1 < \cdots < t_N = t\}$ be a partition of $[0, t]$, with mesh size

$$|\Pi| \;=\; \max_{0\le k\le N-1}(t_{k+1} - t_k). \tag{1.13}$$

The Itô stochastic integral is defined as the mean-square[2] limit of left–point Riemann sums [108]

$$\int_0^t G(X_s)\,\mathrm{d}W_s \;=\; \lim_{|\Pi|\to 0}\sum_{k=0}^{N-1} G\big(X_{t_k}\big)\,\big(W_{t_{k+1}}-W_{t_k}\big), \tag{1.14}$$

where $|\Pi| \to 0$ means that we take finer and finer partitions whose maximal step size tends to zero. Intuitively, the left-point choice reflects that the integrand is evaluated using information available up to time t_k. If, more generally, $\mathrm{d}X_t = \mu(X_t)\,\mathrm{d}t + \sigma(X_t)\,\mathrm{d}W_t$, then Itô's lemma gives

$$\mathrm{d}f(X_t) \;=\; f'(X_t)\,\mu(X_t)\,\mathrm{d}t \;+\; \frac{1}{2}f''(X_t)\,\sigma^2(X_t)\,\mathrm{d}t \;+\; f'(X_t)\,\sigma(X_t)\,\mathrm{d}W_t. \tag{1.15}$$

With $\mu = F$ and $\sigma = \sqrt{2D}\,G$ from (1.12), this becomes

$$\mathrm{d}f(X_t) \;=\; \big[f'(X_t)\,F(X_t) + D\,f''(X_t)\,G^2(X_t)\big]\,\mathrm{d}t \;+\; \sqrt{2D}\,f'(X_t)\,G(X_t)\,\mathrm{d}W_t, \tag{1.16}$$

or, equivalently,

$$\mathrm{d}f(X_t) \;=\; f'(X_t)\,\mathrm{d}X_t + D\,f''(X_t)\,G^2(X_t)\,\mathrm{d}t, \tag{1.17}$$

which exhibits the additional drift $D\,f''G^2$ due to the quadratic variation of W_t.

We contrast this to the Stratonovich discretisation scheme. We define the Stratonovich integral and the Stratonovich chain rule. The Stratonovich integral uses midpoint sums,

$$\int_0^t G(X_s)\circ\mathrm{d}W_s \;=\; \lim_{|\Pi|\to 0}\sum_{k=0}^{N-1} G\Big(\frac{X_{t_k}+X_{t_{k+1}}}{2}\Big)\,\big(W_{t_{k+1}}-W_{t_k}\big), \tag{1.18}$$

and satisfies the traditional chain rule,

$$\mathrm{d}f(X_t) \;=\; f'(X_t)\circ\mathrm{d}X_t, \tag{1.19}$$

[2]"mean-square" means that there exists a random variable I such that $\langle|S_\Pi - I|^2\rangle \to 0$ as $|\Pi| \to 0$, where S_Π denotes the Riemann sum.

where $\circ$ indicates the Stratonovich prescription, but this notation will be dropped. The midpoint prescription is time-symmetric and restores the classical chain rule.

The important takeaway is that in the path integral variational calculus, the Itô chain rule (1.17) produces an order-D contribution at the integration by parts step. For gradient drift $F = -V'$ with additive noise, this yields the Euler–Lagrange equations

$$\ddot{x} \;=\; V'(x)\,V''(x) \;-\; D\,V'''(x) \quad \text{(Itô)}, \qquad \ddot{x} \;=\; V'(x)\,V''(x) \quad \text{(Stratonovich)}, \tag{1.20}$$

the former featuring the D-dependent "tilt". So, even though we work under the assumption of additive white noise, the choice of discretisation scheme alters the saddles of the functional. We derive this explicitly in the following subsection.

1.2.2.2 Itô vs Stratonovich in the variational calculus

Recall that, in the Onsager–Machlup representation in (1.10), the transition probability has the schematic form $P \propto \int \mathcal{D}x\, \exp\big(-\mathcal{S}[x]/(4D)\big)$. For this reason $\mathcal{S}[x]$ plays the role of an *action functional* in the path integral, and writing $\mathcal{S}[x] = \int \mathcal{L}(t,x,\dot{x})\,\mathrm{d}t$ defines the corresponding *Lagrangian* $\mathcal{L}$. The dominant trajectories in the weak-noise regime are obtained by stationarity $\delta\mathcal{S} = 0$, equivalently by the Euler–Lagrange equation associated with $\mathcal{L}$ (with fixed endpoints). A more detailed justification of this stationary-path principle, and the associated "weak-noise tube" picture, is given in § 2.1.6 and § 2.1.7.

Fix $V \in C^3$. Let $x(t)$ be an extremal of $\mathcal{S}$ with Dirichlet data $x(\pm\mathcal{T}/2) = x_{1,2}$. With $\mathcal{L}(t,x,\dot{x}) = (\dot{x} + V'(x))^2$ and a test variation $x_\varepsilon = x + \varepsilon\eta$ where $\eta(\pm\mathcal{T}/2) = 0$ and $|\varepsilon| \ll 1$,

$$\dot{x}_\varepsilon = \dot{x} + \varepsilon\,\dot{\eta}, \qquad V'\big(x_\varepsilon\big) = V'(x) + \varepsilon\,V''(x)\,\eta + \mathcal{O}(\varepsilon^2). \tag{1.21}$$

Hence,

$$\mathcal{S}[x_\varepsilon] = \mathcal{S}[x] + 2\varepsilon \int_{-\mathcal{T}/2}^{+\mathcal{T}/2} (\dot{x} + V'(x))\big(\dot{\eta} + V''(x)\eta\big)\,\mathrm{d}t + \mathcal{O}(\varepsilon^2), \tag{1.22}$$

and the first variation is

$$\delta\mathcal{S} = 2\int_{-\mathcal{T}/2}^{+\mathcal{T}/2} (\dot{x} + V'(x))\big(\dot{\eta} + V''(x)\eta\big)\,\mathrm{d}t. \tag{1.23}$$

Integrate the $\dot{\eta}$ term by-parts (no stochastic correction since the function η is smooth),

$$\int (\dot{x} + V')\,\dot{\eta}\,\mathrm{d}t = \Big[(\dot{x} + V')\,\eta\Big]_{-\mathcal{T}/2}^{+\mathcal{T}/2} - \int \eta\,\frac{\mathrm{d}}{\mathrm{d}t}\big(\dot{x} + V'(x)\big)\,\mathrm{d}t, \tag{1.24}$$

and the boundary term vanishes by the Dirichlet condition. To evaluate $\frac{\mathrm{d}}{\mathrm{d}t}V'(x(t))$, we now insert the Itô chain rule (1.17) with $f = V'$:

$$\frac{\mathrm{d}}{\mathrm{d}t}V'(x(t)) = V''(x)\,\dot{x} + \underbrace{D\,V'''(x)}_{\text{Itô tilt}}. \tag{1.25}$$

Substituting (1.25) into (1.23) and cancelling the $V''\dot{x}$ terms yields

$$\delta\mathcal{S} = 2\int_{-\mathcal{T}/2}^{+\mathcal{T}/2} \eta(t)\,\Big(-\ddot{x} + V'(x)V''(x) - D\,V'''(x)\Big)\,\mathrm{d}t, \tag{1.26}$$

so, since $\delta\mathcal{S} = 0$ for all test functions η, by the fundamental lemma of the calculus of variations,

$$\boxed{\ddot{x}(t) = V'(x)\,V''(x) - D\,V'''(x)}. \tag{1.27}$$

Remarks

- In the Stratonovich convention the chain rule is classical, $\frac{\mathrm{d}}{\mathrm{d}t}V'(x) = V''(x)\dot{x}$, so (1.27) reduces to $\ddot{x} = V'V''$ (without tilt).
- We work with the Onsager–Machlup functional $\mathcal{S} = \int(\dot{x} + V')^2\,\mathrm{d}t$ (cf. (1.43)), and the Itô contribution $D\,V'''$ enters precisely at the integration by parts step via (1.25). This is the key input for steepest descents and for accommodating complex saddles.
- General drift $F(x)$. With $\mathcal{L} = (\dot{x} - F(x))^2$, the same argument gives $\ddot{x} = F\,F' + D\,F''$. Setting

$F = -V'$ recovers (1.27).

1.2.3 Steepest descents for the Onsager–Machlup functional

1.2.3.1 1D method of steepest descents template

This section covers the basics of the steepest descent method in the language of the stochastic path integral, working in the limit $D \to 0$.

Consider the one-dimensional template

$$I(\lambda) = \int_C f(z)\, \exp\big(\lambda g(z)\big)\, \mathrm{d}z, \qquad \lambda \gg 1, \tag{1.28}$$

where f and g are analytic in a domain containing the contour C, and no singularities are crossed under admissible deformations. Write $g = u + iv$ with $u = \operatorname{Re} g$ and $v = \operatorname{Im} g$. By Cauchy's theorem we can deform C into a union of constant phase paths $C' = \bigcup_{\sigma\in\Sigma} \Gamma_\sigma$ chosen so that v is constant along each Γ_σ and u decreases away from a saddle z_σ with

$$g'(z_\sigma) = 0, \qquad g''(z_\sigma) \neq 0. \tag{1.29}$$

Along such a path, the oscillatory factor is fixed, and one has

$$\int_{\Gamma_\sigma} f(z)\, \exp\big(\lambda g(z)\big)\, \mathrm{d}z = \exp\big(i\lambda v(z_\sigma)\big) \int_{\Gamma_\sigma} f(z)\, \exp\big(\lambda u(z)\big)\, \mathrm{d}z\,. \tag{1.30}$$

To capture the contribution near a given saddle, expand g and f about z_σ,

$$g(z) = g_\sigma + \frac{1}{2} g_2\,(z - z_\sigma)^2 + \frac{1}{6} g_3\,(z - z_\sigma)^3 + \cdots, \qquad f(z) = f_0 + f_1\,(z - z_\sigma) + \frac{1}{2} f_2\,(z - z_\sigma)^2 + \cdots, \tag{1.31}$$

where $g_\sigma = g(z_\sigma)$, $g_k = g^{(k)}(z_\sigma)$ and $f_k = f^{(k)}(z_\sigma)$. Let $z - z_\sigma = \kappa_\sigma \rho$ with $\rho \in \mathbb{R}$ and $\kappa_\sigma = \exp(i\alpha_\sigma)$

a unit complex direction chosen so that the quadratic term points along the steepest descent,

$$g_2\,\kappa_\sigma^2 \in \mathbb{R}_{<0} \quad \Longleftrightarrow \quad 2\alpha_\sigma + \arg g_2 \equiv \pi \pmod{2\pi}, \qquad \alpha_\sigma = \frac{\pi - \arg g_2}{2}. \tag{1.32}$$

Indeed, writing $g_2 = |g_2|e^{i\phi}$ gives $g(z) - g_\sigma = \frac{1}{2}|g_2|e^{i(\phi+2\alpha_\sigma)}\rho^2$; the constant phase condition forces $\sin(\phi + 2\alpha_\sigma) = 0$, and the steepest *descent* choice is $\phi + 2\alpha_\sigma \equiv \pi$ (the other solution gives ascent).

Parametrise the local constant phase line by the signed arclength ρ,

$$z(\rho) = z_\sigma + \kappa_\sigma\,\rho, \qquad \mathrm{d}z = \kappa_\sigma\,\mathrm{d}\rho, \tag{1.33}$$

so that

$$g\big(z(\rho)\big) = g_\sigma + \frac{1}{2}g_2\,\kappa_\sigma^2\,\rho^2 + \mathcal{O}(\rho^3) = g_\sigma - \frac{1}{2}A_\sigma\,\rho^2 + \mathcal{O}(\rho^3), \qquad A_\sigma := -(g_2\,\kappa_\sigma^2) > 0, \tag{1.34}$$

and

$$f\big(z(\rho)\big) = f_0 + f_1\,\kappa_\sigma\,\rho + \frac{1}{2}f_2\,\kappa_\sigma^2\,\rho^2 + \mathcal{O}(\rho^3). \tag{1.35}$$

The integral near z_σ becomes

$$\begin{aligned}\int_{\Gamma_\sigma} f(z)\,\exp\big(\lambda g(z)\big)\,\mathrm{d}z &= \int_{-\infty}^{+\infty} f\big(z(\rho)\big)\,\exp\big(\lambda g\big(z(\rho)\big)\big)\,z'(\rho)\,\mathrm{d}\rho \\ &= \exp\big(\lambda g_\sigma\big)\int_{-\infty}^{+\infty}\Big(f_0 + \mathcal{O}(\rho)\Big)\,\exp\!\Big(-\frac{1}{2}\lambda A_\sigma\rho^2 + \mathcal{O}\big(\lambda|\rho|^3\big)\Big)\,\kappa_\sigma\,\mathrm{d}\rho.\end{aligned} \tag{1.36}$$

The dominant region is $|\rho| = \mathcal{O}(\lambda^{-1/2})$, so let us introduce the Laplace rescaling

$$s = \sqrt{\lambda A_\sigma}\,\rho, \qquad \mathrm{d}\rho = \frac{\mathrm{d}s}{\sqrt{\lambda A_\sigma}}, \tag{1.37}$$

to obtain

$$\int_{\Gamma_\sigma} f(z)\,\exp\big(\lambda g(z)\big)\,\mathrm{d}z = \exp\big(\lambda g_\sigma\big)\,\frac{\kappa_\sigma}{\sqrt{\lambda A_\sigma}}\int_{\mathbb{R}}\Big(f_0+\mathcal{O}(\lambda^{-1/2})\Big)\,\exp\!\left(-\frac{1}{2}s^2\right)\mathrm{d}s. \tag{1.38}$$

Evaluating the Gaussian and simplifying the prefactor,

$$\int_{\mathbb{R}}\exp\!\left(-\frac{1}{2}s^2\right)\mathrm{d}s=\sqrt{2\pi},\qquad \frac{\kappa_\sigma}{\sqrt{A_\sigma}}=\frac{\kappa_\sigma}{\sqrt{-\,g_2\,\kappa_\sigma^2}}=\frac{1}{\sqrt{-\,g_2}}\cdot\frac{\kappa_\sigma}{\sqrt{\kappa_\sigma^2}}, \tag{1.39}$$

and fixing the branch so that $\sqrt{-\,g_2}\,\kappa_\sigma\in\mathbb{R}_{>0}$, one obtains the canonical leading term

$$\boxed{\int_{\Gamma_\sigma} f(z)\,\exp\big(\lambda g(z)\big)\,\mathrm{d}z = \exp\big(\lambda g(z_\sigma)\big)\,\frac{\sqrt{2\pi}}{\sqrt{\lambda}}\,\frac{f(z_\sigma)}{\sqrt{-\,g''(z_\sigma)}}\Big(1+\mathcal{O}(\lambda^{-1})\Big)}. \tag{1.40}$$

(The $\mathcal{O}(\lambda^{-1/2})$ term vanishes after integration by parity; the first non-zero correction is $\mathcal{O}(\lambda^{-1})$.)

Summing the contributions from all saddles reached by admissible deformations gives the MOSD asymptotic formula

$$I(\lambda)\sim\sum_{\sigma\in\Sigma}\exp\big(\lambda g(z_\sigma)\big)\,\frac{\sqrt{2\pi}}{\sqrt{\lambda}}\,\frac{f(z_\sigma)}{\sqrt{-\,g''(z_\sigma)}}. \tag{1.41}$$

In the following, we give a plot in Fig. 1.3 of representative steepest descent/ascent curves for an integral of the form

$$I(\lambda,a)=\int_C\exp\big(-\lambda\,\mathcal{W}(z,a)\big)\,\mathrm{d}z,\qquad \mathcal{W}(z,a)=\frac{z^2}{2}-a\,\frac{z^4}{4}. \tag{1.42}$$

Here a is a parameter that we can vary, even to complex values, and we can visualise how the descent curves geometry changes. The saddles solve $\mathcal{W}'(z,a)=0$, i.e.

$$z_0=0,\qquad z_\pm=\pm\,a^{-1/2},$$

with the branch of $a^{-1/2}$ chosen consistently (principal branch unless stated). The leading contributions are of the form $\exp\big(-\lambda\,\mathcal{W}(z_\sigma,a)\big)$, and the *dominant* saddle(s) are those that minimise $\mathrm{Re}\,\mathcal{W}(z_\sigma,a)$.

Varying $\arg a$ steers which saddle minimises $\operatorname{Re}\mathcal{W}$ and how the contours attach. We illustrate two examples below; a more extensive gallery of method of steepest descent/ascent curves is provided in A.

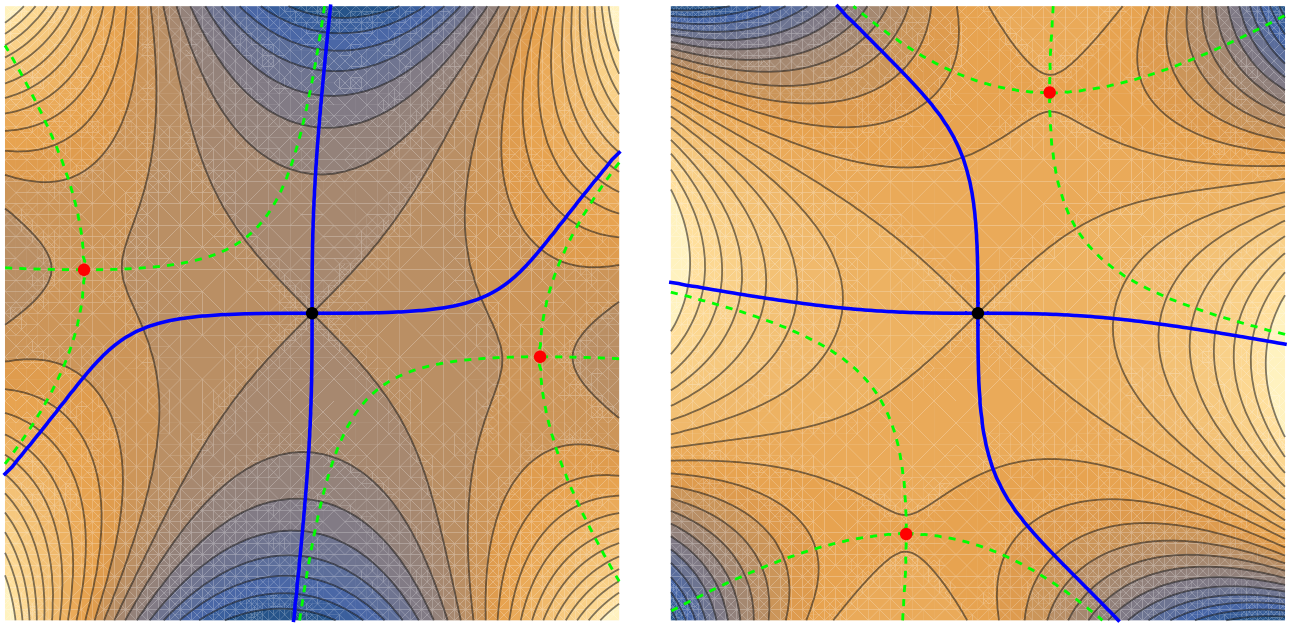

(a) $a = \exp(0.12i\pi)$. (b) $a = \exp(1.2i\pi)$.

Figure 1.3: *MOSD curves for the model integral* $I(\lambda, a) = \int_C \exp\big(-\lambda\,\mathcal{W}(z,a)\big)\,\mathrm{d}z$ *with* $\mathcal{W}(z,a) = \frac{1}{2}z^2 - a\,\frac{1}{4}z^4$*, shown for* $a = \exp(0.12i\pi)$ *and* $a = \exp(1.2i\pi)$ *(taking* $\lambda \in \mathbb{R}_{>0}$*). The background colour indicates the "height function"* $\operatorname{Re}\mathcal{W}(z,a)$*, and the thin black curves are contour lines of* $\operatorname{Re}\mathcal{W}$*. The thick* ***blue*** *curves are steepest descent trajectories: along them* $\operatorname{Im}\mathcal{W}$ *is constant and* $\operatorname{Re}\mathcal{W}$ *increases monotonically away from a saddle (as indicated by the shading/contours). The dashed* ***green*** *curves are the corresponding steepest ascent (dual) trajectories. The black dot marks the saddle* $z_0 = 0$*, and the red dots mark the pair* $z_\pm = \pm a^{-1/2}$ *(principal branch).*

1.2.3.2 Applying MOSD to the Onsager–Machlup functional

With the MOSD framework established, we now extend steepest descent reasoning to the stochastic path integral. In the weak-noise regime $D \to 0^+$, paths are weighted by an Onsager–Machlup action as in (1.10),

$$\mathcal{P}[x] \;\propto\; \exp\Big(-\frac{1}{4D}\,\mathcal{S}[x]\Big), \qquad \mathcal{S}[x] := \int_{-\mathcal{T}/2}^{+\mathcal{T}/2} \big(\dot{x}(t) + V'(x(t))\big)^2\,\mathrm{d}t, \quad \text{(Itô interpretation).} \tag{1.43}$$

Here $\mathcal{P}[x]$ denotes the (unnormalised) weight assigned to an individual trajectory $x(\cdot)$ in the path integral, while $P(x,t)$ denotes the probability density in x-space as in (1.8). In the one-dimensional MOSD template (1.28), the exponent takes the form λg with λ large. In the present setting the same role is played by $\lambda \mapsto (4D)^{-1}$ and $g \mapsto -\mathcal{S}$. Thus, as $D \to 0^+$, trajectories with larger $\mathcal{S}[x]$ are exponentially suppressed, and the dominant contribution comes from a neighbourhood of a stationary point of $\mathcal{S}$. This is the functional analogue of expanding $g(z)$ about its saddle points.

We therefore identify the most probable trajectory $x_{\mathrm{cl}}(t)$ by imposing stationarity $\delta\mathcal{S}/\delta x = 0$ with fixed endpoints. This parallels the saddle condition $g'(z_\sigma) = 0$, except that the saddle is now an entire path. Under the Itô convention the variational calculus yields the D-dependent Euler–Lagrange equation,

$$x_{\mathrm{cl}}(t) \quad \text{solves} \quad \ddot{x} = V'V'' - D\,V''', \tag{1.44}$$

with the D-dependence coming from the Itô chain rule in the variation (see § 1.2.2.2).

To quantify fluctuations about x_{cl}, write $x(t) = x_{\mathrm{cl}}(t) + y(t)$ and expand $\mathcal{S}$ to quadratic order,

$$\mathcal{S}[x] = \mathcal{S}[x_{\mathrm{cl}}] \;+\; \frac{1}{2}\langle y \mid \hat{\mathcal{M}}_\sigma\, y\rangle \;+\; \mathcal{O}(y^3), \tag{1.45}$$

where $\hat{\mathcal{M}}_\sigma$ is the linear operator that governs small deviations y about x_{cl}. This is directly analogous to retaining the quadratic term $g''(z_\sigma)(z - z_\sigma)^2/2$ in the one-dimensional MOSD template (see § 1.2.3). The local contribution from neighbouring paths therefore reduces to a Gaussian functional integral governed by the spectrum of $\hat{\mathcal{M}}_\sigma$ (see (2.61) for the explicit form).

The quadratic form $\langle y \mid \hat{\mathcal{M}}_\sigma\, y\rangle$ encodes the local curvature of $\mathcal{S}$ at the stationary path, and plays the role of the Hessian $g''(z_\sigma)$ in the finite-dimensional template. In particular, the eigenfunctions of $\hat{\mathcal{M}}_\sigma$ pick out distinguished fluctuation directions in path space, while each eigenvalue controls how rapidly $\mathcal{S}$ increases (or decreases) when we move away from x_{cl} along that direction. Steepest descent logic then says that the relevant local integration directions are those along which the quadratic approximation has strictly positive damping in the exponent, so that the fluctuation integral is genuinely Gaussian. This is

the path integral version of choosing, near z_σ, the descent direction κ so that $g''(z_\sigma)\kappa^2 \in \mathbb{R}_{<0}$.

Expanding y in eigenmodes of $\hat{\mathcal{M}}_\sigma$ reduces the functional Gaussian to a product of ordinary one-dimensional Gaussians, one for each mode. Up to overall normalisation, each non-zero eigenvalue contributes an inverse square-root factor, and their product yields the determinant,

$$\int \mathcal{D}y \ \exp\Big(-\frac{1}{8D}\,\langle y \mid \hat{\mathcal{M}}_\sigma\, y\rangle\Big) \ \propto \ \frac{1}{\sqrt{\det{}'\,\hat{\mathcal{M}}_\sigma}}, \tag{1.46}$$

where the prime indicates omission of exact zero modes. An exact zero mode signals a flat direction of $\mathcal{S}$ generated by a continuous symmetry. For instance, an isolated instanton (see § 1.2.4) can be translated in time without altering $\mathcal{S}$, resulting in a vanishing eigenvalue along $\partial_{t_c} x_{\mathrm{cl}}$. Rather than yielding a divergent Gaussian, the method of steepest descents instructs us to treat this direction by introducing the collective coordinate t_c and its Jacobian J_{t_c} (see § 1.2.4 and § 2.115).

In addition to exact symmetries, one often encounters *nearly* flat directions, which we call quasi-zero modes. Geometrically, these correspond to shallow valleys of $\mathcal{S}$ for which the quadratic approximation does not reliably localise the integral. In such cases, the correct leading contribution is obtained by keeping the corresponding one-dimensional integral explicit and evaluating it along the appropriate descent contour. In this thesis, the contour for the soft coordinate θ is fixed by the associated Lefschetz thimble. See § 1.2.7 for an overview and § 3.6 for the detailed implementation.

With this interpretation, the sector contribution is seen to take the form

$$P_\sigma \ \simeq \ \exp\big(-\mathcal{S}[x_{\mathrm{cl}}]/(4D)\big) \ \times \ \frac{1}{\sqrt{\det{}'\,\hat{\mathcal{M}}_\sigma}} \ \times \ \Big(\text{collective coordinate factor}\Big) \ \times \ \Big(\text{soft-mode integral}\Big). \tag{1.47}$$

More explicitly, after separating the time-translation collective coordinate t_c and a single soft coordinate θ, one obtains the template form

$$P_\sigma \ \propto \ \exp\big(-\mathcal{S}[x_{\mathrm{cl}}]/(4D)\big) \ \times \ \frac{1}{\sqrt{\det{}'\,\hat{\mathcal{M}}_\sigma}} \ \times \ \Big(J_{t_c}\int \mathrm{d}t_c\Big) \ \times \ \Big(\int_{\mathcal{J}_\theta} \mathrm{d}\theta \ \exp\big(-\mathcal{S}_{\mathrm{int}}(\theta)/(4D)\big)\Big), \tag{1.48}$$

where J_{t_c} is the collective coordinate Jacobian (derived in § 2.1.9) and $\mathcal{J}_\theta$ denotes the steepest descent contour for θ (see § 3.6). In words, the neighbourhood of a saddle path factorises into stiff directions that are genuinely Gaussian, exact symmetry directions handled by collective coordinates, and softly lifted directions retained as explicit steepest descent integrals on their thimbles.

1.2.3.3 Semiclassical contributions in the context of the stochastic path integral

To clarify terminology, we give a brief recap of perturbative versus non-perturbative contributions and of the term (semi)classical. We use this language by analogy with semiclassical evaluations of quantum-mechanical path integrals, with the weak-noise limit $D \to 0$ playing the role of the semiclassical parameter. Throughout $D > 0$; thus weak-noise means $D \to 0^+$, although we often omit the superscript $+$ when no confusion can arise.

In the stochastic setting, dominant contributions arise from stationary (saddle) paths $x_{\rm cl}$ of the Onsager–Machlup action (i.e. extremals satisfying $\delta\mathcal{S}/\delta x = 0$ with the relevant boundary conditions), which we will refer to as classical paths.

A classical configuration $x_{\rm cl}$ contributes a term of the schematic form

$$\mathcal{A}(D) \;\sim\; \exp\Big(-\frac{\mathcal{S}[x_{\rm cl}]}{4D}\Big) \;\times\; \mathcal{F}(D), \tag{1.49}$$

where $\mathcal{F}(D)$ is the Gaussian (perturbative) prefactor obtained from the fluctuation operator about $x_{\rm cl}$. The exponential factor is *non-perturbative*[3], while $\mathcal{F}(D)$ admits a (typically divergent but asymptotic) expansion in powers of D.

In our setting:

- *Exponent (non–perturbative).* The Arrhenius factor $\exp(-\mathcal{S}[x_{\rm cl}]/(4D))$.

[3] Since it scales like $\exp(-A/(4D))$, its Taylor expansion at $D = 0$ vanishes term-by-term, e.g. $\exp(-1/(4D)) \sim 0 + 0 + 0 + \cdots$. This reflects an essential singularity at $D = 0$, so such terms are invisible to ordinary power-series perturbation theory.

- *Prefactor (perturbative).* Writing $x = x_{\mathrm{cl}} + y$, the quadratic fluctuation operator $\hat{\mathcal{M}}$ yields, up to overall normalisation conventions,

$$\mathcal{F}(D) \;\propto\; \mathrm{Vol}(\mathbf{EZM}) \times \frac{1}{\sqrt{\det{}' \,\hat{\mathcal{M}}}} \times \big(1 + c_1 D + c_2 D^2 + \cdots\big),$$

  where $\det'$ omits exact zero modes (handled by collective coordinates), and the higher-order terms arise from cubic and higher fluctuations.

1.2.4 Introduction to instantons

Instantons $[\mathcal{I}]$ and anti-instantons $[\bar{\mathcal{I}}]$ are distinguished classical solutions that interpolate smoothly between neighbouring critical points of the effective potential in the limit $\mathcal{T} \to \infty$. They are localised in time, and as $\mathcal{T} \to \infty$ they arise on the zero-energy level (finite-$\mathcal{T}$ connecting trajectories have $H > 0$, with the instanton recovered as $H \to 0$). Their derivatives decay exponentially as $t \to \pm\infty$.

Consider an archetypal model with a symmetric, *inverted* double-well effective potential as in Fig. 1.4. Here the effective potential is $\mathfrak{U}(x) = -\big[V'(x)\big]^2 \leq 0$, so its maxima (at critical points of V) sit at zero height. We seek the classical trajectory connecting the two maxima at $\pm\lambda$, namely a path that starts at $x(-\mathcal{T}/2) = -\lambda$ and ends at $x(+\mathcal{T}/2) = +\lambda$, taking $\mathcal{T} \to \infty$ at the end.

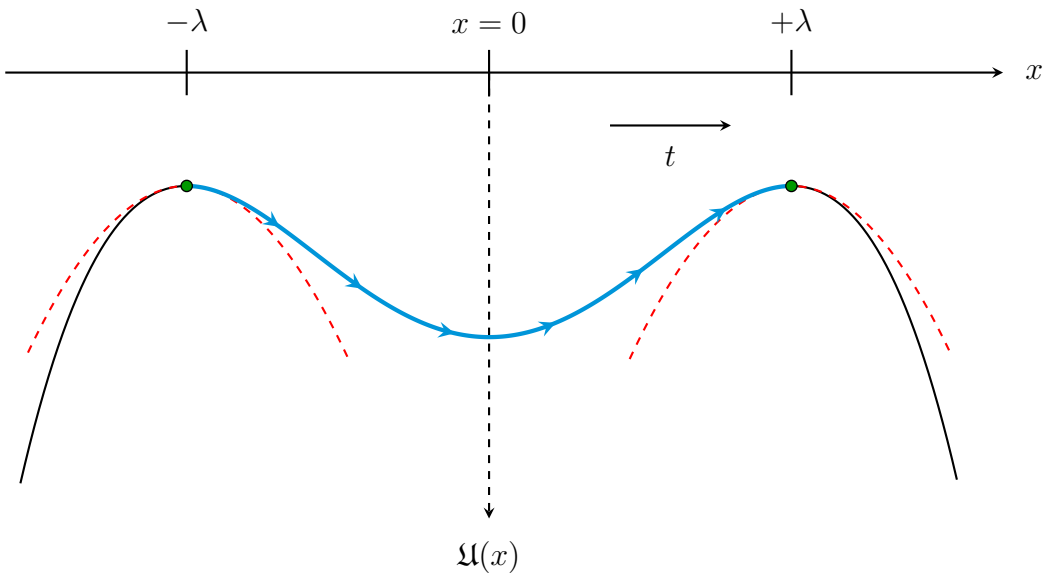

Figure 1.4: *Effective potential with a symmetric inverted double-well structure. Maxima at* $\pm\lambda$ *(green) are at zero height since* $\mathfrak{U} = -[V']^2 \leq 0$*. Dashed red curves show the local inverted harmonic approximation. The cyan curve with arrows illustrates the instanton connecting the maxima; arrows indicate increasing time along* $x_I(t)$*.*

By convention, a rightward transition path with $x_I(t)$ *strictly increasing* in time is called an instanton [148]; an anti-instanton is obtained by time reversal. In the zero-energy limit ($H \to 0$), the first integral $H = \dot{x}^2 + \mathfrak{U}(x)$ (details can be found in (2.51)) reduces to the separable gradient form

$$\dot{x}_I(t) = \sqrt{-\mathfrak{U}\big(x_I(t)\big)} = \big|V'\big(x_I(t)\big)\big| \qquad (H \to 0),$$

where the sign is chosen so that $\dot{x}_I > 0$ for the instanton (and $\dot{x}_{\bar{I}} = -|V'|$ for the anti-instanton [24]).

Under this prescription, the sign in (2.51) is fixed and for instantons we take the positive branch, yielding

$$\int_{-\lambda}^{+\lambda} \frac{\mathrm{d}x_I}{\sqrt{H - \mathfrak{U}(x_I)}} \;=\; +\mathcal{T}. \tag{1.50}$$

Since $\mathfrak{U}(\pm\lambda) = 0$, one has $H = \dot{x}(-\mathcal{T}/2)^2$, so a finite-time connecting trajectory requires $H > 0$. If $H = 0$ the connecting time diverges logarithmically because $\mathfrak{U}(x_I) \to 0$ near the endpoints.

Quantitatively, letting $\omega_\pm := |V''(\pm\lambda)|$, one finds the large–$\mathcal{T}$ behaviour

$$\mathcal{T} \sim \Big(\frac{1}{\omega_-} + \frac{1}{\omega_+}\Big) \log \frac{C}{\sqrt{H}} \quad \Longleftrightarrow \quad H \sim C' \exp\Big(-\frac{2\mathcal{T}}{\frac{1}{\omega_-} + \frac{1}{\omega_+}}\Big), \tag{1.51}$$

for constants $C, C' > 0$ set by the inner (core) region. In the symmetric case $\omega_- = \omega_+ = \omega$ this reduces to the simplified scaling $H \sim \exp(-\omega\,\mathcal{T})$ stated earlier.

Physically, the instanton spends most of its time near the critical points, with the nontrivial excursion occurring over a short interval Δt around $x \approx 0$. The remainder of $\mathcal{T}$ is spent lingering near $\pm\lambda$ in the inverted harmonic regions, and the term "instanton" reflects that the transition happens within an "instant" relative to the total time $\mathcal{T}$.

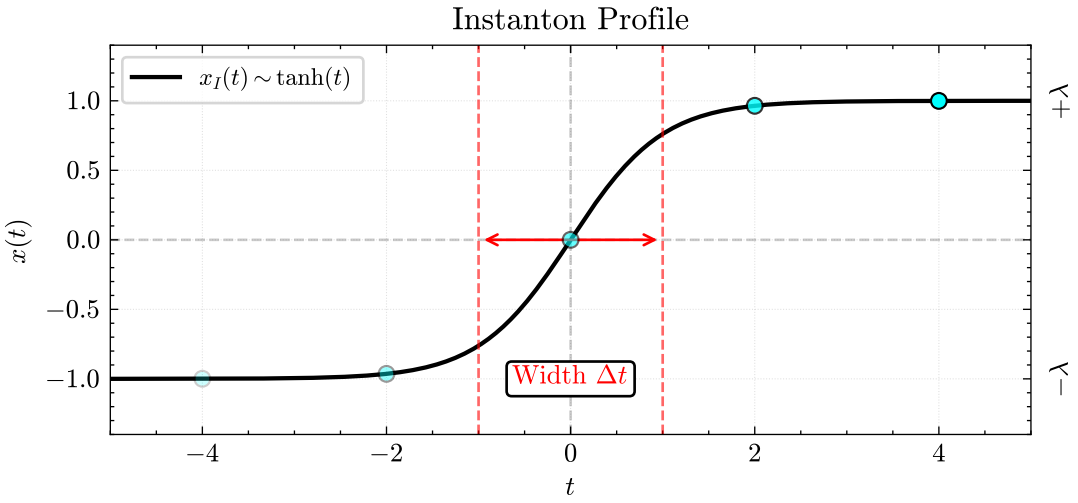

Figure 1.5: *Instanton profile $x_I(t)$, interpolating smoothly between $\pm\lambda$. The transition region Δt is localised relative to the full time interval.*

In specific models the instanton profile can be written in closed form. As an aside, for the quartic double-well in Euclidean quantum mechanics,

$$V_{\text{eff}}(x) = \frac{\omega^2}{4}\left(x^2 - \lambda^2\right)^2, \tag{1.52}$$

the $H = 0$ instanton solving $\dot{x} = \sqrt{2V_{\text{eff}}(x)}$[4] is given by the familiar hyperbolic tangent [61, 190],

$$x_I(t) = \lambda \, \tanh\Big(\frac{\omega\lambda}{\sqrt{2}}\,(t - t_c)\Big), \tag{1.53}$$

illustrating the sharply localised core. In our stochastic setting, the instanton is likewise monotone and localised, and for symmetric wells, its core is well approximated by a $\tanh$ profile.

Since the classical equations are invariant under time translation, any translated instanton $x_I(t - t_c)$ is also a valid solution for arbitrary t_c as $\mathcal{T} \to \infty$. These form a continuous one-parameter family of degenerate saddles ("critical points at infinity"), with t_c specifying the instant of transition.

This time-translation freedom implies that the fluctuation operator $\hat{\mathcal{M}}$ possesses a zero solution we call the *exact zero mode* $\mathrm{EZM(t)} \propto \dot{\mathrm{x}}_{\mathrm{cl}}(\mathrm{t})$ of the homogeneous ODE,

$$\hat{\mathcal{M}}\,\dot{x}_{\text{cl}} = 0, \qquad \dot{x}_{\text{cl}} \neq 0.$$

On a *finite* interval with Dirichlet boundary conditions, this does not, in general, satisfy the endpoint conditions, so there is no Dirichlet zero eigenvalue and the determinant is nonzero; the exact zero mode emerges in the $\mathcal{T} \to \infty$ limit. The flat direction it generates (in t_c) is handled using the method of collective coordinates § 2.1.9.

1.2.5 Bounce solutions and metastable decay in quantum mechanics

This subsection is purely motivational; the stochastic bounce configurations studied in this thesis are defined later from the Onsager–Machlup functional rather than from a Wick-rotated quantum action. We briefly recall the semiclassical picture of quantum tunnelling, where the Euclidean path integral is dominated by non-perturbative saddle point configurations known as *bounce* solutions, originally

[4] The factor $\sqrt{2}$ is specific to the standard Euclidean quantum-mechanical normalisation $S_E = \int(\frac{1}{2}\dot{x}^2 + V)\,\mathrm{d}t$, for which the zero-energy condition gives $\dot{x} = \sqrt{2V}$. In the stochastic setting used in this thesis, the first integral is $H = \dot{x}^2 + \mathfrak{U}(x)$ with $\mathfrak{U} = -[V']^2$, so the corresponding zero-energy limit yields $\dot{x} = \sqrt{-\mathfrak{U}} = |V'|$.

introduced by Coleman [38, 39]. In the Euclidean formulation of quantum mechanics, tunnelling is recast as classical motion in the *inverted* potential $-V(x)$, transforming the problem into one of a particle rolling on a hill. For definiteness, one may take the cubic model $V(x) = -(1/3)x^3 + a^2x$, whose critical points lie at $x = \pm a$ and a full analysis of this potential is given in Chapter 3. In Fig. 1.6 we set $a = 1$ for illustration and observe that the inversion swaps the roles of maxima and minima.

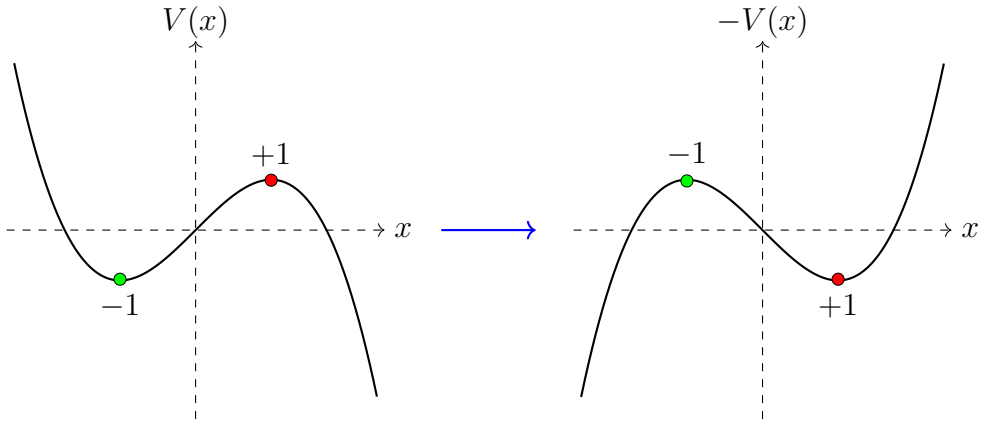

Figure 1.6: *The cubic potential $V(x) = -(1/3)x^3 + x$ (left) and its inverted counterpart $-V(x)$ (right). Inversion swaps the roles of maxima and minima; the marked points are the critical points $x = \pm 1$.*

A quantum bounce corresponds to a classical trajectory in $-V(x)$ that starts and ends at the same point x_{fv} (the false vacuum, i.e. a local minimum of V, equivalently a local maximum of $-V$), but executes a finite excursion to a turning point x_T in between. A schematic $x_b(t)$ profile is shown in Fig. 1.7.

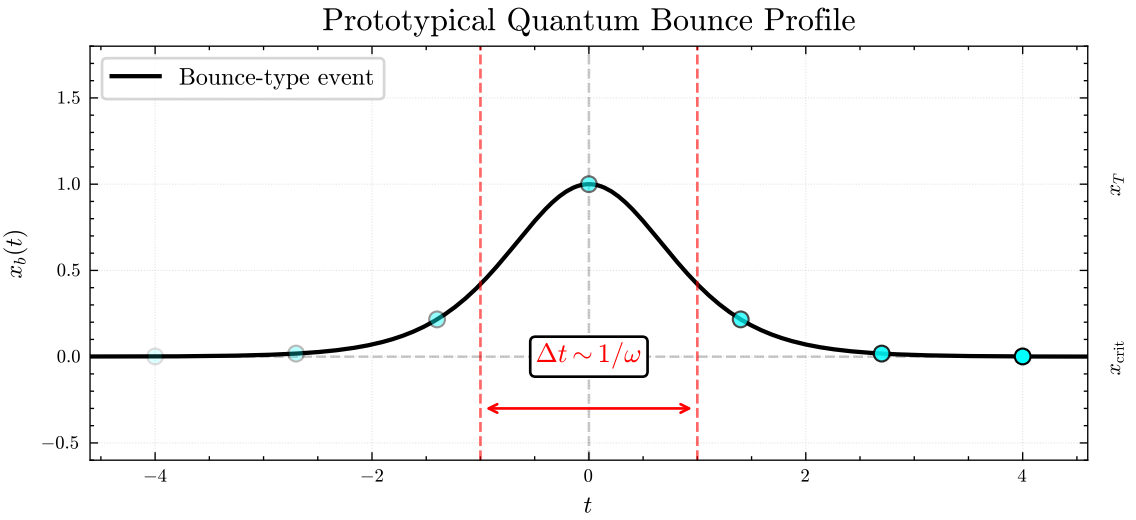

Figure 1.7: *A schematic of the quantum bounce in the inverted potential $-V(x)$. The solution is sharply localised in Euclidean time, with width set by the inverse harmonic frequency about x_{fv}, and reflects rapidly at the turning point.*

The particle spends most of its Euclidean time near $x_{\rm fv}$, then briefly traverses to the turning point x_T, reflects, and returns. Accordingly, bounce trajectories satisfy the boundary conditions

$$x_b(\pm\infty) = x_{\rm fv}, \qquad x_b(0) = x_T. \tag{1.54}$$

In many models, bounce solutions can often be written in terms of elliptic functions [186], and they contribute to the semiclassical expansion through non-perturbative terms of order $\sim \exp(-\mathcal{S}_{\rm bounce}/\hbar)$.

Although bounces are sometimes loosely referred to as "instantons," they are technically distinct. An instanton interpolates between two distinct vacua (different maxima of $-V$), whereas a bounce is a closed excursion based at a single false vacuum and encodes metastable decay.

Bounce solutions play a central role across many areas of theoretical physics, from false vacuum decay in cosmology to metastability in condensed matter and tunnelling phenomena in quantum field theory [83, 112, 113, 127, 131, 160, 177–180].

As we now transition to the Itô stochastic setting, key differences emerge. First, the relevant landscape governing saddle trajectories is no longer the inverted physical potential $-V$. Rather, it is the effective potential $\mathfrak{U}(x)$ induced by the Onsager–Machlup functional (cf. § 1.2.2.2), which in general differs qualitatively from a simple inversion and depends on V (and, in the Itô convention, on D). Second, the stochastic analogue of a bounce is not a sharply reflecting excursion with a time scale set solely by the local harmonic frequency. Instead, the relevant saddle is typically an instanton-anti-instanton composite sector $[\mathcal{I}\bar{\mathcal{I}}]$, whose separation is controlled by a soft (quasi-zero) mode and can lead to logarithmic time scales. Finally, in the weak-noise Onsager–Machlup setting, this composite saddle may lie off the real contour, so complex bounces must be included.

1.2.6 Necessity of complexification

1.2.6.1 Analogy with complex classical trajectories

In conventional classical mechanics, trajectories live on the real phase space $(q(t), p(t)) \in \mathbb{R}^2$. As emphasised by Bender and collaborators (e.g. complexified classical dynamics [3, 17–20]), analytic continuation of (q, p) into $\mathbb{C}^2$ uncovers a rich taxonomy of trajectories that persist even where real motion is classically forbidden.

As a simple illustration, consider the harmonic oscillator

$$\mathcal{H}(p, q) = p^2 + q^2, \qquad \dot{q} = 2p, \;\; \dot{p} = -2q, \tag{1.55}$$

and promote q, p to complex variables $q = r + is$ and $p = u + iv$, with $r, s, u, v \in \mathbb{R}$. Prescribing a real energy $E \in \mathbb{R}$, conservation of $\mathcal{H}$ gives the complex energy shell

$$E = p^2 + q^2 = (u^2 - v^2) + (r^2 - s^2) + 2i(uv + rs).$$

To obtain the one-parameter families plotted in Fig. 1.8, we take the initial position on the real axis,

$$r(0) = a, \qquad s(0) = 0, \qquad u(0) = 0, \tag{1.56}$$

so that $q(0) = a \in \mathbb{R}$ and the initial velocity $\dot{q}(0) = 2p(0)$ is purely imaginary. The condition that the conserved energy equals E then fixes the remaining component of the initial momentum,

$$E = r(0)^2 - v(0)^2 \quad \Longrightarrow \quad v(0) = \pm\sqrt{a^2 - E}, \tag{1.57}$$

which is real provided $a^2 \geq E$. The resulting orbit is an ellipse in the q-plane,

$$q(t) = a\cos(2t) + i\sqrt{a^2 - E}\,\sin(2t), \tag{1.58}$$

so for $E > 0$ the trajectories intersect the real axis orthogonally (at crossings $\operatorname{Im} q(t) = 0$ one has $\sin(2t) = 0$, hence $p(t) = i\sqrt{a^2 - E}\cos(2t)$, so $\dot{q}(t) = 2p(t)$ is vertical), while for $E < 0$ there is no real phase space motion on the energy shell (one always has $p \notin \mathbb{R}$, even when $q \in \mathbb{R}$), although the complex orbit remains smooth.

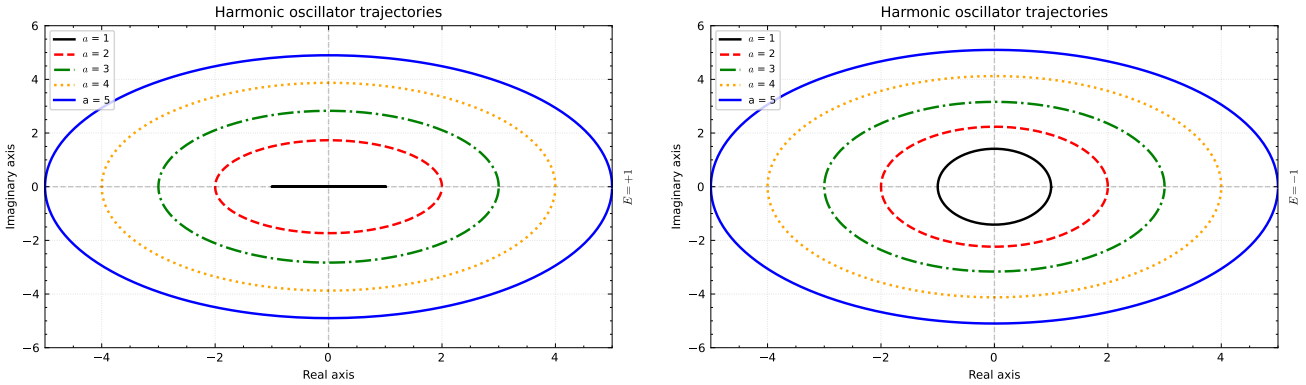

(a) $E = 1$: orbits (1.58) for several $a \geq 1$.

(b) $E = -1$: orbits (1.58) for several $a \in \mathbb{R}$.

Figure 1.8: Complex trajectories of the harmonic oscillator in the q-plane generated from the initial data (1.56) with $v(0)$ fixed by (1.57).

1.2.6.2 Stochastic analogue and persistence of complex bounces beyond the real bounce regime

The same complexification philosophy underpins our stochastic path integral setting. In the Itô Onsager–Machlup formulation, the weak-noise landscape relevant for saddle analysis is the effective potential,

$$\mathfrak{U}(z) \;=\; -\big(V'(z)\big)^2 \;+\; 2D\,V''(z), \tag{1.59}$$

and saddle trajectories satisfy the (Itô-tilted) Euler–Lagrange equation

$$\ddot{z} \;=\; V'(z)\,V''(z) \;-\; D\,V'''(z). \tag{1.60}$$

For the cubic potential $V(x) = -\frac{x^3}{3} + x$ (i.e. $a = 1$ in the model studied rigorously in Chapter 3),

$$\mathfrak{U}(x) \;=\; -\big(x^2-1\big)^2 \;-\; 4D\,x, \tag{1.61}$$

so the Itô tilt $2D\,V''$ deforms $\mathfrak{U}$ as D increases. The real critical points of $\mathfrak{U}$, which control the existence of a real $[\mathcal{I}\bar{\mathcal{I}}]$ bounce on the real contour, satisfy $\mathfrak{U}'(x) = 0 \iff x^3 - x + D = 0$. For $0 < D < D_c$ this equation has three real roots, two of which form the barrier pair relevant to the real bounce, and these coalesce at $D_c = \frac{2}{3\sqrt{3}} \approx 0.385$ in a saddle node bifurcation; for $D > D_c$ the pair disappears.

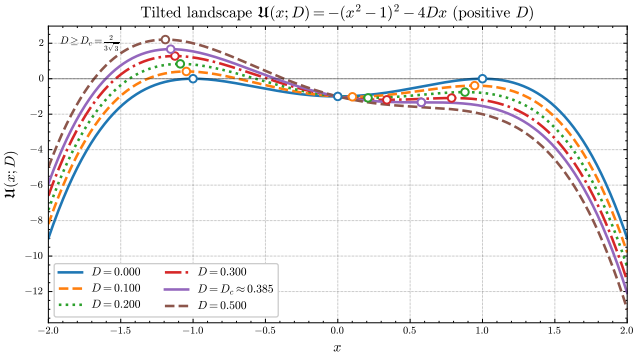

(a) Effective landscape $\mathfrak{U}(x)$ for $D = 0,\ 0.2,\ 0.4,\ 0.5$. The $2D\,V''$ tilt lowers and skews the barrier.

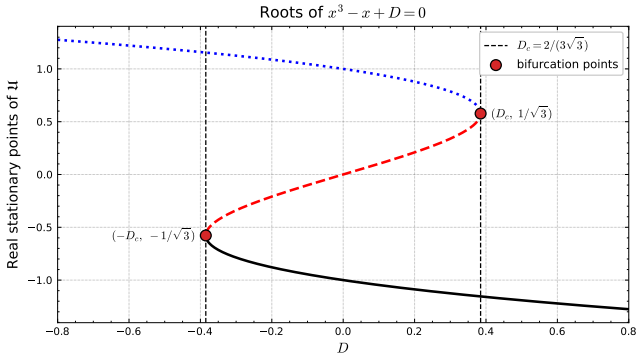

(b) Bifurcation diagram: the relevant real critical point pair coalesces at $D_c = 2/(3\sqrt{3})$ and disappears for $D > D_c$.

Figure 1.9: *Itô tilt of the effective potential and disappearance of the real bounce.*

Beyond D_c the real critical point pair is absent, so the turning point (critical point) condition required to realise a real instanton-anti-instanton ($[\mathcal{I}\bar{\mathcal{I}}]$) bounce no longer has the necessary real solutions. Equivalently, the real bounce saddle $x_{\rm rb}$ ceases to exist as a real trajectory for $D > D_c$ (hence $\mathcal{S}[x_{\rm rb}]$ is not defined as a real-saddle action beyond D_c). Under complexification, however, the same coalescing pair continues as a complex-conjugate pair, and the *stochastic complex bounce* persists for $D > D_c$. Accordingly, the complex bounce action $\mathcal{S}[z_{\rm cb}]$ remains well-defined (and analytic in D) far beyond the real bounce regime, and its contribution is captured by deforming the path integral contour to the appropriate Lefschetz thimble.

1.2.7 Lefschetz thimbles and contour selection

For background on Picard–Lefschetz theory as a method to select convergent integration cycles in oscillatory/complex integrals, we refer to Witten's formulation in quantum mechanics [184] and the AGV text [7]; representative applications in quantum field theory include [15, 71].

On the real contour, the $[\mathcal{I}\bar{\mathcal{I}}]$ sectors contain a soft (quasi-zero) direction, and the associated one-dimensional integral is poorly defined as a Gaussian approximation. We show in Chapters 3 and 4 that the complexification under Picard–Lefschetz theory selects the correct contour, known as the Lefschetz thimble. The path integral measure factorises into an exact symmetry direction (the EZM), a single soft direction (the QZM), and the remaining stable modes, which are genuinely Gaussian:

$$\mathcal{D}z \;\sim\; \mathrm{d}t_c \;\times\; \mathrm{d}\theta \;\times \prod_{n\in\text{hard}} \mathrm{d}a_n, \qquad \text{(EZM)} \;\times\; \text{(QZM)} \;\times\; \text{(stable modes)}. \tag{1.62}$$

A complete account of Lefschetz thimbles and the role of PL theory is given in § 3.6. Intuitively, a thimble is the geometric set spanned by gradient flow lines of a Morse function. We adopt the *upward* flow for $h = \mathrm{Re}(\mathcal{S}/(4D))$, that is,

$$\frac{\partial z(t,u)}{\partial u} \;=\; +\,\overline{\frac{\delta}{\delta z(t,u)}\Big(\frac{\mathcal{S}[z]}{4D}\Big)}, \qquad z(-\mathcal{T}/2,u) = x_i,\;\; z(+\mathcal{T}/2,u) = x_f, \tag{1.63}$$

where u is the auxiliary flow time parameter (distinct from the physical time t). Along solutions of (1.63), $\mathrm{Im}\,\mathcal{S}$ is constant, and h is non-decreasing, so modulus $\exp(-\mathcal{S}/(4D))$ is exponentially damped away from the saddle.

The thimble associated to a saddle trajectory z_σ (an extremal of the action) is the collection of points whose backward flow time [5] is asymptotic to z_σ,

$$\mathcal{J}_\sigma \;:=\; \Big\{\, z(\cdot,0) : [-\mathcal{T}/2, +\mathcal{T}/2] \to \mathbb{C} \;\Big|\; z(t,u) \text{ solves (1.63) and } \lim_{u\to-\infty} z(t,u) = z_\sigma(t) \,\Big\}. \quad (1.64)$$

Along $\mathcal{J}_\sigma$, $\mathrm{Im}\,\mathcal{S}$ is constant (equal to $\mathrm{Im}\,\mathcal{S}[z_\sigma]$), while $h = \mathrm{Re}(\mathcal{S}/(4D))$ increases away from the saddle along the integration direction, ensuring convergence of $\exp(-\mathcal{S}/(4D))$. A heuristic visualisation of the thimble is shown in Fig. 1.10.

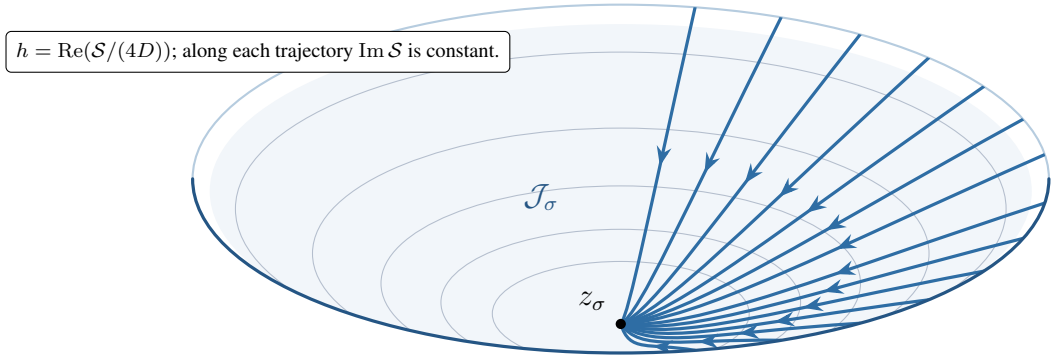

Figure 1.10: The thimble is the manifold of the flow of $h = \mathrm{Re}(\mathcal{S}/(4D))$; $\mathrm{Im}\,\mathcal{S}$ is constant and h increases away from the saddle for increasing u.

Fig. 1.11 summarises, diagrammatically, the central mechanism used throughout this thesis. Picard–Lefschetz theory isolates the QZM integral and, crucially, prescribes its steepest descent evaluation along a refined contour fixed by the thimble (hence fixing the sign/phase of the contribution). For $[\mathcal{I}\bar{\mathcal{I}}]$ configurations the QZM contour is necessarily complex and one finds

$$\mathcal{J}_\theta = \mathbb{R} \pm i\pi,$$

[5] Equivalently, one may use the downward flow and impose $\lim_{u\to+\infty} z(t,u) = z_\sigma(t)$.

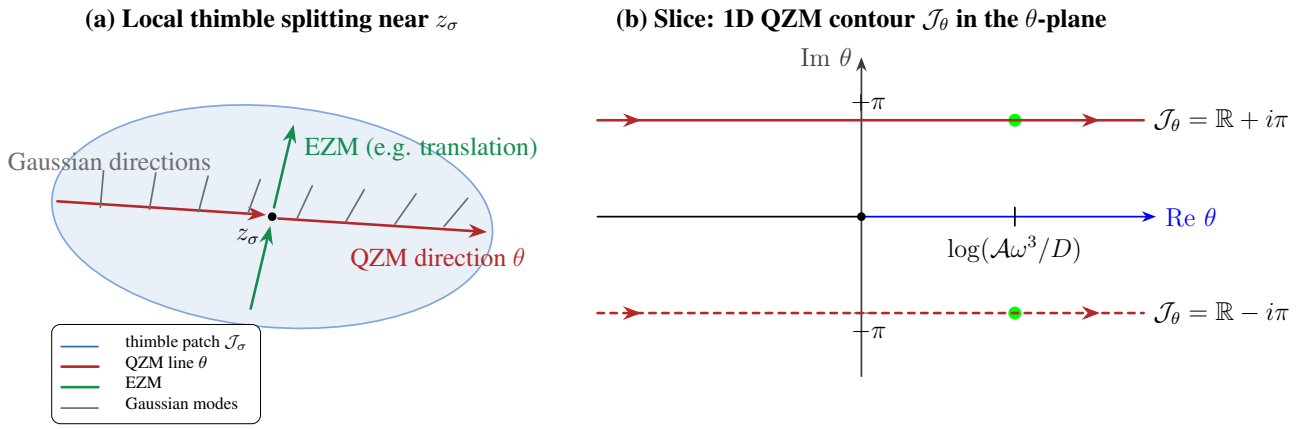

Figure 1.11: Thimble $\mathcal{J}_\sigma$ near a complex saddle z_σ and the 1D QZM slice in the θ-plane. The thimble splits as *EZM direction* $\times$ *QZM line* $\times$ *stable Gaussians*. In the θ-plane, the contributing contours are shifted from the positive half line (blue) and are defined by the lines $\mathcal{J}_\theta = \mathbb{R} \pm i\pi$. The critical point (logarithm term represents the real part) sits on the complex rays (green circles).

which is the familiar BZJ-type $\pm i\pi$ refinement (see § 1.2.8). By contrast, for $[\mathcal{I}\mathcal{I}]$ configurations, the correct contour stays on the real axis,

$$\mathcal{J}_\theta = \mathbb{R},$$

that is, the whole real line rather than the naive half-ray. An alternative approach to complexified integrals is complex Langevin dynamics; for a discussion of its merits and limitations in this context, see, e.g. [1]. In this thesis, we use Picard–Lefschetz geometry to define the integration cycle.

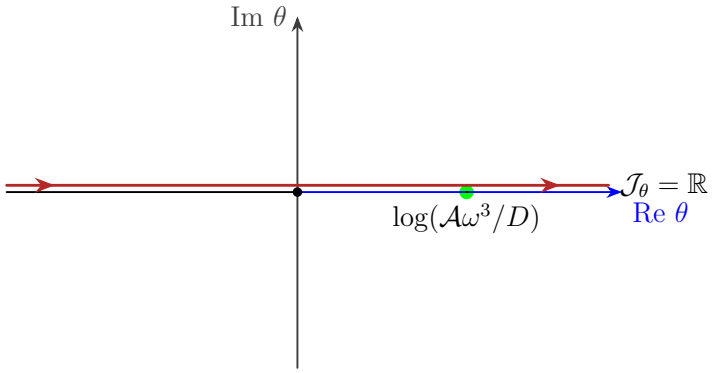

Figure 1.12: The improved contour for $[\mathcal{I}\mathcal{I}]$ pairs (red line). Instead of the half line $\mathbb{R}^+$ (blue line), the correct contour is the full real line. The critical point is a purely real logarithm (green circle).

1.2.8 QZM toy model and geometric sign fixing (BZJ versus thimble)

To isolate how thimbles fix ambiguous phases, consider a toy integral modelling the instanton–anti–instanton quasi-zero mode (QZM), inspired by Dunne *et al.* [14]:

$$\mathcal{I}_{\mathrm{QZM}}(D;A)=\exp\Big(-\frac{2S_I}{4D}\Big)\int_0^\infty \mathrm{d}\theta\,\Big[\exp\Big(\frac{A}{4D}\,e^{-\omega\theta}\Big)-1\Big],\qquad 0<A<2S_I,\ \ \omega>0, \tag{1.65}$$

where the subtraction removes the large–θ plateau (two well–separated events). With $u=e^{-\omega\theta}$ ($\mathrm{d}\theta=-\mathrm{d}u/(\omega u)$),

$$\mathcal{I}_{\mathrm{QZM}}(D;A)=\frac{e^{-2S_I/(4D)}}{\omega}\int_0^1\frac{\mathrm{d}u}{u}\,\big(e^{au}-1\big),\qquad a:=\frac{A}{4D}. \tag{1.66}$$

Here Ei denotes the exponential integral, γ_E the Euler–Mascheroni constant, and $\Gamma(0,\cdot)$ the incomplete gamma function; see e.g. [132]. Using $\displaystyle\int_0^1\frac{e^{au}-1}{u}\,\mathrm{d}u=\mathrm{Ei}(a)-\gamma_E-\ln a$,

$$\boxed{\mathcal{I}_{\mathrm{QZM}}(D;A)=\frac{\exp\big(-\frac{2S_I}{4D}\big)}{\omega}\Big[\,\mathrm{Ei}(a)-\gamma_E-\ln a\Big],\qquad a=\frac{A}{4D}>0.} \tag{1.67}$$

This exact expression is real. Working in the weak-noise limit $D\to 0^+$ (equivalently $a\to\infty$), use $\mathrm{Ei}(a)\sim\dfrac{e^a}{a}\Big(1+\dfrac{1}{a}+\dfrac{2!}{a^2}+\cdots\Big)$ to obtain

$$\begin{aligned}\mathcal{I}_{\mathrm{QZM}}(D;A)&=\frac{\exp\big(-\frac{2S_I}{4D}\big)}{\omega}\Big[\frac{e^a}{a}\Big(1+\mathcal{O}\big(\frac{1}{a}\big)\Big)-\gamma_E-\ln a\Big]\\&=\frac{\exp\big(-\frac{2S_I}{4D}\big)}{\omega}\Big[\exp\Big(\frac{A}{4D}\Big)\,\frac{4D}{A}\Big(1+\mathcal{O}\big(\frac{1}{a}\big)\Big)-\gamma_E-\ln a\Big].\end{aligned} \tag{1.68}$$

Thus, the integral is convergent but, for $a\gg 1$, is dominated by the endpoint $\theta=0$; this is precisely where the physical $[\mathcal{I}\bar{\mathcal{I}}]$ sector is least reliable. Instead, one wants the separation to be large ($\theta\gg 1$), which motivates the continuation method of Bogomolny–Zinn–Justin [24]. This toy model reveals a multivalued phase and a contribution that lacks geometric interpretation. We contrast this with thimble integration, which reproduces the same logarithmic structure and phase with a geometric origin, without any contribution from an ascent direction.

Route A (BZJ on the real axis). Continue to the repulsive interaction $a \to -|a|$ (equivalent to $D \to -D$):

$$\begin{aligned}\int_0^1 \frac{e^{-|a|u}-1}{u}\,\mathrm{d}u &= -\,\Gamma(0,|a|) - \gamma_E - \ln|a| \in \mathbb{R},\\ &= -\,\frac{e^{-|a|}}{|a|}\Big(1+\mathcal{O}\Big(\frac{1}{|a|}\Big)\Big) - \gamma_E - \ln|a|,\end{aligned} \tag{1.69}$$

which follows from $\Gamma(0,a) = -\,\mathrm{Ei}(-a)$. Rotating back across the cut, the logarithm picks up a branch jump and one obtains

$$\boxed{\mathcal{I}^{\mathrm{BZJ}}_{\mathrm{QZM}}(D;A) = \frac{e^{-2S_I/(4D)}}{\omega}\Big[-\gamma_E - \ln\frac{A}{4D} \;\mp\; i\pi \;+\; \mathcal{O}\big(e^{-A/(4D)}\big)\Big].} \tag{1.70}$$

We use the principal branch of $\ln$ with a cut along $\mathbb{R}_-$; under $D \to e^{\pm i\pi}D$ one has $-\ln(-A/(4D)) \mapsto -\ln(A/(4D)) \mp i\pi$. The neglected term is exponentially small on the repulsive sheet; after returning to $\mathrm{Re}\,D > 0$ it corresponds to an ascent direction contribution, so discarding it must ultimately be justified by the contour rather than by size alone (see Chapter 2 for a careful discussion).

Route B (Lefschetz thimble). As shown in Chapters 3 and 4, integrating over the appropriate Lefschetz contour reproduces the BZJ logarithm and phase, with a geometric origin for the $\mp i\pi$ and without any divergent terms.

1.3 Kramers' problem, validation and limits

To benchmark the weak-noise picture and to indicate its limits, we compare Kramers' approximation with (i) the exact one-dimensional mean first passage time (MFPT) formula (derived fully in § 2.1.3.1) and (ii) direct simulations of the overdamped Langevin dynamics. Throughout this section, we take the quartic potential

$$V(x) = x^4 - 4x^3 + 4x^2 - 0.6\,x + 1.6, \qquad V'(x) = 4x^3 - 12x^2 + 8x - 0.6, \tag{1.71}$$

and simulate the SDE given in (1.4) by the Euler–Maruyama scheme (time step Δt)

$$x_{n+1} = x_n - \Delta t\, V'(x_n) + \sqrt{2D\,\Delta t}\,\xi_n, \qquad \xi_n \sim \mathcal{N}(0,1). \tag{1.72}$$

We initialise each trajectory at the metastable well $x_0 = a$ with $a = 0.0857027$ and define the escape time τ as the first hitting time of the barrier, $b = 0.846374$, $\tau := \inf\{t \geq 0 : \ x(t) > b\}$. For each D, the numerical escape rate is estimated as $\Gamma_{\text{num}} \approx 1/\langle\tau\rangle$ from an ensemble of independent paths.[6]

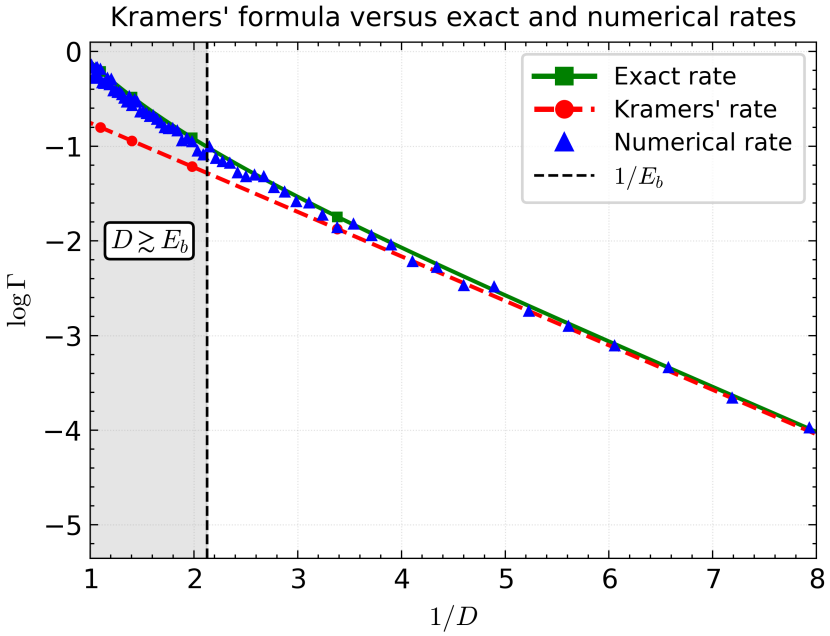

Figure 1.13: *Escape rate Γ from simulation versus the exact MFPT rate and Kramers' approximation for the potential (1.71), with escape defined by first crossing of b. The simulation uses Euler–Maruyama (1.72) with $\Delta t = 0.01$, $N_{\text{steps}} = 10^5$, and $N = 500$ independent trajectories per D. For this parameter set we observe good agreement up to $D \approx 0.30$, beyond which the Kramers approximation deviates markedly.*

In the weak-noise regime (D small compared with the barrier scale), Kramers' estimate tracks both the exact rate and the simulation data. This is the regime in which rare, localised barrier-crossing events dominate escape, and the instanton picture (together with perturbative fluctuations) is quantitatively accurate. As D increases, the Kramers approximation becomes visibly too shallow on the Arrhenius

[6] In the simulations used to produce Fig. 1.13, paths that do not cross b by the final time $T_{\max} = N_{\text{steps}}\Delta t$ are discarded; $T_{\max}$ is chosen sufficiently large that, for the displayed noise range, essentially all paths escape.

plot, signalling the breakdown of the approximation.

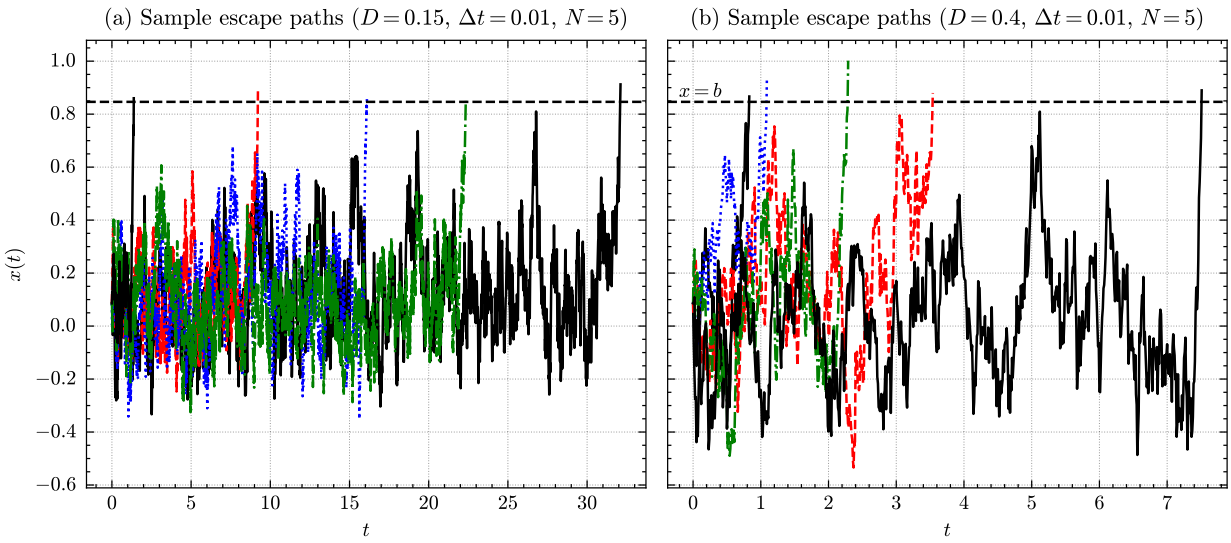

Figure 1.14: *Representative Euler–Maruyama sample paths $x(t)$ for the dynamics in the potential (1.71), started at $x(0) = a$ and stopped upon first crossing of b (dashed line). Left: weak-noise ($D = 0.2$) where trajectories typically spend long times fluctuating near the metastable well before a rare escape. Right: larger noise ($D = 0.4$) where escapes occur more readily.*

For broader perspective on Kramers' law, its domain of validity, and generalisations, see the review by Hänggi–Talkner–Borkovec [85] and the survey by Berglund [21].

1.4 Structure of the thesis

A brief roadmap is as follows.

- **Chapter 1.** Introduction and overview: complexification, steepest descents, BZJ versus thimbles, and the minimal stochastic background needed for the sequel.
- **Chapter 2.** Technical foundations: the Onsager–Machlup path integral (with Itô/Stratonovich conventions), fluctuation operators, exact zero modes and collective coordinates. We also derive

a master formula for the functional determinant, in a form that matches the standard quantum-mechanical instanton prefactors (cf. [14]).

- **Chapters 3 and 4.** Picard–Lefschetz framework for stochastic dynamics and its consequences for escape. We construct new exact two-instanton saddles (real and complex bounces) and apply the resulting thimble prescriptions to escape-rate computations in cubic and periodic (sine–Gordon) models, recovering the correct Kramers prefactor within the complexified framework.

- **Chapter 5.** Summary and outlook: connections to non-equilibrium statistical mechanics and to resurgence, together with a complex-analysis derivation of the universal -1 sign associated with the complex bounce sector.

Chapter 2

The stochastic path integral and escape-rate theory

Chapter summary

This chapter reviews the work of A.J. McKane and H.C. Luckock [117]. We provide a detailed commentary on their results working in the white-noise (Markovian) framework. Our focus is on thermally activated escape processes involving Brownian particles evolving in a metastable potential $V(x)$. We compute the associated escape rate Γ_K across a potential barrier using a perturbative procedure inspired by Feynman's semiclassical path integral formulation of quantum mechanics (with the small parameter $4D$ playing the role of $\hbar \to 0$).

The leading-order term in this expansion is obtained by finding Hamilton's principal function. The next-to-leading-order (NLO) correction accounts for Gaussian fluctuations around the classical path and is encoded in the prefactor, represented by a fluctuation determinant. The determinant is complicated by the presence of exact and quasi-zero modes, arising from continuous symmetries and nearly flat directions in the action, respectively. To treat these, we isolate their contributions from the fluctuation determinant and introduce a *master formula* to compute this determinant systematically. The (exact) zero modes are handled using the method of collective coordinates.

Quasi-zero modes associated with instanton-anti-instanton $[\mathcal{I}\bar{\mathcal{I}}]$ sectors result from the intrinsic mutual attraction between the constituent instantons, captured by an interaction action $\mathcal{S}_{\text{int}}$. The contribution of $[\mathcal{I}\bar{\mathcal{I}}]$ pairs becomes essential in systems that fail to equilibrate, where fluctuations around metastable states persist and nontrivial multi-instanton effects are non-negligible. The sign of $\mathcal{S}_{\text{int}}$ dictates the convergence of the corresponding quasi-zero mode integral I_{QZM}. Although this integral is well defined for repulsive instanton-instanton $[\mathcal{I}\mathcal{I}]$ configurations, it diverges in the attractive $[\mathcal{I}\bar{\mathcal{I}}]$ case unless an analytic continuation $D \to -D$ is performed. This step, the Bogomolny–Zinn–Justin (BZJ) prescription, serves as the conceptual motivation for the broader framework of this thesis. The chapter concludes with a discussion of the necessity and interpretation of this analytic continuation of the noise.

2.1 Path integral formulation and global preliminaries

2.1.1 Bistable potential and escape problem

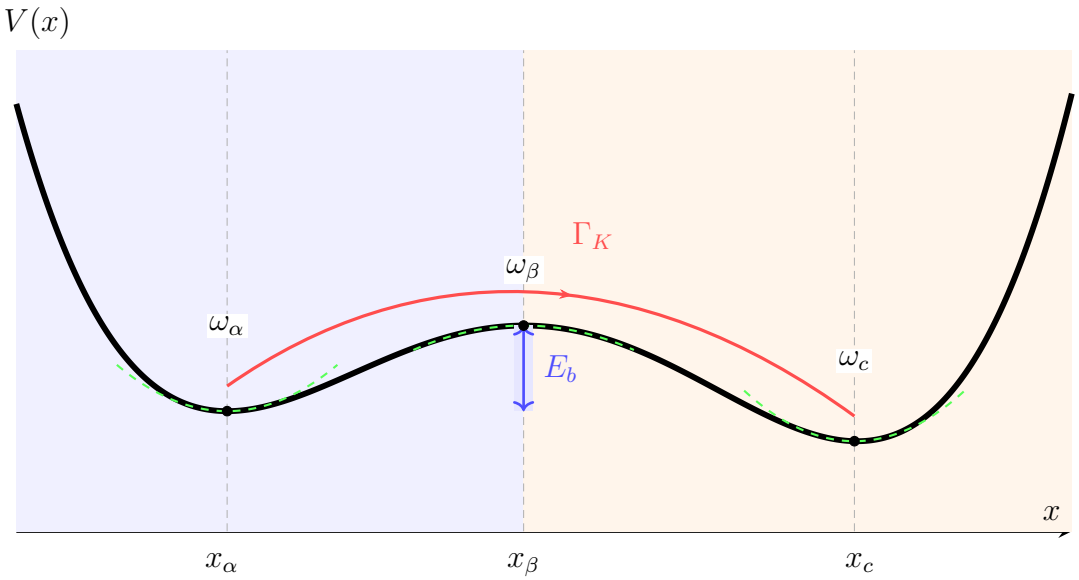

Figure 2.1: *A canonical bistable potential $V(x)$ with three critical points: the metastable minimum x_α, the barrier top x_β, and the global minimum x_c. Forward escape Γ_K proceeds from x_α to x_c via x_β. Dashed parabolas indicate local quadratic approximations with small-oscillation frequencies ω_i. The barrier height is $E_b = V(x_\beta) - V(x_\alpha)$; blue/orange bands indicate pre- and post-barrier regions.*

We begin with a prototypical bistable potential profile [174], as illustrated in Fig. 2.1, characterised by a metastable well at x_α, a barrier at x_β, and a global minimum at x_c. The specific analytic form of the potential is unimportant; we require only that it be at least thrice differentiable, $V(x) \in C^3$, to ensure smoothness and avoid singularities in the formalism.

Throughout, we work in the weak-noise limit $D \to 0$, assuming that the noise strength D is small and constant. The key scale separation is $D \ll E_b$, ensuring that thermally activated barrier-crossing events are exponentially suppressed (rare events) and dominated by saddle-point configurations in path space.

In quantum field theory, bistable configurations model metastable vacuum decay via instanton-mediated tunnelling processes [45,68,97]. In the stochastic context, our aim is to calculate the thermally activated

escape rate of a Brownian particle that begins near the metastable well x_α and surmounts the barrier at x_β.

We are interested in the instanton sectors (see § 1.2.4 for more details), where composite (anti)instanton configurations interpolate between critical points. A stochastic trajectory following the sequence

$$x_\alpha \longrightarrow x_\beta \longrightarrow x_c \tag{2.1}$$

is most naturally viewed as a *two-leg* ($[\mathcal{I}\mathcal{I}]$) configuration: an uphill instanton from x_α to x_β, followed by a downhill relaxation to x_c. In the Onsager–Machlup form

$$\mathcal{S}[x] \;=\; \int_{t_0}^{t_1} \big(\dot{x} + V'(x)\big)^2 \,\mathrm{d}t, \tag{2.2}$$

the downhill leg contributes zero *pointwise* (since $\dot{x} = -V'(x)$ there), so the Arrhenius exponent is set entirely by the uphill instanton. If one instead rewrites

$$\mathcal{S}[x] \;=\; 2\,\Delta V \;+\; \int_{t_0}^{t_1} \big(\dot{x}^2 + V'(x)^2\big)\,\mathrm{d}t, \qquad \Delta V := V\big(x(t_1)\big) - V\big(x(t_0)\big), \tag{2.3}$$

then each leg carries a non-zero bulk cost; however, on the full interval $x_\alpha \to x_c$ the path-independent term $2\Delta V$ cancels the downhill bulk exactly, leaving the same net action. Thus, we will refer to $x_\alpha \to x_\beta \to x_c$ as a two-leg $[\mathcal{I}\mathcal{I}]$ event. In contrast, the (homoclinic) orbit

$$x_\alpha \longrightarrow x_\beta \longrightarrow x_\alpha \tag{2.4}$$

describes an instanton-anti-instanton configuration $[\mathcal{I}\bar{\mathcal{I}}]$, corresponding to a cyclical trajectory that returns to where it started. As in quantum mechanics, instantons and anti-instantons interact: repulsively in $[\mathcal{I}\mathcal{I}]$ configurations and attractively in $[\mathcal{I}\bar{\mathcal{I}}]$ configurations. Crucially, these interactions occur along the time direction rather than the spatial direction.

The attractive interaction in the $[\mathcal{I}\bar{\mathcal{I}}]$ sector renders the quasi-zero mode separation integral non-convergent

in the naive Gaussian approximation, posing a non-trivial challenge for solving the stochastic path integral in the weak-noise limit. The usual fix is the Bogomolny–Zinn–Justin (BZJ) analytic continuation of the noise $D \to -D$. This motivates our later use of complex saddles and thimble contours. This chapter presents a detailed, self-contained derivation of the escape rate in the weak-noise limit, beginning with a formal introduction of the path integral via the Onsager–Machlup action. We follow [117] and set the stage for subsequent developments that involve exact two-instanton solutions and complexified saddles. This chapter contains original work in § 2.2 where we present a new master formula for computing fluctuation determinants with zero modes removed.

2.1.2 Onsager–Machlup functional integral

The probability density functional for a given realisation of *Gaussian white noise* $\xi(t)$ defined over the time interval $[t_0, t_1]$ is formally expressed as

$$P[\xi(t)] \propto \exp\left(-\frac{1}{4D}\int_{t_0}^{t_1} \mathrm{d}t\, \xi(t)^2\right). \tag{2.5}$$

Here, $\xi(t)$ is a Gaussian stochastic process characterised by the mean and covariance [74, 151, 173]

$$\langle \xi(t) \rangle = 0, \qquad \langle \xi(t)\xi(t') \rangle = 2D\,\delta(t-t'), \tag{2.6}$$

where $\langle \cdot \rangle$ denotes expectation and $D > 0$ is the noise strength [118, 135]. The proportionality symbol in (2.5) arises because the Gaussian white-noise measure (the Wiener measure) requires appropriate normalisation; for a rigorous treatment, see Appendix B.1 or Chapter 2 of Wio [182]. The white-noise idealisation corresponds to a noise process with vanishing correlation time. However, many physical systems exhibit coloured-noise correlations, leading to non-Markovian dynamics, as formulated in [28, 117, 123]; see also [139].

Consider the overdamped Langevin dynamics of a Brownian particle moving in a one-dimensional

potential $V : \mathbb{R} \to \mathbb{R}$, subject to stochastic perturbations arising from microscopic collisions. The stochastic differential equation (SDE) governing the particle position X_t is

$$\mathrm{d}X_t = -V'(X_t)\,\mathrm{d}t + \sqrt{2D}\,\mathrm{d}W_t, \tag{2.7}$$

where W_t is a Wiener process [74, 173]. We work in the overdamped regime, assuming that the inertial term $m\ddot{x}$ is negligible compared to frictional damping, that is, $|m\ddot{x}| \ll |\zeta\dot{x}|$. Here m is the mass of the particle and ζ the friction coefficient, which we set to unity henceforth, as it only scales the overall time.

Equivalently, one may express (2.7) as a Langevin equation,

$$\dot{x}(t) := \frac{\mathrm{d}x(t)}{\mathrm{d}t} = -V'(x(t)) + \xi(t), \tag{2.8}$$

where the noise term $\xi(t)$ is interpreted in the distributional sense as the time-derivative of the Wiener process ([133]),

$$\xi(t) := \sqrt{2D}\,\frac{\mathrm{d}W_t}{\mathrm{d}t}. \tag{2.9}$$

For a fixed discretisation and initial condition, this defines a one-to-one mapping

$$\xi(t) \;\mapsto\; x(t), \tag{2.10}$$

whose Jacobian depends on the discretisation scheme (Itô vs. Stratonovich). Substituting $\xi = \dot{x} + V'(x)$ into (2.5) yields the Onsager–Machlup weight for a single path $x(t)$:

$$\mathcal{P}[x(t)] \;\propto\; J_{\mathrm{OM}}[x] \exp\!\left(-\frac{1}{4D}\int_{t_0}^{t_1} \mathrm{d}t\,\big(\dot{x}(t) + V'(x(t))\big)^2\right), \tag{2.11}$$

where $J_{\mathrm{OM}}[x]$ is the (scheme-dependent) Onsager–Machlup Jacobian factor [79, 109][1]. We will adopt a consistent convention (specified in Chapter 3) and keep $J_{\mathrm{OM}}[x]$ explicit when needed. The func-

[1] The Jacobian factor strictly enters once we sum over all paths as done in (2.28).

tional (2.11) exponentially penalises deviations from the deterministic (noise-free) relaxation path, $\dot{x} = -V'(x)$. Before we continue with the path integral formalism, we derive the Kramers' rate probabilistically and then compare it with the path integral derivation of the rate.

2.1.3 Kramers' rate from the exact MFPT formula

Suppose that the system evolves in the metastable potential of Fig. 2.1. We wish to compute the mean escape rate from the basin of attraction of the local minimum $x = x_\alpha$ over the potential barrier at $x = x_\beta > x_\alpha$. Let $\rho_0(x_0)$ be the probability distribution of initial positions supported in the basin $[x_L, x_\beta]$, where $x_L < x_\alpha < x_\beta$. The mean escape time averaged over this distribution is

$$\langle \tau \rangle = \int_{x_L}^{x_\beta} \mathrm{d}x_0 \, \rho_0(x_0) \, \tau(x_0), \tag{2.12}$$

where $\tau(x_0)$ is the mean first passage time (MFPT) for a particle starting at x_0 to reach an absorbing boundary at $x = x_\beta$, assuming a reflecting boundary at x_L.

The exact MFPT satisfies the backward Fokker–Planck boundary-value problem [151]

$$D\,\tau''(x) - V'(x)\,\tau'(x) = -1, \tag{2.13}$$

with boundary conditions

$$\tau'(x_L) = 0 \quad \text{(reflecting)}, \qquad \tau(x_\beta) = 0 \quad \text{(absorbing)}. \tag{2.14}$$

Using the integrating factor $\mu(x) = \exp(-V(x)/D)$ and integrating once from x_L to x yields

$$\tau'(x) = -\frac{1}{D} \exp\Big(\frac{V(x)}{D}\Big) \int_{x_L}^{x} \mathrm{d}y \, \exp\Big(-\frac{V(y)}{D}\Big). \tag{2.15}$$

Integrating τ' from x_0 to x_β and enforcing $\tau(x_\beta) = 0$ gives the standard double-integral formula [149,

151]

$$\tau(x_0) = \frac{1}{D}\int_{x_0}^{x_\beta} \mathrm{d}x\, \exp\Big(\frac{V(x)}{D}\Big) \int_{x_L}^{x} \mathrm{d}y\, \exp\Big(-\frac{V(y)}{D}\Big), \tag{2.16}$$

valid for all $D > 0$. Averaging over the initial data with (2.12) then yields

$$\langle\tau\rangle = \frac{1}{D}\int_{x_L}^{x_\beta} \mathrm{d}u\, \mathrm{e}^{V(u)/D} \int_{x_L}^{u} \mathrm{d}v\, \mathrm{e}^{-V(v)/D} \int_{x_L}^{u} \mathrm{d}x_0\, \rho_0(x_0), \tag{2.17}$$

where we have exchanged the order of integration so that $x_0 \le u \le x_\beta$. The corresponding escape rate is $\Gamma_{\text{Exact}} = 1/\langle\tau\rangle$. We assume a delta-peaked initial condition $\rho_0(x_0) = \delta(x_0 - x_\alpha)$, which reduces to (2.16).

For the asymptotic evaluation below we take the absorbing boundary slightly beyond the barrier, $x = x_b > x_\beta$, so that the barrier top x_β controls the Laplace approximation and the standard overdamped Kramers prefactor is recovered.

2.1.3.1 Recovering Kramers' formula from the exact integral

Suppose that the particle begins precisely at the local minimum x_α, and let the reflecting boundary be located at $x = x_a < x_\alpha$, while the absorbing boundary is placed slightly beyond the barrier, at $x = x_b > x_\beta$. For notational consistency with the exact formula above we may identify $x_a \equiv x_L$. Then the mean first passage time (MFPT) to reach the absorbing boundary is given by the exact expression

$$\tau(x_\alpha) = \frac{1}{D}\int_{x_\alpha}^{x_b} \mathrm{d}x\, \exp\left(\frac{V(x)}{D}\right) \int_{x_a}^{x} \mathrm{d}y\, \exp\left(-\frac{V(y)}{D}\right). \tag{2.18}$$

This formula is valid for arbitrary noise strength $D > 0$, and encodes the precise solution to the backward Fokker–Planck equation with reflecting and absorbing boundary conditions. It becomes especially suited for asymptotic evaluation in the weak-noise limit $D \ll E_b$, where the barrier height is $E_b := V(x_\beta) - V(x_\alpha)$.

To extract the leading-order behaviour of the MFPT in this limit, we apply Laplace's method to both

the inner and outer integrals [43, 185], taking advantage of the fact that they are dominated by neighbourhoods near the extremal points of $V(x)$. The outer integral is sharply peaked near the barrier top at $x = x_\beta$, a local maximum satisfying $V'(x_\beta) = 0,\ V''(x_\beta) < 0$, while the well minimum at $x = x_\alpha$ satisfies $V'(x_\alpha) = 0,\ V''(x_\alpha) > 0$. In each case the dominant contribution arises from a region of width $z \sim \sqrt{D/|V''|}$, so the finite integration limits may be extended to $\pm\infty$ when evaluating the leading-order Gaussian contributions, incurring only exponentially small errors.

We begin with the inner integral. Expanding $V(y)$ about x_α to quadratic order yields

$$V(y) \approx V(x_\alpha) + \frac{1}{2} V''(x_\alpha)\,(y - x_\alpha)^2. \tag{2.19}$$

Substituting this into the integral and extending the limits to $\pm\infty$, we find

$$\int_{x_a}^{x} \exp\!\left(-\frac{V(y)}{D}\right) \mathrm{d}y \approx \exp\!\left(-\frac{V(x_\alpha)}{D}\right) \int_{-\infty}^{+\infty} \exp\!\left(-\frac{1}{2D} V''(x_\alpha)\, z^2\right) \mathrm{d}z, \tag{2.20}$$

where we have made the substitution $z = y - x_\alpha$. Evaluating the resulting Gaussian integral gives

$$\int_{x_a}^{x} \exp\!\left(-\frac{V(y)}{D}\right) \mathrm{d}y \approx \exp\!\left(-\frac{V(x_\alpha)}{D}\right) \sqrt{\frac{2\pi D}{V''(x_\alpha)}}. \tag{2.21}$$

Next, we approximate the outer integral near $x = x_\beta$, expanding the potential as

$$V(x) \approx V(x_\beta) + \frac{1}{2} V''(x_\beta)\,(x - x_\beta)^2. \tag{2.22}$$

Substituting this into the exponential and extending the limits to $\pm\infty$, we obtain

$$\int_{x_\alpha}^{x_b} \exp\!\left(\frac{V(x)}{D}\right) \mathrm{d}x \approx \exp\!\left(\frac{V(x_\beta)}{D}\right) \int_{-\infty}^{+\infty} \exp\!\left(-\frac{1}{2D} |V''(x_\beta)|\, z^2\right) \mathrm{d}z, \tag{2.23}$$

where we used $z = x - x_\beta$. This yields

$$\int_{x_\alpha}^{x_b} \exp\left(\frac{V(x)}{D}\right) \mathrm{d}x \approx \exp\left(\frac{V(x_\beta)}{D}\right) \sqrt{\frac{2\pi D}{|V''(x_\beta)|}}. \tag{2.24}$$

Combining both approximations, the mean first passage time becomes

$$\tau(x_\alpha) \approx \frac{2\pi}{\sqrt{V''(x_\alpha)\,|V''(x_\beta)|}} \exp\left(\frac{V(x_\beta) - V(x_\alpha)}{D}\right). \tag{2.25}$$

Taking the reciprocal yields the classical Kramers escape rate [85, 101] in the overdamped regime:

$$\Gamma_K = \frac{1}{\tau(x_\alpha)} \approx \frac{\sqrt{V''(x_\alpha)\,|V''(x_\beta)|}}{2\pi} \exp\left(-\frac{E_b}{D}\right). \tag{2.26}$$

This expression reproduces the leading-order prediction for thermally activated escape over a potential barrier.

2.1.4 Path integral representation of the transition probability

We wish to compute the transition probability for a particle to be found at position x_1 at time t_1, given that it starts at x_0 at time t_0. For a fixed discretisation scheme and initial condition $x(t_0) = x_0$, each realisation of the noise ξ generates a unique stochastic trajectory via the Langevin equation (2.8). A convenient starting point is the noise path integral, summing over those realisations that satisfy the initial condition and enforcing the terminal condition by a Dirac delta:

$$P(x_1, t_1 \mid x_0, t_0) \;\propto\; \int_{\{\,\xi:\, x_\xi(t_0)=x_0\,\}} \mathcal{D}\xi \;\exp\left(-\frac{1}{4D}\int_{t_0}^{t_1} \mathrm{d}t\, \xi(t)^2\right) \delta\big(x_\xi(t_1) - x_1\big), \tag{2.27}$$

where x_ξ denotes the trajectory obtained from ξ through the SDE. Changing the variables from ξ to the trajectory x (bijection for fixed discretisation and $x(t_0) = x_0$) gives [79, 109, 121]

$$\begin{aligned} P(x_1, t_1 \mid x_0, t_0) &= \int_{x(t_0)=x_0} \mathcal{D}x \, \left|\frac{\mathcal{D}\xi}{\mathcal{D}x}\right| \exp\left(-\frac{\mathcal{S}[x]}{4D}\right) \delta\big(x(t_1) - x_1\big) \\ &= \int_{x(t_0)=x_0} \mathcal{D}x \; J_{\text{OM}}[x] \, \exp\left(-\frac{\mathcal{S}[x]}{4D}\right) \delta\big(x(t_1) - x_1\big), \end{aligned} \tag{2.28}$$

where $J_{\text{OM}}[x]$ is the (scheme-dependent) Onsager–Machlup Jacobian [135] and

$$\mathcal{S}[x] \;=\; \int_{t_0}^{t_1} \mathrm{d}t \, \big(\dot{x} + V'(x)\big)^2. \tag{2.29}$$

The path integral measure is defined as the continuum limit of a discrete product,

$$\mathcal{D}x \;\propto\; \lim_{N\to\infty} \prod_{i=1}^{N} \mathrm{d}x_i, \qquad x_i := x(t_i), \quad t_i := t_0 + i\Delta t, \quad N\Delta t = t_1 - t_0, \tag{2.30}$$

with any overall normalisation absorbed into the measure and fixed *a posteriori* by matching the Ornstein–Uhlenbeck transition kernel [151], which is a well-known solution describing a particle moving in a harmonic well. This matching enforces the short-time limit $\Delta t := t_1 - t_0 \downarrow 0$ [2], for which $P(x_1, t_1 \mid x_0, t_0) \to \delta(x_1 - x_0)$. We place the dynamics on a symmetric time slab $K = [-\mathcal{T}/2, +\mathcal{T}/2]$ and take $\mathcal{T} \to \infty$ at the end, following [35]; cf. [69].

For additive noise, a one-parameter family of time-slicings interpolates between Stratonovich (midpoint) and Itô (left point). Writing $\alpha \in [0, 1]$ for this choice, the Onsager–Machlup Jacobian on K takes the compact form

$$J_{\text{OM}}[x] \;=\; \exp\left(\alpha \int_{-\mathcal{T}/2}^{+\mathcal{T}/2} \mathrm{d}t \, V''(x(t))\right), \tag{2.31}$$

with $\alpha = \frac{1}{2}$ (Stratonovich) and $\alpha = 0$ (Itô [89, 110]). A derivation based on the discretised Langevin equation is provided in Appendix B.2.

[2] $t \downarrow 0$ means there is a sequence $t_n > 0$ with $t_{n+1} \le t_n$ and $t_n \to 0$. So, it is a right-hand limit with monotonic decrease.

Expanding the square in (2.29) yields $\mathcal{S}[x] = \int (\dot{x}^2 + V'(x)^2 + 2\dot{x}\,V'(x))\,\mathrm{d}t$. In Stratonovich calculus, the mixed term is an ordinary Riemann integral and a total derivative,

$$\int_{t_0}^{t_1} 2\,\dot{x}\,V'(x)\,\mathrm{d}t \;=\; 2\int_{t_0}^{t_1} V'(x)\circ \mathrm{d}x \;=\; 2\,\Delta V, \qquad \Delta V := V(x_1) - V(x_0), \tag{2.32}$$

so that

$$\mathcal{S}[x] \;=\; 2\,\Delta V \;+\; \int_{t_0}^{t_1} \left(\dot{x}^2 + V'(x)^2\right) \mathrm{d}t. \tag{2.33}$$

In Itô calculus the chain rule picks up an additional correction (§ 1.2.2.1). Using Itô's lemma for $V(x)$ with $\mathrm{d}x = -V'(x)\,\mathrm{d}t + \sqrt{2D}\,\mathrm{d}W_t$ [133, Ch. 4],

$$\int_{t_0}^{t_1} 2\,\dot{x}\,V'(x)\,\mathrm{d}t \;=\; 2\,\Delta V \;-\; 2D\int_{t_0}^{t_1} V''(x)\,\mathrm{d}t. \tag{2.34}$$

Thus, compared to the Stratonovich identity (2.32), the Itô action carries a $-2D\int V''$ shift. Precisely this shift is supplied by the Jacobian factor (2.31) (with the appropriate α), so that the *combined* weight is convention independent for additive noise.

Collecting the action and Jacobian contributions, one obtains the convention-neutral form

$$P[x(t)] \;\propto\; \exp\!\left(-\frac{1}{4D}\int_{-\mathcal{T}/2}^{+\mathcal{T}/2} \mathrm{d}t\,\left[(\dot{x} + V'(x))^2 - 4D\,\alpha\,V''(x)\right]\right), \tag{2.35}$$

which is independent of the discretisation once J_{OM} is included. For additive white noise, the choice of α merely redistributes contributions between the stochastic action and the Jacobian; genuine physical differences arise only for multiplicative or coloured noise. In what follows, we adopt the Stratonovich convention ($\alpha = \frac{1}{2}$) for algebraic convenience and defer a detailed comparison with Itô to Chapter 3.

To obtain the stochastic path integral representation of transition probabilities, we now integrate over all paths connecting fixed endpoints. Let $P(x_1, +\mathcal{T}/2 \mid x_0, -\mathcal{T}/2)$ denote the probability that the system reaches x_1 at time $+\mathcal{T}/2$, having started at x_0 at time $-\mathcal{T}/2$. This probability is given by the

path integral,

$$P(x_1, +\mathcal{T}/2 \mid x_0, -\mathcal{T}/2) = \mathcal{N} \int_{x(-\mathcal{T}/2)=x_0} \mathcal{D}x \; J_{\text{OM}}[x] \; \exp\left(-\frac{\mathcal{S}[x]}{4D}\right) \delta\big(x(+\mathcal{T}/2) - x_1\big), \tag{2.36}$$

where $\mathcal{N}$ is a normalisation constant, $\mathcal{S}[x]$ is the Stratonovich action, and $J_{\text{OM}}[x]$ denotes the Stratonovich Onsager–Machlup Jacobian. The transformation of the measure $\mathcal{D}\xi \mapsto \mathcal{D}x$ can be made rigorous, e.g., Girsanov's theorem [94], which governs the changes in the measure under drift deformations in the Wiener space.

2.1.5 The semiclassical limit and the Dirac–Feynman insight

The conditional probability in (2.36) satisfies the Fokker–Planck–Smoluchowski equation via the Feynman–Kac formula [22, 92, 93, 163]. This naturally invites a brief comparison with a familiar object from quantum mechanics. In real time, the quantum propagator is the transition amplitude for a particle prepared at q_1 at time $-\mathcal{T}/2$ to be found at q_2 at time $+\mathcal{T}/2$ [161]. Feynman's representation expresses this amplitude as an integral over paths with fixed endpoints, weighted by an oscillatory phase proportional to the classical action [64, 65, 99, 157],

$$K\Big(q_2, +\mathcal{T}/2 \,\Big|\, q_1, -\mathcal{T}/2\Big) = \int_{q(-\mathcal{T}/2)=q_1} \mathcal{D}q \; \exp\left(\frac{\mathrm{i}}{\hbar} \int_{-\mathcal{T}/2}^{+\mathcal{T}/2} \mathrm{d}t \left[\tfrac{1}{2} m\, \dot{q}^{\,2} - V(q)\right]\right) \delta\big(q(+\mathcal{T}/2) - q_2\big), \tag{2.37}$$

where the delta distribution enforces the endpoint constraint at $+\mathcal{T}/2$.

Under Wick rotation $t = -\,\mathrm{i}\,\tau$, one analytically continues real time to imaginary time. This transforms the oscillatory weight into an exponentially damped one and provides the standard imaginary-time form used in semiclassical analysis. In particular, the time integral changes variable and limits,

$$\exp\left(\frac{\mathrm{i}}{\hbar} \int_{-\mathcal{T}/2}^{+\mathcal{T}/2} \mathrm{d}t \left[\tfrac{1}{2} m\, \dot{q}^{\,2} - V(q)\right]\right) \;\longrightarrow\; \exp\left(-\frac{1}{\hbar} \int_{-\mathcal{T}_{\mathrm{E}}/2}^{+\mathcal{T}_{\mathrm{E}}/2} \mathrm{d}\tau \left[\tfrac{1}{2} m\, (q')^2 + V(q)\right]\right), \qquad q' := \frac{\mathrm{d}q}{\mathrm{d}\tau}, \tag{2.38}$$

which defines the Euclidean action [91, 136, 137, 189],

$$\mathcal{S}_E[q] = \int_{-\mathcal{T}_\mathrm{E}/2}^{+\mathcal{T}_\mathrm{E}/2} \mathrm{d}\tau \left(\tfrac{1}{2} m \, (q')^2 + V(q) \right). \tag{2.39}$$

Closed forms exist only for quadratic V; otherwise, one proceeds via asymptotics or numerics. Dirac's idea, developed by Feynman, is to expand in $\hbar$. As $\hbar \to 0$ the integral is dominated by paths near the classical extremum, and the next correction arises from the quadratic expansion, the one-loop term [23, 46, 65, 185].

The weak-noise analysis mirrors this structure. The Onsager–Machlup functional plays the role of $\mathcal{S}_E$, and the identifications

$$4D \;\longleftrightarrow\; \hbar, \qquad D \ll E_b \;\longleftrightarrow\; \hbar \ll 1 \tag{2.40}$$

make the steepest descent the natural tool [69, 135]. Unlike the quantum amplitude, the stochastic path integral is already real and exponentially convergent, so no Wick rotation is required on the stochastic side. These quantum notions are recalled only to highlight the shared semiclassical organisation of the two theories. This mapping of parameters (2.40) gives a weak-noise viewpoint of Kramers' escape [25, 26].

2.1.6 From the semiclassical limit to the weak-noise limit

Building on the structural analogy between the stochastic path integral and the Wick-rotated quantum path integral, we adapt the procedure for the stochastic problem by taking the weak-noise limit $D \to 0$ [69, 158]. The first step is to identify the classical paths that satisfy the Dirichlet boundary conditions.

$$x(-\mathcal{T}/2) = x_1, \qquad x(+\mathcal{T}/2) = x_2. \tag{2.41}$$

These paths are extremals of the Onsager–Machlup functional. Equivalently, they are the most probable paths (minimum-action paths) among

$$\gamma_{\mathcal{T}} = \Big\{ x(t) \;\Big|\; x(-\mathcal{T}/2) = x_1,\; x(+\mathcal{T}/2) = x_2,\; -\mathcal{T}/2 \le t \le +\mathcal{T}/2 \Big\}, \tag{2.42}$$

with minimisers defined by [57, 158]

$$x_{\mathrm{cl},\gamma}(t) \in \arg\min_{\gamma\in\gamma_{\mathcal{T}}} \mathcal{S}[\gamma], \tag{2.43}$$

where

$$\arg\min_{\gamma\in\gamma_{\mathcal{T}}} \mathcal{S}[\gamma] := \left\{ \gamma^\star \in \gamma_{\mathcal{T}} \;:\; \mathcal{S}[\gamma^\star] = \inf_{\gamma\in\gamma_{\mathcal{T}}} \mathcal{S}[\gamma] \right\}. \tag{2.44}$$

Up to the path-independent constant $2\Delta V$ (which we drop for the variational problem), the action reads

$$\mathcal{S}[x] = \int_{-\mathcal{T}/2}^{+\mathcal{T}/2} \mathrm{d}t\, \mathcal{L}(x,\dot{x}), \qquad \mathcal{L}(x,\dot{x}) = \frac{m_p}{2}\,\dot{x}^{\,2} - \mathfrak{U}(x), \qquad \mathfrak{U}(x) := -\,V'(x)^2. \tag{2.45}$$

In our normalisation $m_p = 2$, so $\mathcal{L} = \dot{x}^{\,2} + V'(x)^2$ as used earlier. Thus, the most probable path of an overdamped particle in $V(x)$, connecting x_1 to x_2 in time $\mathcal{T}$, maps to a conservative mechanics problem for a particle of mass 2 in the effective potential $\mathfrak{U}(x) \le 0$. Because $\mathcal{L}$ is time independent, there is a conserved "energy"[3]

$$H \;=\; \dot{x}\,\frac{\partial \mathcal{L}}{\partial \dot{x}} - \mathcal{L} \;=\; \frac{m_p}{2}\,\dot{x}^{\,2} + \mathfrak{U}(x) \;=\; \dot{x}^{\,2} - V'(x)^2, \tag{2.46}$$

which is constant along any classical segment. For heteroclinic connections between critical points of V we have $V'(x) \to 0$ and $\dot{x} \to 0$ at the endpoints, hence $H = 0$ throughout and

$$\dot{x} = \pm\, V'(x). \tag{2.47}$$

[3] Dimensional analysis shows that H is technically a power; we loosely refer to it as energy since we scaled the frictional constant to unity.

The minus sign reproduces deterministic relaxation (downhill drift), while the plus sign is its time-reversal and yields the activated uphill segment (the instanton branch).

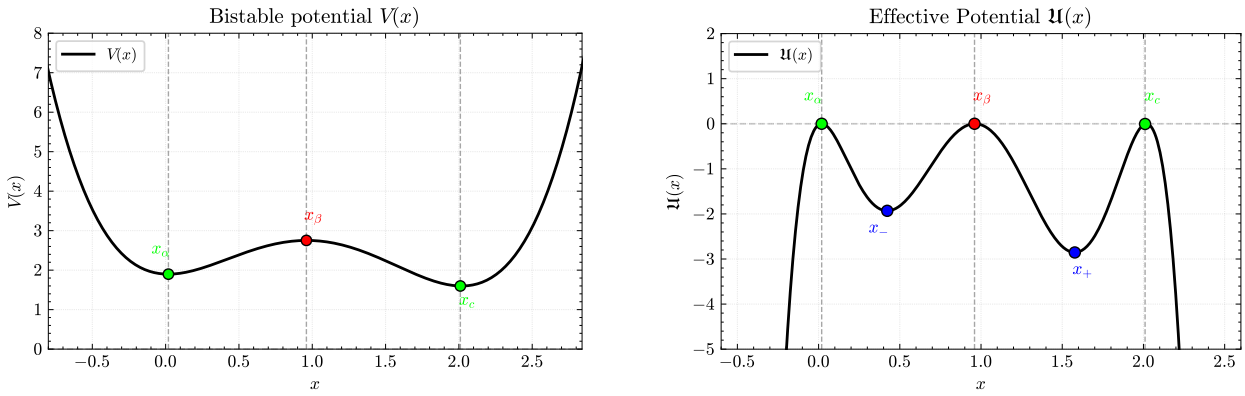

(a) $V(x) = x^4 - 4x^3 + 4x^2 - 0.15x + 1.9$ (b) $\mathfrak{U}(x) = -V'(x)^2$

Figure 2.2: *Effective potential* $\mathfrak{U}(x) = -V'(x)^2$ *associated with the bistable landscape* $V(x)$*. Critical points satisfy* $\mathfrak{U}'(x) = -2V'(x)V''(x) = 0$*. Hence, in addition to the extrema of* V *(where* $V' = 0$*), inflection points of* V *(where* $V'' = 0$*) also appear as stationary points of* $\mathfrak{U}$*. The markers* $x_\pm$ *indicate these additional points, highlighting that the effective dynamics have a richer stationary structure than the original landscape.*

2.1.7 The weak-noise tube and quadratic fluctuations

The system does not literally trace the smooth Hamiltonian path. The stochastic path integral sums over trajectories that are almost surely nowhere differentiable (see, e.g., [133, Ch. 2]). The smooth classical solution is the centreline of maximal probability within an infinitesimal tubular neighbourhood; it is not a typical realisation of the diffusion. In the weak-noise regime, the dominant contributions are confined to a tight tube of radius $\mathcal{O}(\sqrt{D})$ around the classical path (Schulman gives a straightforward heuristic on this point; cf. [157, p. 111]). As $D \to 0$, the tube shrinks, and modelling the transition by a single smooth path becomes a controlled leading-order approximation.

Examining the effective potential where the Hamiltonian dynamics occur (see Fig. 2.2), it becomes clear that the Hamiltonian particle will spend infinite time near the stationary points of $V(x)$. It accumulates infinite dwell time not only near the minima but also at the barrier. Physically, this infinite plateau is unsatisfactory: to ensure barrier crossing in finite time, the effective potential must

acquire an appropriate tilt. In Chapter 3 we show how such a tilt emerges naturally, linking back to the Itô–Stratonovich choice.

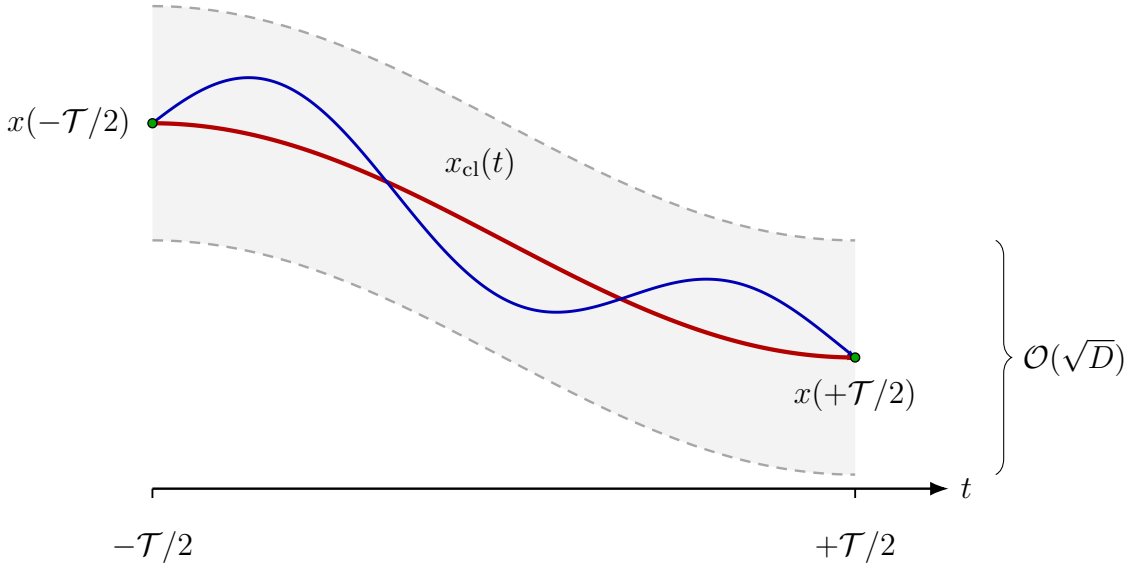

Figure 2.3: *Illustration of the weak-noise tube. Only paths (blue) within a tube of radius $\mathcal{O}(\sqrt{D})$ about the smooth centreline x_{cl} (red) contribute appreciably. The endpoints (green) satisfy Dirichlet boundary conditions at $t = -\mathcal{T}/2$ and $t = +\mathcal{T}/2$.*

Following this stochastic Hamiltonian correspondence, we identify the dominant classical configurations by extremising the action, which gives the Euler–Lagrange equations,

$$\left.\frac{\delta \mathcal{S}[x(t)]}{\delta x(t)}\right|_{x=x_{\mathrm{cl}}} = 0 \quad \Longrightarrow \quad \ddot{x} = -\frac{1}{2}\,\mathfrak{U}'(x). \tag{2.48}$$

As discussed, the parameter H represents the system's energy,

$$H = \dot{x}^2 + \mathfrak{U}(x). \tag{2.49}$$

On classical solutions, H is conserved [10]:

$$\frac{\mathrm{d}H}{\mathrm{d}t} = 2\dot{x}\left(\ddot{x} + \frac{1}{2}\mathfrak{U}'(x)\right) = 0. \tag{2.50}$$

Rearranging (2.49) gives the first integral,

$$\dot{x} = \pm\sqrt{H - \mathfrak{U}(x)}, \tag{2.51}$$

which fully specifies the extremal in one dimension. The action evaluated on this path is Hamilton's principal function [78]. A useful estimate follows from (2.51). Near any stationary point x_* of V one has $V'(x) \approx V''(x_*)(x - x_*)$ and hence

$$\frac{\mathrm{d}t}{\mathrm{d}x} = \frac{1}{\sqrt{H - \mathfrak{U}(x)}} \approx \frac{1}{\sqrt{H + \big(V''(x_*)\big)^2 (x - x_*)^2}}. \tag{2.52}$$

Integrating over a small symmetric interval $[x_* - \Delta,\, x_* + \Delta]$ yields

$$\int \frac{\mathrm{d}x}{\sqrt{H + \big(V''(x_*)\big)^2 (x - x_*)^2}} = \frac{1}{|V''(x_*)|}\,\operatorname{arsinh}\!\Big(\frac{|V''(x_*)|\,\Delta}{\sqrt{H}}\Big) \sim \frac{1}{|V''(x_*)|}\,\log\frac{C}{\sqrt{H}}, \tag{2.53}$$

so for $H \downarrow 0$, the dwell time diverges logarithmically. At $H = 0$, the integral has a $1/|x - x_*|$ singularity, and the plateau is truly infinite. This motivates the effective tilt introduced in Chapter 3.

Having determined the leading-order contribution, we now examine the next-order correction, the quadratic fluctuations around the dominant path. A general path can be written as

$$x(t) = x_{\mathrm{cl}}(t) + y(t), \tag{2.54}$$

where the fluctuations $y(t)$ must vanish at the endpoints,

$$y(-\mathcal{T}/2) = 0 = y(+\mathcal{T}/2). \tag{2.55}$$

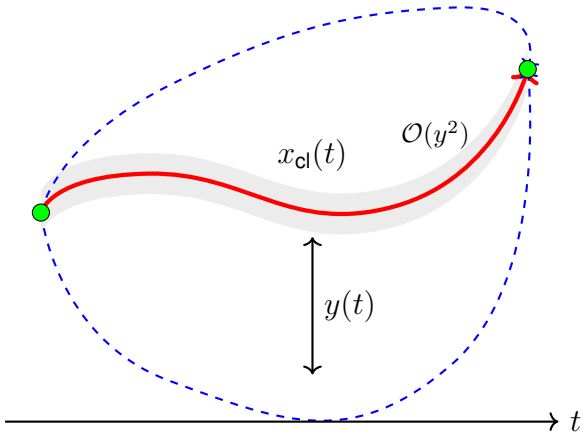

Figure 2.4: *Quadratic fluctuations $y(t)$ about the smooth classical path x_{cl}. The grey band indicates the region where the semiclassical expansion is valid. Endpoints (green) are fixed by the boundary conditions.*

Remark 2.1.1 (On large fluctuations). The fluctuation expansion formally integrates over all paths $y(t)$ satisfying the Dirichlet conditions. However, only small fluctuations of typical amplitude $y \sim \mathcal{O}(\sqrt{D})$ contribute significantly in the weak-noise limit. Larger excursions are exponentially suppressed by the quadratic form in the Onsager–Machlup action, contributing factors like $\exp[-\mathcal{O}(y^2)/(4D)]$ and are thus negligible. The dominant weight is concentrated in a narrow tube around x_{cl}, justifying the local expansion and the picture in Fig. 2.4.

We thus integrate over an infinite set of paths clustered tightly around the extremal solution. By inserting the expansion (2.54) into the action, one performs a functional Taylor expansion [60] up to second order,

$$\mathcal{S}[x] \approx \mathcal{S}[x_{\mathrm{cl}}] + \int_{-\mathcal{T}/2}^{+\mathcal{T}/2} \mathrm{d}t \; y(t) \left[\frac{\delta \mathcal{S}}{\delta x(t)} \bigg|_{x_{\mathrm{cl}}} \right] + \frac{1}{2} \int_{-\mathcal{T}/2}^{+\mathcal{T}/2} \mathrm{d}t \int_{-\mathcal{T}/2}^{+\mathcal{T}/2} \mathrm{d}t' \; y(t) \left[\frac{\delta^2 \mathcal{S}}{\delta x(t) \delta x(t')} \bigg|_{x_{\mathrm{cl}}} \right] y(t') + \mathcal{O}(y^3). \quad (2.56)$$

The first-order term vanishes by the Euler–Lagrange condition, so the action reduces to

$$\mathcal{S}[x] = \mathcal{S}[x_{\rm cl}] + \frac{1}{2}\int_{-\mathcal{T}/2}^{+\mathcal{T}/2} \mathrm{d}t \int_{-\mathcal{T}/2}^{+\mathcal{T}/2} \mathrm{d}t' \; y(t)\, \hat{\mathcal{M}}(t,t')\, y(t') + \mathcal{O}(y^3), \tag{2.57}$$

The single-integral quadratic form obtained by direct computation is then [79]

$$\mathcal{S}[x] = \mathcal{S}[x_{\rm cl}] + \int_{-\mathcal{T}/2}^{+\mathcal{T}/2} \mathrm{d}t \; y(t) \Big[-\frac{\mathrm{d}^2}{\mathrm{d}t^2} - \frac{1}{2}\mathfrak{U}''(x_{\rm cl}) \Big] y(t) + \mathcal{O}(y^3). \tag{2.58}$$

Equivalently, in original units,

$$\mathcal{S}[x] = \mathcal{S}[x_{\rm cl}] + \frac{m_p}{2}\int_{-\mathcal{T}/2}^{+\mathcal{T}/2} \mathrm{d}t \; y(t) \Big[-\frac{\mathrm{d}^2}{\mathrm{d}t^2} - \frac{1}{m_p}\mathfrak{U}''(x_{\rm cl}) \Big] y(t) + \mathcal{O}(y^3), \tag{2.59}$$

making the dependence on m_p explicit. The fluctuation sector is therefore governed by the fluctuation operator,

$$\hat{\mathcal{M}} = -\frac{\mathrm{d}^2}{\mathrm{d}t^2} - \frac{1}{2}\mathfrak{U}''(x_{\rm cl}) = -\frac{\mathrm{d}^2}{\mathrm{d}t^2} + V''(x_{\rm cl})^2 + V'(x_{\rm cl})V'''(x_{\rm cl}), \tag{2.60}$$

which defines the spectrum of Gaussian fluctuations around the dominant trajectory. This is our second-order fluctuation operator. We can write the expansion compactly as

$$\mathcal{S}[x] = \mathcal{S}[x_{\rm cl}] + \langle y \mid \hat{\mathcal{M}}\, y \rangle + \mathcal{O}(y^3). \tag{2.61}$$

The inner product is the standard real inner product on the interval K for real-valued functions[4], where $K = [-\mathcal{T}/2, +\mathcal{T}/2]$,

$$\langle f \mid g \rangle = \int_K \mathrm{d}t \; f(t)\, g(t). \tag{2.62}$$

The term $\langle y \mid \hat{\mathcal{M}}\, y \rangle$ defines the *fluctuation action*, which captures the contribution from quadratic fluctuations about the classical path. This shows that the full path integral naturally factorises into a

[4]Complex conjugation is omitted since the paths are real, for all t, $\overline{g(t)} = g(t)$.

classical part and a fluctuation factor,

$$P \sim P_{\text{classical}} \times P_{\text{fluctuation}}, \tag{2.63}$$

up to an overall normalisation constant. The fluctuation sector is non-trivial. The Euler–Lagrange equations with Dirichlet boundary conditions fix the classical solution, so the Jacobian for the affine shift $x(t) \to y(t)$ is unity, and the path integration measure transforms $\mathcal{D}x = \mathcal{D}y$ [157]. Inserting (2.61) into the original path integral (2.36) gives, up to quadratic order,

$$\begin{aligned} &P(x_2, +\mathcal{T}/2 \mid x_1, -\mathcal{T}/2) \\ &\quad = \exp\Big(-\frac{\mathcal{S}[x_{\text{cl}}]}{4D}\Big) \int_{y(-\mathcal{T}/2)=0} \mathcal{D}y \; J_{\text{OM}}[x_{\text{cl}} + y] \; \exp\Big(-\frac{\langle y \mid \hat{\mathcal{M}}\, y\rangle}{4D} + \mathcal{O}(y^3)\Big) \, \delta\big(y(+\mathcal{T}/2)\big). \end{aligned} \tag{2.64}$$

The decomposition in (2.63) is now explicit: the classical factor comes from $-\mathcal{S}[x_{\text{cl}}]/(4D)$, while the fluctuation piece is a Gaussian path integral about the saddle [189]. Using the earlier form of the Onsager–Machlup Jacobian, at quadratic order, one may replace[5] $J_{\text{OM}}[x_{\text{cl}} + y] \to J_{\text{OM}}[x_{\text{cl}}]$.

To evaluate the Gaussian piece, expand $y(t)$ in an orthonormal basis $\{y_n(t)\}$ that diagonalises $\hat{\mathcal{M}}$:

$$\hat{\mathcal{M}}\, y_n(t) = \lambda_n \, y_n(t), \tag{2.65}$$

with Dirichlet boundary conditions

$$y_n(-\mathcal{T}/2) = 0 = y_n(+\mathcal{T}/2), \tag{2.66}$$

and orthonormality

$$\langle y_n \mid y_m \rangle = \int_{-\mathcal{T}/2}^{+\mathcal{T}/2} \mathrm{d}t \; y_n(t)\, y_m(t) = \delta_{mn}. \tag{2.67}$$

The original action (2.29) is positive semidefinite, $\mathcal{S}[x] \geq 0$ for all real, admissible paths. Hence,

[5] At prefactor accuracy (leading in D), typical fluctuations scale as $y = \mathcal{O}(\sqrt{D})$. Expanding $\log J_{\text{OM}}[x_{\text{cl}} + y]$ then shows that the y-dependent terms modify $\log P$ only by $\mathcal{O}(D)$, so we evaluate the Jacobian at the saddle: $J_{\text{OM}}[x_{\text{cl}} + y] \to J_{\text{OM}}[x_{\text{cl}}]$.

the classical solution with Dirichlet conditions is a local minimum; inspecting (2.61) shows that $\hat{\mathcal{M}}$ is therefore positive semidefinite. With these boundary conditions $\hat{\mathcal{M}}$ is also self-adjoint,[6] which justifies the mode expansion.

Hence, we write

$$x(t) = x_{\mathrm{cl}}(t) + y(t) = x_{\mathrm{cl}}(t) + \sum_{n=0}^{\infty} a_n\, y_n(t), \tag{2.68}$$

with coefficients a_n. The fluctuation action becomes diagonal,

$$\langle y \mid \hat{\mathcal{M}}\, y\rangle = \sum_{n=0}^{\infty} \lambda_n\, a_n^2, \tag{2.69}$$

so integration over the fluctuation space reduces to an integral over the coefficients a_n (see Appendix I of [124] for a detailed justification). This diagonalisation reduces the fluctuation path integral to an infinite product over decoupled Gaussian modes and underpins the computation of fluctuation determinants.

We transform the path integral from an integral over $y(t)$ to an explicit product over $\{a_n\}$:

$$P(x_2, +\mathcal{T}/2 \mid x_1, -\mathcal{T}/2) = \mathcal{N}_D\, \exp\!\Big(-\frac{\mathcal{S}[x_{\mathrm{cl}}]}{4D}\Big)\, J_{\mathrm{OM}}[x_{\mathrm{cl}}]\, \lim_{N\to\infty} \prod_{n=0}^{N} \Big\{ \int_{\mathbb{R}} \mathrm{d}a_n\, \exp\!\Big(-\frac{\lambda_n\, a_n^2}{4D}\Big)\Big\}, \tag{2.70}$$

where the constant $\mathcal{N}_D$ fixes the overall normalisation of the free path measure.

Remark 2.1.2 (Normalisation of the mode expansion). In the continuum formulation, the measure $\mathcal{D}x$ is chosen so that the free Gaussian functional integral equals one. After expanding in the orthonormal eigenmodes of $\hat{\mathcal{M}}$, the measure becomes a product of standard one-dimensional Gaussians over the coefficients a_n, each contributing a factor $\sqrt{4\pi D}$. The constant $\mathcal{N}_D$ cancels the resulting product so that the free theory is correctly normalised [157, 189].

[6] For test functions f, g vanishing at the endpoints,

$$\langle \hat{\mathcal{M}} f \mid g\rangle = \int_{-\mathcal{T}/2}^{+\mathcal{T}/2} \mathrm{d}t\, \Big[-\ddot{f}\, g - \tfrac{1}{2}\, f\, g\, \mathfrak{U}''(x_{\mathrm{cl}})\Big] = \langle f \mid \hat{\mathcal{M}} g\rangle,$$

so the eigenfunctions form a complete orthonormal set.

Carrying out the Gaussian integrals formally yields

$$P(x_2, +\mathcal{T}/2 \mid x_1, -\mathcal{T}/2) = \mathcal{N}_D \, \exp\Big(- \frac{\mathcal{S}[x_{\text{cl}}]}{4D} \Big) \, J_{\text{OM}}[x_{\text{cl}}] \, \lim_{N\to\infty} \prod_{n=0}^{N} \sqrt{\frac{4\pi D}{\lambda_n}}, \tag{2.71}$$

$$= \mathcal{N}_D \, \exp\Big(- \frac{\mathcal{S}[x_{\text{cl}}]}{4D} \Big) \, J_{\text{OM}}[x_{\text{cl}}] \, \Big[\lim_{N\to\infty} \prod_{n=0}^{N} \sqrt{4\pi D} \Big] \, (\det \hat{\mathcal{M}})^{-\frac{1}{2}}. \tag{2.72}$$

Here, $\det\hat{\mathcal{M}}$ denotes the product of the eigenvalues $\{\lambda_n\}$ and is the fluctuation determinant. We assume for simplicity that no zero eigenvalues are present; cases with zero or near-zero modes are treated later.

To begin, consider the simplest solvable case: the free particle with $V(x) = 0$ everywhere. This describes unconstrained diffusion along the real axis. The Fokker–Planck–Smoluchowski equation then reduces to the standard diffusion (heat) equation,

$$\frac{\partial P}{\partial t} = D \, \frac{\partial^2 P}{\partial x^2}, \tag{2.73}$$

whose fundamental solution over the time interval $\mathcal{T}$ is

$$P_{\text{free}}(x_2, +\mathcal{T}/2 \mid x_1, -\mathcal{T}/2) = \frac{1}{\sqrt{4\pi D \, \mathcal{T}}} \, \exp\Big(- \frac{(x_2 - x_1)^2}{4D \, \mathcal{T}} \Big). \tag{2.74}$$

In the path integral representation (2.72), the transition probability for the free particle is

$$P(x_2, +\mathcal{T}/2 \mid x_1, -\mathcal{T}/2) = \mathcal{N}_D \, \exp\Big(- \frac{\mathcal{S}[x_{\text{free}}]}{4D} \Big) \, J_{\text{OM}}[x_{\text{free}}] \, \Big[\lim_{N\to\infty} \prod_{n=1}^{N} \sqrt{4\pi D} \Big] \, \big(\det \hat{\mathcal{M}}_{\text{free}} \big)^{-1/2}. \tag{2.75}$$

The classical solution satisfying the Dirichlet endpoints is elementary,

$$x_{\text{free}}(t) = \frac{x_2 - x_1}{\mathcal{T}} \, t \; + \; \frac{x_1 + x_2}{2}, \tag{2.76}$$

and its action evaluates to

$$\mathcal{S}[x_{\text{free}}] = \frac{(x_2 - x_1)^2}{\mathcal{T}}. \tag{2.77}$$

The Onsager–Machlup Jacobian for free diffusion is trivially unity, $J_{\mathrm{OM}}[x_{\mathrm{free}}] = 1$, and the free fluctuation operator reduces to the negative second derivative,

$$\hat{\mathcal{M}}_{\mathrm{free}} = -\frac{\mathrm{d}^2}{\mathrm{d}t^2}, \tag{2.78}$$

with eigenvalue problem [187]

$$\hat{\mathcal{M}}_{\mathrm{free}}\, y_n(t) = \lambda_n\, y_n(t), \quad y_n(-\mathcal{T}/2) = 0 = y_n(+\mathcal{T}/2). \tag{2.79}$$

The standard Dirichlet modes on $[-\mathcal{T}/2, +\mathcal{T}/2]$ are

$$y_n(t) = \sqrt{\frac{2}{\mathcal{T}}}\, \sin\!\Big(\frac{n\pi}{\mathcal{T}}\big(t + \mathcal{T}/2\big)\Big), \quad \lambda_n = \frac{n^2\pi^2}{\mathcal{T}^2}, \quad n = 1, 2, \dots, \tag{2.80}$$

and note that there is no non-trivial Dirichlet eigenfunction for $n = 0$.

Inserting these results into (2.72) and equating with the fundamental solution fixes the normalisation relation,

$$\mathcal{N}_D \Big[\lim_{N\to\infty} \prod_{n=1}^{N} \sqrt{4\pi D}\Big] \left(\prod_{n=1}^{\infty} \frac{n^2\pi^2}{\mathcal{T}^2}\right)^{-1/2} = \frac{1}{\sqrt{4\pi D\,\mathcal{T}}}. \tag{2.81}$$

This provides the needed reference to fix $\mathcal{N}_D$ once the fluctuation determinant is regularised.

Next, let us assume $V(x) \neq 0$ and consider the elementary case where the particle remains stationary at a fixed point x_0 for all time. Assume x_0 is a *non-degenerate minimum* of V, i.e. $V'(x_0) = 0$ and $V''(x_0) > 0$. That is, at $t = -\mathcal{T}/2$ the particle sits at x_0 and at $t = +\mathcal{T}/2$ it remains there. Returning to the path integral representation (2.72), the conditional probability is

$$P(x_0, +\mathcal{T}/2 \mid x_0, -\mathcal{T}/2) = \mathcal{N}_D\, \exp\!\Big(-\frac{\mathcal{S}[x_0]}{4D}\Big)\, J_{\mathrm{OM}}[x_0] \Big[\lim_{N\to\infty} \prod_{n=1}^{N} \sqrt{4\pi D}\Big] \big(\det \hat{\mathcal{M}}_0\big)^{-1/2}. \tag{2.82}$$

For brevity, define $P_0(\mathcal{T}) := P(x_0, +\mathcal{T}/2 \mid x_0, -\mathcal{T}/2)$, the probability that a trajectory starts and ends at x_0 over time $\mathcal{T}$. In the weak-noise limit, fluctuations about x_0 are infinitesimal, so only paths within

the harmonic region of the potential contribute appreciably. Expanding $V(x)$ around x_0 gives the local quadratic approximation,

$$V(x) \approx V(x_0) + \frac{1}{2}V''(x_0)\,(x-x_0)^2 + \dots \quad \Longrightarrow \quad \omega_0^2 := -\tfrac{1}{2}\mathfrak{U}''(x_0), \tag{2.83}$$

where the harmonic frequency is $\omega_0 = \sqrt{-\frac{1}{2}\mathfrak{U}''(x_0)} = |V''(x_0)|$.

In this stationary limit, the action of the constant path $x(t) = x_0$ is zero, $\mathcal{S}[x_0] = 0$, since $\mathfrak{U}(x) = -(V'(x))^2$ gives $\mathfrak{U}(x_0) = 0$ and $\dot{x} \equiv 0$ makes the kinetic term vanish. The fluctuation operator is now harmonic,

$$\hat{\mathcal{M}}_0 = -\frac{\mathrm{d}^2}{\mathrm{d}t^2} + \omega_0^2, \tag{2.84}$$

and the eigenvalue problem $\hat{\mathcal{M}}_0\, y_n(t) = \lambda_n\, y_n(t)$ with Dirichlet conditions has solutions

$$y_n(t) = \sqrt{\frac{2}{\mathcal{T}}}\,\sin\Big(\sqrt{\lambda_n - \omega_0^2}\,(t + \mathcal{T}/2)\Big), \quad \lambda_n = \omega_0^2 + \frac{n^2\pi^2}{\mathcal{T}^2}, \quad n = 1, 2, \dots. \tag{2.85}$$

The Onsager–Machlup Jacobian for a stationary harmonic minimum is

$$J_{\text{OM}}[x_0] = \exp\big(\tfrac{1}{2}V''(x_0)\,\mathcal{T}\big) = \exp\big(\tfrac{1}{2}\omega_0\,\mathcal{T}\big), \tag{2.86}$$

since $V''(x_0) = \omega_0 > 0$ at a minimum.

Hence, the conditional probability is

$$P_0(\mathcal{T}) = \exp\big(\tfrac{1}{2}\omega_0\,\mathcal{T}\big)\, \underbrace{\mathcal{N}_D\left[\lim_{N\to\infty}\prod_{n=1}^{N}\sqrt{4\pi D}\right]\Big(\prod_{n=1}^{\infty}\tfrac{n^2\pi^2}{\mathcal{T}^2}\Big)^{-1/2}}_{\dfrac{1}{\sqrt{4\pi D\,\mathcal{T}}}} \times \underbrace{\Big(\prod_{n=1}^{\infty} 1 + \tfrac{\omega_0^2\mathcal{T}^2}{n^2\pi^2}\Big)^{-1/2}}_{\sqrt{\dfrac{\omega_0\mathcal{T}}{\sinh(\omega_0\mathcal{T})}}}. \tag{2.87}$$

The first product uses the relation derived in the free particle case (2.81) and the final product follows

from Euler's infinite product expansion [175], resulting in

$$P_0(\mathcal{T}) = \sqrt{\frac{\omega_0}{4\pi D\,\sinh(\omega_0 \mathcal{T})}}\,\exp\!\big(\tfrac{1}{2}\omega_0\,\mathcal{T}\big), \tag{2.88}$$

which matches the Ornstein–Uhlenbeck solution [119]. The $P_0(\mathcal{T})$ fixes the normalisation factor in the full path integral,

$$P(x_2, +\mathcal{T}/2 \mid x_1, -\mathcal{T}/2) = P_0(\mathcal{T})\,\exp\!\Big(-\frac{\mathcal{S}[x_{\rm cl}]}{4D}\Big)\,\frac{J_{\rm OM}[x_{\rm cl}]}{J_{\rm OM}[x_0]}\left(\frac{\det\hat{\mathcal{M}}}{\det\hat{\mathcal{M}}_0}\right)^{-1/2}. \tag{2.89}$$

This confirms that in the weak-noise approximation, the stochastic path integral is properly normalised and matches the exact known solutions in the free and harmonic limits.

In constructing (2.89), we have so far assumed that the fluctuation operator admits only positive, non-zero eigenvalues. Throughout, $\hat{\mathcal{M}}$ acts on $L^2([-\mathcal{T}/2, +\mathcal{T}/2])$ with Dirichlet boundary conditions and the spectrum is discrete. We write

$$\sigma_p(\hat{\mathcal{M}}) := \{\,\lambda \in \mathbb{R} \mid \hat{\mathcal{M}} y = \lambda y \text{ for some } y \neq 0\,\}, \tag{2.90}$$

and when $\lambda_n > 0$ for all n we denote the spectrum by σ_p^+. Since $\hat{\mathcal{M}}$ and $\hat{\mathcal{M}}_0$ share the same interval and BCs, the ratio

$$\frac{\det\hat{\mathcal{M}}}{\det\hat{\mathcal{M}}_0}$$

is finite even though the individual determinants are divergent. Fluctuation determinants in this context are meaningful only when expressed as a ratio. As all other components of (2.89) are standard, the chief task is to evaluate this fluctuation determinant ratio.

We could impose the Ornstein–Uhlenbeck result a priori, but this example illustrates how determining the full spectrum quickly becomes non-trivial. Rather than summing the eigenvalues explicitly, we use the *Gel'fand–Yaglom (GY) method*, which computes determinants from a well-posed initial value problem without solving for the entire spectrum. It states that if y solves $\hat{\mathcal{M}} y = 0$ with $y(-\mathcal{T}/2) = 0$,

$y'(-\mathcal{T}/2) = 1$ (and y_0 for $\hat{\mathcal{M}}_0$), then $\det \hat{\mathcal{M}} / \det \hat{\mathcal{M}}_0 = y(+\mathcal{T}/2)/y_0(+\mathcal{T}/2)$.

Cases with a zero eigenvalue are handled via the McKane–Tarlie boundary-perturbation [125]: we slightly perturb one boundary condition so the zero eigenvalue lifts to $\lambda_\varepsilon = \kappa\,\varepsilon + \mathcal{O}(\varepsilon^2)$ (with κ fixed by the zero mode), compute $\det \hat{\mathcal{M}}_\varepsilon$ (e.g. by Gel'fand–Yaglom), and define the reduced determinant

$$\det{}' \hat{\mathcal{M}} \;=\; \lim_{\varepsilon \to 0} \frac{\det \hat{\mathcal{M}}_\varepsilon}{\kappa\,\varepsilon}\,.$$

The full details of this case are given in § 2.2, but first we present the GY method assuming that all $\lambda_n > 0$.

2.1.8 Gel'fand–Yaglom formula and the functional determinant

Rather than resolving the entire set of eigenvalues, we evaluate fluctuation determinants using the GY method [75]. We consider the second-order operator

$$\hat{\mathcal{M}}_R \;:=\; -\frac{d^2}{dt^2} + R(t), \tag{2.91}$$

acting on $K = [-\mathcal{T}/2, +\mathcal{T}/2]$ with *Dirichlet* boundary conditions $y(\pm\mathcal{T}/2) = 0$.[7] For smooth R with a strictly positive Dirichlet spectrum on the *same interval and boundary conditions* as $\hat{\mathcal{M}}_{R_0}$, GY gives the determinant ratio [67]

$$\frac{\det \hat{\mathcal{M}}_R}{\det \hat{\mathcal{M}}_{R_0}} \;=\; \frac{\psi_R(+\mathcal{T}/2)}{\psi_{R_0}(+\mathcal{T}/2)}, \qquad \psi_R''(t) = R(t)\,\psi_R(t), \quad \psi_R(-\mathcal{T}/2) = 0,\ \psi_R'(-\mathcal{T}/2) = 1, \tag{2.92}$$

i.e., the determinant is fixed relative to a reference operator by solving a single initial value problem (IVP). Only ratios such as (2.92) enter (2.89).

[7] The GY formula applies to any interval $[t_1, t_2]$; we use the symmetric interval K for later convenience.

Harmonic reference. Taking $R_1(t) = \omega_0^2$ gives

$$\psi_{R_1}(+\mathcal{T}/2) = \frac{\sinh(\omega_0 \mathcal{T})}{\omega_0} \quad \Longrightarrow \quad \det \hat{\mathcal{M}}_{\omega_0^2} \propto \frac{\sinh(\omega_0 \mathcal{T})}{\omega_0}. \tag{2.93}$$

We will always define determinant ratios against this reference. This fixes the form of the normalisation constant in (2.70),

$$\mathcal{N}_D := \Big[\lim_{N\to\infty} \prod_{n=1}^{N} \sqrt{4\pi D} \Big]^{-1} = \lim_{N\to\infty} (4\pi D)^{-N/2}. \tag{2.94}$$

non-trivial fluctuation operator along x_{cl}. For

$$R_2(t) = V'(x_{\text{cl}}(t))\, V'''(x_{\text{cl}}(t)) + \big[V''(x_{\text{cl}}(t))\big]^2, \tag{2.95}$$

define the classical velocity $\rho(t) := \dot{x}_{\text{cl}}(t)$. From

$$\dddot{x}_{\text{cl}} = \big(V''(x_{\text{cl}})^2 + V'(x_{\text{cl}})\, V'''(x_{\text{cl}})\big)\, \dot{x}_{\text{cl}} \tag{2.96}$$

we have $\hat{\mathcal{M}}_{R_2}\rho = 0$, i.e. ρ is a zero solution of the ODE. Using the reduction of order method [187], let $\phi(t) = \rho(t) \int^t \mathrm{d}t' \,/\rho(t')^2$ and by imposing the initial GY data at $-\mathcal{T}/2$ we find

$$\psi_{R_2}(+\mathcal{T}/2) = \rho(-\mathcal{T}/2)\, \rho(+\mathcal{T}/2) \int_{-\mathcal{T}/2}^{+\mathcal{T}/2} \frac{\mathrm{d}t'}{\rho(t')^2}. \tag{2.97}$$

Therefore, combining (2.92), (2.93) and (2.97),

$$\frac{\det \hat{\mathcal{M}}_{R_2}}{\det \hat{\mathcal{M}}_{\omega_0^2}} = \frac{\rho(-\mathcal{T}/2)\, \rho(+\mathcal{T}/2)}{\sinh(\omega_0 \mathcal{T})/\omega_0} \int_{-\mathcal{T}/2}^{+\mathcal{T}/2} \frac{\mathrm{d}t'}{\rho(t')^2}. \tag{2.98}$$

Using energy conservation (2.49), $\rho^2 = H + \big(V'(x)\big)^2$ and $\mathrm{d}t = \mathrm{d}x\,/\rho$, this becomes the position-space representation [98]

$$\frac{\det \hat{\mathcal{M}}_{R_2}}{\det \hat{\mathcal{M}}_{\omega_0^2}} = \frac{\sqrt{H + V'(x_1)^2}\, \sqrt{H + V'(x_2)^2}}{\sinh(\omega_0 \mathcal{T})/\omega_0} \int_{x_1}^{x_2} \frac{\mathrm{d}x}{\big(H + V'(x)^2\big)^{3/2}}. \tag{2.99}$$

Equations (2.98)-(2.99) complete the determinant part of the transition probability $P(x_2, +\mathcal{T}/2 \mid x_1, -\mathcal{T}/2)$ for operators without a Dirichlet zero mode.

2.1.9 The method of collective coordinates

In setting up the path integral, we arrived at a step involving formal Gaussian integration over all mode coefficients $\{a_n\}$. As demonstrated above, there is a *zero mode* [39,99] associated with time-translation invariance. On a finite interval with Dirichlet boundary conditions this mode does not, in general, satisfy the endpoints exactly and its eigenvalue is exponentially small in $\mathcal{T}$; in the strict infinite-time limit $\mathcal{T} \to \infty$ it satisfies the boundary conditions and becomes an EZM. We reserve the notation EZM for this limit.

Isolating the zero mode in the mode expansion gives

$$\lim_{N\to\infty} \prod_{n=0}^{N} \Big\{ \int_{\mathbb{R}} \mathrm{d}a_n \, \exp\Big(- \frac{\lambda_n \, a_n^2}{4D} \Big) \Big\} = \int_{\mathbb{R}} \mathrm{d}a_0 \, \lim_{N\to\infty} \prod_{n=1}^{N} \Big\{ \int_{\mathbb{R}} \mathrm{d}a_n \, \exp\Big(- \frac{\lambda_n \, a_n^2}{4D} \Big) \Big\}, \tag{2.100}$$

since $\lambda_0 = 0$ in the $\mathcal{T} \to \infty$ limit. The standard Gaussian approximation then breaks down since the a_0-integral is unsuppressed and diverges [117]. This reflects that the instanton is not isolated but lies on a one-parameter family of degenerate saddles generated by time translations (the *instanton valley* [4, 5, 120]).

The moduli space of single-instanton solutions is

$$\mathcal{F}_I \;=\; \big\{ \, x_{\mathrm{cl}}(t - t_c) \mid t_c \in \mathbb{R} \big\} \subset \text{Path Space}. \tag{2.101}$$

Its tangent vector is $\dot{x}_{\mathrm{cl}}$, as seen by expanding about an arbitrary reference $\bar{t}_c$:

$$x_{\mathrm{cl}}\big(t - [\,\bar{t}_c + \delta t\,]\big) = x_{\mathrm{cl}}(t - \bar{t}_c) - \delta t \, \dot{x}_{\mathrm{cl}}(t - \bar{t}_c) + \mathcal{O}(\delta t^2). \tag{2.102}$$

Thus, to leading order, exciting the zero mode with amplitude a_0 is equivalent to a local shift δt,

$$x_{\rm cl}(t-\bar{t}_c) - \delta t\, \dot{x}_{\rm cl}(t-\bar{t}_c) = x_{\rm cl}(t-\bar{t}_c) + a_0\, y_0(t-\bar{t}_c), \qquad y_0(t) \;=\; \frac{\dot{x}_{\rm cl}(t)}{\sqrt{\langle \dot{x}_{\rm cl} \mid \dot{x}_{\rm cl}\rangle}}. \tag{2.103}$$

Promoting δt to the global collective coordinate t_c spans the entire family.

Matching the expansion yields the following relationship between coordinates [76, 167]

$$\mathrm{d}a_0 \;=\; -\sqrt{\langle \dot{x}_{\rm cl} \mid \dot{x}_{\rm cl}\rangle}\; \mathrm{d}t_c, \qquad \Rightarrow \qquad \big|\mathrm{d}a_0\big| \;=\; \sqrt{\langle \dot{x}_{\rm cl} \mid \dot{x}_{\rm cl}\rangle}\; \mathrm{d}t_c, \tag{2.104}$$

where the measure picks up the absolute value of the Jacobian and the collective coordinate Jacobian is

$$\big\langle \dot{x}_{\rm cl} \mid \dot{x}_{\rm cl}\big\rangle = \int_{-\mathcal{T}/2}^{+\mathcal{T}/2} \dot{x}_{\rm cl}(t)^2\, \mathrm{d}t = \int_{x_1}^{x_2} \sqrt{H + \big(V'(x)\big)^2}\, \mathrm{d}x \xrightarrow[H\to 0]{} \int_{x_1}^{x_2} |V'(x)|\, \mathrm{d}x, \tag{2.105}$$

using $\rho^2 = \dot{x}_{\rm cl}^2 = H + \big(V'(x_{\rm cl})\big)^2$ and $\mathrm{d}t = \mathrm{d}x/\rho$.

Hence, the divergent zero-mode integral is replaced by an integral over the collective coordinate spanning the moduli space,

$$\int_{\mathbb{R}} \mathrm{d}a_0 = \sqrt{\langle \dot{x}_{\rm cl} \mid \dot{x}_{\rm cl}\rangle} \int_{-\mathcal{T}/2}^{+\mathcal{T}/2} \mathrm{d}t_c\,. \tag{2.106}$$

Substituting this back into the fluctuation expansion,

$$\begin{aligned} &\lim_{N\to\infty} \prod_{n=0}^{N} \Big\{ \int_{\mathbb{R}} \mathrm{d}a_n\, \exp\Big(-\frac{\lambda_n\, a_n^2}{4D}\Big)\Big\} \\ &\qquad = \underbrace{\sqrt{\langle \dot{x}_{\rm cl} \mid \dot{x}_{\rm cl}\rangle} \int_{-\mathcal{T}/2}^{+\mathcal{T}/2} \mathrm{d}t_c}_{\text{zero-mode (EZM) contribution}} \lim_{N\to\infty} \prod_{n=1}^{N} \Big\{ \int_{\mathbb{R}} \mathrm{d}a_n\, \exp\Big(-\frac{\lambda_n\, a_n^2}{4D}\Big)\Big\}, \end{aligned} \tag{2.107}$$

which shows that the functional determinant must have its null eigenvalue removed, denoted by a prime.

Putting everything together, the properly regularised transition probability with the EZM treated exactly

reads:

$$P(x_2, +\mathcal{T}/2 \mid x_1, -\mathcal{T}/2)$$
$$= P_0(\mathcal{T})\, \exp\Big(- \frac{\mathcal{S}[x_{\rm cl}]}{4D} \Big)\, \frac{J_{\rm OM}[x_{\rm cl}]}{J_{\rm OM}[x_0]} \sqrt{\frac{\langle \dot{x}_{\rm cl} \mid \dot{x}_{\rm cl} \rangle}{4\pi D}} \int_{-\mathcal{T}/2}^{+\mathcal{T}/2} \mathrm{d}t_c \left(\frac{\det{}' \hat{\mathcal{M}}}{\det \hat{\mathcal{M}}_0} \right)^{-1/2} . \quad (2.108)$$

2.2 Master formula for regularised fluctuation determinants

In the Gel'fand–Yaglom approach of Section 2.1.8, we assumed that the fluctuation operator admits no exact or exponentially small zero eigenvalues. We now present a refined version that allows for the calculation of the fluctuation determinant *with* the EZM correctly removed. The limit $\mathcal{T} \to \infty$ is always taken at the end. While we omit a detailed derivation here, this result is a natural modification of the method developed by McKane and Tarlie [125].

There are two differences from the standard quantum mechanical presentation which together introduce an overall factor -4 in our stochastic normalisation: (i) our fluctuation operator carries the opposite sign convention, which flips the sign after integrating by parts (cf. Eq. (3.3) of [125]); and (ii) the stochastic weight is $\exp[-\mathcal{S}/(4D)]$ (with D playing the role of $\hbar$), so the Gaussian normalisation differs by a factor of 4 compared to $\exp[-\mathcal{S}/\hbar]$.

Consider the fluctuation operator

$$\hat{\mathcal{M}} = -\frac{\mathrm{d}^2}{\mathrm{d}t^2} - \frac{1}{2}\,\mathfrak{U}''(x_{\rm cl})\,, \quad (2.109)$$

where $\mathfrak{U} = -[V']^2$. The regularised functional determinant with the EZM removed is

$$\det{}' \hat{\mathcal{M}} = -\frac{1}{4}\, \frac{\langle \dot{x}_{\rm cl} \mid \dot{x}_{\rm cl} \rangle}{\ddot{x}_{\rm cl}(-\mathcal{T}/2)\, \ddot{x}_{\rm cl}(+\mathcal{T}/2)}\,. \quad (2.110)$$

To render this finite we normalise by the Dirichlet harmonic operator

$$\hat{\mathcal{M}}_0 = -\frac{\mathrm{d}^2}{\mathrm{d}t^2} + \omega_0^2, \qquad \text{with} \quad \omega_0^2 = -\tfrac{1}{2}\,\mathfrak{U}'' \text{ (at the endpoint).} \tag{2.111}$$

Using the GY result (2.93), we obtain our *master formula*:

$$\frac{\det' \hat{\mathcal{M}}}{\det \hat{\mathcal{M}}_0} = -\frac{\omega_0}{4\,\sinh(\omega_0 \mathcal{T})}\,\frac{\langle \dot{x}_{\mathrm{cl}} \mid \dot{x}_{\mathrm{cl}} \rangle}{\ddot{x}_{\mathrm{cl}}(-\mathcal{T}/2)\,\ddot{x}_{\mathrm{cl}}(+\mathcal{T}/2)}\,. \tag{2.112}$$

Equivalently, using $\ddot{x}_{\mathrm{cl}} = -\frac{1}{2}\,\mathfrak{U}'(x_{\mathrm{cl}})$,

$$\frac{\det' \hat{\mathcal{M}}}{\det \hat{\mathcal{M}}_0} = -\frac{\omega_0}{\sinh(\omega_0 \mathcal{T})}\,\frac{\langle \dot{x}_{\mathrm{cl}} \mid \dot{x}_{\mathrm{cl}} \rangle}{\mathfrak{U}'(x_{\mathrm{cl}}(-\mathcal{T}/2))\,\mathfrak{U}'(x_{\mathrm{cl}}(+\mathcal{T}/2))}\,. \tag{2.113}$$

Since the EZM is the time derivative of the classical solution and the instanton profile decays exponentially, it admits the asymptotics

$$\dot{x}_{\mathrm{cl}}(t) \;\sim\; \alpha_-\, e^{\omega_0 t} \quad (t \to -\infty), \qquad \dot{x}_{\mathrm{cl}}(t) \;\sim\; \alpha_+\, e^{-\omega_0 t} \quad (t \to +\infty), \tag{2.114}$$

where we define $\alpha_\pm > 0$ as the positive amplitudes. Combining these with $\sinh(\omega_0 \mathcal{T}) \sim \frac{1}{2} e^{\omega_0 \mathcal{T}}$ and $\ddot{x}_{\mathrm{cl}}(\pm\mathcal{T}/2) \sim \pm\,\omega_0 \alpha_\pm e^{\mp \omega_0 \mathcal{T}/2}$, the master formula reduces in the infinite-time limit to

$$\lim_{\mathcal{T}\to\infty} \frac{\det' \hat{\mathcal{M}}}{\det \hat{\mathcal{M}}_0} = \frac{1}{2\,\omega_0}\,\frac{\langle \dot{x}_{\mathrm{cl}} \mid \dot{x}_{\mathrm{cl}} \rangle}{\alpha_-\,\alpha_+}\,. \tag{2.115}$$

For an instanton one has $\dot{x}_I = +V'(x_I)$ at $H = 0$, so

$$\mathcal{S}_{\mathrm{Inst}}[x] = \int_{-\mathcal{T}/2}^{+\mathcal{T}/2} \mathrm{d}t\, \left[\dot{x}_I + V'(x_I)\right]^2 = 4\,\langle \dot{x}_{\mathrm{cl}} \mid \dot{x}_{\mathrm{cl}} \rangle, \tag{2.116}$$

and hence the fully explicit instanton determinant

$$\lim_{\mathcal{T}\to\infty} \frac{\det' \hat{\mathcal{M}}_{\text{Inst}}}{\det \hat{\mathcal{M}}_0} = \frac{1}{8\,\omega_0} \frac{\mathcal{S}_{\text{Inst}}}{\alpha_-\,\alpha_+}\,. \tag{2.117}$$

In summary, the reduced fluctuation determinant is determined by three ingredients: the endpoint harmonic frequency ω_0, the action of the saddle, and the asymptotic falloff amplitudes $\alpha_\pm$ of the zero mode. Equation (2.117) agrees in structure with known QFT results on reduced determinants and zero modes; see, e.g., [14, 54].

2.2.1 Instanton configurations and explicit forms

The expression in (2.108) is strictly valid only in the limit $\mathcal{T} \to \infty$. However, it also holds approximately for large but finite $\mathcal{T}$, provided the derivatives of the classical solution decay exponentially at the endpoints. Returning to the method of collective coordinates on a long but finite interval, a perturbation of the form $\Delta t\, \dot{x}_{\text{cl}}(t)$, corresponding to a slight time shift of the classical solution, will nearly satisfy the boundary conditions. In this scenario, $\dot{x}_{\text{cl}}$ is approximately proportional to an eigenfunction y_0 that exactly satisfies the boundary conditions but carries a small positive eigenvalue $\lambda_0 \ll 1$.

Physically, this means the nearly flat direction in the path integral (the translation mode) is lifted slightly by the finite-time cutoff: the fluctuation must bend near the endpoints to satisfy the imposed conditions, and this gentle bending costs a small positive "energy" in the spectrum of $\hat{\mathcal{M}}$. As $\mathcal{T} \to \infty$, this small eigenvalue vanishes exponentially, recovering the exact zero mode.

Thus, for any sufficiently large $\mathcal{T}$, we may still apply the method of collective coordinates in an approximate sense. We replace the integral over the near-zero mode by an integral over the collective

coordinate t_c, giving

$$P(x_\beta, +\mathcal{T}/2 \mid x_\alpha, -\mathcal{T}/2) \simeq P_0(\mathcal{T}) \int_{-\mathcal{T}/2}^{+\mathcal{T}/2} \mathrm{d}t_c \, \exp\Big(- \frac{\mathcal{S}[x_{\mathrm{cl}}]}{4D} \Big) \frac{J_{\mathrm{OM}}[x_{\mathrm{cl}}]}{J_{\mathrm{OM}}[x_0]} \sqrt{\frac{\langle \dot{x}_{\mathrm{cl}} \mid \dot{x}_{\mathrm{cl}} \rangle}{4\pi D}} \left(\frac{\det' \hat{\mathcal{M}}}{\det \hat{\mathcal{M}}_0} \right)^{-1/2}, \quad (2.118)$$

where x_α and x_β denote the asymptotic initial and final positions,

$$x_\alpha = \lim_{t \to -\infty} x_{\mathrm{cl}}(t), \qquad x_\beta = \lim_{t \to +\infty} x_{\mathrm{cl}}(t).$$

For a large but finite interval, the classical action, the Onsager–Machlup Jacobian, and the fluctuation determinant all depend explicitly on t_c through the shifted solution $x_{\mathrm{cl}}(t - t_c)$. The t_c-integral must therefore sit in front to reflect this dependence. Only in the strict limit $\mathcal{T} \to \infty$ does this dependence drop out, restoring exact time-translation symmetry; the integral then factorises as a trivial moduli volume. Hence, one checks that (2.118) reproduces (2.108) as $\mathcal{T} \to \infty$.

Next, we write explicit forms for each factor. Using the fluctuation determinant master formula (2.112) and the equation of motion

$$\ddot{x}_{\mathrm{cl}}(t) = V'(x_{\mathrm{cl}})\, V''(x_{\mathrm{cl}}) \quad \text{(equivalently, } \ddot{x}_{\mathrm{cl}} = -\tfrac{1}{2}\, \mathfrak{U}'(x_{\mathrm{cl}})\text{)}, \quad (2.119)$$

we find

$$\frac{\det' \hat{\mathcal{M}}}{\det \hat{\mathcal{M}}_0} = \frac{\omega_0}{4 \, \sinh(\omega_0 \mathcal{T})} \frac{\langle \dot{x}_{\mathrm{cl}} \mid \dot{x}_{\mathrm{cl}} \rangle}{\rho(-\mathcal{T}/2)\, \rho(+\mathcal{T}/2)\, |V''_\alpha|\, |V''_\beta|}, \quad (2.120)$$

where we recall $\rho = \dot{x}_{\mathrm{cl}}$. At the endpoints, $\ddot{x}_{\mathrm{cl}} \approx V'' \, \rho$; writing $|V''_{\alpha,\beta}|$ makes the overall sign manifestly positive. For a right-moving instanton, $\rho(-\frac{\mathcal{T}}{2})\, \rho(+\frac{\mathcal{T}}{2}) > 0$, and the exponential factors from $\sinh(\omega_0 \mathcal{T})$ and the endpoint asymptotics of ρ cancel, leaving a finite prefactor as $\mathcal{T} \to \infty$.

By construction, the right-moving instanton connecting $x_\alpha \to x_\beta$ with $x_\beta > x_\alpha$ follows the uphill

branch

$$\dot{x}_u(t) = +\,V'(x_u(t)), \tag{2.121}$$

while the time-reversed profile corresponds to the downhill branch

$$\dot{x}_d(t) = -\,V'(x_d(t)). \tag{2.122}$$

Each depends implicitly on the collective coordinate t_c.

The Onsager–Machlup Jacobian along the uphill branch is

$$\frac{J_{\mathrm{OM}}[x_u]}{J_{\mathrm{OM}}[x_0]} = \sqrt{\frac{\dot{x}_u(+\mathcal{T}/2)}{\dot{x}_u(-\mathcal{T}/2)}}\,\exp\Big(-\,\frac{1}{2}\,\omega_0\,\mathcal{T}\Big), \tag{2.123}$$

while for the downhill branch it is

$$\frac{J_{\mathrm{OM}}[x_d]}{J_{\mathrm{OM}}[x_0]} = \sqrt{\frac{\dot{x}_d(-\mathcal{T}/2)}{\dot{x}_d(+\mathcal{T}/2)}}\,\exp\Big(-\,\frac{1}{2}\,\omega_0\,\mathcal{T}\Big), \tag{2.124}$$

with the sign of the endpoint velocity reversing and swapping which endpoint dominates the ratio.

Collecting all factors, the uphill probability in the infinite-time limit [8] reads

$$P(x_\beta, +\mathcal{T}/2 \mid x_\alpha, -\mathcal{T}/2)_u \simeq \frac{\sqrt{|V''_\alpha|\,|V''_\beta|}}{2\pi D}\int_{-\mathcal{T}/2}^{+\mathcal{T}/2} \mathrm{d}t_c\,\exp\Big(-\,\frac{\mathcal{S}[x_u]}{4D}\Big)\,\big|\dot{x}_u(+\mathcal{T}/2)\big|. \tag{2.125}$$

For the downhill path,

$$P(x_\alpha, +\mathcal{T}/2 \mid x_\beta, -\mathcal{T}/2)_d \simeq \frac{\sqrt{|V''_\alpha|\,|V''_\beta|}}{2\pi D}\int_{-\mathcal{T}/2}^{+\mathcal{T}/2} \mathrm{d}t_c\,\big|\dot{x}_d(-\mathcal{T}/2)\big|. \tag{2.126}$$

Along the downhill branch, the classical action is zero.[9] This explicit separation into uphill and down-

[8] We retain the leading-order terms of the path integral components; taking the exact $\mathcal{T} \to \infty$ limit in the integration bounds would turn $\simeq$ into $=$.

[9] We emphasise that (2.126) is used here in this pre-normalised form to isolate the translation mode before passing to the

hill contributions will feed directly into the Kramers rate derived next.

2.3 Escape rate over a potential barrier

Having presented the foundational aspects of the stochastic path integral, we now demonstrate how to compute the escape rate over a potential barrier using instanton methods.

2.3.1 Escape rate analysis for instanton-instanton pairs

We analyse the escape process by examining composite instanton-instanton ($[\mathcal{II}]$) pairs. Our goal is to determine the probability that a particle initially near a metastable well at x_α escapes over the barrier x_β and settles near a stable minimum x_c. This is described by glueing together an uphill segment and a downhill segment, forming a single continuous Hamiltonian trajectory mapped by the stochastic Hamiltonian correspondence (see Fig. 2.5). For later use, set

$$\omega_u := |V''(x_\beta)|, \qquad \omega_d := V''(x_c) > 0.$$

rate. The extracted zero mode appears explicitly as $\int_{-\mathcal{T}/2}^{+\mathcal{T}/2} \mathrm{d}t_c \sim \mathcal{T}$. After dividing out this explicit factor, the corresponding normalised downhill contribution tends to unity as $\mathcal{T} \to \infty$.

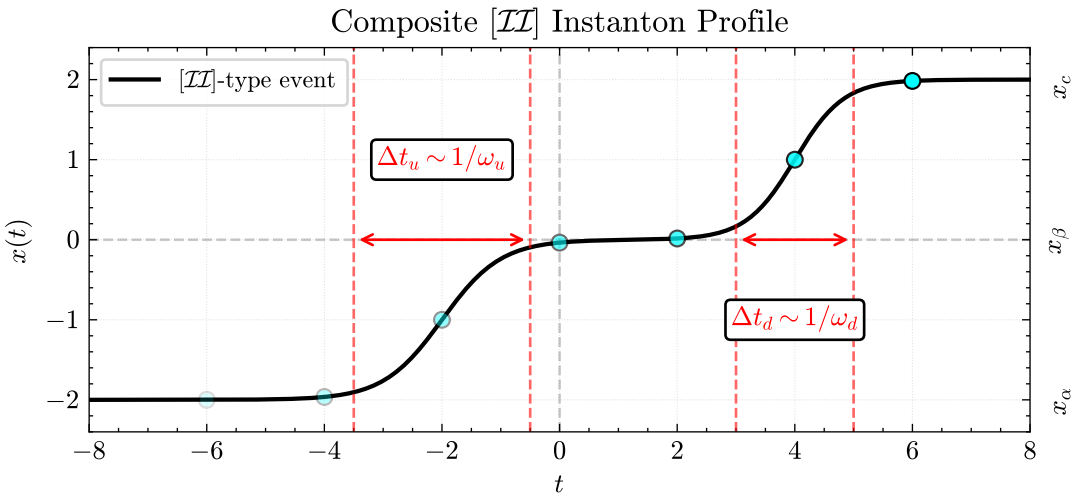

Figure 2.5: *A schematic composite* $[\mathcal{II}]$ *solution plotted as a function of time. The black curve represents the double kink profile, while the fading cyan points indicate the direction of time evolution, progressing from left to right. Dashed red lines and annotated arrows mark the characteristic widths* Δt_u *and* Δt_d *of the uphill and downhill excursions, inversely proportional to the corresponding local barrier and well curvatures,* $\omega_u = |V''(x_\beta)|$ *and* $\omega_d = V''(x_c)$.

We introduce an intermediate matching time $\mathcal{T}_0$ at which the trajectory transitions from the uphill to the downhill segment. A minimal ansatz for the path is

$$x_{\rm cl}(t) = \begin{cases} x_u(t), & t \in [-\mathcal{T}/2,\, \mathcal{T}_0], \\ x_d(t), & t \in [\mathcal{T}_0,\, +\mathcal{T}/2], \end{cases} \qquad \mathcal{T}_0 \in [-\mathcal{T}/2,\, +\mathcal{T}/2]. \tag{2.127}$$

At the barrier, we enforce *position continuity*

$$x_u(\mathcal{T}_0) = x_d(\mathcal{T}_0) = x_\beta, \tag{2.128}$$

while the *slope* generally does not match, $\dot{x}_u(\mathcal{T}_0) \neq \dot{x}_d(\mathcal{T}_0)$. In practice, the uphill and downhill pieces are weakly coupled through their overlapping exponential tails; the resulting smooth $[\mathcal{II}]$ configuration is obtained by including a small interaction that corrects this C^1 mismatch (see Appendix B).

The composite path admits *two* time-translation zero modes in the large-$\mathcal{T}$ limit: one shifting the uphill

segment and one shifting the downhill segment. Hence, the collective coordinate method uses two moduli, t_u (uphill midpoint) and t_d (downhill midpoint). The intermediate time $\mathcal{T}_0$ depends implicitly on both. The full functional integral for the $[\mathcal{II}]$ pair reads

$$P(x_c, +\mathcal{T}/2 \mid x_\alpha, -\mathcal{T}/2) \simeq P_0(\mathcal{T}) \int_{-\mathcal{T}/2}^{+\mathcal{T}/2} \mathrm{d}t_u \int_{t_u}^{+\mathcal{T}/2} \mathrm{d}t_d \, \exp\Big(- \frac{\mathcal{S}[x_{\mathrm{cl}}]}{4D} \Big) \frac{J_{\mathrm{OM}}[x_{\mathrm{cl}}]}{J_{\mathrm{OM}}[x_0]} \times \sqrt{\frac{\langle \dot{x}_u \mid \dot{x}_u \rangle}{4\pi D}} \sqrt{\frac{\langle \dot{x}_d \mid \dot{x}_d \rangle}{4\pi D}} \left(\frac{\det{}'' \, \hat{\mathcal{M}}}{\det \hat{\mathcal{M}}_0} \right)^{-1/2}, \quad (2.129)$$

where the double prime removes the two near-zero eigenvalues associated with (t_u, t_d). The second integral starts at t_u to enforce temporal ordering (the downhill relaxation starts after the uphill segment reaches the barrier).

Determinant factorisation on split intervals. Let $K = [-\mathcal{T}/2, +\mathcal{T}/2]$, $K_1 = [-\mathcal{T}/2, \mathcal{T}_0]$, and $K_2 = [\mathcal{T}_0, +\mathcal{T}/2]$. On K_1 and K_2 we impose Dirichlet BCs at the outer ends and enforce continuity at $\mathcal{T}_0$.[10] In the limit of large separation $(t_d - t_u) \to \infty$, the determinant on K factorises approximately into the determinants on K_1 and K_2, and comparing the harmonic Gel'fand–Yaglom solutions on K versus K_1, K_2 yields the interface correction,

$$P_0(\mathcal{T}) \left[\frac{\det \hat{\mathcal{M}}|_K}{\det \hat{\mathcal{M}}_0|_K} \right]^{-\frac{1}{2}} \simeq \sqrt{\frac{2\pi D}{|V_\beta''|}} \; P_0(\mathcal{T}_0 + \mathcal{T}/2) \, P_0(\mathcal{T}/2 - \mathcal{T}_0) \left[\frac{\det \hat{\mathcal{M}}|_{K_1}}{\det \hat{\mathcal{M}}_0|_{K_1}} \right]^{-\frac{1}{2}} \left[\frac{\det \hat{\mathcal{M}}|_{K_2}}{\det \hat{\mathcal{M}}_0|_{K_2}} \right]^{-\frac{1}{2}}. \quad (2.130)$$

The factor $\sqrt{2\pi D/|V_\beta''|}$ removes the duplicated local harmonic contribution at the barrier created by

[10] Equivalently, one can phrase the composition using the Forman determinant formula for concatenated intervals; we only need the leading large-separation limit.

splitting the interval [67]. Removing the two infinitesimal eigenvalues consistently gives

$$P_0(\mathcal{T})\left[\frac{\det''\hat{\mathcal{M}}|_K}{\det\hat{\mathcal{M}}_0|_K}\right]^{-\frac{1}{2}}$$
$$\simeq \sqrt{\frac{2\pi D}{|V''_\beta|}}\; P_0(\mathcal{T}_0+\mathcal{T}/2)\,P_0(\mathcal{T}/2-\mathcal{T}_0)\left[\frac{\det'\hat{\mathcal{M}}|_{K_1}}{\det\hat{\mathcal{M}}_0|_{K_1}}\right]^{-\frac{1}{2}}\left[\frac{\det'\hat{\mathcal{M}}|_{K_2}}{\det\hat{\mathcal{M}}_0|_{K_2}}\right]^{-\frac{1}{2}}. \quad (2.131)$$

Other factors. The Onsager–Machlup Jacobian factorises cleanly:

$$\frac{J_{\text{OM}}[x_{\text{cl}}]|_K}{J_{\text{OM}}[x_0]|_K}=\frac{J_{\text{OM}}[x_{\text{cl}}]|_{K_1}}{J_{\text{OM}}[x_0]|_{K_1}}\cdot\frac{J_{\text{OM}}[x_{\text{cl}}]|_{K_2}}{J_{\text{OM}}[x_0]|_{K_2}}. \quad (2.132)$$

Using the improved ansatz from Appendix B, the classical action separates as

$$\mathcal{S}[x_{\text{cl}}]=\mathcal{S}[x_u]+\underbrace{\mathcal{S}[x_d]}_{=0\text{ at leading order}}+\mathcal{S}_{\text{int}}(t_u,t_d), \quad (2.133)$$

where $\mathcal{S}[x_d]=0$ follows from $\dot{x}_d=-V'(x_d)$ (downhill along the drift), up to exponentially small corrections. The interaction term arises from matching the linearised (inverted) harmonic tails at the barrier and minimising the slope mismatch; it takes the form

$$\mathcal{S}_{\text{int}}(t_u,t_d)=\frac{4}{|V''_\beta|}\left[\dot{x}_u(\mathcal{T}_0)\right]^2. \quad (2.134)$$

Change of variables. Set the centre and separation

$$t_c:=\frac{t_u+t_d}{2},\qquad s:=t_d-t_u\geq 0, \quad (2.135)$$

so that

$$\int_{-\mathcal{T}/2}^{+\mathcal{T}/2}\mathrm{d}t_u\int_{t_u}^{+\mathcal{T}/2}\mathrm{d}t_d=\int_{-\mathcal{T}/2}^{+\mathcal{T}/2}\mathrm{d}t_c\int_0^{\mathcal{T}-2|t_c|}\mathrm{d}s\,. \quad (2.136)$$

Collecting all factors, the double integral (2.129) simplifies to

$$P(x_c, +\mathcal{T}/2 \mid x_\alpha, -\mathcal{T}/2) \simeq \sqrt{\frac{|V_\alpha''|\,|V_\beta''|\,|V_c''|}{(2\pi D)^3}}\,\exp\Big(-\frac{\mathcal{S}[x_u]}{4D}\Big)\,\mathcal{Z}_{[\mathcal{II}]}, \tag{2.137}$$

with the integral

$$\mathcal{Z}_{[\mathcal{II}]} = \int_{-\mathcal{T}/2}^{+\mathcal{T}/2} \mathrm{d}t_c \int_0^{\mathcal{T}-2|t_c|} \mathrm{d}s\;\Big|\dot{x}_u(\mathcal{T}_0)\Big|^2\,\exp\Big(-\frac{\big[\dot{x}_u(\mathcal{T}_0)\big]^2}{D\,|V_\beta''|}\Big), \qquad \mathcal{T}_0 = \mathcal{T}_0(t_c, s), \tag{2.138}$$

where, in the limit of large separation, $\mathcal{T}_0 = t_c + \mathcal{O}(e^{-\omega\mathcal{T}})$. The prefactor in (2.137) will be cross-checked against the Kramers prefactor in the next subsection.

Effective interaction and QZM integral. Define the function

$$\nu(s) := \Big|\dot{x}_u(\mathcal{T}_0)\Big|^2. \tag{2.139}$$

For well separated segments, $\dot{x}_u$ decays exponentially from the barrier top, hence

$$\nu(s) \;\simeq\; \mathcal{A}\,e^{-\kappa s}, \qquad \kappa := |V_\beta''|, \quad \mathcal{A} := \nu(0) > 0. \tag{2.140}$$

Using (2.136) and extending the s-upper limit to $+\infty$ gives

$$\mathcal{Z}_{[\mathcal{II}]} \;\simeq\; \mathcal{T}\int_0^\infty \mathrm{d}s\;\nu(s)\,\exp\Big(-\frac{\nu(s)}{D\,\kappa}\Big). \tag{2.141}$$

The integral in (2.141) is the *quasi-zero mode* (QZM) integral. A convenient way to display its saddle structure is to absorb the prefactor $\nu(s)$ into the exponential. Writing $\nu(s) = \mathcal{A}e^{-\kappa s} = \exp(\ln\mathcal{A} - \kappa s)$ and pulling constants out, one may define (up to an additive constant)

$$\mathcal{V}_+(s) \;:=\; \frac{4\mathcal{A}}{\kappa}\,e^{-\kappa s} \;+\; 4D\,\kappa\,s, \tag{2.142}$$

so that $\nu(s)\,\exp[-\nu(s)/(D\kappa)] \propto \exp\big[-\mathcal{V}_+(s)/(4D)\big]$.[11] The first term in $\mathcal{V}_+$ encodes the repulsive

[11] Explicitly, $\nu(s)\,\mathrm{e}^{-\nu/(D\kappa)} = \exp\big(-\frac{1}{4D}[\frac{4\mathcal{A}}{\kappa}e^{-\kappa s} + 4D\kappa s - 4D\ln\mathcal{A}]\big)$. The $-4D\ln\mathcal{A}$ term is an s-independent normalisation and can be dropped.

interaction between the uphill and downhill pieces; the linear term is the "tilt" originating algebraically from the $\nu(s) = \mathcal{A}e^{-\kappa s}$ prefactor when recast in the exponent (equivalently, from the Gaussian measure/Jacobian once the mode expansion is performed).

The critical point of $\mathcal{V}_+$ is

$$\mathcal{V}'_+(s^*) = 0 \quad \Longrightarrow \quad e^{-\kappa s^*} = \frac{D\kappa}{\mathcal{A}} \quad \Rightarrow \quad s^* = \frac{1}{\kappa}\,\log\Big(\frac{\mathcal{A}}{D\kappa}\Big), \tag{2.143}$$

so, the dominant contribution sits at a separation $s^* \sim \kappa^{-1}\log(1/D)$. **Exact evaluation of the QZM integral.** Using (2.140) directly in (2.141), set $u = e^{-\kappa s}$ so that $\mathrm{d}s = -(\mathrm{d}u)/(\kappa u)$. Then

$$\int_0^\infty \mathrm{d}s\ \nu(s)\,\exp\Big(-\frac{\nu(s)}{D\kappa}\Big) = \int_0^\infty \mathrm{d}s\ \mathcal{A}e^{-\kappa s}\,\exp\Big(-\frac{\mathcal{A}e^{-\kappa s}}{D\kappa}\Big) \tag{2.144}$$

$$= \frac{\mathcal{A}}{\kappa}\int_0^1 \mathrm{d}u\ \exp\Big(-\frac{\mathcal{A}}{D\kappa}\,u\Big) \;=\; D\Big[1-\exp\Big(-\frac{\mathcal{A}}{D\kappa}\Big)\Big]. \tag{2.145}$$

Hence,

$$\boxed{\mathcal{Z}_{[\mathcal{I}\mathcal{I}]} \;\simeq\; D\,\mathcal{T}\Big[1-\exp\Big(-\frac{\mathcal{A}}{D\,|V''_\beta|}\Big)\Big]} \;\xrightarrow[D\to 0]{}\; D\,\mathcal{T}. \tag{2.146}$$

The exponentially small term $\exp\big[-\mathcal{A}/(D|V''_\beta|)\big]$ is an important correction that will reappear in the $[\mathcal{I}\bar{\mathcal{I}}]$.

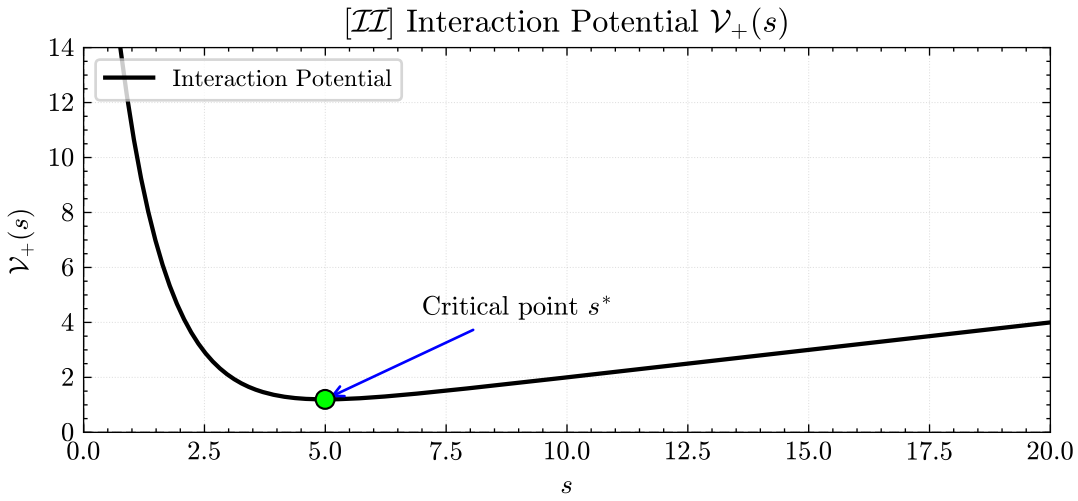

Figure 2.6: *Effective interaction potential $\mathcal{V}_+(s)$ governing the separation s between the uphill and downhill segments of the $[\mathcal{II}]$ configuration; cf. (2.142). The exponential term encodes the repulsion between segments, while the linear term arises when the overlap factor $\nu(s) = \mathcal{A}e^{-\kappa s}$ is absorbed into the exponential. The unique critical point $s^* = \kappa^{-1}\log(\mathcal{A}/(D\kappa))$ (green) stabilises the pair at a finite separation.*

Combining the large separation evaluation of the quasi-zero mode integral with (2.137) yields

$$P(x_c, +\mathcal{T}/2 \mid x_\alpha, -\mathcal{T}/2) \simeq \mathcal{T}\,\frac{\sqrt{|V''_\alpha|\,|V''_\beta|\,|V''_c|}}{2\pi\sqrt{2\pi D}}\,\exp\Big(-\frac{\mathcal{S}[x_u]}{4D}\Big). \tag{2.147}$$

To extract a physical escape rate from this density at the final point, note that for a long observation time, the system depends only on the well label of the initial condition (not its precise microscopic position). By the Markov property and the fast intrawell relaxation on the time scale $1/\omega_c$ (with $\omega_c := V''_c > 0$ the local curvature scale at the stable minimum), the dependence on the exact starting point is washed out:

$$P(x_3, +\mathcal{T}/2 \mid x_\alpha, -\mathcal{T}/2) \;\longrightarrow\; P(x_3, +\mathcal{T}/2 \mid a, -\mathcal{T}/2), \qquad a \simeq x_\alpha. \tag{2.148}$$

Near the stable minimum x_c, the particle rapidly equilibrates, so for x_3 in the capture region of the well the final distribution factorises (again by the Markov property together with rapid relaxation) (see,

e.g., [74, 151]):

$$P(x_3, +\mathcal{T}/2 \mid a, -\mathcal{T}/2) \simeq P(c, +\mathcal{T}/2 \mid a, -\mathcal{T}/2)\, P_S(x_3) \;+\; \mathcal{O}\big(e^{-\omega_c \mathcal{T}}\big), \tag{2.149}$$

and

$$P_S(x_3) = \sqrt{\frac{V_c''}{2\pi D}}\, \exp\Big(-\frac{V_c''}{2D}(x_3 - x_c)^2\Big). \tag{2.150}$$

Hence, the total probability of being captured in the well is obtained by integrating the density over the capture region (width $\sim \sqrt{D/V_c''}$, that is, the standard deviation of the local harmonic equilibrium),

$$P(c, +\mathcal{T}/2 \mid a, -\mathcal{T}/2) \;\approx\; \int_{\mathbb{R}} P(x_3, +\mathcal{T}/2 \mid a, -\mathcal{T}/2)\, \mathrm{d}x_3 \;\simeq\; P(x_c, +\mathcal{T}/2 \mid a, -\mathcal{T}/2) \sqrt{\frac{2\pi D}{V_c''}}, \tag{2.151}$$

where we used that the capture region is narrow and P_S is sharply peaked and normalised, so the integral is well approximated by the value at the peak times its width (Laplace's method around x_c [16]).

Dividing by the observation time then defines the escape rate Γ:

$$\Gamma \;=\; \lim_{\mathcal{T}\to\infty} \frac{1}{\mathcal{T}} \int_{\mathbb{R}} P(x_3, +\mathcal{T}/2 \mid a, -\mathcal{T}/2)\, \mathrm{d}x_3 \;\simeq\; \lim_{\mathcal{T}\to\infty} \frac{1}{\mathcal{T}}\, P(x_c, +\mathcal{T}/2 \mid a, -\mathcal{T}/2) \sqrt{\frac{2\pi D}{V_c''}}. \tag{2.152}$$

Using (2.147) in (2.152) gives the coarse-grained probability and the escape rate,

$$P(c, +\mathcal{T}/2 \mid a, -\mathcal{T}/2) \;=\; \Gamma_{[\mathcal{I}\mathcal{I}]}\, \mathcal{T}, \qquad \Gamma_{[\mathcal{I}\mathcal{I}]} \;=\; \frac{\sqrt{|V_\alpha''|\,|V_\beta''|}}{2\pi}\, \exp\Big(-\frac{\mathcal{S}[x_u]}{4D}\Big). \tag{2.153}$$

Finally, for gradient flows $\dot{x} = \pm V'(x)$ one has $\mathcal{S}[x_u] = 4\,\Delta V$, so

$$\Gamma_{[\mathcal{I}\mathcal{I}]} \;=\; \frac{\sqrt{|V_\alpha''|\,|V_\beta''|}}{2\pi}\, \exp\Big(-\frac{\Delta V}{D}\Big), \tag{2.154}$$

which is the classic overdamped Kramers rate in the weak-noise limit (cf. [85, 101]).

Remarks on regime and accuracy. The derivation above is valid for $D \ll E_b$, large $\mathcal{T}$, and large instan-

ton segment separation $t_d - t_u$; neglected corrections are $\mathcal{O}(D)$, $O(e^{-\omega_c \mathcal{T}})$, and subleading interaction corrections beyond the large separation approximation. Units are transparent: the path integral output at fixed x_3 is a density in [length^{-1}]; multiplying by the capture width $\sqrt{2\pi D/V_c''}$ yields a probability, and dividing by $\mathcal{T}$ yields a rate [time^{-1}].

2.3.2 Escape rate associated with instanton-anti-instanton events

We now analyse the analogous contribution from composite instanton-anti-instanton ($[\mathcal{I}\bar{\mathcal{I}}]$) pairs. This configuration describes a closed fluctuation loop: the pseudoparticle climbs the barrier via an instanton and then returns via an anti-instanton, ending in the original metastable well.

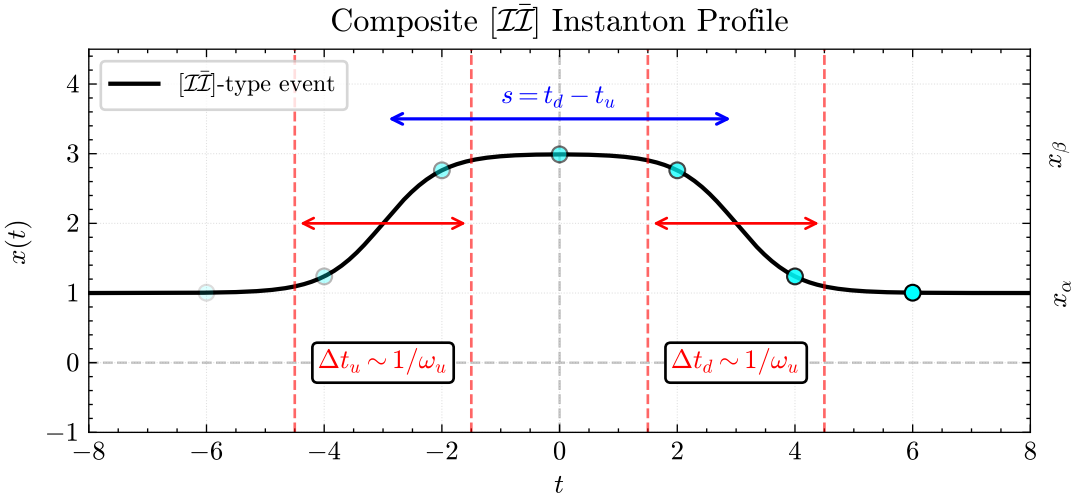

Figure 2.7: *A schematic composite $[\mathcal{I}\bar{\mathcal{I}}]$ solution as a function of time. The black curve shows the pseudoparticle compound, the fading cyan points indicate the time direction, red dashed lines mark the characteristic excursion widths Δt_u and Δt_d (equal by symmetry), and the breathing mode s (the plateau between events) is shown in blue.*

The setup mirrors the $[\mathcal{I}\mathcal{I}]$ case: we glue an uphill instanton trajectory from x_α to x_β to its time-reversed anti-instanton that returns to x_α. Time reversal implies the Onsager–Machlup Jacobians and fluctuation

determinants match segment-wise. The double integral for the $[\mathcal{I}\bar{\mathcal{I}}]$ sector is

$$P(x_\alpha, +\mathcal{T}/2 \mid x_\alpha, -\mathcal{T}/2)$$
$$\simeq P_0(\mathcal{T}) \int_{-\mathcal{T}/2}^{+\mathcal{T}/2} \mathrm{d}t_u \int_{t_u}^{+\mathcal{T}/2} \mathrm{d}t_d \, \exp\Big(- \frac{\mathcal{S}[x_{\mathrm{cl}}]}{4D} \Big) \frac{J_{\mathrm{OM}}[x_{\mathrm{cl}}]}{J_{\mathrm{OM}}[x_0]} \frac{\langle \dot{x}_u \mid \dot{x}_u \rangle}{4\pi D} \left(\frac{\det{}'' \, \hat{\mathcal{M}}}{\det \, \hat{\mathcal{M}}_0} \right)^{-1/2} . \quad (2.155)$$

Here the factor $\langle \dot{x}_u \mid \dot{x}_u \rangle / (4\pi D)$ comes from the product of two identical collective coordinate Jacobians (one for the instanton shift and one for the anti-instanton shift), each contributing $\sqrt{\langle \dot{x}_u \mid \dot{x}_u \rangle / (4\pi D)}$.

Determinant factorisation (large separation). With $K = [-\mathcal{T}/2, +\mathcal{T}/2]$ and an intermediate time $\mathcal{T}_0$, let $K_1 = [-\mathcal{T}/2, \mathcal{T}_0]$ and $K_2 = [\mathcal{T}_0, +\mathcal{T}/2]$. In the regime $t_d - t_u \to \infty$ (well-separated segments),

$$P_0(\mathcal{T}) \left[\frac{\det{}'' \, \hat{\mathcal{M}}\big|_K}{\det \, \hat{\mathcal{M}}_0\big|_K} \right]^{-1/2} \simeq \sqrt{\frac{2\pi D}{|V_\beta''|}} \, P_0(\mathcal{T}_0 + \mathcal{T}/2) \, P_0(\mathcal{T}/2 - \mathcal{T}_0) \left[\frac{\det{}' \, \hat{\mathcal{M}}\big|_{K_1}}{\det \, \hat{\mathcal{M}}_0\big|_{K_1}} \right]^{-1} . \quad (2.156)$$

Since K_1 and K_2 are mirror images in the $[\mathcal{I}\bar{\mathcal{I}}]$ configuration, their two identical factors with exponent $-\frac{1}{2}$ combine to the single bracket with exponent -1 shown above; the prefactor $\sqrt{2\pi D/|V_\beta''|}$ corrects the double-counting of the local harmonic piece at the barrier.

Interaction sign and instability. The crucial difference with the $[\mathcal{I}\mathcal{I}]$ case is the *sign* of the interaction action. Reversing the second segment flips the velocity near the barrier and yields (Appendix B.3)

$$\mathcal{S}_{\mathrm{int}}(t_u, t_d) = - \frac{4}{|V_\beta''|} \big[\dot{x}_u(\mathcal{T}_0) \big]^2 , \quad (2.157)$$

which is negative definite. Thus the $[\mathcal{I}\bar{\mathcal{I}}]$ composite is a *local maximum* along the quasi-zero mode $s := t_d - t_u$ and is intrinsically unstable on the real axis.

Quasi-zero mode integral and the need to complexify. Changing variables to centre and separation,

$$t_c = \frac{t_u + t_d}{2}, \qquad s = t_d - t_u \geq 0,$$

and using the same large separation estimates as in the $[\mathcal{I}\mathcal{I}]$ case, the quasi-zero mode (QZM) integral takes the form

$$\mathcal{Z}_{[\mathcal{I}\bar{\mathcal{I}}]} = \mathcal{T}\,\mathcal{A}\int_0^\infty \mathrm{d}s\,\exp\Big(-\frac{1}{4D}\,\mathcal{V}_-(s)\Big), \qquad \mathcal{V}_-(s) = -\frac{4\,\mathcal{A}}{\omega_\beta}\,e^{-\omega_\beta s} + 4D\,\omega_\beta\,s, \quad \omega_\beta := |V_\beta''| > 0. \tag{2.158}$$

There is no real saddle for s since

$$\partial_s\mathcal{V}_- = 4\mathcal{A}\,e^{-\omega_\beta s} + 4D\,\omega_\beta = 0 \quad \Longrightarrow \quad s_\star = \frac{1}{\omega_\beta}\Big[\log\frac{\mathcal{A}}{D\,\omega_\beta} + i\,(2k+1)\pi\Big], \qquad k \in \mathbb{Z}, \tag{2.159}$$

is complex. Consequently, $\mathbb{R}_+$ is not a steepest descent contour because the integral has no saddle on the real axis and is dominated by the endpoint $s = 0$, signalling the breakdown of the large separation approximation.

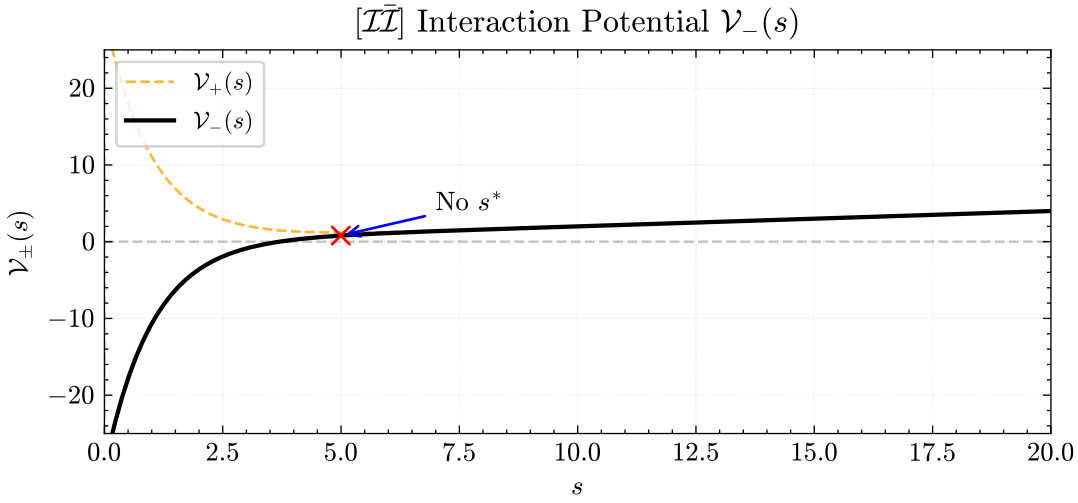

Figure 2.8: *Comparison of the effective interaction potentials for instanton-instanton ($\mathcal{V}_+$, dashed) and instanton-anti-instanton ($\mathcal{V}_-$, solid) configurations. The repulsive $\mathcal{V}_+$ has a unique minimum s^* (stabilising the pair), whereas the attractive $\mathcal{V}_-$ has no real critical point and the pair collapses.*

A common workaround is the ad hoc analytic continuation $D \to D\,e^{\pm i\pi}$ to flip the sign in the exponent and force convergence [24, 188]. However, this choice ($\pm$) is ambiguous and, more seriously, it turns the exponentially suppressed factor $e^{-\mathcal{A}/(D\omega_\beta)}$ that appeared in the $[\mathcal{I}\mathcal{I}]$ analysis into an exponentially

enhanced one, so dropping it becomes inconsistent.

Remark 2.3.1 (Why instanton-instanton pairs behave but instanton-anti-instanton do not). The $[\mathcal{I}\mathcal{I}]$ sector has an effective interaction

$$\mathcal{V}_+(s) = +\frac{4\mathcal{A}}{\omega_\beta}\, e^{-\omega_\beta s} + 4D\,\omega_\beta s, \qquad \omega_\beta := |V_\beta''| > 0, \tag{2.160}$$

with a real critical point

$$\partial_s \mathcal{V}_+ = -4\mathcal{A}\, e^{-\omega_\beta s} + 4D\,\omega_\beta = 0 \implies s^* = \frac{1}{\omega_\beta}\log\frac{\mathcal{A}}{D\,\omega_\beta}, \tag{2.161}$$

and $\partial_s^2 \mathcal{V}_+(s^*) = 4\mathcal{A}\omega_\beta e^{-\omega_\beta s^*} > 0$, so s^* is a local minimum. Hence, the real s-axis already contains a steepest descent contour (a Lefschetz thimble) through s^*, and the QZM integral over $\mathbb{R}_+$ does not need contour deformation. By contrast, for $[\mathcal{I}\bar{\mathcal{I}}]$ the interaction is

$$\mathcal{V}_-(s) = -\frac{4\mathcal{A}}{\omega_\beta}\, e^{-\omega_\beta s} + 4D\,\omega_\beta s, \tag{2.162}$$

whose critical points solve $\partial_s \mathcal{V}_- = 4\mathcal{A}e^{-\omega_\beta s} + 4D\omega_\beta = 0$, giving

$$s_\star = \frac{1}{\omega_\beta}\Big[\log\frac{\mathcal{A}}{D\,\omega_\beta} \pm i\pi\Big], \tag{2.163}$$

a conjugate pair of complex saddles with no real critical point. Thus, the real contour $\mathbb{R}_+$ is not a valid contour (thimble), and the QZM integral is not valid in a Gaussian approximation. The well-defined prescription is to deform to the thimble(s) through $s_\star$ (details in § 3.6).

We shall demonstrate that the correct weak-noise prescription is to keep $D > 0$ and deform the s-contour into the complex plane to the steepest descent thimble(s) through the complex saddle(s) $s_\star$ (Picard–Lefschetz theory [42, 70, 143, 169, 184]). Only one of the conjugate saddles contributes, with the choice fixed by intersection numbers [50–52, 71]. This replaces the ill-posed real integral by a well-defined thimble integral and removes the need for the ad hoc $D \to -D$ flip. We develop this

construction in Chapter 3 and show that it preserves the leading Kramers exponent while providing a contour-consistent treatment of the $[\mathcal{I}\bar{\mathcal{I}}]$ sector.

Chapter 3

Case Study I – Stochastic Cubic Formulation

Chapter Summary

We calculate the escape rate of a Brownian particle in the weak-noise limit ($D \to 0$) using Picard–Lefschetz theory, focusing on the stochastic cubic potential. We reformulate the dynamics using the Onsager–Machlup functional in the Itô discretisation, mapping the problem to classical motion in an effective tilted quartic landscape, where the tilt arises from the Itô calculus.

In the Itô framework, we find that in the weak-noise regime, a new trajectory emerges: the stochastic real bounce ($[\mathcal{RB}]$). This path shows an extended plateau near the classical turning point, unlike quantum bounces. However, the saddle-point approximation fails because an attractive quasi-zero mode makes the fluctuation determinant divergent. The standard Bogomolny–Zinn–Justin prescription, continuing $D \to -D$ to fix this, lacks justification in the stochastic setting and introduces ambiguity $\pm i\pi$.

Picard–Lefschetz theory directly addresses these challenges. It complexifies the path space and selects the appropriate integration cycle, a Lefschetz thimble. This supports another solution: stochastic complex bounce ($[\mathcal{CB}]$), an exact solution to the holomorphic Euler–Lagrange equations on a non-vanishing energy manifold.

With this method, deforming to the thimble allows an exact evaluation of the quasi-zero mode integral and fixes the $\pm i\pi$ factor geometrically via thimble orientation, ensuring that $D > 0$ throughout.

3.1 The Itô Onsager–Machlup formulation

In contrast to Chapter 2, where we used the Stratonovich prescription, we now adopt the Itô discretisation in formulating the stochastic path integral. Since our analysis concerns additive white noise, the Onsager–Machlup Jacobian simplifies to unity, provided that the stochastic integral is interpreted in the Itô sense [106]. Concretely, this choice does not change the physics for additive noise, but it changes where the $\frac{1}{2}\int \mathrm{d}t\ V''$ contribution appears in the path integral formulation. While the Stratonovich formalism packages the order-D^0 contribution into the Onsager–Machlup Jacobian,

$$J_{\text{OM}}[x] = \exp\left(\frac{1}{2}\int_{-\mathcal{T}/2}^{+\mathcal{T}/2} \mathrm{d}t\ V''(x(t))\right), \tag{3.1}$$

the Itô formalism absorbs this term directly into the action functional, as demonstrated in §1.2.2.1. The origin of this difference lies in how the cross-term $\int \mathrm{d}t\ 2\dot{x}V'(x)$ is evaluated.

Viewing the cross term as an Itô integral, this expression acquires an additional correction due to the Itô chain rule.

$$\text{Itô}\left\{\int_{-\mathcal{T}/2}^{+\mathcal{T}/2} \mathrm{d}t\ 2\dot{x}V'(x)\right\} = 2\Delta V - 2D\int_{-\mathcal{T}/2}^{+\mathcal{T}/2} \mathrm{d}t\ V''(x). \tag{3.2}$$

Thus, the Stratonovich Jacobian re-emerges now as a built-in feature of the action. In equivalent formulations, this same contribution may be described as Jacobian-induced loop effects. The Itô formulation, therefore, yields an effective action of the form

$$\mathcal{S}[x] = \int \mathrm{d}t\left[\dot{x}^2 + V'(x)^2 - 2D\,V''(x)\right], \tag{3.3}$$

where the final term encodes the tilt induced by the stochastic calculus itself. For a complementary discussion of tilt effects in Onsager–Machlup functionals (in a closely related setting), see [159].

In the quantum field theory setting studied by Dunne *et al.* [12–14], the tilt arises from 'fermionic loop effects' and enters at order $\mathcal{O}(g)$, with g the coupling constant [183]. The effective potential here takes

the form

$$-V_{\pm} = -\frac{1}{2}(W'(x))^2 \mp pg\, W''(x). \tag{3.4}$$

In the stochastic analogue, the tilt arises not from quantum corrections but from the discretisation scheme[1]. It emerges at order $\mathcal{O}(D)$ in the action, giving

$$\mathfrak{U}(x) = -(V'(x))^2 + 2DV''(x), \tag{3.5}$$

which shares a structure similar to (3.4). From a strictly perturbative viewpoint, adding the order-D correction directly to the action contaminates the expansion. It mixes different orders in noise strength and disrupts the order-by-order hierarchy seen in the Stratonovich formalism. This conventional view keeps the Onsager–Machlup Jacobian outside the action, preserving the clean stratification of the weak-noise expansion.

Yet, we will show that both formalisms yield the same escape rate up to the prefactor when D is small. More importantly, the Itô framework naturally reveals complex saddles and presents a clear picture of the $D \to -D$ continuation. Thus, the Itô prescription goes beyond convenience and enhances compatibility between the stochastic path integral and complexified geometry.

3.1.1 The tilt term and the effective landscape

We now give a brief overview of the geometry generated by the Itô choice and discuss how the formulation differs from the Stratonovich path integral formulation presented in Chapter 2. Some well-known potentials are plotted, in which the classical mechanics takes place, with the $2DV''$ term added.

[1] The point at which the force is evaluated in the discrete-time Langevin equation determines the structure of the Onsager–Machlup measure.

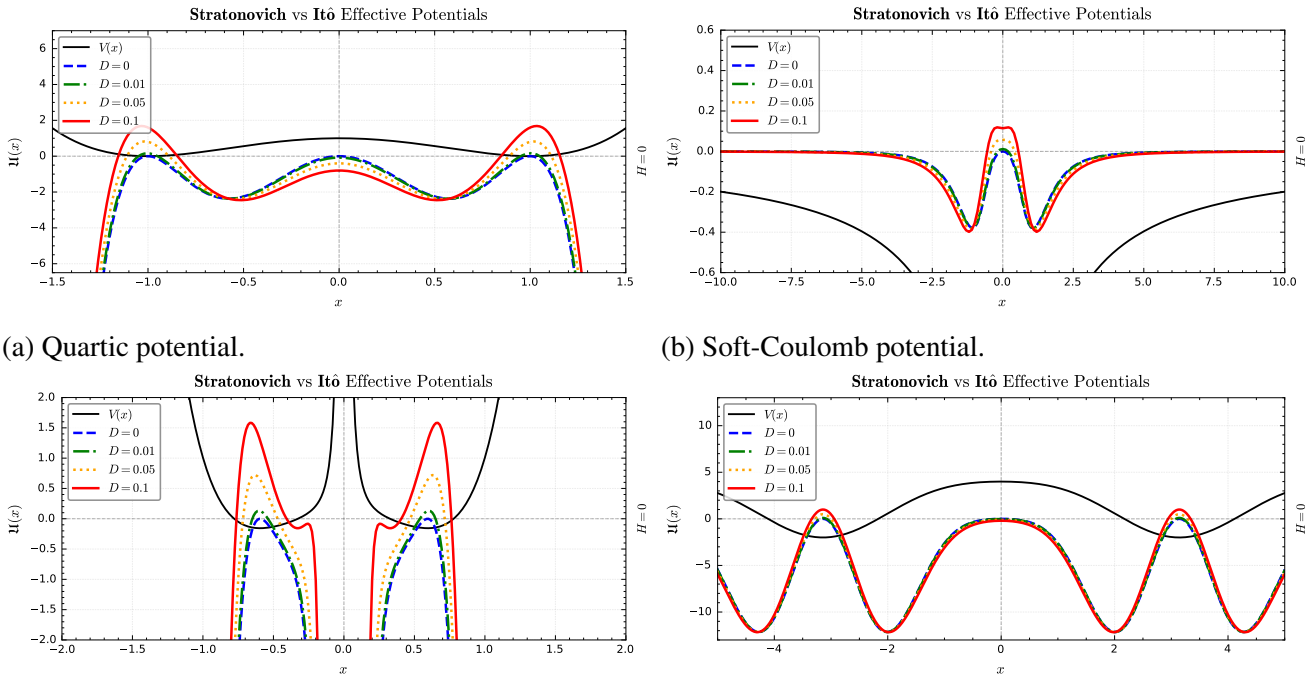

(a) Quartic potential.

(b) Soft-Coulomb potential.

(c) Augmented sextic potential.

(d) Mathieu-type potential.

Figure 3.1: *Geometry of the Itô effective potential. The black curve indicates the original potential $V(x)$ governing the stochastic dynamics, and the coloured curves represent the Itô effective potential $\mathfrak{U}(x)$, which governs the Hamiltonian evolution. (a) A symmetric quartic potential [162], $V(x) = (x^2 - 1)^2$, mapped to an inverted and tilted sextic effective potential. (b) A soft-Coulomb-type potential [115], $V(x) = -\frac{1}{\sqrt{1+(x-\frac{1}{2})^2}} - \frac{1}{\sqrt{1+(x+\frac{1}{2})^2}}$. (c) A sextic potential augmented by a centrifugal barrier [47], $V(x) = \frac{1}{100x^2} - x^2 + x^4 + x^6$, mapped to a highly deformed Itô landscape. (d) A Mathieu-type potential [166], $V(x) = 1 + 3\cos(x) + \sin^2(x)$.*

In Fig. 3.1, the bold black curve shows the original stochastic potential $V(x)$. The dashed blue curve gives its effective Stratonovich landscape $-[V'(x)]^2$. The coloured curves display the effective Itô landscape $\mathfrak{U}(x) = -[V'(x)]^2 + 2DV''(x)$ for the indicated values of D. The $2DV''$ tilt shifts the critical points and removes their degeneracy. Under Stratonovich's formalism, $-[V']^2$ keeps all critical points at zero. In contrast, $\mathfrak{U}$ raises or lowers them by terms of order D, splitting minima and maxima. This deformation of the landscape then produces qualitatively different Hamiltonian trajectories under the Itô Euler–Lagrange dynamics $\ddot{x} = V'V'' - DV'''$ (see § 1.2.2.2).

3.1.2 Itô and Stratonovich compared

With this new classical landscape in mind, we now derive the path integral up to equation (2.108) from Chapter 2. Here, we work within Itô's framework, with the choice $\alpha = 0$ (see B.2) in the discretised Langevin equation. The derivation follows the earlier steps closely, but subtle differences arise. Using the self-adjointness of the Hamiltonian fluctuation operator, we obtain the analogue of equation (2.72):

$$P(x_2, +\mathcal{T}/2|x_1, -\mathcal{T}/2) = \mathcal{N}_D \exp\left(-\frac{\mathcal{S}[x_{\text{cl}}]}{4D}\right) \underbrace{J_{\text{OM}}[x_{\text{cl}}]}_{=1} \left[\lim_{N\to\infty} \prod_{n=0}^{N} \sqrt{4\pi D}\right] (\det \hat{\mathcal{M}})^{-\frac{1}{2}}. \tag{3.6}$$

The Onsager–Machlup Jacobian evaluates to unity along any Itô path; we thus omit it from all further expressions. Its structural role is now absorbed into the action functional, which becomes

$$\mathcal{S}[x] = 2\Delta V + \int_{-\mathcal{T}/2}^{+\mathcal{T}/2} \mathrm{d}t\ \mathcal{L}(x, \dot{x}, t), \tag{3.7}$$

with Lagrangian

$$\mathcal{L}(x, \dot{x}, t) = \frac{m_p}{2}\left(\frac{\mathrm{d}x}{\mathrm{d}t}\right)^2 - \mathfrak{U}(x), \quad \mathfrak{U}(x) = -V'(x)^2 + 2DV''(x). \tag{3.8}$$

As before, we may set $m_p/2 = 1$ without loss of generality. The classical paths that extremise this action satisfy the modified Euler–Lagrange equation,

$$\left.\frac{\delta\mathcal{S}[x(t)]}{\delta x(t)}\right|_{x=x_{\text{cl}}} = 0 \quad \Longrightarrow \quad \left.\frac{\mathrm{d}^2x}{\mathrm{d}t^2}\right|_{x=x_{\text{cl}}} = -\frac{1}{2}\mathfrak{U}'(x)\Big|_{x=x_{\text{cl}}}. \tag{3.9}$$

This leads to the Hamiltonian dynamics,

$$\left.\frac{\mathrm{d}^2x}{\mathrm{d}t^2}\right|_{x=x_{\text{cl}}} = \left[V'(x)V''(x) - DV'''(x)\right]\big|_{x=x_{\text{cl}}}. \tag{3.10}$$

Previously, the term $-DV'''(x)$ was absent in Stratonovich's formalism, and the extremising solutions were instantons obeying the first-order equation

$$\frac{\mathrm{d}x_I}{\mathrm{d}t} = V'(x_I). \tag{3.11}$$

Differentiating this with respect to time yields the associated second-order differential equation,

$$\frac{\mathrm{d}^2x_I}{\mathrm{d}t^2} = V'(x_I)V''(x_I). \tag{3.12}$$

This trajectory is entirely independent of the noise strength D. In contrast, within the Itô formalism, the saddle equations acquire an explicit D-dependence. This quantitative modification introduces a qualitative deformation of the space of extremising paths.

To obtain a first integral for the Itô Euler–Lagrange equation (3.9), we multiply it by $2\dot{x}$ and use

$$\frac{\mathrm{d}}{\mathrm{d}t}\big(\dot{x}^2\big) = 2\dot{x}\ddot{x}, \qquad \frac{\mathrm{d}}{\mathrm{d}t}\big(V'(x)^2 - 2DV''(x)\big) = 2\dot{x}V'(x)V''(x) - 2D\dot{x}V'''(x).$$

Along any classical trajectory satisfying (3.9) this gives

$$\frac{\mathrm{d}}{\mathrm{d}t}\big(\dot{x}^2 - V'(x)^2 + 2DV''(x)\big) = 0,$$

so the combination $\dot{x}^2 - V'(x)^2 + 2DV''(x)$ is constant in time. We denote this real integration constant by H; it plays the role of an effective conserved energy for the tilted Itô dynamics. The conserved quantity can therefore be written as

$$\dot{x}^2 = H + V'^2 - 2DV'', \tag{3.13}$$

so that the corresponding first integral is

$$\frac{\mathrm{d}x}{\mathrm{d}t} = \pm\sqrt{H + V'^2 - 2DV''}. \tag{3.14}$$

This first integral solves the Euler–Lagrange equation (3.9) for fixed H. As we shall later demonstrate in equations (3.3.4) and (3.4.4), the tilt term also deforms the fluctuation operator through a modification of the associated fluctuation potential.

Finally, the normalisation constant must also be reevaluated. Consider a particle that begins and ends at a minimum of the original potential. One may either use the Ornstein–Uhlenbeck propagator or follow the explicit eigenvalue analysis beginning with equation (2.73), yielding

$$\mathcal{N}_D = \left[\lim_{N\to\infty}\prod_{n=0}^{N}(4\pi D)^{-\frac{1}{2}}\right](\det\hat{\mathcal{M}}_0)^{+\frac{1}{2}}P_0(\mathcal{T}), \tag{3.15}$$

where the time-dependent factor becomes

$$P_0(\mathcal{T}) = \sqrt{\frac{\omega_0}{4\pi D\sinh(\omega_0\mathcal{T})}}. \tag{3.16}$$

Unlike in the Stratonovich setting, the exponential factor $\exp(\omega_0\mathcal{T}/2)$ appearing in equation (2.88) is absent from the Itô normalisation function.

The corresponding harmonic fluctuation operator is given by

$$\begin{aligned}\hat{\mathcal{M}}_0 &= -\frac{\mathrm{d}^2}{\mathrm{d}t^2} - \frac{1}{2}\mathfrak{U}''(x_0)\\ &= -\frac{\mathrm{d}^2}{\mathrm{d}t^2} + V'(x_0)V'''(x_0) + [V''(x_0)]^2 - DV''''(x_0),\end{aligned} \tag{3.17}$$

which exhibits an explicit dependence on the noise strength D. Around a critical point x_0, the fluctuation operator simplifies to

$$\hat{\mathcal{M}}_0 = -\frac{\mathrm{d}^2}{\mathrm{d}t^2} + \omega_0^2, \tag{3.18}$$

with effective frequency

$$\omega_0^2 = V'(x_0)V'''(x_0) + [V''(x_0)]^2 - DV''''(x_0). \tag{3.19}$$

A natural assumption is that the noise dependence in the fluctuation spectrum stems solely from the term involving the fourth derivative of the potential. For example, in a cubic potential where $V''''(x) = 0$, one might expect the harmonic frequency ω_0 to be noise-independent. However, this intuition is incorrect: as we demonstrate in Section 3.3, there are *two* distinct mechanisms through which D-dependence enters the frequency.

Even when $V''''(x) = 0$, the frequency ω_0 can still acquire dependence on D. This arises because the point x_0 entering the harmonic operator corresponds not to a critical point of the original potential, but to the critical point $x_{\rm cr}$ of the *Itô effective potential*, defined by the condition $\mathfrak{U}'(x_{\rm cr}) = 0$. Crucially, the extrema of $\mathfrak{U}(x)$ generally do not coincide with those of $V(x)$. As illustrated in Fig. 3.1, these critical points can be displaced relative to their Stratonovich counterparts. In such cases, $x_{\rm cr}$ may be perturbatively expanded in D, and the condition $V'(x_{\rm cr}) = 0$ is violated by a small remainder. That is,

$$V'(x_{\rm cr}) = \mathcal{E}(D), \tag{3.20}$$

where $\mathcal{E}(D)$ admits a power series expansion in D. Consequently, the frequency inherits a noise dependence of the form

$$\omega = b_0 + b_1 D + b_2 D^2 + \dots . \tag{3.21}$$

This contrasts with the Stratonovich formalism, where x_0 is fixed by $V'(x_0) = 0$, eliminating such corrections by construction.

The method of collective coordinates introduced in § 2.1.9 carries over directly to the Itô framework. As before, we isolate the divergent contribution associated with the translational zero mode of $\hat{\mathcal{M}}$, and replace it by an integration over the collective coordinate t_c:

$$\sqrt{\frac{4\pi D}{\lambda_0}} \quad \mapsto \quad \sqrt{\langle \dot{x}_{\rm cl} | \dot{x}_{\rm cl} \rangle} \int_{-\mathcal{T}/2}^{+\mathcal{T}/2} \mathrm{d}t_c \, . \tag{3.22}$$

The resulting Itô path integral, which incorporates quadratic fluctuations around the saddle, reads

$$P(x_2,+\mathcal{T}/2|x_1,-\mathcal{T}/2)=\sqrt{\frac{\omega_0}{4\pi D\sinh(\omega_0\mathcal{T})}}\exp\left(-\frac{\mathcal{S}[x_{\rm cl}]}{4D}\right)\\ \times\sqrt{\frac{\langle\dot{x}_{\rm cl}|\dot{x}_{\rm cl}\rangle}{4\pi D}}\int_{-\mathcal{T}/2}^{+\mathcal{T}/2}\mathrm{d}t_c\left(\frac{\det'\hat{\mathcal{M}}}{\det\hat{\mathcal{M}}_0}\right)^{-\frac{1}{2}}. \quad (3.23)$$

We now compare the weak-noise asymptotics of the stochastic path integral derived in the Itô formalism with its Stratonovich counterpart (2.108). The key structural differences are as follows:

- **Measure / Jacobian.** For additive noise the Onsager–Machlup Jacobian is

$$J_{\rm OM}^{\rm Strat}[x]=\exp\Big(\frac{1}{2}\int V''(x)\,\mathrm{d}t\Big),\qquad J_{\rm OM}^{\rm Itô}[x]\equiv 1.$$

  In the weak-noise expansion, this factor is evaluated at $x_{\rm cl}$ and multiplies the weight. We may equivalently absorb it into the exponent (see the following item).

- **Exponent and equations of motion.** We keep the canonical action $\mathcal{S}[x]=\int(\dot{x}+V')^2\mathrm{d}t$ and weight $\exp[-\mathcal{S}/(4D)]$ in both schemes. The total exponent differs by

$$\Phi_D^{\rm Strat}[x]=-\frac{1}{4D}\mathcal{S}[x]+\frac{1}{2}\int V''(x)\,\mathrm{d}t,\qquad \Phi_D^{\rm Itô}[x]=-\frac{1}{4D}\mathcal{S}[x],$$

  which are algebraically equivalent to the total exponent

$$-\frac{1}{4D}\int\left(\dot{x}^{\,2}+V'^2-2D\,V''\right)\mathrm{d}t.$$

  For the Itô action functional, the equations of motion acquire an additional term through the calculus of variations,

$$\ddot{x}=V'V''-DV'''$$

  .

- **Stationary points and harmonic operator.** In Stratonovich the effective landscape is $\mathfrak{U}_S(x) = -[V'(x)]^2$, so $\mathfrak{U}'_S(x) = -2V'V''$ and generic stationary points satisfy $V'(x) = 0$ (inflection points with $V'' = 0$ may also appear). In Itô the landscape is $\mathfrak{U}(x) = -[V']^2 + 2D\,V''$, so $\mathfrak{U}'(x) = -2V'V'' + 2DV'''$ and stationary points solve $V'V'' - DV''' = 0$, that do not need to have $V' = 0$. Expanding near a Stratonovich extremum x_* with $V'(x_*) = 0$, $V''(x_*) \neq 0$ ($\delta x = \mathcal{O}(D)$),

$$x_{\rm cr} = x_* + \delta x, \qquad \delta x = \frac{D\,V'''(x_*)}{[V''(x_*)]^2} + \mathcal{O}(D^2), \quad V'(x_{\rm cr}) = \frac{D\,V'''(x_*)}{V''(x_*)} + \mathcal{O}(D^2).$$

  Linearising the EL equation about $x_{\rm cr}$ gives the local frequency

$$\omega^2 \;=\; [V''(x_{\rm cr})]^2 + V'(x_{\rm cr})\,V'''(x_{\rm cr}) - D\,V''''(x_{\rm cr}).$$

- **Fluctuations and determinant.** In Stratonovich the quadratic operator about $x_{\rm cl}$ is $\hat{\mathcal{M}}_S = -\partial_t^2 - \frac{1}{2}\mathfrak{U}''_S(x_{\rm cl})$, which is real and D-independent. In Itô one has $\hat{\mathcal{M}} = -\partial_t^2 - \frac{1}{2}\mathfrak{U}''(x_{\rm cl})$, which depends on D both through $\mathfrak{U}$ and through the D-shift of $x_{\rm cr}$, making the spectrum and determinant D-dependent.

- **Zero-noise limit.** Both formalisms coincide at $D = 0$ (the Jacobian contributes only at order D^0 and the Euler–Lagrange equations agree). For any $D > 0$ they differ in the stationary set, the fluctuation operator, and the prefactors, while yielding the same leading Arrhenius exponent.

We now proceed to apply the Itô formalism to a concrete physical example. Our goal is to compute the components of the Itô stochastic path integral explicitly and recover the corresponding escape rate. We begin by formally introducing the stochastic cubic potential and setting up the relevant semiclassical framework.

3.2 Stochastic cubic potential preliminaries

We begin by considering a prototypical non-confining potential that supports metastable dynamics, namely the cubic potential

$$V(x) = -\frac{1}{3}x^3 + a^2 x, \tag{3.24}$$

where $a > 0$ determines the positions of the extrema. This function has a local minimum at $x = -a$ and a local maximum at $x = +a$. Physically, the minimum at $x = -a$ plays the role of a metastable state, from which thermally activated escape occurs.

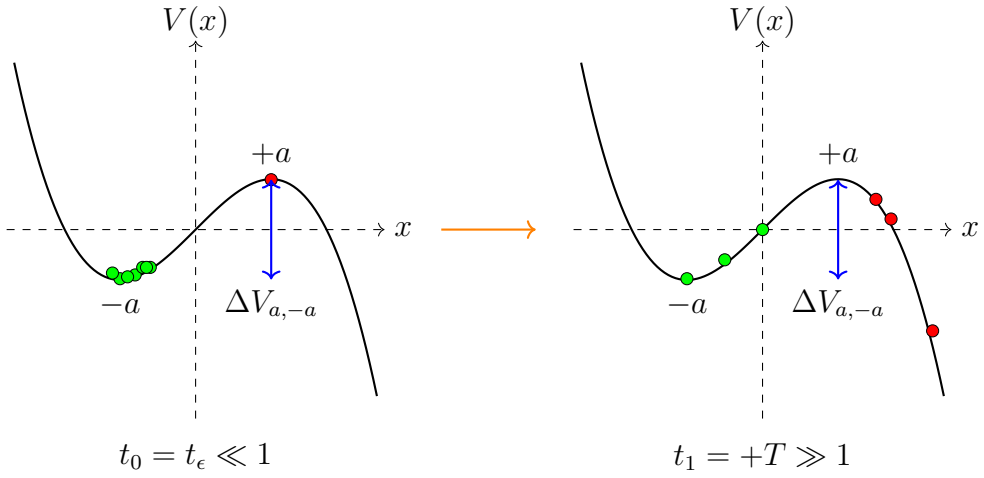

Figure 3.2: *The cubic potential $V(x)$, illustrated at two distinct times. The orange arrow denotes the forward direction of time. Initially (left), particles are localised near the metastable well at $x = -a$. At later times (right), escape events over the barrier at $x = +a$ have occurred.*

To meaningfully discuss thermally activated escape in the potential $V(x)$, the noise strength D must be small compared to the barrier height,

$$\Delta V_{a,-a} = V(+a) - V(-a) = \frac{4}{3}a^3. \tag{3.25}$$

We assume a is sufficiently large such that $a \gg D^{1/3}$, ensuring a clear separation of scales between thermal fluctuations and the potential barrier.

As illustrated in Fig. 3.2, the potential is non-confining. Once particles cross the barrier at $x = +a$, they irreversibly escape into a running channel as $x \to +\infty$, effectively reaching an absorbing boundary. The system therefore admits no stationary distribution [2, 126], and, in analogy with quantum field theory, one may regard it as lacking a true ground state [81].

In computing the forward escape rate, the detailed structure of the potential beyond the barrier is largely irrelevant. This justifies the use of asymptotic methods that focus on local bounce-like configurations, which we proceed to analyse next.

3.3 The stochastic real bounce

Starting from the cubic potential (3.24), we consider the problem of evaluating the transition probability $P(-a, +\mathcal{T}/2 \,|\, -a, -\mathcal{T}/2)$, corresponding to escape over the barrier at $x = +a$ for a Brownian particle initialised in the metastable well at $x = -a$. We analyse this using the Itô path integral formalism, expanding around the dominant weak-noise trajectory and incorporating Gaussian fluctuations.

Under the Markovian stochastic Hamiltonian correspondence (as discussed in § 2.1.7), the escape dynamics reduces to a classical problem: the motion of a Hamiltonian particle in the Itô effective potential

$$\mathfrak{U}(x) = -[V'(x)]^2 + 2D\,V''(x). \tag{3.26}$$

A plot of the effective potential $\mathfrak{U}(x)$ associated with the stochastic cubic model (3.24) is shown in Fig. 3.3.

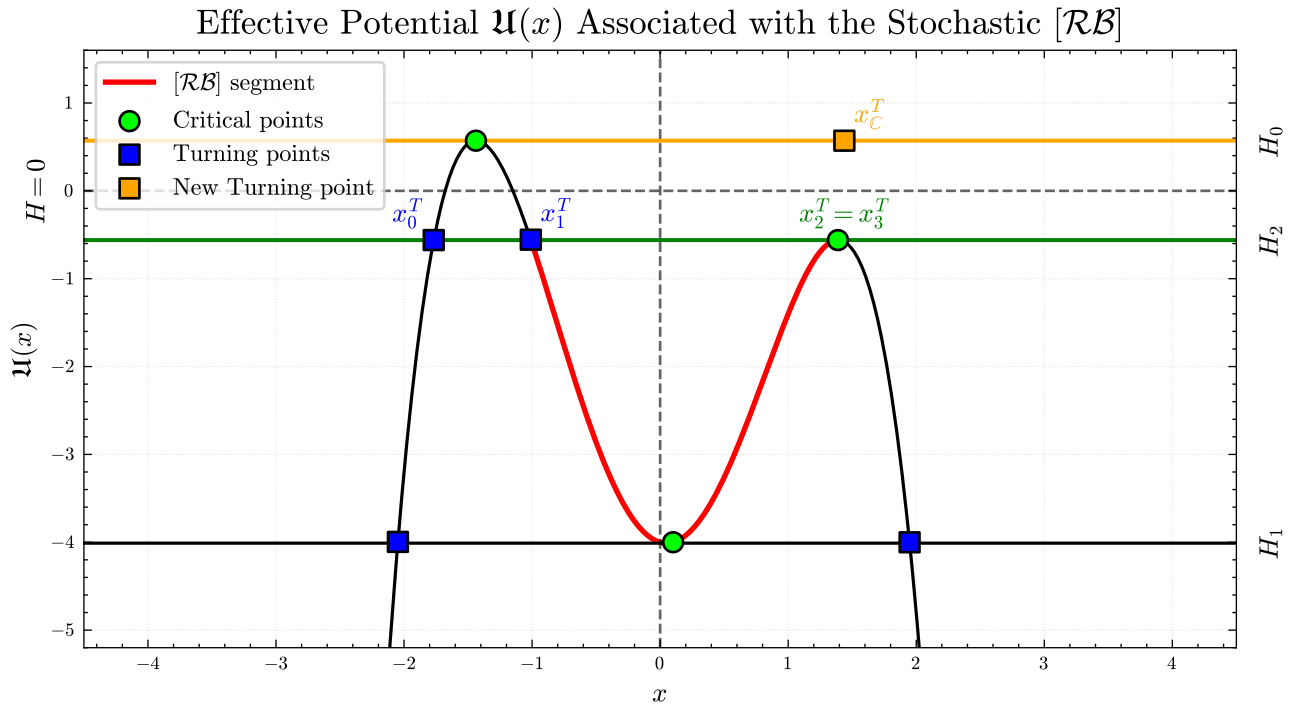

Figure 3.3: *Itô effective potential* $\mathfrak{U}(x)$ *(with* $a = \sqrt{2}, D = 0.1$*) governing the stochastic* $[\mathcal{RB}]$ *dynamics. The horizontal lines indicate three representative energy levels* $H_1 < H_2 < H_0$ *defined in Eq.* (3.30)*. Green circles mark the critical points of* $\mathfrak{U}(x)$*, while squares denote the corresponding turning points of the Itô dynamics at these energy levels. The orange square anticipates the position of a complex turning point after analytic continuation into the complex plane, foreshadowing the need for complexified dynamics. The qualitative structure closely follows Figure 10 of Behtash et al. [13].*

Inspection of the effective potential reveals that the noise-induced tilt significantly deforms its geometry such that a conventional bounce trajectory no longer exists. Consider, for instance, a Hamiltonian particle with energy infinitesimally below the global maximum of $\mathfrak{U}(x)$. The particle acquires sufficient kinetic energy to surpass the secondary peak and escape to asymptotically large values of x, which prevents any return. Accordingly, there exists no real, bounded classical solution satisfying the relevant boundary conditions. The standard bounce paradigm thus fails to compute $P(-a, +\mathcal{T}/2 \,|\, -a, -\mathcal{T}/2)$.

A natural alternative is to consider the transition probability $P(a, +\mathcal{T}/2 \,|\, a, -\mathcal{T}/2)$, where the particle begins and ends at the top of the barrier. At this energy level, the Hamiltonian trajectory is bounded between real turning points: the particle descends to a turning point and returns, yielding a real closed classical solution that satisfies the desired boundary conditions. Although this setup may initially ap-

pear artificial, it offers a controlled setting in which to study bounce dynamics within the Itô formalism and to build intuition for the influence of noise and asymmetry. We refer to this configuration as the **stochastic real bounce**, denoted by $[\mathcal{RB}]$. Its trajectory is depicted as the thick red curve in Fig. 3.3.

3.3.1 Critical points, energies and turning points

To begin our analysis of the stochastic real bounce $[\mathcal{RB}]$, we examine the geometry of its classical trajectory. The natural starting point is the set of critical points of the effective potential, defined by the stationarity condition $\mathfrak{U}'(x_{\rm cr}^k) = 0$. For the cubic potential $V(x) = -\frac{1}{3}x^3 + a^2 x$, this yields the depressed cubic equation,

$$(x_{\rm cr}^k)^3 - a^2 x_{\rm cr}^k + D = 0, \tag{3.27}$$

which admits three distinct real roots, provided the discriminant satisfies $\Delta = 4(-a^2)^3 + 27D^2 < 0$. These roots may be expressed explicitly in trigonometric form [2]:

$$x_{\rm cr}^k = -\frac{2a}{\sqrt{3}} \cos\left(\frac{1}{3}\arccos\left(\frac{3\sqrt{3}}{2a^3}D\right) - \frac{2\pi k}{3}\right), \qquad k = 0,\, 1,\, 2. \tag{3.28}$$

This agrees with the set of critical points found by Dunne *et al.* in Equation (128) in [13]. The stochastic $[\mathcal{RB}]$ trajectory is time-symmetric, reflecting off a turning point $x_1^{\rm T}$ at $t = t_c = 0$ (without loss of generality), and approaching the lower maximum of $\mathfrak{U}(x)$ as $\mathcal{T} \to \pm\infty$. At the energy level associated with $[\mathcal{RB}]$, the turning points $x_2^{\rm T}$ and $x_3^{\rm T}$ coalesce.

In the weak-noise regime, corresponding physically to a small tilt in the effective potential, the roots of

[2] This follows via the substitution $x_{\rm cr}^k = -\frac{2a}{\sqrt{3}}\cos(\theta)$ and the identity $\cos(3\theta) = 4\cos^3\theta - 3\cos\theta$.

the depressed cubic (3.27) admit asymptotic expansions in powers of D:

$$\begin{aligned} x_0^{\mathrm{cr}} &\approx -a - \frac{D}{2a^2} + \frac{3D^2}{8a^5} + \mathcal{O}(D^3), \\ x_1^{\mathrm{cr}} &\approx \quad \frac{D}{a^2} + \frac{D^3}{a^8} + \mathcal{O}(D^5), \\ x_2^{\mathrm{cr}} &\approx \quad a - \frac{D}{2a^2} - \frac{3D^2}{8a^5} + \mathcal{O}(D^3). \end{aligned} \tag{3.29}$$

These expansions confirm that the critical points of the Itô effective potential are slightly shifted compared to their Stratonovich counterparts. In the noiseless limit $D = 0$, the tilt vanishes exactly and $\mathfrak{U}(x)$ becomes symmetric, recovering the critical point structure of the classical Stratonovich framework. The three critical points collapse to the zero-energy level $H = 0$. In contrast, for non-zero noise, this symmetry breaks and the degeneracy is lifted.

To determine the energy associated with each critical point, we evaluate the effective potential at the corresponding roots,

$$H_k = \mathfrak{U}(x_{\mathrm{cr}}^k), \qquad k = 0,\ 1,\ 2. \tag{3.30}$$

These energy levels explicitly depend on the noise strength D, and remain finite (typically negative for real bounces) even in the infinite-time limit $\mathcal{T} \to \infty$. The energy level governing the stochastic real bounce is the value at the rightmost critical point x_2^{cr}, which admits the expansion

$$H_2 = \mathfrak{U}(x_2^{\mathrm{cr}}) \approx -4aD + \frac{D^2}{a^2} + \mathcal{O}(D^3). \tag{3.31}$$

To determine the corresponding turning points, we proceed by analysing the square of the particle's velocity via energy conservation. Turning points are defined as locations where the Hamiltonian particle momentarily comes to rest, i.e., where its velocity vanishes,

$$\begin{aligned} \left(\frac{\mathrm{d}x}{\mathrm{d}t}\right)^2 &= H - \mathfrak{U}(x) \\ &= H + 4Dx + x^4 - 2a^2x^2 + a^4 \\ &\equiv \Phi(x), \end{aligned} \tag{3.32}$$

where $\Phi(x)$ is the *turning point function*. This function encodes the kinematically accessible region of the Hamiltonian particle and admits a transparent algebraic structure. Since the critical points x_{cr}^k lie on constant-energy surfaces, they satisfy $\Phi(x_{\text{cr}}^k) = 0$ by construction. Differentiating and evaluating at x_{cr}^k yields $\Phi'(x_{\text{cr}}^k) = -\mathfrak{U}'(x_{\text{cr}}^k) = 0$, confirming that each x_{cr}^k is a degenerate double root of $\Phi(x)$. This reflects the vanishing of both the velocity and its derivative at that point. As a monic quartic, $\Phi(x)$ factorises as

$$\Phi(x) = (x - x_{\text{cr}})^2(x - x_T)(x - x_T'), \tag{3.33}$$

where $x_{\text{cr}} \in \mathbb{R}$ is a double root corresponding to a critical point and $x_T, x_T' \in \mathbb{R}$ are the associated non-degenerate turning points. Expanding both sides and comparing with (3.32) yields the coefficient identities:

$$\begin{aligned}
&\text{(i)} \quad \text{Coefficient of } x^3: \quad 2x_{\text{cr}} + x_T + x_T' = 0, \\
&\text{(ii)} \quad \text{Coefficient of } x^2: \quad 2x_{\text{cr}}(x_T + x_T') + x_T x_T' + x_{\text{cr}}^2 = -2a^2, \\
&\text{(iii)} \quad \text{Coefficient of } x^1: \quad -2x_{\text{cr}} x_T x_T' - x_{\text{cr}}^2(x_T + x_T') = 4D, \\
&\text{(iv)} \quad \text{Coefficient of } x^0: \quad x_{\text{cr}}^2 x_T x_T' = H + a^4.
\end{aligned} \tag{3.34}$$

Using (i), we eliminate one root: $x_T' = -2x_{\text{cr}} - x_T$. Substituting into (iii) yields a quadratic in x_T, leading to

$$x_T = -x_{\text{cr}} + \sqrt{\frac{2D}{x_{\text{cr}}}} \qquad \text{and} \qquad x_T' = -x_{\text{cr}} - \sqrt{\frac{2D}{x_{\text{cr}}}}, \tag{3.35}$$

provided $x_{\text{cr}} > 0$. Substituting these into (ii) yields the constraint

$$x_{\text{cr}}^2 + \frac{D}{x_{\text{cr}}} = a^2, \tag{3.36}$$

which is algebraically equivalent to the critical point condition $\mathfrak{U}'(x_{\text{cr}}) = 0$, or equivalently the depressed cubic (3.27). These identities will help streamline the analytic study of the stochastic bounce configuration and its fluctuations.

3.3.2 Exact analytic solution for the stochastic real bounce

The motion of the stochastic $[\mathcal{RB}]$ satisfies the second-order ODE,

$$\begin{aligned}\frac{\mathrm{d}^2x}{\mathrm{d}t^2} &= -\frac{1}{2}\mathfrak{U}'(x)\\ &= 2x^3 - 2a^2x + 2D,\end{aligned} \tag{3.37}$$

subject to the conditions

$$x(\pm\infty) = x_2^{\mathrm{cr}}, \quad x(t_c) = x_T, \tag{3.38}$$

where x_2^{cr} is given explicitly in (3.28) and the turning point, x_T, satisfies the relation of (3.35). We solve this equation numerically to extract the structural features of the solution.

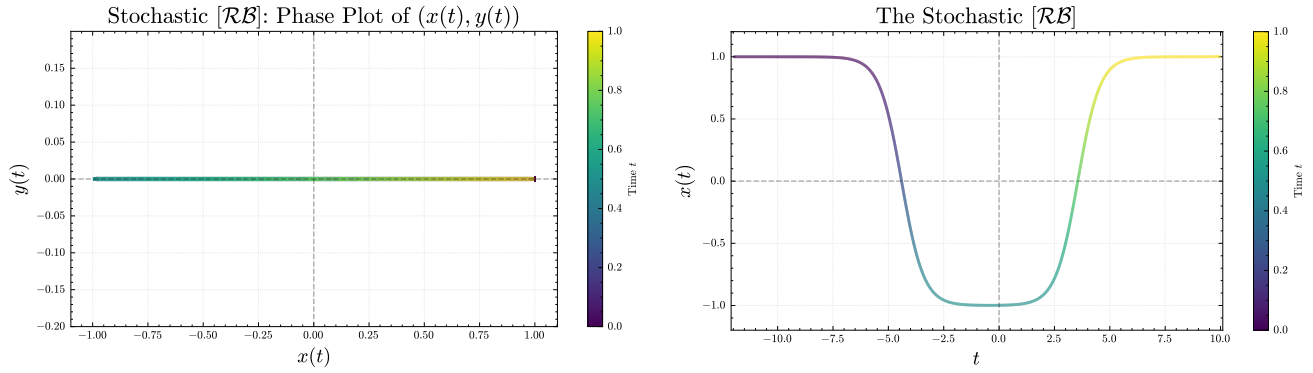

(a) A phase plot of the stochastic $[\mathcal{RB}]$.

(b) Evolution of the stochastic $[\mathcal{RB}]$.

Figure 3.4: Numerically solving the ODE ($t_c = 0$) with $a = 1$ and $D = 10^{-6}$. The colour bar on the right indicates the direction of time. On the colour bar, the time is normalised to unity.

The phase plot in Fig. 3.4a shows that the stochastic $[\mathcal{RB}]$ remains confined to the real axis since $y(t) = 0\,\forall\, t$, returning to its initial position at the end of its trajectory. In Fig. 3.4b, we plot the solution as a function of time against position, revealing the loop-like structure characteristic of a composite ansatz pair $[\bar{\mathcal{I}}\mathcal{I}]$ introduced in Chapter 2. We will now derive the exact analytic solution that exhibits this behaviour.

To elucidate the structure of the solution, we begin in a general setting, postponing the substitution of

explicit values for the critical and turning points until the final step. Although their specific locations vary across energy levels, the underlying ODE structure remains invariant. The classical path satisfies the algebraic curve equation (3.33), which is equivalent to the differential equation

$$\left(\frac{\mathrm{d}x}{\mathrm{d}t}\right)^2 = (x - x_{\mathrm{cr}})^2(x - x_T)(x - x_T'), \tag{3.39}$$

and admits an implicit solution via quadrature:

$$\int_{t_c}^{t} 1 \, \mathrm{d}t' = \int_{x_T}^{x} \frac{\mathrm{d}x'}{\sqrt{(x' - x_{\mathrm{cr}})^2(x' - x_T)(x' - x_T')}} =: F(x), \tag{3.40}$$

yielding the relation

$$t - t_c = \int_{x_T}^{x} \frac{\mathrm{d}x'}{\sqrt{(x' - x_{\mathrm{cr}})^2(x' - x_T)(x' - x_T')}} = F(x). \tag{3.41}$$

Without loss of generality, we assume the particle reaches the turning point x_T at time $t = t_c = 0$. This choice amounts to a global time translation $t \mapsto t - t_c$, which leaves the underlying dynamics invariant due to time-translation symmetry. At this stage, the solution is implicit in the form $t - t_c = F(x)$, and must be inverted to yield the classical path $x(t - t_c) = F^{-1}(t - t_c)$.

Rather than solving (3.39) directly using special functions such as the Weierstrass elliptic function $\wp$ [111], we adopt a constructive and algebraically transparent approach.[3] This method systematically transforms the original equation through a sequence of invertible maps into a solvable form. The solution strategy is depicted below as a commutative diagram of transformations.

[3]The idea of reducing the ODE to more accessible forms was motivated by discussions with Professor Alan McKane. The illustration and implementation of commutative diagrams was an original contribution of the author.

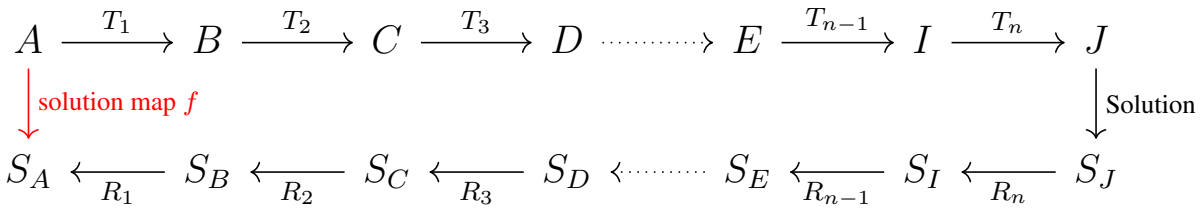

Figure 3.5: *An abstract blueprint for solving nonlinear ODEs via sequential transformations.*

Here, the objects $A, B, \ldots, J$ denote successive forms of the ODE obtained by transformations T_i. Each transformation T_i represents a (possibly non-linear) change of variables designed to simplify the algebraic structure of the differential equation, while the reverse maps $R_i = T_i^{-1}$ reconstruct the original variables. This defines the *solution map* f, expressed as the composition

$$f(A) = R_1 \circ R_2 \circ \cdots \circ R_n \circ \text{Solution} \circ T_n \circ \cdots \circ T_1(A), \tag{3.42}$$

where $\circ$ denotes function composition. The order of composition is essential. We now proceed to solve the bounce equation explicitly. We first introduce a coordinate shift to centre the dynamics at the critical point,

$$(\varphi(x), \varphi_T, \varphi_T') := (x - x_{\text{cr}}, x_T - x_{\text{cr}}, x_T' - x_{\text{cr}}). \tag{3.43}$$

This recasts the quartic ODE (3.39) into the translated form

$$\left(\frac{\mathrm{d}\varphi}{\mathrm{d}t}\right)^2 = \varphi^2(\varphi - \varphi_T)(\varphi - \varphi_T'), \tag{3.44}$$

i.e., a quartic equation with a double root at the origin. We now apply a reciprocal transformation to simplify the quartic structure,

$$(\psi(x), \psi_T, \psi_T') := \left(\frac{1}{\varphi(x)}, \frac{1}{\varphi_T}, \frac{1}{\varphi_T'}\right). \tag{3.45}$$

Under this change of variables, Equation (3.44) becomes

$$\left(\frac{\mathrm{d}\psi}{\mathrm{d}t}\right)^2 = \frac{1}{\psi_T \psi_T'}(\psi - \psi_T)(\psi - \psi_T'). \tag{3.46}$$

The prefactor simplifies upon identifying the square of the local angular frequency around the critical point,

$$\omega^2 := (x_T - x_{\mathrm{cr}})(x_T' - x_{\mathrm{cr}}) = \frac{1}{\psi_T \psi_T'}. \tag{3.47}$$

This arises from the linearisation of the effective potential around x_{cr}, where the operator has the form $\hat{\mathcal{M}} = -\frac{\mathrm{d}^2}{\mathrm{d}t^2} + 6(x_{\mathrm{cr}})^2 - 2a^2 = -\frac{\mathrm{d}^2}{\mathrm{d}t^2} + (x_T - x_{\mathrm{cr}})(x_T' - x_{\mathrm{cr}})$. Introducing the scaled time variable $\tilde{t} := \omega t$, we obtain the simplified equation

$$\left(\frac{\mathrm{d}\psi}{\mathrm{d}\tilde{t}}\right)^2 = (\psi - \psi_T)(\psi - \psi_T'). \tag{3.48}$$

To fix the freedom associated with the time-translation symmetry, we choose the initial condition $x(0) = x_T$, which implies $\psi(0) = \psi_T$. This convention fixes the position modulus, selecting a unique bounce trajectory up to global time shifts. Define

$$r := \psi_T - \psi_T', \qquad \eta(\tilde{t}) := \psi(\tilde{t}) - \psi_T, \tag{3.49}$$

so that Equation (3.48) becomes

$$\left(\frac{\mathrm{d}\eta}{\mathrm{d}\tilde{t}}\right)^2 = \eta(\eta + r). \tag{3.50}$$

We now rescale η to symmetrise the right-hand side. Define

$$\eta(\tilde{t}) = \frac{r}{2}\big(K(\tilde{t}) - 1\big), \qquad \text{with} \quad K(0) = 1. \tag{3.51}$$

This transforms the ODE into the elementary form

$$\left(\frac{\mathrm{d}K}{\mathrm{d}\tilde{t}}\right)^2 = K^2 - 1, \tag{3.52}$$

whose solution is the standard hyperbolic cosine,

$$K(\tilde{t}) = \cosh\big(\tilde{t}\big). \tag{3.53}$$

Since each transformation is invertible, we reconstruct the original bounce solution by reversing the sequence. The result is an exact analytic expression,

$$x_{\mathrm{cl}}(t) = x_{\mathrm{cr}} + \frac{(x_T - x_{\mathrm{cr}})(1 + C)}{\cosh(\omega t) + C}, \tag{3.54}$$

where the constant

$$C = \frac{2x_{\mathrm{cr}} - (x_T + x'_T)}{x_T - x'_T} \tag{3.55}$$

quantifies the asymmetry of the turning points relative to the critical point.

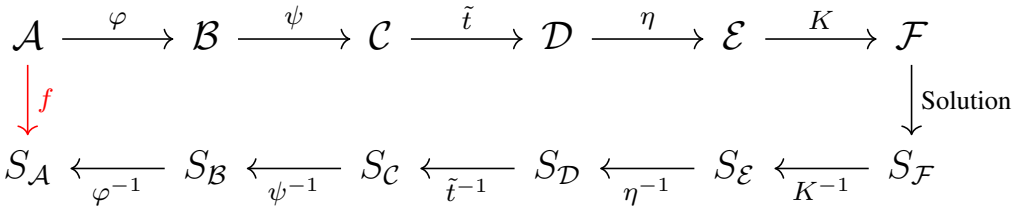

Figure 3.6: *Commutative diagram illustrating the transformation sequence yielding the exact bounce solution. The maps are defined as*
$\varphi = x - x_{cr}, \quad \psi = 1/\varphi, \quad \tilde{t} = \omega t, \quad \eta(\tilde{t}) = \psi(\tilde{t}) - \psi_T, \quad K(\tilde{t}) = 1 + \frac{2}{r}\eta(\tilde{t}).$

The diagram above compactly summarises the sequence of transformations employed to obtain the exact solution. For example, the solution in the canonical form, denoted by $S_{\mathcal{F}}$, is given by $K = \cosh\big(\tilde{t}\big)$, while $S_{\mathcal{E}} = \frac{r}{2}[\cosh\big(\tilde{t}\big) - 1]$ represents the form of the solution after inverting the final simplifying transformation, and so on.

The explicit stochastic $[\mathcal{RB}]$ solution is obtained by substituting the relevant critical and turning point values into the general solution structure (3.54). This yields

$$x_{\rm cl}(t) = x_2^{\rm cr} + \frac{(x_1^{\rm T} - x_2^{\rm cr})(1 + C_{rb})}{\cosh(\omega_{rb} t) + C_{rb}}, \tag{3.56}$$

where the turning point is perturbed very slightly from $-a$,

$$x_1^{\rm T} = -a + \sqrt{\frac{2D}{a}} + \frac{D}{2a^2} + \mathcal{O}(D^{3/2}), \tag{3.57}$$

and the asymmetry constant is

$$C_{rb} = \frac{2x_2^{\rm cr} - (x_1^{\rm T} + x_0^{\rm T})}{x_1^{\rm T} - x_0^{\rm T}}. \tag{3.58}$$

Note that this constant is real and very large in the weak-noise limit,

$$C_{rb} = \sqrt{\frac{2a^3}{D}} - \frac{3}{2}\sqrt{\frac{D}{2a^3}} - \frac{15}{16}\sqrt{\frac{D^3}{2a^9}} + \cdots \sim \sqrt{\frac{2a^3}{D}} \quad \text{as} \quad D \to 0. \tag{3.59}$$

At first glance, the structure of the solution may appear opaque. However, using the exact expressions for the turning points and the identity (3.36), the solution can be reorganised into a more transparent expression that naturally admits a physical interpretation in terms of a composite anti-instanton-instanton configuration, reminiscent of the language in Chapter 2. Explicitly, algebraic rearrangement yields

$$x_{\rm cl}(t) = x_2^{\rm cr} + (x_1^{\rm T} - x_2^{\rm cr}) \left[\frac{\left(\dfrac{x_2^{\rm cr}}{\sqrt{2a^2 - 2(x_2^{\rm cr})^2}} + \dfrac{1}{2} \right)}{\cosh^2(\omega_{rb} t/2) + \left(\dfrac{x_2^{\rm cr}}{\sqrt{2a^2 - 2(x_2^{\rm cr})^2}} - \dfrac{1}{2} \right)} \right]. \tag{3.60}$$

To reveal the compound structure, we define a new temporal separation parameter[4]

$$\mu_{rb} = \frac{2}{\omega_{rb}} \operatorname{arcosh}\left(\sqrt{\frac{x_2^{\rm cr}}{\sqrt{2a^2 - 2(x_2^{\rm cr})^2}} + \frac{1}{2}} \right), \tag{3.61}$$

[4]This follows from the identity $[\cosh(\operatorname{arcosh}(x))]^2 = x^2$, and $[\sinh(\operatorname{arcosh}(x))]^2 = x^2 - 1$.

where

$$\omega_{rb} := \sqrt{-\frac{1}{2}\mathfrak{U}''(x_2^{\rm cr})} \approx 2a - \frac{3D}{2a^2} - \frac{21D^2}{16a^5} + \mathcal{O}(D^3), \tag{3.62}$$

denotes the local curvature of the effective Itô potential at the lower peak. Then, we obtain a more illuminating expression,

$$\begin{aligned} x_{\rm cl}(t) &= x_2^{\rm cr} + (x_1^{\rm T} - x_2^{\rm cr}) \left[\frac{\cosh^2(\omega_{rb}\mu_{rb}/2)}{\cosh^2(\omega_{rb}t/2) + \sinh^2(\omega_{rb}\mu_{rb}/2)}\right] \\ &= x_1^{\rm T} + (x_2^{\rm cr} - x_1^{\rm T}) \left[\frac{\sinh^2(\omega_{rb}t/2)}{\cosh^2(\omega_{rb}\mu_{rb}/2) + \sinh^2(\omega_{rb}t/2)}\right]. \end{aligned} \tag{3.63}$$

Finally, to exhibit the anti-instanton-instanton structure in closed form, we recast the stochastic $[\mathcal{RB}]$ solution as

$$x_{\rm cl}(t) = x_2^{\rm cr} - \frac{1}{2}(x_2^{\rm cr} - x_1^{\rm T})\,\coth\left(\frac{\omega_{rb}\mu_{rb}}{2}\right)\left[\tanh\left(\frac{\omega_{rb}}{2}(t+\mu_{rb})\right) - \tanh\left(\frac{\omega_{rb}}{2}(t-\mu_{rb})\right)\right]. \tag{3.64}$$

It follows directly from this expression that the boundary conditions are satisfied,

$$\lim_{t\to\pm\infty} x_{\rm cl}(t) = x_2^{\rm cr}, \qquad x_{\rm cl}(0) = x_1^{\rm T}. \tag{3.65}$$

If we had chosen to retain the collective coordinate t_c, the $[\mathcal{RB}]$ would instead take the form

$$\begin{aligned} x_{\rm cl}(t) = x_2^{\rm cr} - \frac{1}{2}(x_2^{\rm cr} - x_1^{\rm T})\,\coth\left(\frac{\omega_{rb}\mu_{rb}}{2}\right) \\ \times \left[\tanh\left(\frac{\omega_{rb}}{2}(t-t_c+\mu_{rb})\right) - \tanh\left(\frac{\omega_{rb}}{2}(t-t_c-\mu_{rb})\right)\right]. \end{aligned} \tag{3.66}$$

This representation demonstrates the two-instanton structure of the stochastic $[\mathcal{RB}]$ solution, derived entirely from first principles without recourse to an ansatz. The solution is understood as an *exact* composite anti-instanton-instanton configuration. This matches the expression derived by Dunne *et al.* in Equation (143) in [13]. The instantonic substructures are explicitly captured by the two $\tanh$ functions, each localised near its respective centre. Concretely, the trajectory consists of an anti-instanton event

$[\bar{\mathcal{I}}]$ centred at $t = t_c - \mu_{rb}$, followed by an instanton event $[\mathcal{I}]$ centred at $t = t_c + \mu_{rb}$.

The collective coordinate t_c serves as the centre-of-mass of the instanton compound, reflecting its underlying time-translation invariance. The parameter μ_{rb} governs the temporal separation between the two instantonic events. In the weak-noise limit $D \to 0$, this separation diverges logarithmically and the configuration becomes dilute, factorising into two weakly interacting segments. The asymptotic expansion of μ_{rb} in this regime is given by

$$\mu_{rb} = \frac{1}{4a} \log\left(\frac{8a^3}{D}\right) + \frac{D}{16a^4}\left[-7 + \log\left(\frac{512a^9}{D^3}\right)\right] + \cdots, \tag{3.67}$$

confirming the emergence of widely separated instantons in the weak-noise limit, where the total separation is dominated by

$$2\mu_{rb} \sim \frac{1}{2a} \log\left(\frac{8a^3}{D}\right). \tag{3.68}$$

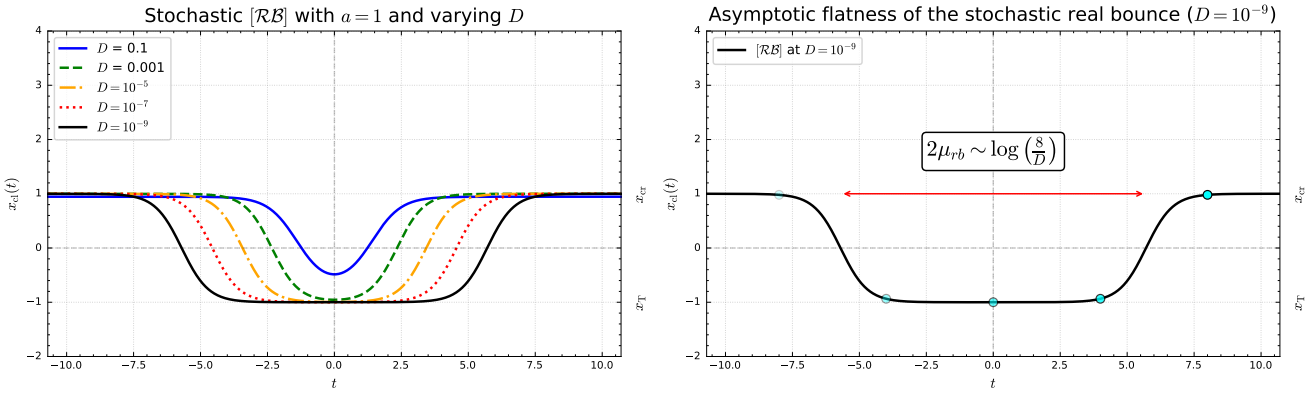

(a) Stochastic $[\mathcal{RB}]$ trajectories for decreasing noise strength D.

(b) Logarithmic growth of the bounce width at fixed $D = 10^{-9}$.

Figure 3.7: Qualitative structure of the stochastic real bounce $[\mathcal{RB}]$ for $a = 1$. **(a)** As the noise strength D decreases, the solution flattens and separates into a dilute anti-instanton-instanton compound. **(b)** At fixed small D, the temporal separation $2\mu_{rb} \sim \log(1/D)$ becomes clearly resolved, confirming the logarithmic scaling of the bounce width in the weak-noise limit, as also observed in [12].

In the weak-noise limit, the temporal gap between the anti-instanton and instanton grows large, as shown by the logarithmic dependence of μ_{rb} on the inverse noise strength. This highlights a key trait

of the $[\mathcal{RB}]$ solution: the path starts at the lower maximum of the effective potential $x_2^{\rm cr}$ as $t \to -\infty$, lingering there for a long period. The system then quickly moves to the turning point $x_1^{\rm T}$ at time $t = t_c$. Unlike quantum tunnelling trajectories, which change over time scale $1/\omega$, the stochastic $[\mathcal{RB}]$ stays near the turning point for about $2\mu_{rb} \approx (1/2a)\log(8a^3/D)$. Thus, the stochastic bounce has a much wider temporal footprint than its quantum counterparts, with a long plateau separating the instantonic events.

This long middle segment shapes the spectrum of the fluctuation operator around the $[\mathcal{RB}]$, discussed in further detail in Section 3.3.4. In one-dimensional systems, knowing the exact analytic form of the $[\mathcal{RB}]$ is not necessary to compute its stochastic action. As shown in the following, the action can be found independently of the explicit trajectory.

3.3.3 The stochastic real bounce action

If the total duration $\mathcal{T}$ is assumed to be large but finite, the particle does not start exactly at the critical point. Instead, it begins with a small distance δ to the left, that is, $x_{\rm cl}(-\mathcal{T}/2) = x_{\rm cr} - \delta$, where δ is a function to be determined. We will demonstrate that δ is exponentially suppressed in time and can be neglected. Assuming $\mathcal{T}$ is large but finite, the action functional evaluated along the extremal path takes the form

$$\begin{aligned}\mathcal{S}[x_{\rm cl}] &= \int_{-\mathcal{T}/2}^{+\mathcal{T}/2} \mathrm{d}t\,[H - 2\,\mathfrak{U}(x)] = \int_{-\mathcal{T}/2}^{+\mathcal{T}/2} \mathrm{d}t\,[2H - 2\,\mathfrak{U}(x) - H] \\ &= -H\mathcal{T} + 2\int_{-\mathcal{T}/2}^{+\mathcal{T}/2} \mathrm{d}t\,[H - \mathfrak{U}(x)] \\ &= -H\mathcal{T} + 4\int_{x_{\rm cr}-\delta}^{x_T} \mathrm{d}x\,\sqrt{H - \mathfrak{U}(x)},\end{aligned} \tag{3.69}$$

where we have used time-reversal symmetry and the fact that $\Delta V = 0$, since the particle returns to its initial position. The trajectory traces the path $x_{\rm cr} - \delta \to x_T \to x_{\rm cr} - \delta$, which, due to symmetry, corresponds to twice the journey $x_{\rm cr} - \delta \to x_T$. The resulting action is a line integral over the square root of a quartic polynomial scaled by a multiplicative factor of 2, and reads

$$\mathcal{S}[x] = -H\mathcal{T} + 4\int_{x_{\rm cr}-\delta}^{x_T} \mathrm{d}x\,\sqrt{(x - x_{\rm cr})^2(x - x_T)(x - x'_T)}. \tag{3.70}$$

This integral can be evaluated exactly, yielding [5]

$$\begin{aligned}\mathcal{S}[x] = -H\mathcal{T}&\\ &+ \frac{1}{6}\Bigg\{\sqrt{(x_{\rm cr} - \delta - x_T)(x_{\rm cr} - \delta - x'_T)}[3(x_T - x'_T)^2 + 4(x_{\rm cr} - \delta - x_T)(x_{\rm cr} - \delta - x'_T)] \\ &- 3(x_T - x'_T)^2(2x_{\rm cr} - 2\delta - x_T - x'_T)\log\left(\sqrt{\frac{x_{\rm cr} - \delta - x_T}{x_T - x'_T}} + \sqrt{\frac{x_{\rm cr} - \delta - x'_T}{x_T - x'_T}}\right)\Bigg\}.\end{aligned} \tag{3.71}$$

[5] The logarithmic term corresponds to the explicit form of $\operatorname{arsinh}\left(\sqrt{\frac{x_{\rm cr}-x_T}{x_T-x'_T}}\right)$, assuming the principal branch is taken. To avoid subtle issues with branch cuts in inverse hyperbolic functions, we prefer to express the result explicitly in terms of logarithms.

The correction δ behaves as $\delta \propto \exp(-\omega\mathcal{T}/2)(1+\mathcal{O}(\exp(-\omega\mathcal{T})))$. For sufficiently large $\mathcal{T}$, δ becomes exponentially suppressed and negligible. In the limit $\mathcal{T} \to \infty$, $\delta \to 0$, and the action simplifies to

$$\mathcal{S}[x] = -H\mathcal{T} + \frac{1}{6}\Bigg\{ \sqrt{(x_{\text{cr}} - x_T)(x_{\text{cr}} - x'_T)}[3(x_T - x'_T)^2 + 4(x_{\text{cr}} - x_T)(x_{\text{cr}} - x'_T)] \\ - 3(x_T - x'_T)^2(2x_{\text{cr}} - x_T - x'_T)\log\left(\sqrt{\frac{x_{\text{cr}} - x_T}{x_T - x'_T}} + \sqrt{\frac{x_{\text{cr}} - x'_T}{x_T - x'_T}}\right)\Bigg\}. \tag{3.72}$$

Removing the tilt corresponds to the coalescence of the turning points, $x_T \to x'_T$, which recovers the instanton limit, where $H = 0$. In that case, the instanton action becomes

$$\mathcal{S}_{\text{inst}}[x] = \frac{2}{3}(x_{\text{cr}} - x_T)^3, \tag{3.73}$$

with $x_{\text{cr}} = a$ and $x_T = -a$. This yields $\mathcal{S}_{\text{inst}} = \frac{16a^3}{3} = 4\Delta V_{a,-a}$. Thus, exponentiating and dividing by $-4D$ recovers the expected Boltzmann factor $\exp(-\Delta V/D)$. We now simplify the general form of the action ((3.72)) for the stochastic real bounce using the relations established in Eq. 3.34. The classical action then becomes

$$\begin{aligned}\mathcal{S}_{rb}[x] &= -H\mathcal{T} + \frac{8a^2}{3}\sqrt{6(x_2^{\text{cr}})^2 - 2a^2} - 16D\log\left(\sqrt{\frac{1}{2} + \sqrt{\frac{(x_2^{\text{cr}})^3}{2D}}} + \sqrt{-\frac{1}{2} + \sqrt{\frac{(x_2^{\text{cr}})^3}{2D}}}\right) \\ &= -H\mathcal{T} + \frac{16a^3}{3}\sqrt{1 - \frac{3D}{2a^2x_2^{\text{cr}}}} - 16D\log\left(\sqrt{\frac{1}{2} + \sqrt{\frac{(x_2^{\text{cr}})^3}{2D}}} + \sqrt{-\frac{1}{2} + \sqrt{\frac{(x_2^{\text{cr}})^3}{2D}}}\right).\end{aligned} \tag{3.74}$$

This agrees with the action functional expression found by Dunne *et al.* in Equation (159a) in [13] left in terms of the logarithm. For small D, we obtain the asymptotic expansion:

$$\mathcal{S}_{rb}[x] = -H\mathcal{T} + \frac{16a^3}{3} - 4D - 4D\log\left(\frac{8a^3}{D}\right) + \frac{7D^2}{2a^3} + \mathcal{O}(D^3). \tag{3.75}$$

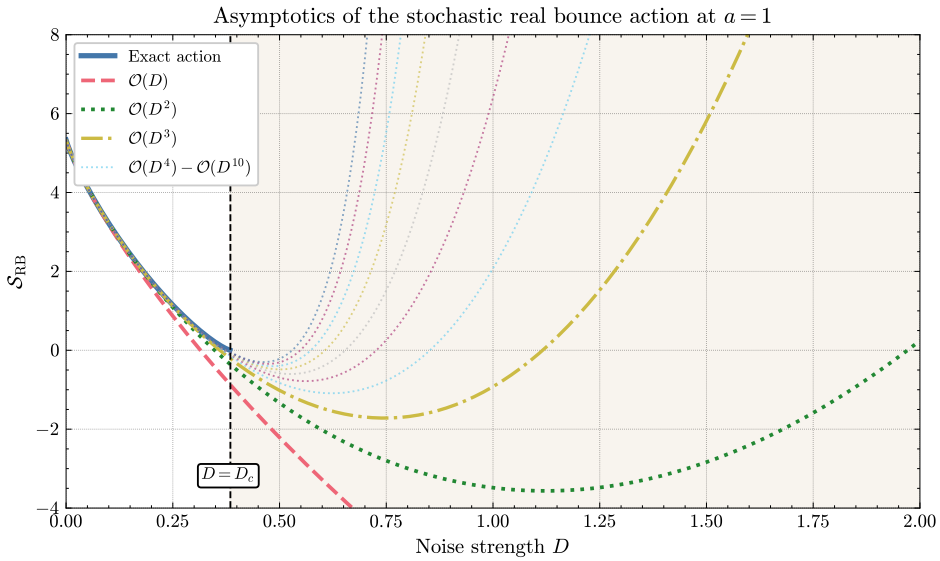

Figure 3.8: *Plot of the stochastic real bounce action, $\mathcal{S}[\mathcal{RB}]$, for $a = 1$ as a function of D, omitting the energy-dependent term. The black curve represents the exact action (Eq. (3.74)), while the green, red and blue curves correspond to the asymptotic approximations at orders $\mathcal{O}(D)$, $\mathcal{O}(D^2)$ and $\mathcal{O}(D^3)$ to $\mathcal{O}(D^{10})$ respectively.*

The critical value $D = D_c = 2a^3/(3\sqrt{3})$ represents a saddle-node bifurcation. At this value, the turning points coalesce and, beyond this noise strength, no real bounce is possible because the barrier completely collapses. In the physical region $D < D_c$, we see that as more orders are retained, the better the approximation to the exact action value. To illustrate this, we plot the error in the asymptotic series against the exact action value as D varies in Fig. 3.9.

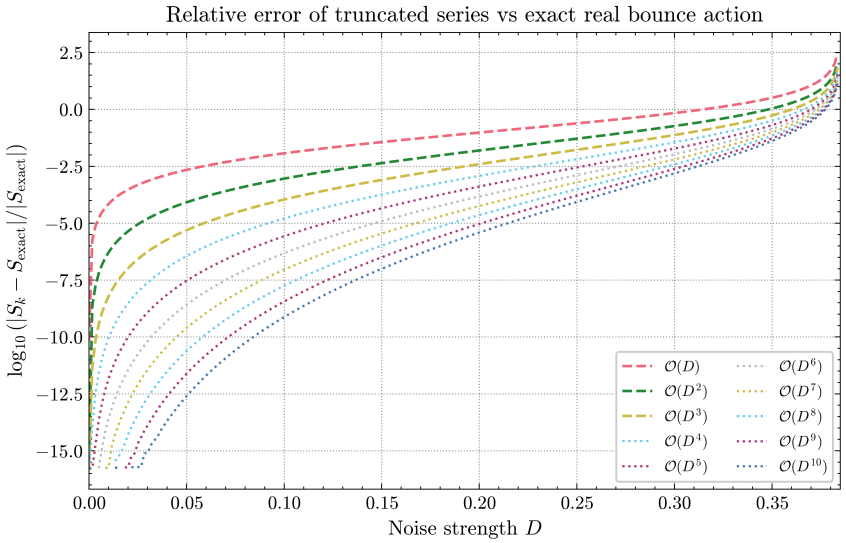

Figure 3.9: *Asymptotic weak-noise expansion of the real bounce action at* $a = 1$. *Truncated series* $S_k(D)$ *for* $k = 1, 2, \ldots, 10$ *are compared with the exact action* $S_{\text{RB}}(D)$. *Higher orders consistently outperform lower orders.*

The leading-order contribution to the escape rate is obtained by exponentiating Hamilton's principal function and dividing by $-4D$,

$$\begin{aligned}\Gamma_{rb} &\sim \exp\left(-\frac{\mathcal{S}_{rb}[x]}{4D}\right) \\ &= \exp\left(-\frac{\Delta V}{D}\right) \cdot \exp\left(\frac{H\mathcal{T}}{4D}\right) \cdot \exp(1) \cdot \left(\frac{8a^3}{D}\right) \cdot (\text{higher-order terms}).\end{aligned} \tag{3.76}$$

The divergent exponential $\exp(H\mathcal{T}/(4D))$ poses no problem, as it cancels against an equivalent term arising from the Itô normalisation factor $P_0(\mathcal{T})$. The factor of e comes from the term $-4D$ and the factor of $8a^3/D$ comes from the logarithm term $-4D\log(8a^3/D)$. Although the Hamiltonian principal function governs the leading exponential behaviour, our objective is to determine the full prefactor. To this end, we must analyse the fluctuation determinant associated with the stochastic real bounce.

3.3.4 Stochastic real bounce fluctuations and functional determinant

We proceed with the analysis of quadratic fluctuations around the stochastic $[\mathcal{RB}]$ solution in the weak-noise limit. These fluctuations are governed by the second variation of the Itô stochastic action, leading to a Schrödinger-type operator of the form

$$\hat{\mathcal{M}} = -\frac{\mathrm{d}^2}{\mathrm{d}t^2} - \frac{1}{2}\mathfrak{U}''(x_{\mathrm{cl}}), \tag{3.77}$$

where the Itô effective potential associated with the cubic potential is defined as $\mathfrak{U}(x) = -(x^2 - a^2)^2 - 4Dx$. Consequently, the fluctuation operator around the stochastic $[\mathcal{RB}]$ solution is expressed as

$$\begin{aligned}\hat{\mathcal{M}}_{[\mathcal{RB}]} &= -\frac{\mathrm{d}^2}{\mathrm{d}t^2} + 6[x_{\mathrm{cl}}(t)]^2 - 2a^2 \\ &= -\frac{\mathrm{d}^2}{\mathrm{d}t^2} + \omega_{rb}^2\left[1 - \frac{3}{2}\left(\mathrm{sech}^2\left(\frac{\omega_{rb}}{2}(t+\mu_{rb})\right) + \mathrm{sech}^2\left(\frac{\omega_{rb}}{2}(t-\mu_{rb})\right)\right)\right],\end{aligned} \tag{3.78}$$

where $\omega_{rb}^2 = 6(x_2^{\mathrm{cr}})^2 - 2a^2$ represents the local curvature at x_2^{cr}, and μ_{rb} controls the separation between the anti-instanton and instanton substructures embedded within the stochastic bounce. We denote the time-dependent term in the fluctuation operator as the *fluctuation potential*, so that the general form of the fluctuation operator assumes the schematic structure

$$\hat{\mathcal{M}} = -\frac{\mathrm{d}^2}{\mathrm{d}t^2} + \text{“fluctuation potential”}. \tag{3.79}$$

Thus, the fluctuation potential associated with the stochastic $[\mathcal{RB}]$ is given by a linear combination of sech^2 functions. The invariance of the action under time translations implies the existence of an exact zero eigenvalue of $\hat{\mathcal{M}}_{[\mathcal{RB}]}$. The zero mode (EZM) is defined as the time derivative of the bounce profile,

$$\begin{aligned}y_{\text{zero mode}}^{[\mathcal{RB}]}(t) &= \frac{\mathrm{d}}{\mathrm{d}t}x_{\mathrm{cl}}(t) \\ &= +\frac{\beta\omega_{rb}}{2}\left[\mathrm{sech}^2\left(\frac{\omega_{rb}}{2}(t+\mu_{rb})\right) - \mathrm{sech}^2\left(\frac{\omega_{rb}}{2}(t-\mu_{rb})\right)\right],\end{aligned} \tag{3.80}$$

where $\beta = \frac{1}{2}(x_1^{\mathrm{T}} - x_2^{\mathrm{cr}}) \coth\left(\frac{\omega_{rb}\mu_{rb}}{2}\right)$ is a μ_{rb}-dependent amplitude factor of the stochastic $[\mathcal{RB}]$. Note that the derivative with respect to t is equivalent (up to a sign change) to the derivative with respect to the centre-of-mass collective coordinate t_c, i.e.,

$$y^{[\mathcal{RB}]}_{\text{zero mode}}(t) \propto \frac{\mathrm{d}x_{\text{cl}}(t)}{\mathrm{d}t_c}. \tag{3.81}$$

The formal definition of the zero mode involves differentiating with respect to t_c, but our definition remains valid and does not affect the computation of the fluctuation determinant. The normalised zero mode is given by $y_0 = \dot{x}_{\text{cl}}/\sqrt{\langle \dot{x}_{\text{cl}} | \dot{x}_{\text{cl}} \rangle}$. It is straightforward to verify that either function satisfies

$$\hat{\mathcal{M}}_{[\mathcal{RB}]}\left[y^{[\mathcal{RB}]}_{\text{zero mode}}(t)\right] = 0, \tag{3.82}$$

confirming the exactness of the zero mode. In the forthcoming graphical analysis, we compare the fluctuation potential and zero mode of the stochastic real bounce with those of its quantum mechanical counterpart. This comparison highlights the distinctive features of the stochastic solution, particularly the reflection symmetry and the double-well structure of its fluctuation potential, which encapsulates its composite anti-instanton-instanton nature.

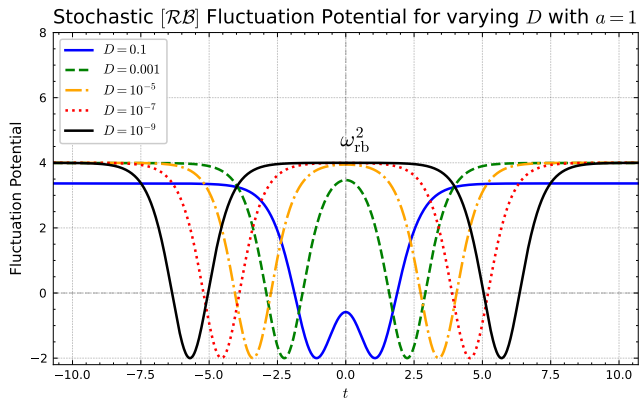

(a) $[\mathcal{RB}]$ fluctuation potential for different noise strengths D.

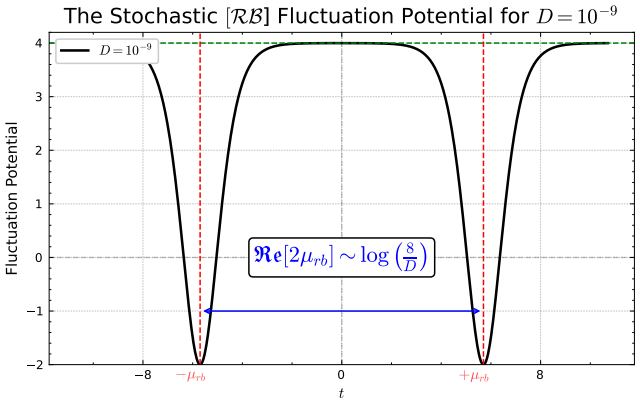

(b) $[\mathcal{RB}]$ fluctuation potential for $D = 1 \times 10^{-9}$.

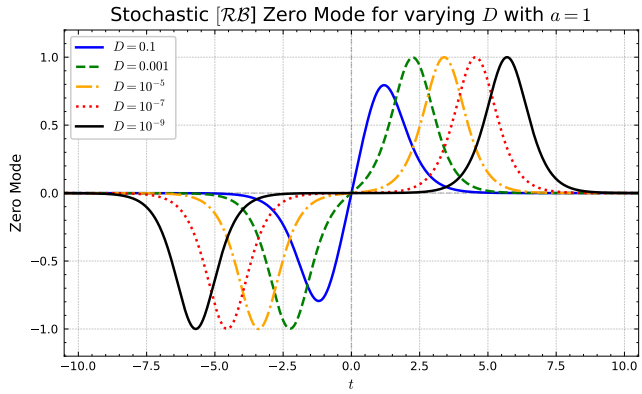

(c) The (normalised) $[\mathcal{RB}]$ zero mode for different D.

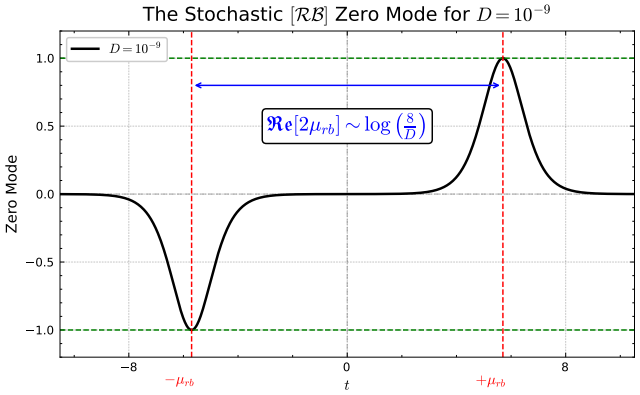

(d) The (normalised) $[\mathcal{RB}]$ zero mode for $D = 1 \times 10^{-9}$.

Figure 3.10: *A plot of the fluctuation potential and normalised zero mode in the background of the stochastic real bounce solution. The plots in the left panel (Fig. 3.10a and Fig. 3.10c) are shown for five different noise strengths D. By contrast, the plots in the right panel (Fig. 3.10b and Fig. 3.10d) are shown at fixed noise strength $D = 1 \times 10^{-9}$, with the parameter $a = 1$.*

The fluctuation potential and the zero mode of the stochastic $[\mathcal{RB}]$ encode essential information about the pre-exponential factor and perturbative structure of the escape rate. Fig. 3.10a shows the fluctuation potential derived from the linearised operator $\hat{\mathcal{M}}_{[\mathcal{RB}]}$ about the stochastic $[\mathcal{RB}]$ configuration. As the noise strength D decreases, the potential smoothly deforms into a double-well profile. This deformation signals the emergence of two quasi-independent instanton substructures within the Itô effective potential, symmetrically placed around the midpoint $t = t_c = 0$. The growing separation of the wells reflects the anti-instanton-instanton composition of the stochastic $[\mathcal{RB}]$, where the constituent instanton

events become increasingly decoupled as $D \to 0$.

Fig. 3.10b presents the fluctuation potential at small noise. The inter-well separation scales logarithmically as $\log(8/D)$, which is consistent with the asymptotic behaviour of the separation parameter μ_{rb}. The potential maximum is ω_{rb}^2, determined by the leading-order term in $\hat{\mathcal{M}}_{[\mathcal{RB}]}$. The minima are located near $t = \pm\mu_{rb}$, where the anti-instanton and instanton peaks reside.

Fig. 3.10c displays the normalised zero mode $y^{[\mathcal{RB}]}_{\text{zero mode}}(t)$, which arises from the time translation symmetry of the classical path $x_{\text{cl}}(t)$. As $D \to 0$, this mode becomes increasingly antisymmetric and concentrates into two narrow lobes supported near $t = \pm\mu_{rb}$ with a node at $t = 0$. Near the origin, the mode flattens significantly, aligning with the physical interpretation that the instanton structures are localised near the turning points of the path and effectively remain at rest between transitions. This behaviour reflects the slow dynamics of the system near the critical points, where the fluctuations are minimal.

Fig. 3.10d depicts the same zero mode at very small noise. The structure reveals two sharply peaked, oppositely signed lobes of equal amplitude, whose separation scales again as $\log(8/D)$. The sign structure of the zero mode reflects the temporal orientation of the solution: the particle first moves leftward (anti-instanton) before reversing direction rightward (instanton). The peak amplitudes are symmetric, indicating equal-magnitude peak speed in the two transition events.

The antisymmetry of the zero mode carries critical spectral implications: by the Sturm–Liouville nodal theorem [84], the existence of a node (a zero crossing) implies a lower-lying eigenfunction with no nodes, that is, a negative eigenvalue of the fluctuation operator $\hat{\mathcal{M}}_{[\mathcal{RB}]}$. Consequently, in the spectral hierarchy, the zero mode is not the ground state but the first excited state of the fluctuation operator, a fundamental result with implications for the perturbative expansion of the escape rate.

This observation is crucial, as it directly leads to the conclusion that the stochastic $[\mathcal{RB}]$ is a saddle point rather than a true minimum. Consequently, the fluctuation determinant is negative. After removing the zero mode from the spectrum, the remaining eigenvalues consist of one negative eigenvalue and $N - 2$

positive eigenvalues in the $N \to \infty$ limit. The reduced functional determinant, after omitting the zero mode, then takes the form

$$\det{}' \hat{\mathcal{M}}_{[\mathcal{RB}]} = \lambda_{-1}^{-} \cdot \lim_{N\to\infty} \prod_{n=1}^{N-2} \lambda_n^{+} < 0, \tag{3.83}$$

where the prime indicates the omission of the zero mode. This spectrum is consistent with the general structure of the bounce-type saddle points in semiclassical tunnelling [33], where the presence of a single negative mode indicates instability in one fluctuation direction, a hallmark of saddle points in the tunnelling process.

In contrast, the quantum mechanical bounce exhibits a simpler fluctuation structure, typically governed by a single-well Pöschl–Teller potential [40, 66, 147], reflecting its simpler, single-event nature. The absence of the two-event structure makes the quantum bounce's fluctuation operator much less complex than that of the stochastic $[\mathcal{RB}]$, which is a coherent anti-instanton-instanton composite.

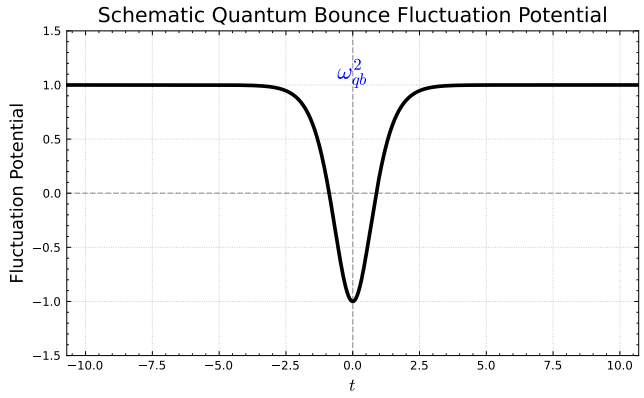

(a) *Fluctuation potential of the quantum bounce. A single-well Pöschl–Teller potential.*

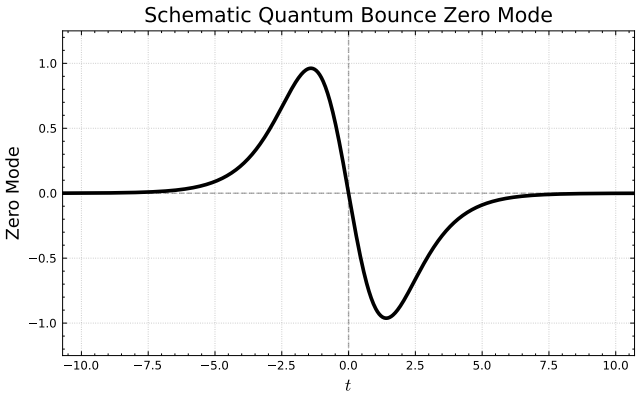

(b) *Quantum bounce zero mode. Antisymmetric with a single node.*

Figure 3.11: Fluctuation potential and zero mode for the quantum bounce solution.

Fig. 3.11 illustrates this contrast. The left panel shows the symmetric fluctuation potential with a single peak at ω_{qb}^2, while the right panel displays the corresponding antisymmetric zero mode. Unlike the stochastic $[\mathcal{RB}]$, the quantum zero mode has a smooth profile and lacks any flattening near the origin, reflecting the simplicity of its single-event structure.

Explicit Computation of the Stochastic Real Bounce Fluctuation Determinant

We now compute the fluctuation determinant associated with the stochastic $[\mathcal{RB}]$ configuration and show that it is negative. The computation proceeds via the master formula established in (2.115), which relates the functional determinant to the asymptotic data of the zero mode. The key computational aspect is the extraction of the asymptotic prefactors $\alpha_\pm$ characterising the exponential decay of the normalised zero mode EZM as $t \to \pm\mathcal{T}/2$, with $\mathcal{T} \to \infty$.

The asymptotic constants can be extracted by differentiating the classical solution twice and examining the asymptotic decay of $\ddot{x}_{\rm cl}(t)$ for large $\mathcal{T}$, while keeping $\mathcal{T}$ finite. In our case, we find,

$$\ddot{x}_{\rm cl}(+\mathcal{T}/2) = \ddot{x}_{\rm cl}(-\mathcal{T}/2) \simeq 4\beta\omega_{rb}^2 \sinh(\omega_{rb}\mu_{rb})\, \exp(-\omega_{rb}\mathcal{T}/2). \tag{3.84}$$

The fact that the asymptotic particle acceleration is the same at both endpoints is physically intuitive. The stochastic $[\mathcal{RB}]$ is time-reversal symmetric about the bounce centre $t = t_c = 0$, so $x_{\rm cl}(t) = x_{\rm cl}(-t)$. As a consequence, its derivatives satisfy $\dot{x}_{\rm cl}(t) = -\dot{x}_{\rm cl}(-t)$ and $\ddot{x}_{\rm cl}(t) = \ddot{x}_{\rm cl}(-t)$. This symmetry ensures that both the exponential decay rate and the prefactor of the fluctuations are identical for both ends of the bounce, which are mirror images of each other under time reversal. Substituting this into the master formula and taking the $\mathcal{T} \to \infty$ limit yields a well-defined expression for the fluctuation determinant ratio,

$$\begin{aligned}\lim_{\mathcal{T}\to\infty} \frac{1}{\langle \dot{x}_{\rm cl}|\dot{x}_{\rm cl}\rangle} \cdot \frac{\det{}' \hat{\mathcal{M}}_{[\mathcal{RB}]}}{\det \hat{\mathcal{M}}_0} &= -\frac{1}{32\beta^2\omega_{rb}^3 \sinh^2(\omega_{rb}\mu_{rb})} \\ &= -\frac{D}{512a^8} - \frac{23D^2}{2048a^{11}} + \mathcal{O}(D^{5/2}).\end{aligned} \tag{3.85}$$

Thus, to leading order in the weak-noise expansion, the fluctuation determinant is manifestly negative,

$$\lim_{\mathcal{T}\to\infty} \frac{1}{\langle \dot{x}_{\rm cl}|\dot{x}_{\rm cl}\rangle} \frac{\det{}' \hat{\mathcal{M}}_{[\mathcal{RB}]}}{\det \hat{\mathcal{M}}_0} = -\frac{D}{512a^8} + \cdots \tag{3.86}$$

3.3.5 Conclusion for the stochastic real bounce

The negative fluctuation determinant signals that the Gaussian integral over the unstable mode is ill-defined on the real contour. In particular, for the mode with eigenvalue $\lambda_{-1} < 0$,

$$\int_{\mathbb{R}} \mathrm{d}a_{-1}\, \exp\!\left(-\frac{1}{4D}\,\lambda_{-1}\, a_{-1}^2\right) \quad \text{diverges.} \tag{3.87}$$

Moreover, this direction is *soft* since $|\lambda_{-1}| \sim \mathcal{O}(D)$ due to a quasi-zero mode. This is the familiar instability of the $[\mathcal{I}\bar{\mathcal{I}}]$ sector, already encountered in Chapter 2.

The Bogomolny–Zinn-Justin (BZJ) prescription rectifies the problem by analytic continuation $D \mapsto e^{\pm i\pi} D$, which renders the Gaussian (and the full QZM integral) convergent, and then returning across the branch cut; this produces the characteristic $\pm i\pi$ phase. While operationally effective, this manoeuvre leaves a branch choice and lacks geometric rigour.

In the next section, we resolve this cleanly by complexifying the path space and deforming the contour to the Lefschetz thimble of the contributing complex saddle (the stochastic complex bounce). On this thimble, the unstable direction is translated into a decaying one, the quadratic form has a positive real part, and the phase is fixed by thimble orientation, so the entire analysis proceeds at fixed $D > 0$. Thus, although the path integral is formally real, its weak-noise asymptotics are governed by saddles in the complexified configuration space.

3.4 Complexification and the stochastic complex bounce

The motivation behind studying the stochastic real bounce arose from inspecting the Hamiltonian dynamics governed by the effective potential depicted in Fig. 3.3. The stochastic real bounce $[\mathcal{RB}]$ emerges as the only suitable classical trajectory to describe the escape rate over the barrier. It is an exact and purely real solution to the Euler–Lagrange equations derived from the stochastic action.

However, we face difficulties posed by the negative fluctuation determinant.

We demonstrate that a rigorous framework exists to place this analytic continuation on a firm footing. This framework requires considering an alternative classical trajectory, fundamentally different from the real bounce, defined in a complex configuration space. The strength of complexification is that it elevates $[\mathcal{I}\bar{\mathcal{I}}]$-type saddles to the same rigorous footing as the more conventional $[\mathcal{I}\mathcal{I}]$-type instantons.

Until now, our analysis has been restricted to real-valued trajectories $x(t) \in \mathbb{R}$. However, through the lens of Picard–Lefschetz theory, there is no fundamental obstruction to extending the stochastic path integral contour into the complex plane. This raises critical questions:

- Do complex-valued classical solutions to the Euler–Lagrange equations exist?
- If they do, do these complex solutions carry physical significance?

The answer is affirmative. Not only do complex classical solutions exist, they provide the relevant saddles governing the non-perturbative sectors of the weak-noise expansion. In particular, for the $[\mathcal{I}\bar{\mathcal{I}}]$-type configurations, complex trajectories provide the canonical saddles on which the path integral should be defined.

Revisiting the effective potential landscape from Fig. 3.3, we initially dismissed trajectories emanating from the global maximum of the potential because they "escape" to infinity in the real configuration space. Particle trajectories that roll off to infinity correspond to configurations with divergent Euclidean action since $|x(t)| \to \infty$ for some t. As such, they do not contribute to the weak-noise expansion of the stochastic path integral since their weight $\exp(-\mathcal{S}/(4D)) \to 0$ vanishes. This criterion serves as a natural filter, excluding physically irrelevant solutions that do not correspond to true saddle points of finite action.

However, this conclusion applies only under the restriction to real trajectories. By allowing trajectories to explore the complex plane, one discovers exact complex bounce solutions initialised at the global maximum that remain bounded, thereby providing genuine non-perturbative saddles that contribute to

the path integral. This was foreshadowed by the orange turning point in Fig. 3.3.

Formally, to properly compute the conditional probability that a particle starts and finishes at $-a$ over a duration $\mathcal{T}$, we extend the stochastic path integral into the complexified configuration space. This extension is essential for capturing the non-perturbative contributions that are inaccessible through real-valued trajectories alone. We write the stochastic path integral as

$$P(-a, +\mathcal{T}/2 \mid -a, -\mathcal{T}/2) = \int_{\gamma} \mathcal{D}z \, \exp\left(-\frac{\mathcal{S}[z]}{4D}\right), \tag{3.88}$$

where $\mathcal{D}z$ represents the integration over complex paths $z(t)$, and we choose an integration contour γ. The choice of integration contour γ and the subsequent decomposition of the stochastic path integral are determined by Picard-Lefschetz theory, which ensures the correct saddle points are captured and the integral converges, which we will explore in detail in § 3.6. We focus on the structural impact of this complexification on the path integral.

All elements of the path integral, including the measure, are promoted to complex variables. The action functional $\mathcal{S}[z]$ is holomorphically extended to the complex domain, with the real-valued terms of the action now extended as complex functions. Specifically, the action is given by

$$\mathcal{S}[z] = \int_{-\mathcal{T}/2}^{+\mathcal{T}/2} \mathrm{d}t \, \left[\dot{z}^2(t) - \mathfrak{U}(z(t))\right], \tag{3.89}$$

where the effective Itô potential $\mathfrak{U}(z)$ is analytically continued to the complex plane, yielding the following holomorphic form

$$\mathfrak{U}(z) = -(z^2 - a^2)^2 - 4Dz, \tag{3.90}$$

which is now a holomorphic function on $\mathbb{C}$. We emphasise the mathematical consequences of complexification.

We start by understanding how the complexification in (3.88) affects the diagonalisation procedure and the derivation of the Itô path integral that previously took the form (3.23).

3.4.1 Complex paths, fluctuations and diagonalisation of the non-Hermitian fluctuation operator

We extend the stochastic path integral to complex particle trajectories. In Chapter 2, we derived the one-loop factor for real paths by expanding about a classical trajectory $x_{\mathrm{cl}}(t) \in \mathbb{R}$ and treating quadratic fluctuations $y(t)$ as real-valued. After complexification, the classical trajectory becomes

$$z_{\mathrm{cl}}(t) = x_{\mathrm{cl}}(t) + i\, y_{\mathrm{cl}}(t), \tag{3.91}$$

and fluctuations $w(t)$ are taken in the complexified path space. Complexification does *not* double the number of integration directions on the cycle: later we will show, using Picard–Lefschetz theory, that there remains one real steepest descent direction per mode, with quasi-zero modes handled separately (cf. [143]). Let $\hat{\mathcal{M}}$ denote the fluctuation operator (the Hessian of the holomorphic action) at z_{cl}. For the stochastic $[\mathcal{RB}]$ on the real contour, the operator is self-adjoint. At a genuinely complex saddle the Hessian is in general non-Hermitian but complex symmetric, so $\hat{\mathcal{M}} \neq \hat{\mathcal{M}}^{\dagger}$, where † denotes the conjugate transpose. In particular, with the (sesquilinear [146]) pairing $\langle \cdot\,, \cdot \rangle$ where $\langle u, v \rangle = \int \overline{u(t)} v(t)\, \mathrm{d}t$ one has

$$\langle \hat{\mathcal{M}} f, g \rangle \neq \langle f, \hat{\mathcal{M}} g \rangle, \tag{3.92}$$

while the (complex) pairing $\langle u \mid v \rangle = \int u(t) v(t)\, \mathrm{d}t$ renders the Hessian symmetric in the sense $\langle \hat{\mathcal{M}} f \mid g \rangle = \langle f \mid \hat{\mathcal{M}} g \rangle$ (see, e.g., [88]). For a finite-mode truncation, the complex symmetric matrix representing $\hat{\mathcal{M}}$ admits the Autonne–Takagi [9, 168] factorisation

$$\hat{\mathcal{M}} = U\, \Sigma\, U^{\mathsf{T}}, \qquad U \in \mathrm{U}(N), \quad \Sigma = \mathrm{diag}(\sigma_0, \sigma_1, \dots), \;\; \sigma_n \geq 0, \tag{3.93}$$

so that, in the Takagi basis $s = U^{\mathsf{T}} c$, the quadratic form diagonalises to

$$\sum_n \sigma_n s_n^2, \tag{3.94}$$

with U unitary and Σ real non-negative [9, 31, 88, 168]. Here, $\sigma_0 = 0$ corresponds to the translation zero mode. The mode factors then integrate along their steepest descent rays,

$$\int_{\gamma_n} \mathrm{d}s_n \, \exp\!\left(-\frac{\sigma_n s_n^2}{4D}\right) \;=\; \sqrt{\frac{4\pi D}{\sigma_n}}, \qquad \gamma_n = \mathbb{R} \text{ in Takagi variables,} \tag{3.95}$$

as in the standard multidimensional saddle-point method [143]. The product over all non-zero modes yields $(\det{}' \hat{\mathcal{M}})^{-1/2}$ up to a global orientation phase[6] induced by the contour choice. With the translation zero mode isolated, the transition probability reads

$$P(z_2, +\mathcal{T}/2 \mid z_1, -\mathcal{T}/2) = \mathcal{N}_D \, \exp\!\left(-\frac{\mathcal{S}[z_{\mathrm{cl}}]}{4D}\right) \mathfrak{P} \sqrt{\frac{\omega_0}{4\pi D \, \sinh(\omega_0 \mathcal{T})}} \times \sqrt{\frac{\langle \dot{z}_{\mathrm{cl}} \mid \dot{z}_{\mathrm{cl}} \rangle}{4\pi D}} \int_{-\mathcal{T}/2}^{\mathcal{T}/2} \mathrm{d}t_c \, \left(\frac{\det{}' \hat{\mathcal{M}}}{\det \hat{\mathcal{M}}_0}\right)^{-1/2}, \tag{3.96}$$

where $\langle \cdot \# \cdot \rangle$ denotes the chosen pairing, $\hat{\mathcal{M}}_0$ is the free operator, and

$$\mathfrak{P} = \exp(i\mu/2) \tag{3.97}$$

is an orientation factor with phase μ that is later identified with a complex Morse/Maslov index [6, 49, 122] in the Picard–Lefschetz framework.

3.4.2 Exact analytic solution for the stochastic complex bounce

Let us return to individual elements of the complex stochastic path integral. As shown in (3.90), now the Itô effective potential describes a holomorphic surface where the particle motion takes place. This represents a shift in the kinematical landscape of classical particles. If we separate the complex path $z(t)$ into real and imaginary components, i.e., let $z(t) = x(t) + iy(t)$, the holomorphic surface takes

[6] The magnitude of the measure is unchanged, but the overall phase and the choice of steepest descent directions across modes produce a net phase (called a complex Morse/Maslov index).

the following form,

$$\begin{aligned} \mathrm{Re}[\mathfrak{U}(z)] &= -x^4 - y^4 + 6x^2y^2 - 2a^2(y^2 - x^2) - 4Dx - a^4, \\ \mathrm{Im}[\mathfrak{U}(z)] &= 4xy^3 - 4x^3y + 4a^2xy - 4Dy. \end{aligned} \tag{3.98}$$

On the line $y = 0$, we return to the original real potential where the stochastic $[\mathcal{RB}]$ analysis was carried out. Leaving y to vary, the effective potential geometry becomes much more intricate. A visualisation of this landscape is shown below.

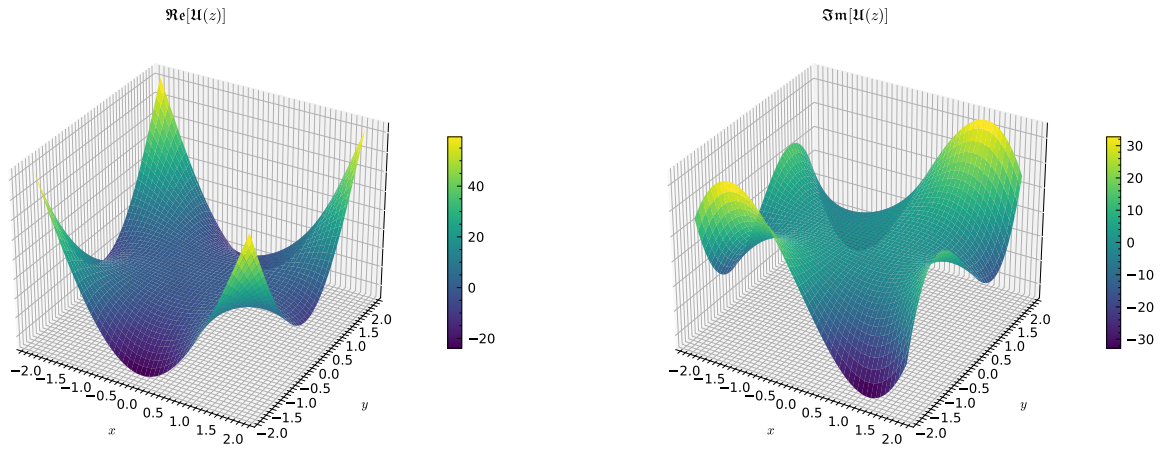

(a) Real part of holomorphic function.

(b) Imaginary part of holomorphic function.

Figure 3.12: Visualising the hypersurface corresponding to the complexified version of the Itô effective potential. The surfaces are plotted over a complex square of radius 2, $-2 \leq x \leq 2,\ -2 \leq y \leq 2$. Lighter regions indicate large peaks, whereas darker regions indicate deep wells.

The new solution space is spanned by particle paths that interpolate from the (real) global maximum of the Itô effective potential and reflect from a turning point that lies in the complex plane. This is what was hinted at in Fig. 3.3 by the orange turning point. We re-plot the diagram to give a simple visualisation of the stochastic $[\mathcal{CB}]$ trajectory.

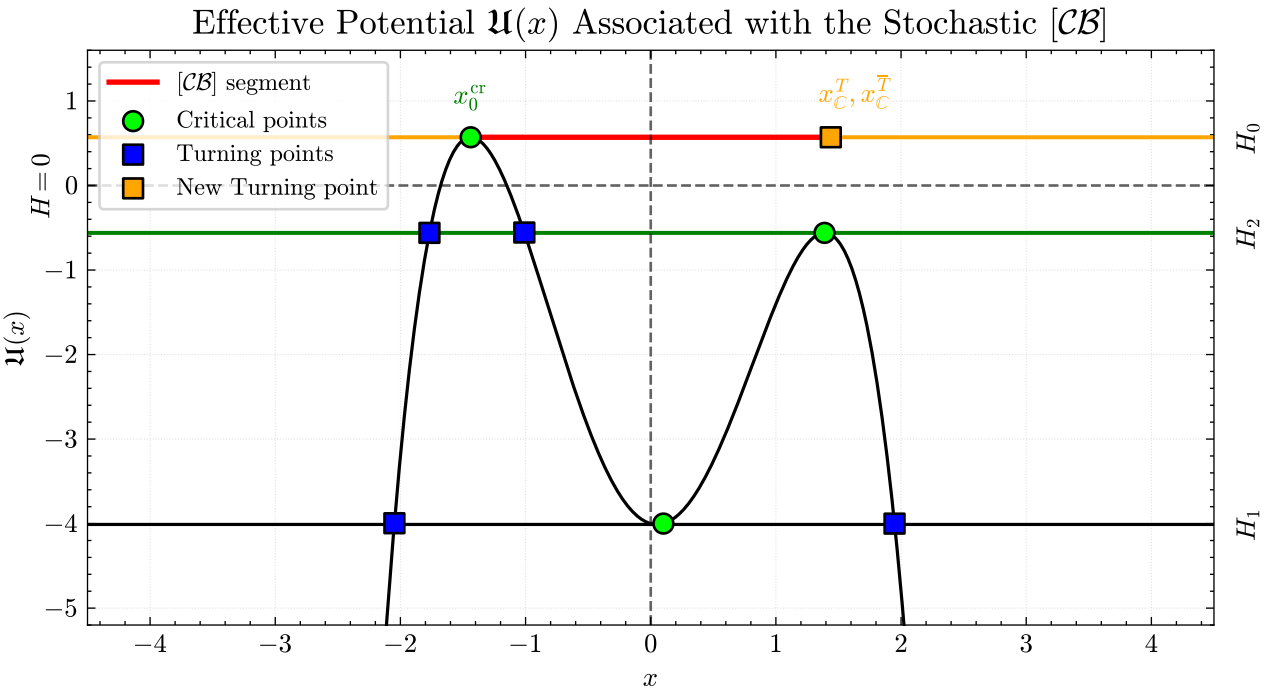

Figure 3.13: *Effective potential* $\mathfrak{U}(x)$ *(with* $a = \sqrt{2}, D = 0.1$*) governing the stochastic* $[\mathcal{CB}]$ *dynamics. Green circles mark the critical points of* $\mathfrak{U}(x)$*, while blue squares denote real turning points along the representative energy level* H_0*. The orange square denotes a complex conjugate turning point pair with a non-zero imaginary part.*

The critical point is real and negative, as already found in (3.28),

$$x_0^{\mathrm{cr}} = -\frac{2a}{\sqrt{3}} \cos\left(\frac{1}{3} \arccos\left(\frac{3\sqrt{3}}{2a^3} D\right)\right). \tag{3.99}$$

We shall let $z_0^{\mathrm{cr}} = x_0^{\mathrm{cr}}$ in the spirit of working in a complex configuration space, but the critical point here is purely real. Referring to Fig. 3.13, now the turning points have a non-zero imaginary part and are, in fact, a complex conjugate pair. We denote complex turning points by z_0^{T} (or $\overline{z_0^{\mathrm{T}}}$), and there is currently ambiguity about which path we choose. Intersection coefficients will formalise this choice in § 3.6.

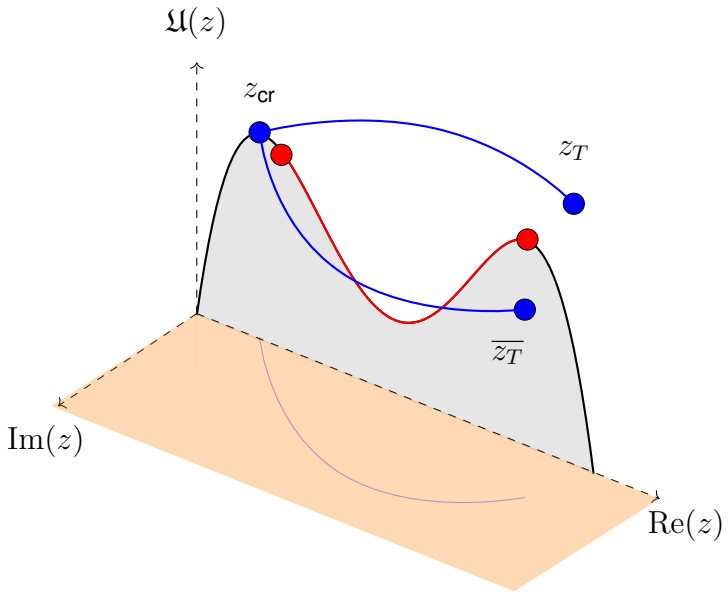

Figure 3.14: *Illustration of the effective, inverted double-well potential $\mathfrak{U}(z)$ where the stochastic $[\mathcal{RB}]$ motion (red line) and the stochastic $[\mathcal{CB}]$ motion (blue lines) take place. As explained in Fig. 3.12, the actual structure of the effective potential is much more elaborate, but here we highlight the shift of the particle paths onto the complex plane. This was inspired by Fig. 1 of [12].*

Let us assign z_0^{T} to the path with a positive imaginary part. The energy level here is positive and can be expanded in powers of D,

$$H_0 = \mathfrak{U}(z_0^{\mathrm{cr}}) \approx 4aD + \frac{D^2}{a^2} + \mathcal{O}(D^3). \tag{3.100}$$

The critical point is a double degenerate root, and the turning points form a conjugate pair, which means the turning point equation (3.33) takes the form of

$$\left(\frac{\mathrm{d}z}{\mathrm{d}t}\right)^2 = (z - z_0^{\mathrm{cr}})^2 (z - z_0^{\mathrm{T}})(z - \overline{z_0^{\mathrm{T}}}), \tag{3.101}$$

where

$$\begin{pmatrix} z_0^{\mathrm{T}} \\ \overline{z_0^{\mathrm{T}}} \end{pmatrix} = z_0^{\mathrm{cr}} \begin{pmatrix} -1 \\ -1 \end{pmatrix} + \sqrt{\frac{2D}{z_0^{\mathrm{cr}}}} \begin{pmatrix} 1 \\ -1 \end{pmatrix}. \tag{3.102}$$

Then, expanding in small powers of D, we find that

$$z_0^{\mathrm{T}} = a + i\sqrt{\frac{2D}{a}} + \frac{D}{2a^2} + \mathcal{O}(D^{3/2}), \tag{3.103}$$

and $\overline{z_0^{\mathrm{T}}}$ admits the same real powers but all imaginary components are conjugated. The equations of motion are found by extremising the holomorphic action $\mathcal{S}[z]$ which is equivalent to applying the condition of vanishing first-order functional derivative,

$$\frac{\delta \mathcal{S}}{\delta z} = 0. \tag{3.104}$$

Therefore, saddle points of the complexified stochastic path integral correspond to classical trajectories $z_{\mathrm{cl}}(t)$ solving the *holomorphic* Euler–Lagrange equation,

$$\frac{d^2 z_{\mathrm{cl}}}{dt^2} = -\frac{1}{2}\left.\frac{\partial \mathfrak{U}}{\partial z}\right|_{z=z_{\mathrm{cl}}}, \tag{3.105}$$

subject to the boundary conditions,

$$\lim_{\mathcal{T}/2\to\infty} z_{\mathrm{cl}}(\pm\mathcal{T}/2) = z_{\mathrm{cr}}, \quad z(t=t_c) = z_0^{\mathrm{T}}. \tag{3.106}$$

From the equations of motion, if we set $z(t) = x(t) + iy(t)$, we find the following system of coupled second-order ODEs,

$$\begin{aligned} \frac{\mathrm{d}^2 x}{\mathrm{d}t^2} &= 2x^3 - 6xy^2 - 2a^2 x + 2D, \\ \frac{\mathrm{d}^2 y}{\mathrm{d}t^2} &= -2y^3 - 2a^2 y + 6x^2 y, \end{aligned} \tag{3.107}$$

subject to the conditions

$$x(\pm\infty) = \operatorname{Re} z_0^{\mathrm{cr}}, \quad x(t_c) = \operatorname{Re} z_0^{\mathrm{T}} > 0, \quad y(\pm\infty) = \operatorname{Im} z_0^{\mathrm{cr}}, \quad y(t_c) = \operatorname{Im} z_0^{\mathrm{T}}, \tag{3.108}$$

where z_0^{cr} is given explicitly in (3.28) and the turning point, z_T, satisfies the relation of (3.35) and we choose the branch with positive imaginary component. We can solve these ODEs numerically to develop an insight into the new dynamics.

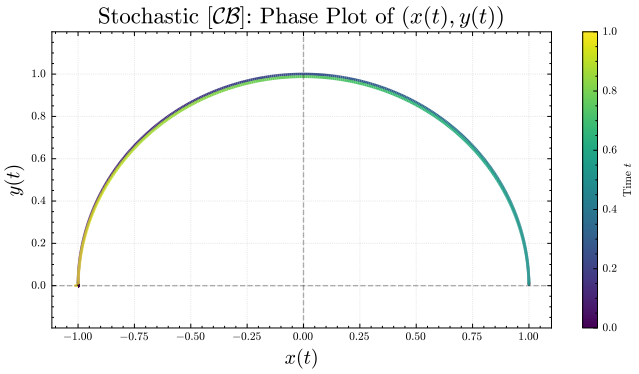

(a) Phase plot of $(x(t), y(t))$.

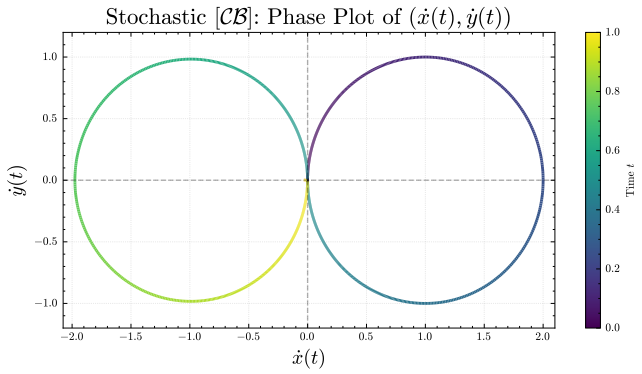

(b) Phase plot of $(\dot{x}(t), \dot{y}(t))$.

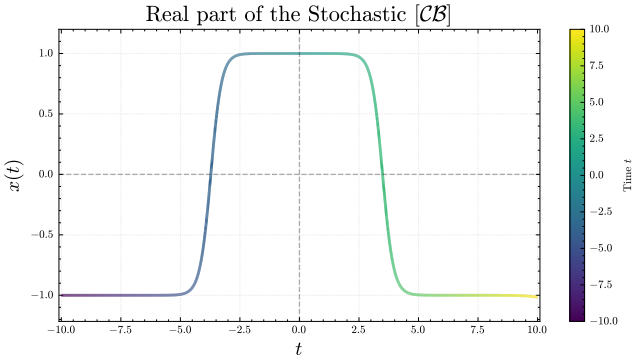

(c) Real part of the [$\mathcal{CB}$].

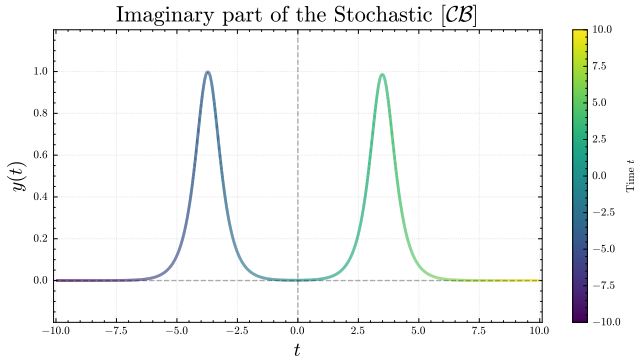

(d) Imaginary part of the [$\mathcal{CB}$].

Figure 3.15: *A numerical investigation into the* [$\mathcal{CB}$] ($t_c = 0$) *with* $a = 1$ *and* $D = 10^{-6}$.

Fig. 3.15a shows the characteristic loop of the stochastic [$\mathcal{CB}$] in the complex plane, a hallmark of a [$\mathcal{I}\bar{\mathcal{I}}$]-type trajectory. Rather than lying on the real axis, the orbit traces a semicircular arc with $\operatorname{Im} z \neq 0$. The particle reaches a complex turning point whose real part lies just beyond the barrier, then retraces the arc. Choosing the conjugate turning point reflects the arc across the real axis, producing the same shape in $\operatorname{Im} z < 0$.

Fig. 3.15b displays the velocity portrait $(\operatorname{Re} \dot{z}, \operatorname{Im} \dot{z})$, consisting of two adjacent, symmetric lobes.

Fig. 3.15c–Fig. 3.15d show that $\operatorname{Re} x(t)$ realises a pair of [$\mathcal{I}\bar{\mathcal{I}}$] pseudo-events rather than the [$\bar{\mathcal{I}}\mathcal{I}$]

structure seen for the stochastic $[\mathcal{RB}]$. The imaginary component supplies a well-defined excursion away from the real axis. The exact analytic solution derived below accurately reproduces these features.

Because the turning point condition depends only on the constant energy level, the analytic construction of the stochastic $[\mathcal{CB}]$ follows the $[\mathcal{RB}]$ derivation almost verbatim, with relabelled parameters and complex boundary data. The complex classical path satisfies the algebraic curve equation (3.101) and can be solved implicitly by quadrature,

$$\int_{t_c}^{t} 1 \, \mathrm{d}t' = \int_{z_0^{\mathrm{T}}}^{z} \frac{\mathrm{d}z'}{\sqrt{(z'-z_0^{\mathrm{cr}})^2(z'-z_0^{\mathrm{T}})(z'-\overline{z_0^{\mathrm{T}}})}} =: F(z). \tag{3.109}$$

Again, we can set $t_c = 0$ and, to make the inversion of the solution $z(t) = F^{-1}(t)$ clear, we follow the transformative procedure summarised in the commutative diagram.

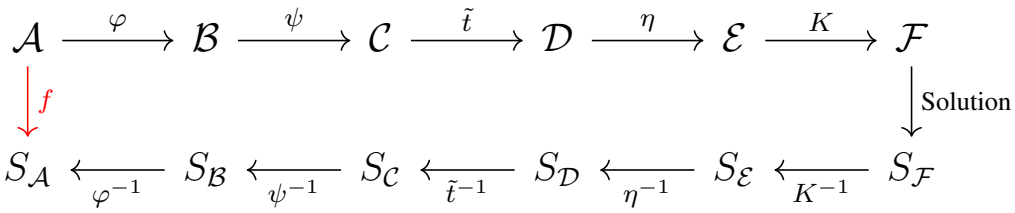

Figure 3.16: *Commutative diagram illustrating the transformation sequence yielding the exact bounce solution. The maps are defined as* $\varphi = z - z_0^{cr}$, $\psi = 1/\varphi$, $\tilde{t} = \omega t$, $\eta(\tilde{t}) = \psi(\tilde{t}) - \psi_T$, $K(\tilde{t}) = 2\eta(\tilde{t})/r + 1$. *with the condition* $z(0) = z_0^T$.

This yields

$$z_{\mathrm{cl}}(t) = z_0^{\mathrm{cr}} + \frac{(z_0^{\mathrm{T}} - z_0^{\mathrm{cr}})(1 + C_{cb})}{\cosh(\omega_{cb} t) + C_{cb}}, \tag{3.110}$$

where the constant,

$$C_{cb} = \frac{2z_0^{\mathrm{cr}} - (z_0^{\mathrm{T}} + \overline{z_0^{\mathrm{T}}})}{z_0^{\mathrm{T}} - \overline{z_0^{\mathrm{T}}}}, \tag{3.111}$$

is now purely imaginary, which can be seen with some algebra using (3.102) and expanding in small

powers of D,

$$C_{cb} = i\sqrt{\frac{2a^3}{D}} + \frac{3i}{2}\sqrt{\frac{D}{2a^3}} - \frac{15i}{16}\sqrt{\frac{D^3}{2a^9}} + \cdots \sim i\sqrt{\frac{2a^3}{D}} \quad \text{as} \quad D \to 0. \tag{3.112}$$

Following the same algebraic approach as in the $[\mathcal{RB}]$ case 3.3.2, we find the stochastic complex bounce solution as

$$z_{\text{cl}}(t) = z_0^{\text{cr}} - \frac{1}{2}(z_0^{\text{cr}} - z_0^{\text{T}}) \coth\left(\frac{\omega_{cb}\mu_{cb}}{2}\right)\left[\tanh\left(\frac{\omega_{cb}}{2}(t+\mu_{cb})\right) - \tanh\left(\frac{\omega_{cb}}{2}(t-\mu_{cb})\right)\right], \tag{3.113}$$

where the separation parameter is defined as

$$\mu_{cb} := \frac{2}{\omega_{cb}} \operatorname{arcosh}\left(\sqrt{\frac{z_0^{\text{cr}}}{\sqrt{2a^2 - 2(z_0^{\text{cr}})^2}} + \frac{1}{2}}\right), \tag{3.114}$$

and the frequency about the critical point is

$$\omega_{cb} = \sqrt{-\frac{1}{2}\mathfrak{U}''(z_0^{\text{cr}})} \approx 2a + \frac{3D}{2a^2} - \frac{21D^2}{16a^5} + \mathcal{O}(D^3). \tag{3.115}$$

Setting $t_c = 0$ was arbitrary; the most general form of the $[\mathcal{CB}]$ solution is

$$\begin{aligned} z_{\text{cl}}(t) = z_0^{\text{cr}} - \frac{1}{2}(z_0^{\text{cr}} - z_0^{\text{T}})\, \coth\left(\frac{\omega_{cb}\mu_{cb}}{2}\right) \\ \times \left[\tanh\left(\frac{\omega_{cb}}{2}(t - t_c + \mu_{cb})\right) - \tanh\left(\frac{\omega_{cb}}{2}(t - t_c - \mu_{cb})\right)\right]. \end{aligned} \tag{3.116}$$

This matches the expression (150) in [13]. Now, the frequency (3.115) is purely real and admits a series expansion in D, however, the separation (3.114) is now shifted into the complex plane, as seen through the series expansion,

$$\mu_{cb} = \frac{1}{4a}\left[\log\left(\frac{8a^3}{D}\right) + i\pi\right] + \frac{D}{16a^4}\left[-3i\pi + 7 - \log\left(\frac{512a^9}{D^3}\right)\right] + \cdots, \tag{3.117}$$

where the total separation is dominated by

$$2\mu_{cb} \sim \frac{1}{2a}\left[\log\left(\frac{8a^3}{D}\right) + i\pi\right]. \tag{3.118}$$

If we instead chose the path that was centred at the conjugate turning point $\overline{z_0^{\mathrm{T}}}$, then the $i\pi$ factor would flip sign while all other elements remain the same. In light of this, we shall write

$$2\mu_{cb} \sim \frac{1}{2a}\left[\log\left(\frac{8a^3}{D}\right) + (2\sigma-1)i\pi\right] = \frac{1}{2a}\left[\log\left(\frac{8a^3}{D}\right) \pm i\pi\right], \tag{3.119}$$

where the multivalued imaginary part is directly attached to the choice of the complex path $\sigma = \{0, +1\}$. This choice will be fully understood in § 3.6.

The explicit stochastic $[\mathcal{CB}]$ solution (3.113) reveals another two-instanton structure. The solution is understood as an exact composite instanton-anti-instanton $[\mathcal{I}\bar{\mathcal{I}}]$ configuration, which is the relevant complex saddle for a particle initialised in the metastable well. The full trajectory consists of an instanton event $[\mathcal{I}]$ centred at $t = t_c - \mu_{cb}$, followed by an anti-instanton event $[\bar{\mathcal{I}}]$ centred at $t = t_c + \mu_{cb}$ where the separation between the events inherits an imaginary component.

3.4.3 Stochastic complex bounce action and asymptotics

The classical action associated with the complex bounce can be written as

$$\begin{aligned}\mathcal{S}_{cb}[z] &= -H\mathcal{T} + \frac{8a^2}{3}\sqrt{6(z_0^{\mathrm{cr}})^2 - 2a^2} + 16D\log\left(\sqrt{\frac{1}{2} + \sqrt{\frac{(z_0^{\mathrm{cr}})^3}{2D}}} + \sqrt{-\frac{1}{2} + \sqrt{\frac{(z_0^{\mathrm{cr}})^3}{2D}}}\right) \\ &= -H\mathcal{T} + \frac{16a^3}{3}\sqrt{1 - \frac{3D}{2a^2(z_0^{\mathrm{cr}})}} + 16D\log\left(\sqrt{\frac{1}{2} + \sqrt{\frac{(z_0^{\mathrm{cr}})^3}{2D}}} + \sqrt{-\frac{1}{2} + \sqrt{\frac{(z_0^{\mathrm{cr}})^3}{2D}}}\right).\end{aligned} \tag{3.120}$$

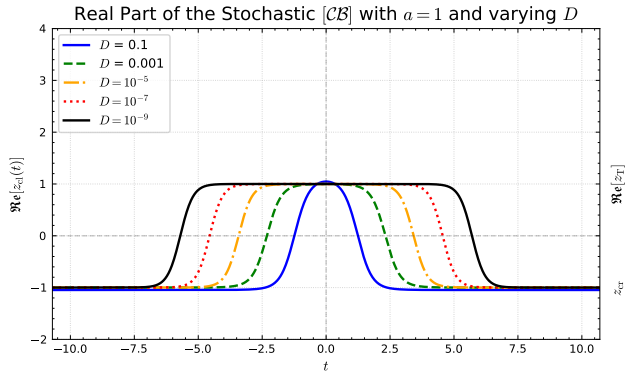

(a) Real part of the $[\mathcal{CB}]$.

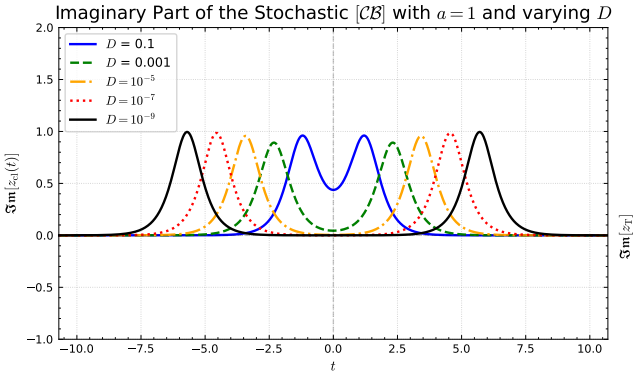

(b) Imaginary part of the $[\mathcal{CB}]$.

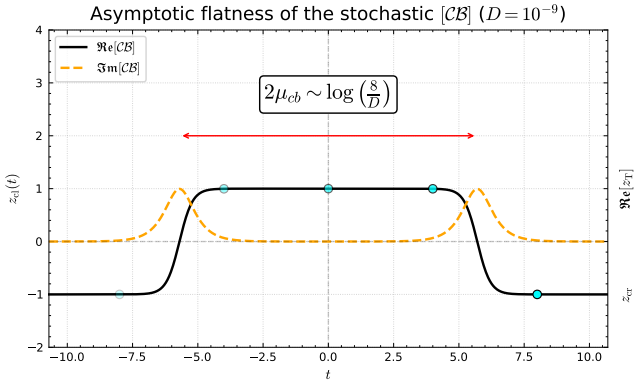

(c) Width/flatness of the $[\mathcal{CB}]$.

Figure 3.17: *Investigating the $[\mathcal{CB}]$ solution and decomposing it into its real and imaginary constituents. All curves shown are generated from the exact analytic complex bounce solution derived in this section, rather than from numerical integration of the equations of motion. We observe all the features of our numerical solution and the $[\mathcal{RB}]$ solution, except that the transition events ordering has changed, and there is clear particle motion beyond the real axis.*

This agrees with the action functional expression found by Dunne *et al.* in Equation (159a) in [13] left in terms of the logarithm. For small D, we obtain the asymptotic expansion,

$$\mathcal{S}_{cb}[z] = -H\mathcal{T} + \frac{16a^3}{3} + 4D \pm 4Di\pi - 4D\log\left(\frac{D}{8a^3}\right) + \frac{7D^2}{2a^3} + \mathcal{O}(D^3). \tag{3.121}$$

Omitting the energy-dependent term and imaginary factor, we can analyse the asymptotic expansion.

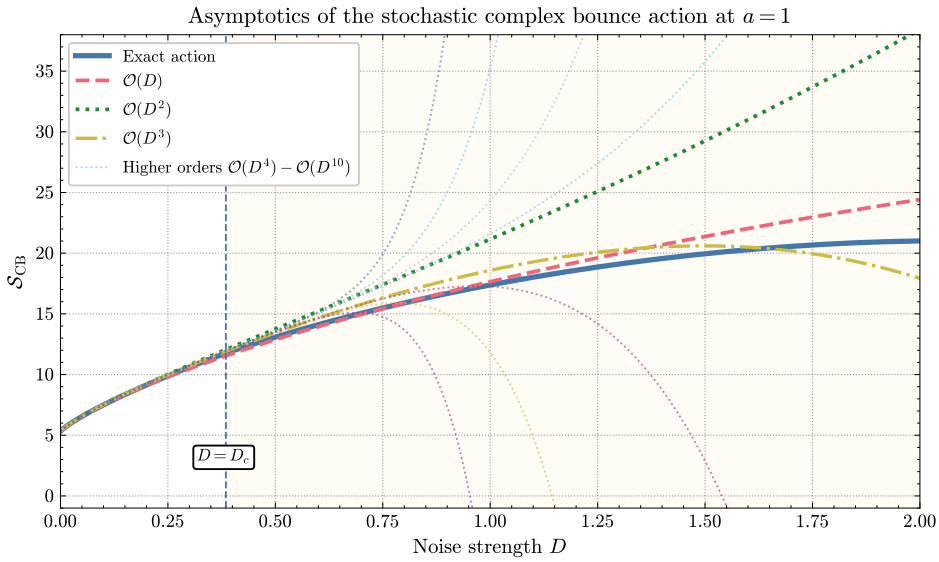

Figure 3.18: *Plot of the real part of the complex stochastic bounce action, $\mathcal{S}[\mathcal{CB}]$, for $a = 1$ as a function of D, omitting the energy-dependent term. The black curve represents the exact action ((3.120)), while the red, green, yellow and thin, dashed curves correspond to the asymptotic approximations at orders $\mathcal{O}(D)$, $\mathcal{O}(D^2)$ and $\mathcal{O}(D^3)$ to $\mathcal{O}(D^{10})$ respectively (Eq. (3.121)).*

In contrast to the stochastic $[\mathcal{RB}]$ asymptotics presented in Fig. 3.8 whose action has no meaning beyond D_c due to a saddle-node bifurcation, the exact stochastic $[\mathcal{CB}]$ action (blue) persists for all D. The trade-off in accessing higher D regimes (where the Kramers approximation breaks down) is that the higher-order approximations are less controlled; i.e., sometimes lower-order truncations outperform higher-order truncations. The asymptotics are quite controlled up until $D \approx 0.5$, a significant proportion past where the real barrier vanishes.

This "lower-beats-higher" behaviour is a consequence of complexification. We can plot the errors in the asymptotics against the noise strength to clearly observe this phenomenon.

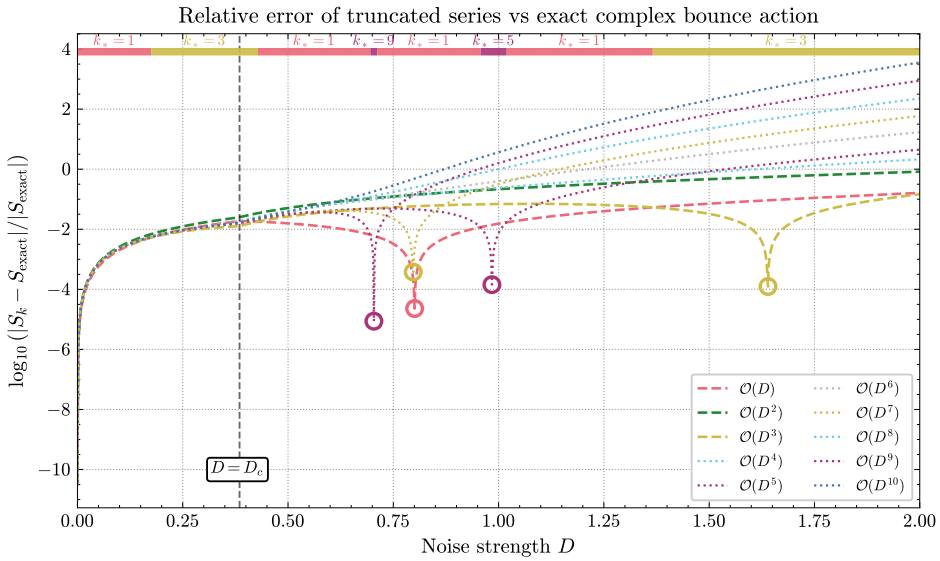

Figure 3.19: *Asymptotic weak-noise expansion of the complex bounce action at $a = 1$. Truncated series $S_k(D)$ for $k = 1, 2, \ldots, 10$ are compared with the exact action $S_{\mathrm{CB}}(D)$. For each fixed D there is an optimal truncation index $k_*(D) \sim \mathrm{Re}\, \mathcal{S}_{\mathrm{CB}}/D$ at which the error is minimised; beyond k_* higher orders degrade the approximation.*

Proceeding with the computation, we apply the master formula of the fluctuation determinant. The fluctuation operator about the cubic $[\mathcal{CB}]$ solution is

$$\begin{aligned}\hat{\mathcal{M}}_{[\mathcal{CB}]} &= -\frac{\mathrm{d}^2}{\mathrm{d}t^2} + 6[z_{\mathrm{cl}}(t)]^2 - 2a^2 \\ &= -\frac{\mathrm{d}^2}{\mathrm{d}t^2} + \omega_{cb}^2\left[1 - \frac{3}{2}\left(\mathrm{sech}^2\left(\frac{\omega_{cb}}{2}(t+\mu_{cb})\right) + \mathrm{sech}^2\left(\frac{\omega_{cb}}{2}(t-\mu_{cb})\right)\right)\right],\end{aligned} \tag{3.122}$$

and the fluctuation operator has one EZM corresponding to the time translational symmetry of the $[\mathcal{CB}]$,

$$\begin{aligned}y^{[\mathcal{CB}]}_{\text{zero mode}}(t) &= \frac{\mathrm{d}}{\mathrm{d}t} z_{\mathrm{cl}}(t) \\ &= +\frac{\beta\omega_{cb}}{2}\left[\mathrm{sech}^2\left(\frac{\omega_{cb}}{2}(t+\mu_{cb})\right) - \mathrm{sech}^2\left(\frac{\omega_{cb}}{2}(t-\mu_{cb})\right)\right],\end{aligned} \tag{3.123}$$

where β is a constant independent of time but dependent on the separation μ_{cb} given by the prefactor in the explicit $[\mathcal{CB}]$ solution, $\beta = \frac{1}{2}(z_0^{\mathrm{T}} - z_0^{\mathrm{cr}})\coth\left(\frac{\omega\mu_{cb}}{2}\right)$. It is easily checked that $\hat{\mathcal{M}}_{[\mathcal{CB}]} y^{[\mathcal{CB}]}_{\text{zero mode}}(t) = 0$.

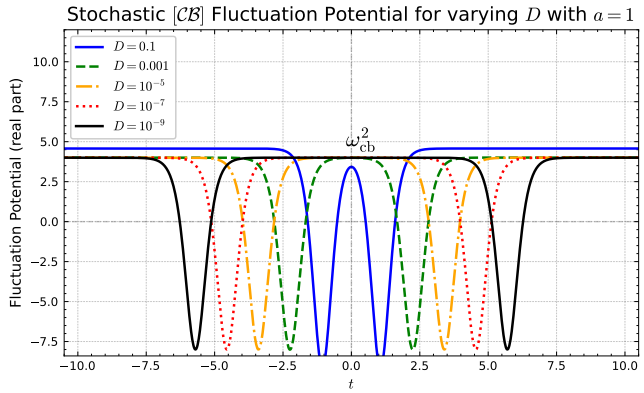

(a) [$\mathcal{CB}$] fluctuation potential for different noise strengths D.

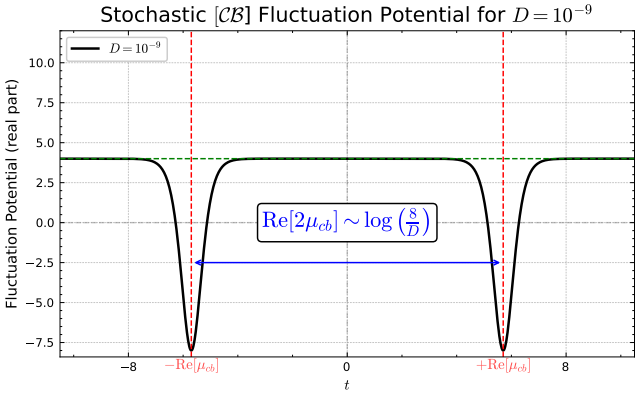

(b) [$\mathcal{CB}$] fluctuation potential for $D = 1 \times 10^{-9}$.

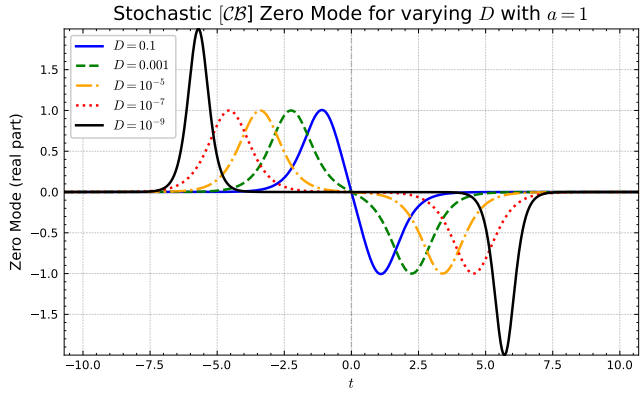

(c) The [$\mathcal{CB}$] zero mode for different D.

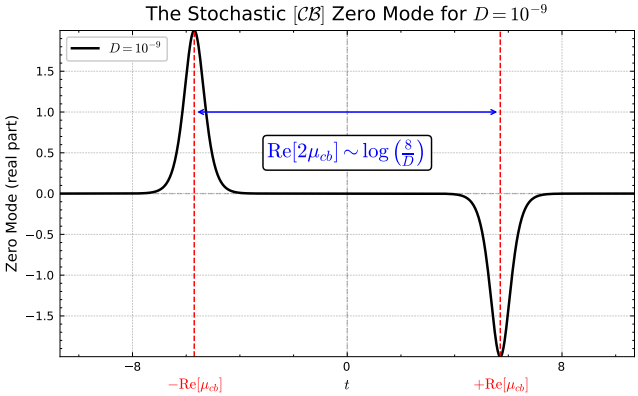

(d) The (normalised) [$\mathcal{CB}$] zero mode for $D = 1 \times 10^{-9}$.

Figure 3.20: *A plot of the fluctuation potential and zero mode in the background of the stochastic complex bounce solution. The plots in the left panel (Fig. 3.20a and Fig. 3.20c) are shown for five different noise strengths D. By contrast, the plots in the right panel (Fig. 3.20b and Fig. 3.20d) are shown at fixed noise strength $D = 1 \times 10^{-9}$, with the parameter $a = 1$.*

3.4.4 Stochastic complex bounce fluctuations and functional determinant

Computing the fluctuation determinant, we find

$$\begin{aligned} \lim_{\mathcal{T}\to\infty} \frac{\det' \hat{\mathcal{M}}_{[\mathcal{CB}]}}{\det \hat{\mathcal{M}}_0} &= -\frac{\langle \dot{z}_{\rm cl} | \dot{z}_{\rm cl} \rangle}{32\beta^2 \omega_{cb}^3 \sinh^2(\omega_{cb}\mu_{cb})} \\ &= +\frac{D}{512 a^8} + \mathcal{O}(D^2). \end{aligned} \tag{3.124}$$

The grave instability in the fluctuation determinant is no longer present. Using the formulation of the path integral under Itô, the escape rate using the $[\mathcal{CB}]$ is found as

$$-|\Gamma_{[\mathcal{CB}]}|\mathcal{T} = -\frac{2a}{\mathrm{e}\sqrt{2\pi}}\exp(-\Delta V/D)\mathcal{T}, \tag{3.125}$$

whereas using Kramers' formula, we should get

$$-|\Gamma_K|\mathcal{T} = -\frac{a}{\pi}\exp(-\Delta V/D)\mathcal{T}. \tag{3.126}$$

Hence, the $[\mathcal{CB}]$ has produced the correct negative sign, but there are some additional unwanted terms in the formula. By looking at the ratio of these answers, we deduce that we have a multiplicative error to resolve,

$$\mathcal{R} = \frac{|\Gamma_{[\mathcal{CB}]}|}{|\Gamma_K|} = \frac{\sqrt{2\pi}}{\mathrm{e}}. \tag{3.127}$$

From a mathematician's perspective, the fact that we have both π and e in the error is exciting and makes one believe there must be a deeper story behind the mistake. At first glance, one may be tempted to think that the $\sqrt{2\pi}$ factor is just a normalisation error (perhaps of the measure or eigenvalues) and that in fact we are only trying to correct a factor of e. However, as we will show, this is not the case; the factors arise together, originating from the same source.

The results so far have been entirely consistent with Section 5 of Dunne *et al.* in [13]. We have reproduced many similar results, but in a stochastic, rather than quantum, setting.

3.5 Quasi-zero modes and the prefactor problem

This error factor, $\mathcal{R}$, is related to the quasi-zero mode (QZM) issue for the $[\mathcal{I}\bar{\mathcal{I}}]$ pairs discussed in Chapter 2. Viewing the $[\mathcal{CB}]$ solution as a correlated instanton-anti-instanton $[\mathcal{I}\bar{\mathcal{I}}]$ pair, care is needed with their interaction. As discussed, $[\mathcal{I}\bar{\mathcal{I}}]$ configurations attract. Let μ_{cb} denote the fixed separation in

the $[\mathcal{CB}]$ solution. If we instead allow the separation to vary, the interaction weakens as the separation grows, and μ_{cb} serves as a collective coordinate. Because the interaction is weak, this direction in configuration space is nearly flat or *pseudo-flat* direction of the $[\mathcal{I}\bar{\mathcal{I}}]$ action. As with the exact zero mode (EZM), a naive Gaussian treatment of this *soft* QZM direction is inaccurate: the associated integral is large and must be handled exactly. We now show how this mistreatment of a non-Gaussian mode in a Gaussian approximation is the source of the error factor.

In the functional integral step of (2.70) we should therefore separate the modes as

$$\lim_{N\to\infty}\prod_{n=0}^{N}\Big\{\int_{\mathbb{R}}\mathrm{d}a_n\,\exp\Big(-\frac{\lambda_n a_n^2}{4D}\Big)\Big\} = \underbrace{\Big[\int_{\mathbb{R}}\mathrm{d}a_0\Big]}_{\text{EZM}}\underbrace{\Big(\int_C I_{\text{QZM}}\Big)}_{\text{QZM}}\cdot\lim_{N\to\infty}\prod_{n=2}^{N}\Big\{\int_{\mathbb{R}}\mathrm{d}a_n\,\exp\Big(-\frac{\lambda_n a_n^2}{4D}\Big)\Big\}, \tag{3.128}$$

where C is a contour that will be fixed later, and standard collective coordinates treat the EZM. The product starts at $n=2$ precisely because the integral over the QZM direction ($n=1$) must be extracted from the infinite ladder of Gaussians and handled independently.

3.5.1 Quasi-zero eigenvalue and eigenfunction

We prove that such a QZM direction exists by relating the $[\mathcal{CB}]$ fluctuation determinant with standard instanton determinants. With zero tilt, the cubic instanton reads $x_I(t) = a\,\tanh\big(a(t-t_c)\big)$. The fluctuation operator is Pöschl–Teller [147],

$$\hat{\mathcal{M}}_{\text{Inst}} = -\frac{\mathrm{d}^2}{\mathrm{d}t^2} + \omega_I^2\big[1 - 2\,\mathrm{sech}^2(at)\big], \tag{3.129}$$

and its determinant ratio with zero mode removed is

$$\lim_{\mathcal{T}\to\infty}\frac{1}{\langle\dot{x}_I|\dot{x}_I\rangle}\frac{\det{}'\,\hat{\mathcal{M}}_{\text{Inst}}}{\det\hat{\mathcal{M}}_0} = \frac{1}{64\,a^5}. \tag{3.130}$$

Having computed the $[\mathcal{CB}]$ fluctuation determinant explicitly, we can relate the two functional determinants as

$$\lim_{\mathcal{T}\to\infty} \frac{1}{\langle \dot{z}_{\rm cl}|\dot{z}_{\rm cl}\rangle} \frac{\det' \hat{\mathcal{M}}_{[\mathcal{CB}]}}{\det \hat{\mathcal{M}}_0} = 8a^2 D \left[\lim_{\mathcal{T}\to\infty} \frac{1}{\langle \dot{x}_I|\dot{x}_I\rangle} \frac{\det' \hat{M}_{\rm Inst}}{\det \hat{M}_0} \right]^2, \tag{3.131}$$

thus, a small eigenvalue is embedded in $\hat{\mathcal{M}}_{[\mathcal{CB}]}$ as $D \to 0$ of order D, indicating the existence of a pseudo-flat direction in the action. The fact that the instanton determinant appears squared reflects the two-instanton composition of the $[\mathcal{CB}]$. The prefactor $8a^2D$ is model-dependent and builds the quasi-eigenvalue. Computing the inner products to leading order numerically,

$$\lambda_D = 8a^2 D \frac{\langle \dot{z}_{\rm cl}|\dot{z}_{\rm cl}\rangle}{[\langle \dot{x}_I|\dot{x}_I\rangle]^2} \approx \frac{12D}{a} \qquad (D \to 0), \tag{3.132}$$

and we see explicitly the $\mathcal{O}(D)$ softness. An analytical derivation, inspired by conversations with Professor Steve Fitzgerald on this quasi-eigenvalue, is presented in the Appendix C.1 to confirm the numerical findings. With this, the Gaussian integral over this mode is

$$\int \mathrm{d}a_1 \, \exp\left(-\frac{\lambda_D}{4D} a_1^2\right) = \sqrt{\frac{\pi a}{3}}. \tag{3.133}$$

If we also take the QZM factor out from the fluctuation determinant,

$$\det'' \hat{\mathcal{M}}_{[\mathcal{CB}]} = \frac{\det' \hat{\mathcal{M}}_{[\mathcal{CB}]}}{\lambda_D}, \tag{3.134}$$

we would find to leading order

$$\lim_{\mathcal{T}\to\infty} \frac{1}{\langle \dot{z}_{\rm cl}|\dot{z}_{\rm cl}\rangle} \frac{\det'' \hat{\mathcal{M}}_{[\mathcal{CB}]}}{\det \hat{\mathcal{M}}_0} = \frac{a}{12D} \cdot \frac{D}{512a^8} = \frac{1}{6144a^7}, \tag{3.135}$$

so the QZM-stripped determinant is independent of D. Hence, softness is solely a result of this QZM. We can also deduce data about the structure of the quasi-eigenfunction. An approximate form of the quasi-eigenfunction is given by taking the derivative of the classical solution with respect to the collective coordinate μ_{cb}. Unlike the exact zero mode, the prefactor contains μ_{cb}, so the derivative picks

up an additional term by the product rule,

$$
\begin{aligned}
y_{\mathrm{QZM}}(t) \;&=\; \partial_{\mu_{cb}} z_{\mathrm{cl}}(t) \\
&= \;+\; \frac{\omega_{cb}}{4}\,(z_{\mathrm{cr}} - z_{\mathrm{T}})\,\operatorname{csch}^2\!\Big(\frac{\omega_{cb}\,\mu_{cb}}{2}\Big)\left[\tanh\!\Big(\frac{\omega_{cb}}{2}\big(t - t_c + \mu_{cb}\big)\Big) - \tanh\!\Big(\frac{\omega_{cb}}{2}\big(t - t_c - \mu_{cb}\big)\Big)\right] \\
&\quad -\; \frac{\omega_{cb}}{4}\,(z_{\mathrm{cr}} - z_{\mathrm{T}})\,\coth\!\Big(\frac{\omega_{cb}\,\mu_{cb}}{2}\Big)\left[\operatorname{sech}^2\!\Big(\frac{\omega_{cb}}{2}\big(t - t_c + \mu_{cb}\big)\Big) + \operatorname{sech}^2\!\Big(\frac{\omega_{cb}}{2}\big(t - t_c - \mu_{cb}\big)\Big)\right].
\end{aligned}
\tag{3.136}
$$

It is 'quasi' in the sense that it is not an exact solution to the eigenvalue problem,

$$
\hat{\mathcal{M}}_{[\mathcal{CB}]}\, y_{\mathrm{QZM}} \;=\; \lambda_D\, y_{\mathrm{QZM}} \;+\; (\text{small residual})\,, \tag{3.137}
$$

with the residual suppressed by the exponentially small overlap of the two wells, $\propto\, e^{-\omega_{cb}\mu_{cb}}$. Consequently, if one attempted to solve the eigenvalue problem y_{QZM}, one would obtain an effective t-dependent eigenvalue; the correct scalar eigenvalue is read using the Rayleigh-Ritz formula [41, 152] (as used in the Appendix C.1). Using parity, a computation can show y_{QZM} is orthogonal to the EZM,

$$
\big\langle \partial_{\mu_{cb}} z_{\mathrm{cl}} \;\big|\; \partial_{t_c} z_{\mathrm{cl}} \big\rangle = 0, \tag{3.138}
$$

for the centred bounce ($t_c = 0$) and $\langle y_{\mathrm{QZM}} \mid y_{\mathrm{QZM}} \rangle = 8a^3/3 + \cdots$.

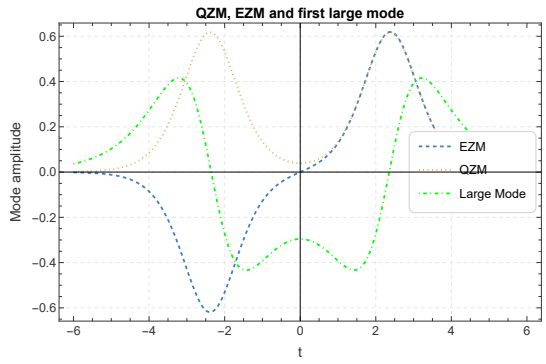

(a) First 3 eigenmodes.

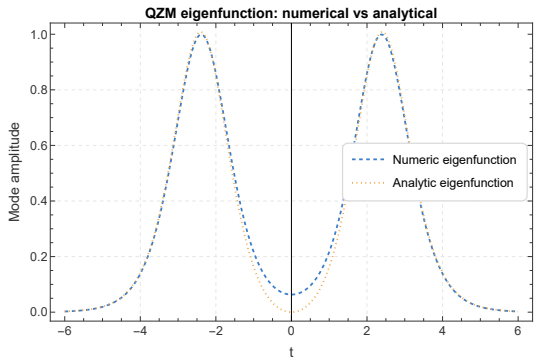

(b) QZM eigenfunction comparison.

Figure 3.21: *The first three eigenmodes exhibit an exact zero mode, a quasi-zero mode, and then a significantly larger mode, confirming the structure we expected. Taking the derivative of the classical solution with respect to μ_{cb} gives a very good approximate solution, only deviating from the true curve (Figure (b)) around a small neighbourhood about the origin $(t-\delta, t+\delta)$.*

3.5.2 Origin of the $\sqrt{2\pi}/\mathrm{e}$ factor

To model the QZM direction and set up the correct integral, we use the large separation $[\mathcal{I}\bar{\mathcal{I}}]$ ansatz

$$z^{\text{ansatz}}_{[\mathcal{I}\bar{\mathcal{I}}]}(t,\theta) = -a - a\,\tanh\Big[\frac{\omega^{\text{ansatz}}_{\mathcal{I}\bar{\mathcal{I}}}}{2}\Big(t-\frac{\theta}{2}\Big)\Big] + a\,\tanh\Big[\frac{\omega^{\text{ansatz}}_{\mathcal{I}\bar{\mathcal{I}}}}{2}\Big(t+\frac{\theta}{2}\Big)\Big], \tag{3.139}$$

with separation θ. This is an approximation to our exact $[\mathcal{C}\mathcal{B}]$ solution. Inserting this expression into the action and retaining leading order terms yields the interaction potential

$$\mathcal{V}_-(\theta) = -32\,a^3\exp(-\omega_{cb}\theta) + 4D\,\omega_{cb}\,\theta, \tag{3.140}$$

where we have matched $\omega_{cb} = \omega^{\text{ansatz}}_{\mathcal{I}\bar{\mathcal{I}}}$. This potential is purely attractive for $[\mathcal{I}\bar{\mathcal{I}}]$ sectors. For $[\mathcal{I}\mathcal{I}]$ pairs, the interaction action is repulsive and free from divergences. The naive (Gaussian) QZM integral therefore has the form

$$I_{\text{Gauss}} = \int_{\mathbb{R}} \mathrm{d}\theta\ \exp\Big(-\frac{\mathcal{V}_-(\theta)}{4D}\Big), \tag{3.141}$$

and the interaction potential has a complex critical point,

$$\mathcal{V}_-'(\theta_{\text{crit}}) = 0 \quad \Longrightarrow \quad \theta_{\text{crit}} = \frac{1}{\omega_{cb}}\Big[\ln\Big(\frac{8a^3}{D}\Big) \pm i\pi\Big], \tag{3.142}$$

which matches the leading $[\mathcal{CB}]$ separation μ_{cb}. Following the MOSD, we expand the interaction potential about the critical point,

$$\mathcal{V}_-(\theta) \approx \mathcal{V}_-(\theta_{\text{crit}}) + \frac{1}{2}\,\mathcal{V}_-''(\theta_{\text{crit}})\,(\theta - \theta_{\text{crit}})^2, \tag{3.143}$$

and one finds

$$\mathcal{V}_-(\theta_{\text{crit}}) = 4D\Big[1 + \ln\Big(\frac{8a^3}{D}\Big) \pm i\pi\Big], \qquad \mathcal{V}_-''(\theta_{\text{crit}}) = 4D\,\omega_{cb}^2. \tag{3.144}$$

Changing variable to $u = \omega_{cb}\theta$ so that $\mathrm{d}u = \omega_{cb}\,\mathrm{d}\theta$ and letting $\omega = \omega_{cb}$, the Gaussian integral gives

$$\begin{aligned} I_{\text{Gauss}} &= \frac{1}{\omega}\int_{\mathbb{R}} \mathrm{d}(\omega\theta)\ \exp\Big(-\frac{\mathcal{V}_-(\theta_{\text{crit}})}{4D}\Big)\ \exp\Big(-\frac{1}{8D}\mathcal{V}_-''(\theta_{\text{crit}})\,(\theta-\theta_{\text{crit}})^2\Big) \\ &= \exp(\pm i\pi)\,\frac{1}{\omega}\,\underbrace{\frac{\sqrt{2\pi}}{e}}_{\text{Stirling}}\,\Big(\frac{D}{8a^3}\Big). \end{aligned} \tag{3.145}$$

The frequency scale is a consequence of the measure change $\mathrm{d}\theta = \mathrm{d}(\omega\theta)/\omega$ and will later cancel an identical factor. The Stirling factor $\sqrt{2\pi}/e$ is the "peculiar error factor" $\mathcal{R}$: it arises solely from treating the QZM by a naive Gaussian on an incorrect contour. The cure is to evaluate the QZM integral *exactly* on the appropriate Lefschetz contour C determined by the PL gradient flow. In the next subsection, we justify the QZM isolation by clarifying the measure factorisation in (3.128) and specify the contour C; doing so removes this Stirling factor.

3.6 Picard–Lefschetz resolution of the quasi-zero mode

Our aim is not to survey Stokes phenomena and Morse theory (see, e.g., [129, 176]), but to implement a method that allows for a precise factorisation of the measure that isolates the non-Gaussian QZM and fixes its integration cycle, similar to the work presented on the quasi-zero mode integral in [71, 72] and the work by Tanizaki [95, 169, 171]. Picard–Lefschetz (PL) theory provides exactly this: a canonical deformation of the original real cycle to a sum of "Lefschetz thimbles" on which the phase is stationary and the integral is convergent, together with a geometric interpretation of the $\pm i\pi$ phase that appears in the BZJ continuation.

We apply the thimble path integral decomposition as in [12, 15, 71, 169, 170, 184] to the stochastic path integral; to our knowledge, this is the first explicit treatment in the stochastic context. We begin by complexifying all components of the path integral, $x(t) \mapsto z(t) \in \mathbb{C}$ and the stochastic action is promoted to a holomorphic function. $\mathcal{S}[z]$. Using the PL theory framework, the stochastic path integral may be written as

$$P \;=\; \int_{\gamma} \mathcal{D}z \;\exp\!\left(-\frac{\mathcal{S}[z]}{4D}\right) \;=\; \sum_{\sigma\in\Sigma} n_\sigma \, P_\sigma, \tag{3.146}$$

where Σ is the set of critical points of $\mathcal{S}$, and $n_\sigma \in \mathbb{Z}$ are the intersection numbers that encode how the original real integration cycle decomposes into thimbles. We now focus on the global cycle γ. Assuming for the moment no exact/near-zero directions, each saddle contributes

$$P_\sigma \;=\; \int_{\mathcal{J}_\sigma} \mathcal{D}z \;\exp\!\left(-\frac{\mathcal{S}[z]}{4D}\right). \tag{3.147}$$

3.6.1 Thimble decomposition and flow equations

We compute $\mathcal{J}_\sigma$ in (3.147) by the antiholomorphic *upward* flow with flow time u:

$$\frac{\partial z}{\partial u} = +\,\overline{\frac{\delta \mathcal{S}}{\delta z}} = +\Big(2\,\overline{z}''(t) + \partial_{\overline{z}}\overline{\mathfrak{U}}\Big), \qquad \frac{\partial \overline{z}}{\partial u} = +\,\frac{\delta \mathcal{S}}{\delta z} = +\Big(2\,z''(t) + \partial_z \mathfrak{U}\Big), \tag{3.148}$$

with the convention that the thimble consists of points whose flow originates at the critical point as $u \to -\infty$: if $\delta\mathcal{S}/\delta z|_{z_\sigma} = 0$, then $\lim_{u\to-\infty} z(\cdot, u) = z_\sigma$. Accordingly,

$$\mathcal{J}_\sigma := \big\{\, z(\cdot,0) \mid z(\cdot,u) \text{ solves (3.148) and } \lim_{u\to-\infty} z(\cdot,u) = z_\sigma \,\big\}. \tag{3.149}$$

Furthermore, the dual thimbles are defined by (flow time reversal)

$$\mathcal{K}_\sigma := \big\{\, z(\cdot,0) \mid \lim_{u\to+\infty} z(\cdot,u) = z_\sigma \,\big\}. \tag{3.150}$$

Along $\mathcal{J}_\sigma$ the imaginary part of the action is constant and $\mathrm{Re}\,\mathcal{S}$ is *increasing* with u (upward flow):

$$\frac{d}{du}\,\mathrm{Re}\,\mathcal{S} \;=\; \left\|\frac{\delta\mathcal{S}}{\delta z}\right\|^2 \;\geq\; 0, \qquad \frac{d}{du}\,\mathrm{Im}\,\mathcal{S} \;=\; 0. \tag{3.151}$$

This ensures a good convergence behaviour. The original integration cycle can be expressed as a sum over the thimbles coupled with an intersection number $\mathcal{C}_\mathbb{R} = \sum_\sigma n_\sigma\, \mathcal{J}_\sigma$, and the full stochastic path integral is decomposed into a sum over the thimbles,

$$P \;=\; \sum_{\sigma\in\Sigma} n_\sigma \int_{\mathcal{J}_\sigma} \mathcal{D}z\; \exp\!\left(-\frac{\mathcal{S}[z]}{4D}\right). \tag{3.152}$$

The intersection coefficients n_σ are determined by the number of times the dual thimble intersects the original integration cycle. Therefore, it is the geometry of the dual thimbles that dictates whether a saddle contributes to the stochastic path integral. We plot the thimble geometry for our QZM integration example in Fig. 3.22 where the intersection coefficients will become clear.

To understand the structure of the cycle, we only need the local structure near the stochastic complex bounce z_{cl} solution. Around z_{cl} the quadratic form defined by the fluctuation operator $\hat{\mathcal{M}}_{[\mathcal{CB}]}$ decouples into: (i) the exact zero mode (translation), (ii) a single soft quasi-mode (the separation QZM), and (iii)

a family of hard Gaussian modes. Consequently, the functional measure factorises as

$$\mathcal{D}z \;\simeq\; (\mathrm{d}t_c)\,(\mathrm{d}\theta)\prod_{n\geq 2}\mathrm{d}a_n, \quad \mathcal{J}\simeq \mathcal{J}_{\mathrm{EZM}}\times\mathcal{J}_{\mathrm{QZM}}\times\prod_{n\geq 2}\mathbb{R} \tag{3.153}$$

and the integration cycle decomposes accordingly: only the QZM slice is deformed to its Lefschetz thimble contour, while the EZM and hard Gaussians remain on their real cycles. This fact is also given in (2.9) of [15]. Crucially, the PL theory provides the exact one-dimensional contour for the QZM direction beyond the Gaussian approximation, and we will integrate the interaction potential factor exactly along that contour.

3.6.2 The quasi-zero mode contour and the $\pm i\pi$ phase

To make the geometry of the thimbles clear, we introduce a regulator ν to the interaction potential and take the limits above and below $\nu \to 0^{\pm}$. This will be seen as analogous to taking the limit $D \to D\exp(\pm i\pi)$. The interaction potential deformed by ν is

$$\mathcal{V}_{-}(\theta,\nu) = -32a^3\mathrm{e}^{-\omega\theta-i\nu} + 4D\,\omega\,\theta. \tag{3.154}$$

We shall work with

$$S_\nu(\theta) = \frac{1}{4D}\mathcal{V}_{-}(\theta,\nu) = -\frac{8a^3}{D}\mathrm{e}^{-\omega\theta-i\nu} + \omega\theta. \tag{3.155}$$

Following the PL gradient flow equations (3.151), we find that

$$\frac{\mathrm{d}\theta}{\mathrm{du}} = +\overline{\frac{\partial S_\nu(\theta)}{\partial\theta}} = \frac{8a^3\omega}{D}\mathrm{e}^{-\omega\bar{\theta}+i\nu} + \omega. \tag{3.156}$$

Allowing θ to take complex values, we let $\theta = x + iy$ and find the following system of coupled differential equations,

$$\frac{\mathrm{d}x}{\mathrm{d}u} = \frac{8a^3\omega}{D}\mathrm{e}^{-\omega x}\cos(\omega y+\nu) + \omega, \quad \frac{\mathrm{d}y}{\mathrm{d}u} = \frac{8a^3\omega}{D}\mathrm{e}^{-\omega x}\sin(\omega y+\nu). \tag{3.157}$$

This gives an ODE for x and y,

$$\frac{\mathrm{d}x}{\mathrm{d}y} = \cot(\omega y + \nu) + \frac{D\mathrm{e}^{\omega x}}{8a^3\omega}\sin(\omega y + \nu). \tag{3.158}$$

Using the fact that the imaginary part of the thimble is constant by construction (stationary phase), and letting K be such a constant, one finds

$$K - \omega y = \frac{8a^3\omega}{D}\mathrm{e}^{-\omega x}\sin(\omega y + \nu). \tag{3.159}$$

Using this result, we can integrate (3.158) to find the general form of the dual thimbles as

$$x(y) = \frac{1}{\omega}\log\left(A\frac{\sin(\omega y + \nu)}{K - \omega y}\right). \tag{3.160}$$

It will be convenient to clearly distinguish between the two saddles by introducing a saddle tracking parameter, $\sigma = \{0, +1\}$. Then,

$$\theta_\sigma = \frac{1}{\omega}\left[\ln\left(\frac{8a^3}{D}\right) + (2\sigma - 1)i\pi - i\nu\right]. \tag{3.161}$$

One finds

$$K = K_\sigma = -\nu - (2\sigma - 1)\pi, \quad A = 8a^3/D, \tag{3.162}$$

hence we can relate the real and imaginary part of the dual thimble through the equation[7]

$$x(y) = \frac{1}{\omega}\log\left(\frac{8a^3}{D}\frac{\sin(\omega y + b_\sigma)}{\omega y + b_\sigma}\right), \quad b_\sigma = -\nu - (2\sigma - 1)\pi. \tag{3.163}$$

This matches Equation (4.34) in [71], but reproduced in the stochastic context. To find the thimbles $\mathcal{J}_\sigma$ we impose $\mathrm{Im}\,\mathcal{V}_-(\theta) = \mathrm{Im}\,\mathcal{V}_-(\theta_{\mathrm{crit}}) = \pm 4D\pi$ giving

$$32a^3 e^{-\omega\theta_R}\sin(\omega\theta_I) + 4D\omega\,\theta_I = \pm 4D\pi \quad \Longrightarrow \quad \theta_I = \pm\frac{\pi}{\omega}, \qquad \theta_R \in \mathbb{R}, \tag{3.164}$$

[7] Use the fact that $\sin(\omega y + \nu) = -\sin(\omega y + \nu + (2\sigma - 1)\pi)$.

so the QZM thimble is the horizontal line

$$\mathcal{J}_\sigma = \mathbb{R} \pm i\,\frac{\pi}{\omega}. \tag{3.165}$$

3.6.3 Exact quasi-zero mode integral and recovery of the Kramers prefactor

With $\xi = e^{-\omega\theta}$,

$$I_{\mathrm{QZM}} = \int_{\mathcal{J}_\sigma} \mathrm{d}\theta\ \exp\Big(-\frac{\mathcal{V}_-(\theta)}{4D}\Big) = \frac{1}{\omega}\, e^{\pm i\pi} \int_0^\infty \mathrm{d}\xi\ e^{-(8a^3/D)\,\xi} = \frac{e^{\pm i\pi}}{\omega}\,\Big(\frac{D}{8a^3}\Big)\Gamma(1), \tag{3.166}$$

where the sign in the exponent $\exp(\pm i\pi)$ depends on the saddle we choose. This exact thimble evaluation replaces the naive Gaussian (which yields the Stirling remnant $\sqrt{2\pi}/e$) and is the only non-trivial deformation we need: the rest of the modes stay on their real cycles.

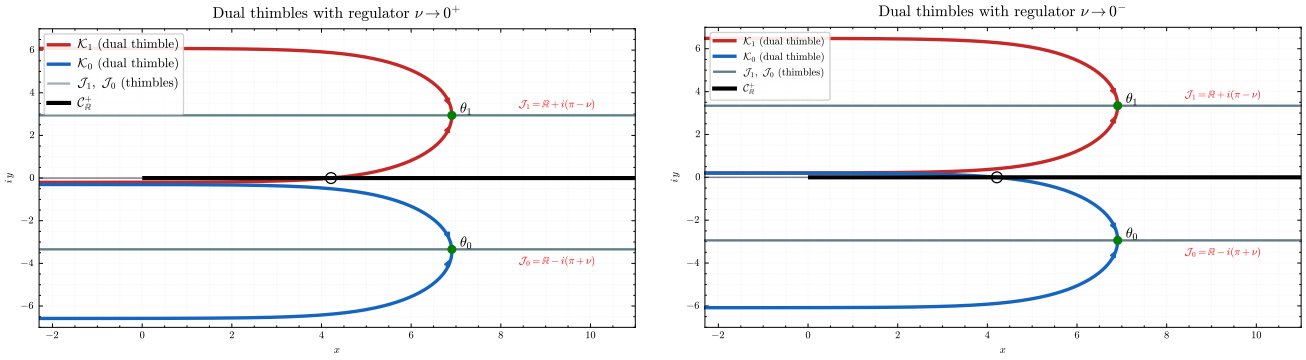

(a) *Taking the limit above.* (b) *Taking the limit below.*

Figure 3.22: Plotting the thimbles $\mathcal{J}_\sigma$ and the dual thimbles $\mathcal{K}_\sigma$.

The two horizontal thimbles are complex conjugates and enter with equal intersection number for our boundary data; equivalently, one may work with a single real integral and keep the overall $e^{\pm i\pi}$ phase as in (3.166). Compared with the Gaussian result $I_{\mathrm{Gauss}} = \frac{e^{\pm i\pi}}{\omega}\,(\sqrt{2\pi}/e)\,(D/8a^3)$ we find

$$\frac{I_{\mathrm{Gauss}}}{I_{\mathrm{QZM}}} = \frac{\sqrt{2\pi}/e}{\Gamma(1)} = \frac{\sqrt{2\pi}}{e}\,, \tag{3.167}$$

identifying the "peculiar error factor" as nothing but Stirling's approximation sneaking in from a naively chosen contour. This matches the work in [14, 71] and we see that the PL theory supplies the correct contour $\mathcal{J}_\sigma$ and removes $\mathcal{R}$ *exactly*. Putting everything together, the path integral about the stochastic complex bounce splits as

$$\int_{\mathbb{R}} \mathcal{D}x\, e^{-\mathcal{S}[x]/(4D)} = \sum_{\sigma\in\Sigma} n_\sigma \Big[\int_{\mathbb{R}} \mathrm{d}t_c\Big] \Big[\underbrace{\int_{\mathcal{J}_\sigma} \mathrm{d}\theta\, e^{-\mathcal{V}_-(\theta)/(4D)}}_{\text{QZM on thimble}}\Big] \Big[\prod_{n\geq 2}\int_{\mathbb{R}} \mathrm{d}a_n\, e^{-\lambda_n a_n^2/(4D)}\Big], \tag{3.168}$$

i.e., only the QZM factor is deformed to its Lefschetz thimble while the EZM and orthogonal Gaussian factors stay on the real axis. No poles are crossed in our problem, so there are no residue contributions. Reading off Fig. 3.22, we see for $\nu \to 0^+$, the intersection numbers are $(n_0, n_1) = (0, 1)$ and for $\nu \to 0^-$, the intersection numbers are $(n_0, n_1) = (1, 0)$. This is the PL decomposition of the stochastic path integral that fixes the QZM contour.

We conclude that $\pm i\pi$ in (3.166) is the geometric avatar of the BZJ phase ambiguity: it simply records which of the two horizontal thimbles $\mathbb{R} \pm i\pi/\omega$ contributes.

3.7 Itô corrections and a stochastic real and complex bounce dictionary

Recall that the main ingredients for the escape rate formula using the $[\mathcal{CB}]$ under Itô is given informally by

$$-|\Gamma_{\text{Ito}}| = \exp(-\mathcal{S}'[z_{\text{cl}}]/(4D)) \times (\text{fluctuation operator})^{-\frac{1}{2}} \times \frac{1}{\sqrt{4\pi D}}, \tag{3.169}$$

where $'$ in the action indicates the removal of energy divergence $-H\mathcal{T}$, the fluctuation operator is assumed to have the EZM removed and the $1/\sqrt{4\pi D}$ factor is from a length scale from smearing. Unlike when deriving the escape rate traditionally using Stratonovich calculus, the Itô framework gives an escape rate that has a non-terminating expansion in D. Here, we have an exact formula (when

$\mathcal{T} \to \infty$) for the stochastic bounce action and fluctuation determinant that are coupled to D. If one were to expand these quantities in small powers of D, one would find the series

$$\Gamma_{\text{Ito}} = \left[\frac{a}{\pi} + \cdots\right] \exp\left(-\Delta V/D + 7D/8a^3 + \cdots\right). \tag{3.170}$$

Full equivalence between Itô and Stratonovich is at the level of the exact path integral, i.e., if we could sum everything. However, to leading order under the weak-noise limit, these frameworks agree. The additional terms generated in the Itô case may be tied to a more global complex analysis framework called *resurgence*. For this thesis, we do not concern ourselves with the additional corrections and work strictly to leading order.

3.7.1 Comparing the stochastic real bounce and stochastic complex bounce

The stochastic $[\mathcal{RB}]$ sector on the real contour has a divergent quasi-zero mode. Instead of doing a $D \to -D$ operation, Picard-Lefschetz theory keeps $D > 0$ and instead deforms the contour to the Lefschetz thimble of the stochastic $[\mathcal{CB}]$. In the QZM variable θ this is the horizontal extension and vertical translation $\theta \in [0, \infty) \ \to \ [-\infty, \infty) \pm i\pi/\omega$.

So, instead of following the $[\mathcal{RB}]$ and BZJ procedure, we follow the $[\mathcal{CB}]$ with the contour chosen by the PL theory. This explains why the $[\mathcal{CB}]$ data matches the $[\mathcal{RB}]$ data and why they are related through the algebraic substitution $D \mapsto -D$.

To illustrate this relationship, note that the fluctuation determinant of the $[\mathcal{CB}]$ is $+D/512a^8$ compared to the fluctuation determinant of the real bounce that is $-D/512a^8$. This algebraic relation persists for higher order D. We also see that we do not have an additional phase factor (Maslov-Morse index). The same relation holds between the separations μ_{rb} and μ_{cb}, the frequencies ω_{rb} vs ω_{cb}, the actions, and so on. The factor $\pm i\pi$ emerges from the branch of the logarithmic term.

In short, the $[\mathcal{CB}]$ and PL theory combination refines the analytic continuation programme of the BZJ

method and tells us that for $[\mathcal{I}\bar{\mathcal{I}}]$-type configurations, we should deform the contour of the real axis. This analysis is consistent with the double-well potential analysis of Dunne *et al.* in [12], but the context is within the Markovian white-noise setting and not quantum field theory.

3.8 Using thimble integration to resolve the error factor for more general cases

The exact integral presented in 3.6.3 is a very special case, but the integration method extends into more general cases. As established, when studying $[\mathcal{I}\bar{\mathcal{I}}]$-type configurations, a generic form of the interaction potential is

$$\mathcal{V}_{\text{int}} = -Aa^3 \exp(-\omega\theta) + \mathcal{B}4D\omega\theta, \tag{3.171}$$

for $A, \mathcal{B} > 0$. Provided $a > 0$, the first term in the interaction potential is strictly negative and represents that the induced interaction between an $[\mathcal{I}\bar{\mathcal{I}}]$ pair is attractive. The constant $\mathcal{B}$ will depend on the form of the second derivative of the original potential V''. Now, let us compute the integral naively using a Gaussian approximation. The Gaussian integral evaluates to

$$I_{\text{naive}} = \exp(\pm\mathcal{B}i\pi) \cdot \left(\frac{4\mathcal{B}D}{Aa^3\text{e}}\right)^{\mathcal{B}} \cdot \sqrt{\frac{2\pi}{\mathcal{B}}}. \tag{3.172}$$

Comparing with the exact integral over the thimble,

$$I_{\text{exact}} = \exp(\pm\mathcal{B}i\pi) \cdot \left(\frac{4D}{Aa^3}\right)^{\mathcal{B}} \cdot \Gamma(\mathcal{B}), \tag{3.173}$$

gives a clear visual of the rate correction factor, $\mathcal{R}^{-1}$. Upon computing the ratio of the exact quantity to the approximate value,

$$\mathcal{R}^{-1} = I_{\text{exact}}/I_{\text{naive}} = \frac{\Gamma(\mathcal{B})}{\left(\frac{\mathcal{B}}{\text{e}}\right)^{\mathcal{B}}\sqrt{2\pi/\mathcal{B}}}. \tag{3.174}$$

Stirling's approximation for the gamma function can be expressed as

$$\Gamma(z) = \sqrt{\frac{2\pi}{z}} \left(\frac{z}{\mathrm{e}}\right)^z \left(1 + O\left(\frac{1}{z}\right)\right). \tag{3.175}$$

It is clear that, upon replacing $z \mapsto \mathcal{B}$, the error ratio is precisely the difference between Stirling's asymptotics for the Gamma function and the exact value of the Gamma function. In the stochastic cubic potential, we found the simplest case where $\mathcal{B} = 1$, giving the $\sqrt{2\pi}/\mathrm{e}$ error.

Note that this argument is not restricted to $[\mathcal{I}\bar{\mathcal{I}}]$ configurations where the interaction potential (3.171) is attractive. In fact, if the interaction potential is repulsive, as it is for pairs $[\mathcal{I}\mathcal{I}]$, the same error factor would emerge. The difference is that there would be no phase factors of the form $\exp(\pm\mathcal{B}i\pi)$ in either integral expression, but these factors cancel each other anyway.

3.9 Using the Stratonovich approach

We can follow (2.129) and recover Kramers' rate using the Stratonovich framework, so long as we integrate over the thimble exactly. Under the Stratonovich formulation, this leads to formally solving

$$P(-a, +\mathcal{T}/2 \mid -a, -\mathcal{T}/2) \simeq P_0(\mathcal{T}) \int_{-\mathcal{T}/2}^{+\mathcal{T}/2} \mathrm{d}t_u \int_{t_u}^{+\mathcal{T}/2} \mathrm{d}t_d \, \exp\Big(-\frac{\mathcal{S}[x_{\mathrm{cl}}]}{4D}\Big) \frac{J_{\mathrm{OM}}[x_{\mathrm{cl}}]}{J_{\mathrm{OM}}[x_0]} \times \sqrt{\frac{\langle \dot{x}_u \mid \dot{x}_u \rangle}{4\pi D}} \sqrt{\frac{\langle \dot{x}_d \mid \dot{x}_d \rangle}{4\pi D}} \left(\frac{\det{}'' \hat{\mathcal{M}}}{\det \hat{\mathcal{M}}_0}\right)^{-1/2}. \tag{3.176}$$

Instead of studying a complex bounce solution, we study traditional instanton excursions,

$$x_I(t) = a \tanh\left(a\left(t - t_c \pm \frac{\theta}{2}\right)\right). \tag{3.177}$$

The instanton and anti-instanton trajectories have the same fluctuation determinant, giving the "instanton-squared" determinant. P_0 cancels the smearing factor $\sqrt{\pi D/a}$, the Onsager–Machlup Jacobian $J_{\mathrm{OM}}[x_0]$

and the $H\mathcal{T}$ term, meaning that we can simplify (3.176) to

$$P(-a,+\mathcal{T}/2 \mid -a,-\mathcal{T}/2) \simeq \frac{1}{4\pi D}\int_{-\mathcal{T}/2}^{+\mathcal{T}/2} \mathrm{d}t_u \int_{t_u}^{+\mathcal{T}/2} \mathrm{d}t_d \, \exp\Big(-\frac{\mathcal{S}[x_{\mathrm{cl}}]}{4D}\Big)\, J_{\text{OM}}[x_{\mathrm{cl}}] \times \left(\frac{\det' \hat{\mathcal{M}}_I}{\det \hat{\mathcal{M}}_0}\right)^{-1} \mathcal{T}$$
$$= \frac{\mathcal{T}}{4\pi D}\left(\frac{\det' \hat{\mathcal{M}}_I}{\det \hat{\mathcal{M}}_0}\right)^{-1} \left[\exp(-2\mathcal{S}_I) \int_{\mathcal{J}_\theta} \exp(-\mathcal{V}_-(\theta)/(4D))\right]. \quad (3.178)$$

The instanton determinant factor is $\det = 64a^5$, twice the instanton action gives the Boltzmann factor $\exp(-\Delta V/D)$, and the thimble integral over $\mathbb{R} \pm i\pi$ gives $-D/8a^3$. Hence, the sector contribution is

$$P(-a,+\mathcal{T}/2 \mid -a,-\mathcal{T}/2)_{[\mathcal{I}\bar{\mathcal{I}}]} = -\frac{a}{\pi}\exp(-\Delta V/D)\mathcal{T}, \quad (3.179)$$

recovering Kramers' rate cleanly with no $D \to -D$ tricks involved. The exact integral on the slice of the thimble in the QZM direction reproduces the $[\mathcal{I}\bar{\mathcal{I}}]$ escape rate as in [117] but is now on the same footing as the calculation $[\mathcal{I}\mathcal{I}]$. The Stratonovich scheme gives no additional corrections to the escape rate as there is no mixing of perturbation orders.

A natural question to ask is, are there any other discretisation schemes that could be chosen? Within the class of additive-noise discretisations captured by an effective tilt, consistency of the weak-noise saddle expansion forces $\varepsilon \in \{0, D\}$, corresponding to Stratonovich/Itô.

3.10 Tilt rigidity and why the discretisation is not a dial

We now allow an *a priori* arbitrary tilt ε in the Onsager–Machlup functional and track its impact through the saddle, Jacobian, and QZM thimble integral. Consistency of the weak-noise asymptotics forces ε onto the two canonical choices, recovering precisely the Itô and Stratonovich discretisations.

Let us pick $\varepsilon > 0$. Then, the Onsager–Machlup Jacobian takes the form

$$J_{\text{OM}}[x,\varepsilon] \;=\; \exp\Big[\Big(\frac{1}{2}-\frac{\varepsilon}{2D}\Big)\int_{-\mathcal{T}/2}^{+\mathcal{T}/2}\mathrm{d}t\;\; V''(x(t))\Big], \tag{3.180}$$

while the action functional is

$$\mathcal{S}[x,\varepsilon] = \int_{-\mathcal{T}/2}^{+\mathcal{T}/2}\mathrm{d}t\;\; \big[\dot{x}^2 + V'(x)^2 - 2\,\varepsilon\, V''(x)\big]. \tag{3.181}$$

Then, we can keep the results for the fluctuation determinant and action functional as already obtained, but replace $D \mapsto \varepsilon$. However, the denominator $-4D$ must remain in terms of D. Instead of the Onsager–Machlup Jacobian being unity, it now has a more complicated form. Using the classical solution (in terms of ε), note that $V''(x) = -2x$, so we can integrate the classical solution directly to find the Onsager–Machlup Jacobian. One finds,

$$\log J_{\text{OM}} \;=\; -4\,i\left(\frac{\varepsilon}{D}-1\right)\arctan\left(\frac{C-1}{\sqrt{1-C^2}}\tanh\frac{\omega\,\mathcal{T}}{4}\right), \tag{3.182}$$

where $C \in i\mathbb{R}$ and, to leading order, $C \sim i\sqrt{2a^3/\varepsilon}$. Then, Kramers' rate has the form

$$-|\Gamma|\mathcal{T} \;\approx\; \frac{\mathcal{T}}{\sqrt{4\pi D}}\left[\frac{\det'\hat{\mathcal{M}}}{\det\hat{\mathcal{M}}_0}\right]^{-\frac{1}{2}} J_{\text{OM}}[x,\varepsilon]\;\exp(-\mathcal{S}[x,\varepsilon]/(4D))\times\text{error correction}. \tag{3.183}$$

Now we can look at the asymptotics of each term and build our general Kramers' rate expression. We find,

$$\lim_{\mathcal{T}\to\infty}\frac{1}{\langle\dot{z}_{\text{cl}}|\dot{z}_{\text{cl}}\rangle}\Big[\frac{\det'\,\hat{\mathcal{M}}}{\det\,\hat{\mathcal{M}}_0}\Big] = \frac{\varepsilon}{512\,a^8}+\cdots. \tag{3.184}$$

$$\log J_{\text{OM}} \;=\; \big[\mp i\pi + \log\big(\varepsilon/8a^3\big)\big]\,(1-\varepsilon/D)+\cdots, \tag{3.185}$$

and

$$-\mathcal{S}/(4D) \;=\; -\Delta V/D + \frac{\varepsilon}{D}\,[-1\mp i\pi - \log\big(\varepsilon/8a^3\big)]+\cdots. \tag{3.186}$$

The integral over the thimble is now

$$I_{\mathrm{QZM}} = \frac{1}{\omega}\int_{\mathcal{J}_\sigma} \mathrm{d}(\,\omega\theta)\ \exp\Big(-\mathcal{V}_-/(4D)\Big) = \frac{\exp(\pm i\pi\varepsilon/D)}{\omega}\left(\frac{D}{8a^3}\right)^{\varepsilon/D}\Gamma(\varepsilon/D), \tag{3.187}$$

meaning that the error factor using the results of § 3.8 is

$$\mathrm{err}(\varepsilon/D) = \frac{\Gamma(\varepsilon/D)}{\left(\dfrac{\varepsilon}{\mathrm{e}D}\right)^{\varepsilon/D}\sqrt{\dfrac{2\pi D}{\varepsilon}}}. \tag{3.188}$$

If we momentarily ignore the Onsager–Machlup Jacobian factor, we would find

$$\Gamma_{\varepsilon} = \frac{a}{\pi}\left(\frac{D}{8a^3}\right)^{\varepsilon/D-1}\Gamma\left(\frac{\varepsilon}{D}\right)\exp(-\Delta V/D)\ \exp(\mp i\pi\varepsilon/D). \tag{3.189}$$

The phase factor $\exp(\mp i\pi\varepsilon/D)$ contributes to the overall sign. The Onsager–Machlup Jacobian contains this factor of opposite sign and cancels it perfectly, but leaves behind a definite $\exp(\mp i\pi) = -1$ term. Adding the Jacobian asymptotics, we arrive at the most general form of Kramers' rate using the complex saddle approach,

$$\Gamma_{\varepsilon} = -\frac{a}{\pi}\left(\frac{\varepsilon}{D}\right)^{1-\varepsilon/D}\Gamma\left(\frac{\varepsilon}{D}\right)\exp(-\Delta V/D). \tag{3.190}$$

Kramers' rate is recovered if and only if $\varepsilon \in \{0, D\}$.

Chapter 4

Case Study II – Sine-Gordon Formulation

Chapter Summary

We apply the Picard–Lefschetz machinery of Chapter 3 to a periodic cosine potential where the dynamics are mapped to an effective sine–Gordon model. The periodic landscape admits an additional well-defined instanton-instanton alongside the instanton-anti-instanton sector. The complex trajectory resolves the instanton-anti-instanton computation. This chapter shows that the weak-noise asymptotics, determinant signs, and quasi-zero mode structure carry over from the cubic case, with some new features induced by periodicity.

4.1 The periodic sine–Gordon landscape

Periodic energy landscapes naturally arise in condensed matter and materials science, particularly in models of dislocations and adatom motion on crystalline lattices. For example, the Frenkel–Kontorova [8, 27] chain reduces to the sine–Gordon (SG) model in the continuum limit. In SG, *three* saddle families govern rare events:

1. **Stochastic real bounce** $[\mathcal{RB}]$: a real saddle confined to a single cell; on the real contour, it

possesses a soft negative mode in the $[\mathcal{I}\bar{\mathcal{I}}]$ sector.

2. **Instanton-instanton-type event** $[\mathcal{I}\mathcal{I}]$: a two-instanton trajectory that advances the coordinate by one period; in SG, this saddle is well defined and contributes.[1]

3. **Stochastic complex bounce** $[\mathcal{C}\mathcal{B}]$: the complexified $[\mathcal{I}\bar{\mathcal{I}}]$ saddle selected by contour deformation at fixed $D > 0$. It reproduces the $[\mathcal{I}\bar{\mathcal{I}}]$ rate and determines the $\pm i\pi$ phase via thimble orientation.

4.1.1 Critical points, energies and turning points

Unlike the cubic case in Chapter 3, SG admits a genuinely contributing $[\mathcal{I}\mathcal{I}]$ saddle. We show how $[\mathcal{R}\mathcal{B}]$, $[\mathcal{I}\mathcal{I}]$, and $[\mathcal{C}\mathcal{B}]$ fit together in this periodic landscape: the complex trajectory yields the correct $[\mathcal{I}\bar{\mathcal{I}}]$ contribution at fixed $D > 0$, and $[\mathcal{I}\mathcal{I}]$ controls intercell hops. The classical mechanics results agree with those of Dunne *et al.* in Section 6 of [13].

We work in a simple periodic potential,

$$V(x) \;=\; -\,4a^3\,\cos\!\Big(\frac{x}{2a}\Big), \qquad a > 0, \tag{4.1}$$

which sets the barrier scale for the dynamics. Its basic geometry is as follows:

$$V'(x) = 2a^2\,\sin\!\Big(\frac{x}{2a}\Big), \qquad V''(x) = a\,\cos\!\Big(\frac{x}{2a}\Big), \tag{4.2}$$

$$\text{minima: } x_k^{\min} = 4\pi a\,k,\;\; V(x_k^{\min}) = -4a^3,\;\; V''(x_k^{\min}) = +a, \tag{4.3}$$

$$\text{maxima: } x_k^{\max} = (2k+1)\,2\pi a,\;\; V(x_k^{\max}) = +4a^3,\;\; V''(x_k^{\max}) = -a, \tag{4.4}$$

$$\text{period: } L = 4\pi a, \qquad \text{barrier height (adjacent wells): } \Delta V = 8a^3. \tag{4.5}$$

The harmonic curvatures at the bottom of the well and the top of the barrier coincide in magnitude $|V''(x_k^{\max})| = V''(x_k^{\min}) = a$, and the baseline Kramers escape rate from one well to either neighbour

[1] In this section, we refer to this solution simply as the $[\mathcal{I}\mathcal{I}]$ solution.

is

$$\Gamma_K(D) \;=\; \frac{1}{2\pi}\sqrt{V''(x_k^{\min})\,|V''(x_k^{\max})|}\;\exp\Big(-\frac{\Delta V}{D}\Big) \;=\; \frac{a}{2\pi}\;\exp\Big(-\frac{8a^3}{D}\Big). \tag{4.6}$$

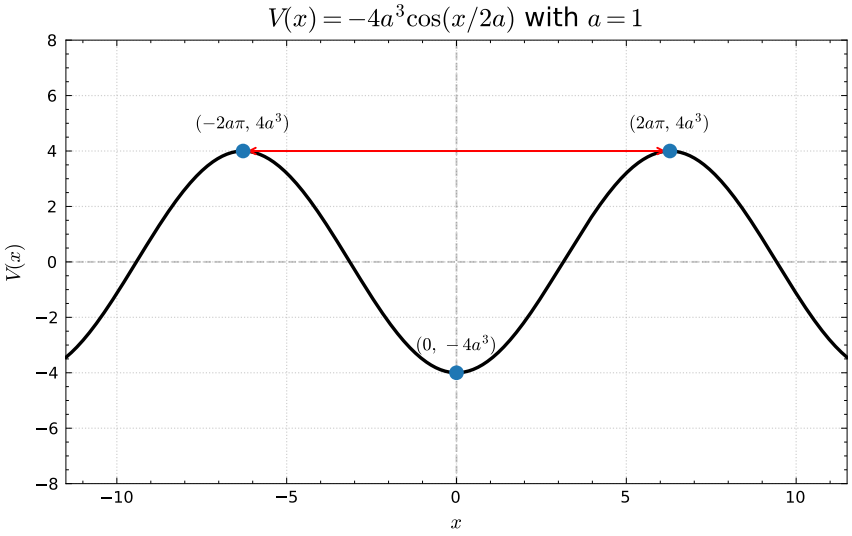

Figure 4.1: *The periodic potential* $V(x) = -4a^3\cos(x/2a)$ *with* $a = 1$. *Adjacent wells are separated by a barrier of height* $\Delta V = 8a^3$ *and period* $L = 4\pi a$.

In what follows, we (i) use $[\mathcal{RB}]$ to demonstrate the necessity of complexification and the breakdown of a purely real contour; (ii) characterise glued $[\mathcal{II}]$ paths, for which the QZM integral is already well posed on the full real line; and (iii) evaluate the $[\mathcal{CB}]$ contribution by integrating the QZM exactly along its Lefschetz thimble slice, yielding the exact Γ function factor and restoring the correct sign structure for $[\mathcal{I}\bar{\mathcal{I}}]$ events. It is important to note that while the $[\mathcal{II}]$-type event is already defined on the real line, the QZM integral is non-Gaussian. In both channels, the one-dimensional QZM integral produces the universal non-Gaussian factor $\mathrm{e}/\sqrt{2\pi}$. Because V is periodic, the dynamics repeat with spatial period $4\pi a$. In the weak-noise limit, the stochastic Hamiltonian correspondence lets us analyse the exit geometry by studying the Hamiltonian trajectory in the *tilted effective potential* under Itô's discretisation,

$$\mathfrak{U}(x) \;=\; -\,V'(x)^2 \;+\; 2D\,V''(x). \tag{4.7}$$

For the cosine potential

$$V(x) = -4a^3 \cos\big(x/2a\big) \tag{4.8}$$

we have

$$V'(x) = 2a^2 \sin\Big(\frac{x}{2a}\Big), \qquad V''(x) = a\cos\Big(\frac{x}{2a}\Big), \tag{4.9}$$

so, the total form of the effective potential is

$$\mathfrak{U}(x) = -4a^4 \sin^2\Big(\frac{x}{2a}\Big) + 2aD\,\cos\Big(\frac{x}{2a}\Big) = 4a^4\cos^2\Big(\frac{x}{2a}\Big) + 2aD\cos\Big(\frac{x}{2a}\Big) - 4a^4. \tag{4.10}$$

The stationary points of the effective potential $\mathfrak{U}(x) = -V'(x)^2 + 2D\,V''(x)$ organise into three distinct energy levels (one period $4\pi a$):

- **The highest level** $H_{\rm hi} = \mathfrak{U}(x_k^{\rm hi}) = 2aD$, achieved at

  $$x_k^{\rm hi} = 4\pi a\, k, \qquad k \in \mathbb{Z},$$

  with $\mathfrak{U}''(x_k^{\rm hi}) = -(4a^3 + D)/(2a) < 0$ (local maxima).

- **The middle level** $H_{\rm mid} = \mathfrak{U}(x_k^{\rm mid}) = -\,2aD$, achieved at

  $$x_k^{\rm mid} = (2k+1)\,2\pi a, \qquad k \in \mathbb{Z},$$

  with $\mathfrak{U}''(x_k^{\rm mid}) = (D - 4a^3)/(2a)$. Hence, for the weak-noise regime $0 < D < 4a^3$, these are also local *maxima*.

- **Lowest level** (two symmetric minima per period), existing for $0 < D < 4a^3$:

  $$\cos\Big(\frac{x}{2a}\Big) = -\,\frac{D}{4a^3} \implies x_{k,\pm}^{\rm lo} = 2a\Big(\pi \pm \arccos\frac{D}{4a^3}\Big) + 4\pi a\, k, \quad k \in \mathbb{Z},$$

with energy

$$H_{\mathrm{lo}} = \mathfrak{U}(x^{\mathrm{lo}}_{k,\pm}) = -\,4a^4 - \frac{D^2}{4a^2}, \qquad \mathfrak{U}''(x^{\mathrm{lo}}_{k,\pm}) = 2a^2\left(1 - \frac{D^2}{16a^6}\right) > 0.$$

Equivalently, using $\arccos u = \arctan\!\left(\sqrt{1-u^2}/\,u\right)$ (for $u \in (0,1]$), the two low-level critical points in each cell can be written as

$$x^{\mathrm{lo}}_{k,\pm} = (2k+1)\,2\pi a \;\pm\; 2a\,\arctan\!\left(\frac{\sqrt{16a^6 - D^2}}{D}\right).$$

As $D \uparrow 4a^3$ the pair $x^{\mathrm{lo}}_{k,\pm}$ coalesces with x^{mid}_k in a saddle-node bifurcation at energy $-8a^4$.

Thus, for $0 < D < 4a^3$ each period contains two maxima at $x = 4\pi a\,k$ with energy $2aD$ and $x = (2k+1)\,2\pi a$ with energy $-2aD$ and a symmetric pair of minima at $x^{\mathrm{lo}}_{k,\pm}$. As $D \to 4a^{3-}$ these minima coalesce (saddle-node) at $x = (2k+1)\,2\pi a$. This agrees with the classical mechanics structure given by Dunne *et al.* in Section 6 [13].

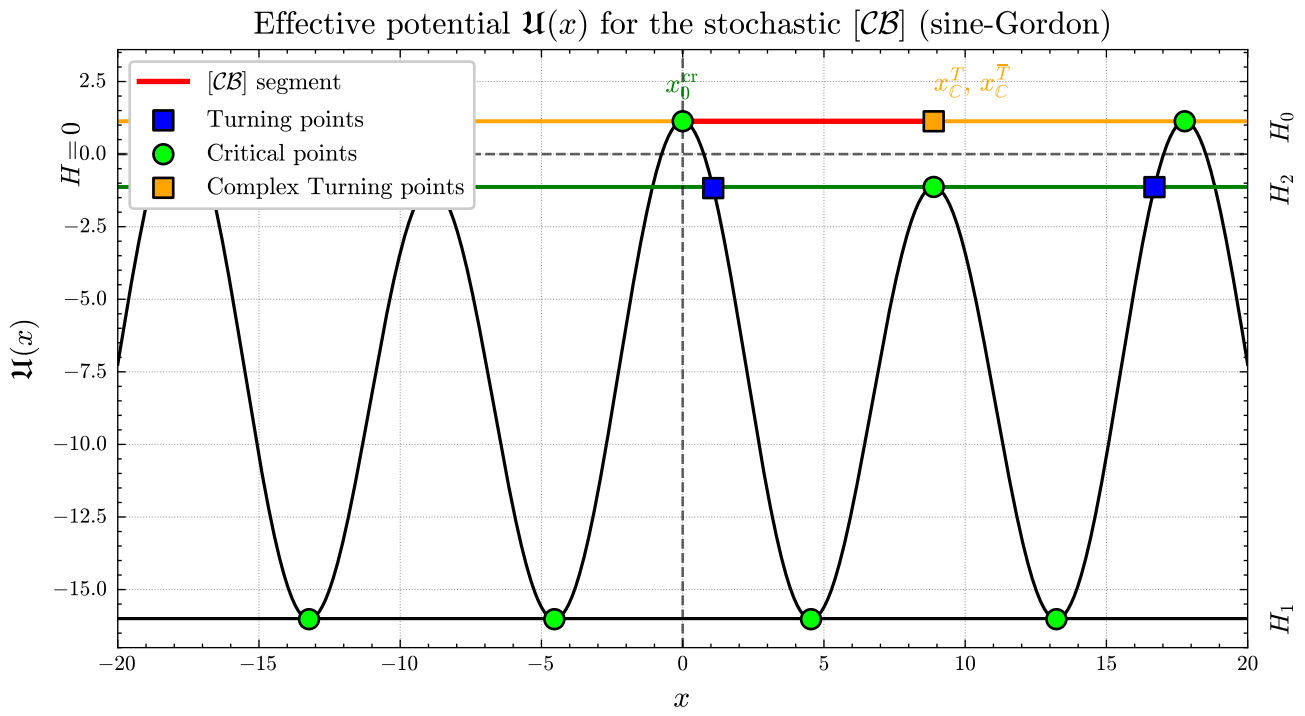

Figure 4.2: *Effective potential $\mathfrak{U}(x)$ (with $a=\sqrt{2}, D=0.4$) governing the stochastic $[\mathcal{CB}]$ dynamics. Green circles mark the critical points of $\mathfrak{U}(x)$, while blue squares denote real turning points along the representative energy level H. The orange square denotes a complex conjugate turning point pair with non-zero imaginary part.*

4.2 Stochastic real bounce

Consider the motion of a Hamiltonian particle that starts at $x_{\mathrm{cr}} = 2a\pi + 4a\pi k_1,\ k_1 \in \mathbb{Z}$, in the infinite past $t \to -\infty$ at the energy level $H = -2aD$. Assume that the particle bounces off a turning point at $t_c = 0$ and returns to x_{cr} as $t \to +\infty$. The turning points are

$$x_{\mathrm{T}} = \pm 2a \arccos\left(1 - \frac{D}{2a^3}\right) + 4a\pi k_2, \qquad k_2 \in \mathbb{Z}, \tag{4.11}$$

obtained by setting the velocity to zero in the first integral

$$\left(\frac{\mathrm{d}x}{\mathrm{d}t}\right)^2 = 4a^4\Big(1+\cos\frac{x}{2a}\Big)\Big[1-\cos\frac{x}{2a}-\frac{D}{2a^3}\Big]. \tag{4.12}$$

Integrating by quadrature gives,

$$\int_0^t \mathrm{d}t' = \int_{x_T}^{x} \frac{\mathrm{d}x'}{\sqrt{4a^4\Big(1+\cos\frac{x'}{2a}\Big)\Big[1-\cos\frac{x'}{2a}-\frac{D}{2a^3}\Big]}}. \tag{4.13}$$

At the critical point x_{cr}, the fluctuation operator has a simple closed form,

$$\hat{\mathcal{M}} = -\frac{\mathrm{d}^2}{\mathrm{d}t^2} - \frac{1}{2}\,\mathfrak{U}''(x_{\mathrm{cr}}) = -\frac{\mathrm{d}^2}{\mathrm{d}t^2} + a^2 - \frac{D}{4a} \tag{4.14}$$

where the frequency is

$$\omega_{\mathrm{rb}} = \sqrt{a^2 - \frac{D}{4a}} \;=\; a\sqrt{1-\frac{D}{4a^3}}. \tag{4.15}$$

4.2.1 Exact analytic solution for the stochastic real bounce

We solve (4.12) by a sequence of elementary transformations (summarised in Fig. 4.3). Upon inversion, the classical trajectory takes the equivalent closed forms[2]

$$\begin{aligned} x_{\mathrm{cl}}(t) &= 2a\,\arccos\left(\frac{1-\dfrac{D}{4a\omega_{\mathrm{rb}}^2}\cosh^2\omega_{\mathrm{rb}}t}{1+\dfrac{D}{4a\omega_{\mathrm{rb}}^2}\cosh^2\omega_{\mathrm{rb}}t}\right) \\ &= 4a\,\arctan\left(\frac{1}{2\omega_{\mathrm{rb}}}\sqrt{\frac{D}{a}}\;\cosh(\omega_{\mathrm{rb}}t)\right) \;=\; 4a\,\arctan\left(\sqrt{\frac{D}{4a^3-D}}\;\cosh(\omega_{\mathrm{rb}}t)\right). \end{aligned} \tag{4.16}$$

This solution satisfies the boundary conditions modulo $4a\pi$.

[2] Using the identity $\arctan\sqrt{X} = \frac{1}{2}\arccos\big(\frac{1-X}{1+X}\big)$.

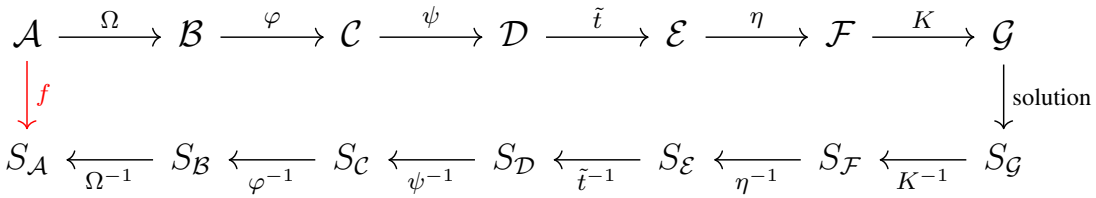

Figure 4.3: *Transformations used to obtain the closed form:* $\Omega = \cos(x/2a),\ \varphi = \Omega + 1,\ \psi = 1/\varphi,$ $\tilde{t} = 2\omega_{\rm rb} t,\ \eta = \mu - \mu_D,\ K = 2\eta/r + 1$ *with* $\mu_D = (2 - \frac{D}{2a^3})^{-1}$ *and* $r = \frac{D}{8a\,\omega_{\rm rb}^2}$.

To exhibit the solution as a composite $[\mathcal{I}\bar{\mathcal{I}}]$ pair, write

$$x_{\rm cl}(t) = 4a\,\arctan\left(\frac{1}{4\omega_{\rm rb}}\sqrt{\frac{D}{a}}\,e^{\omega_{\rm rb}\mu_{\rm rb}}\left[e^{\omega_{\rm rb}(t-\mu_{\rm rb})} + e^{-\omega_{\rm rb}(t+\mu_{\rm rb})}\right]\right), \tag{4.17}$$

where the separation $\mu_{\rm rb}$ is fixed by the addition formula $\arctan X + \arctan Y = \arctan\left(\frac{X+Y}{1-XY}\right)$ (mod π). Setting $X = e^{\omega_{\rm rb}(t-\mu_{\rm rb})}$, $Y = e^{-\omega_{\rm rb}(t+\mu_{\rm rb})}$ yields

$$\frac{1}{4\omega_{\rm rb}}\sqrt{\frac{D}{a}}\,e^{\omega_{\rm rb}\mu_{\rm rb}} = \frac{1}{1 - e^{-2\omega_{\rm rb}\mu_{\rm rb}}}, \tag{4.18}$$

and hence the explicit separation

$$\mu_{\rm rb} = \frac{1}{\omega_{\rm rb}}\,\mathrm{arsinh}\left(2\omega_{\rm rb}\sqrt{\frac{a}{D}}\right), \tag{4.19}$$

which is purely real. Its weak-noise expansion is

$$\mu_{\rm rb} = \frac{1}{2a}\log\left(\frac{16a^3}{D}\right) + \frac{D}{16a^4}\left[-1 + \log\left(\frac{16a^3}{D}\right)\right] + \frac{D^2}{512a^7}\left[-7 + 6\log\left(\frac{16a^3}{D}\right)\right] + \mathcal{O}(D^3). \tag{4.20}$$

Thus, the time near the turning point is again logarithmically growing,

$$2\mu_{\rm rb} \sim \frac{1}{a}\log\left(\frac{16a^3}{D}\right), \tag{4.21}$$

as $D \to 0$. Using $\arctan(x^{-1}) = \frac{\pi}{2} - \arctan x$ for $x > 0$, we also have the $[\mathcal{I}\bar{\mathcal{I}}]$ form

$$\begin{aligned} x_{\rm cl}(t) &= 4a\Big[\arctan\big(e^{\omega_{\rm rb}(t-\mu_{\rm rb})}\big) + \arctan\big(e^{-\omega_{\rm rb}(t+\mu_{\rm rb})}\big)\Big] \\ &= 4a\pi - 4a\Big[\arctan\big(e^{\omega_{\rm rb}(t+\mu_{\rm rb})}\big) + \arctan\big(e^{-\omega_{\rm rb}(t-\mu_{\rm rb})}\big)\Big], \end{aligned} \tag{4.22}$$

i.e., an instanton at $t = -\mu_{\rm rb}$ followed by an anti-instanton at $t = +\mu_{\rm rb}$. (4.22) matches (184) in [13].

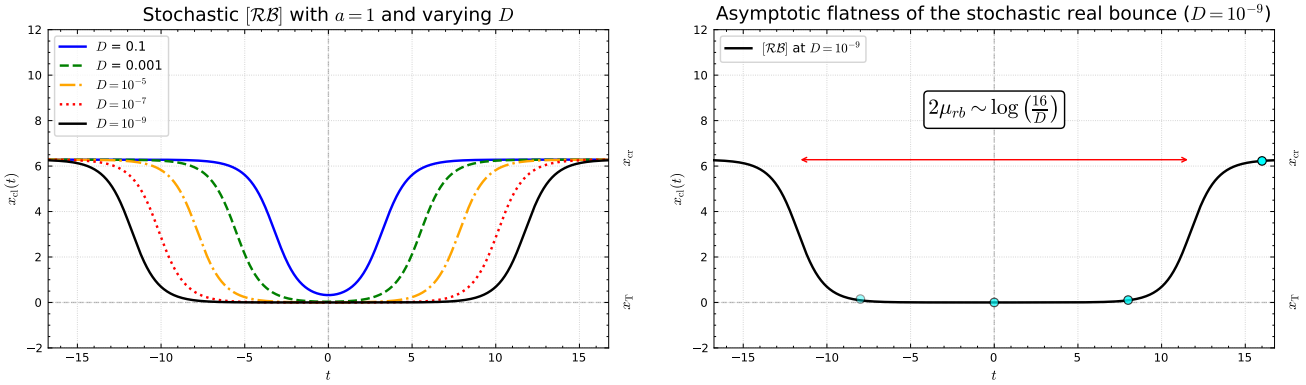

(a) Stochastic $[\mathcal{RB}]$ for varying D. (b) $[\mathcal{RB}]$ at $D = 10^{-9}$.

Figure 4.4: Stochastic $[\mathcal{RB}]$ in the sine–Gordon model with $a = 1$.

4.2.2 The stochastic real bounce action

The associated action can be written as a line integral,

$$\mathcal{S}[x] = -H\mathcal{T} + 4\int_{x_{\rm cr}}^{x_T} {\rm d}x\, \sqrt{4a^4\Big(1+\cos\frac{x}{2a}\Big)\Big[1-\cos\frac{x}{2a}-\frac{D}{2a^3}\Big]}\,, \tag{4.23}$$

which evaluates in closed form to

$$\mathcal{S}[x] = -H\mathcal{T} + 32a^3\sqrt{1-\frac{D}{4a^3}} - 4D\,\log\left(\frac{1+\sqrt{1-\frac{D}{4a^3}}}{1-\sqrt{1-\frac{D}{4a^3}}}\right). \tag{4.24}$$

Our action functional agrees with the logarithmic expression given in (187b) in [13]. The weak-noise asymptotic expansion of the action is

$$\mathcal{S}[x] = -H\mathcal{T} + 32a^3 - 4D - 4D\log\left(\frac{16a^3}{D}\right) + \frac{D^2}{4a^3} + \mathcal{O}(D^3). \tag{4.25}$$

The real bounce solution exists for $0 < D < D_c$ with $D_c = 4a^3$.

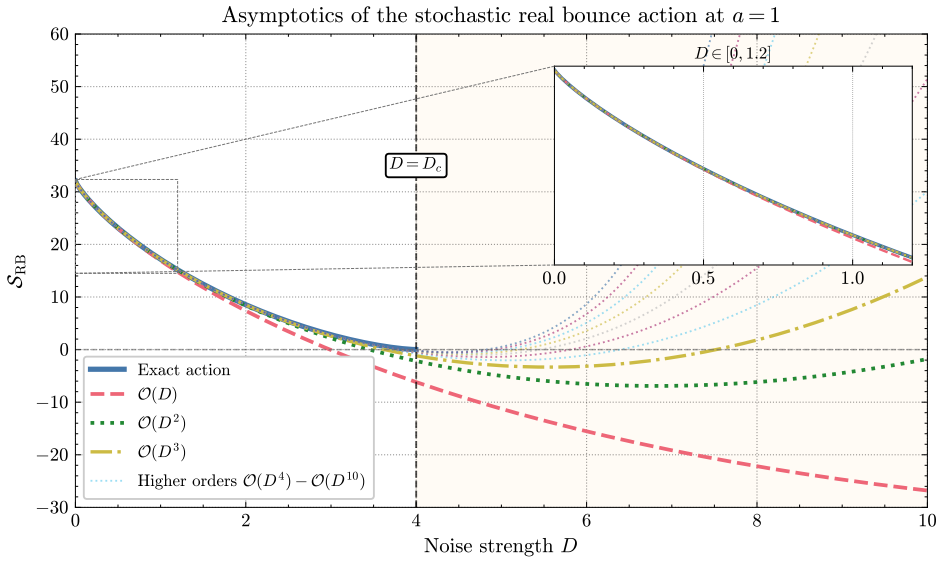

Figure 4.5: *Asymptotics of the stochastic real bounce action for the sine–Gordon potential at* $a = 1$. *The solid curve is the exact* $\mathcal{S}_{\mathrm{RB}}$ *with the* $-H\mathcal{T}$ *term removed; dashed/dotted curves show weak-noise truncations at orders* $\mathcal{O}(D)$, $\mathcal{O}(D^2)$, $\mathcal{O}(D^3)$, *and* $\mathcal{O}(D^4)$–$\mathcal{O}(D^{10})$. *The vertical line marks* $D_c = 4a^3$; *for* $D > D_c$ *no real bounce exists (shaded). The inset zooms into* $D \in [0, 1.2]$.

4.2.3 Stochastic real bounce functional determinant

The fluctuation determinant around the stochastic $[\mathcal{RB}]$ has one negative mode that is soft, and using the master formula § 2.2, one finds the same leading-order expression as for the cubic $[\mathcal{RB}]$,

$$\lim_{\mathcal{T}\to\infty} \frac{1}{\langle \dot{x}_{\mathrm{cl}} \mid \dot{x}_{\mathrm{cl}} \rangle} \frac{\det' \hat{\mathcal{M}}}{\det \hat{\mathcal{M}}_0} = -\frac{D}{512\, a^8} + \text{higher-order terms}, \tag{4.26}$$

exhibiting the same instability. In the same manner, we address this by passing to the complex bounce in the next subsection, and then analyse the $[\mathcal{II}]$ event.

4.3 The stochastic complex bounce

Write the complex path as $z(t) = x(t) + i\,y(t)$ and set $u := x/(2a)$, $v := y/(2a)$. For the Itô effective potential $\mathfrak{U}(z) = -\big[V'(z)\big]^2 + 2D\,V''(z)$ with $V'(z) = 2a^2 \sin\!\big(\frac{z}{2a}\big)$, one has

$$\begin{aligned} \mathrm{Re}\ \mathfrak{U}(z) &= 4a^4\big[\cos^2 u\,\cosh^2 v - \sin^2 u\,\sinh^2 v\big] + 2aD\cos u\,\cosh v - 4a^4, \\ \mathrm{Im}\ \mathfrak{U}(z) &= -4a^4 \sin(2u)\cosh v\,\sinh v \;-\; 2aD\sin u\,\sinh v, \end{aligned} \tag{4.27}$$

and the holomorphic Euler–Lagrange equations

$$\begin{aligned} \ddot{x} &= a^3 \sin(2u)\cosh(2v) + \frac{D}{2}\sin u\,\cosh v, \\ \ddot{y} &= a^3 \cos(2u)\sinh(2v) + \frac{D}{2}\cos u\,\sinh v, \end{aligned} \tag{4.28}$$

obtained from $\ddot{z} = V'(z)V''(z) - D\,V'''(z)$ with $V''(z) = a\cos\!\big(\frac{z}{2a}\big)$, $V'''(z) = -\frac{1}{2}\sin\!\big(\frac{z}{2a}\big)$.

We expand about the well at the origin $z_{\mathrm{cr}} = 0$. The fluctuation operator is

$$\hat{\mathcal{M}} \;=\; -\frac{\mathrm{d}^2}{\mathrm{d}t^2} - \frac{1}{2}\,\mathfrak{U}''(z_{\mathrm{cr}}) \;=\; -\frac{\mathrm{d}^2}{\mathrm{d}t^2} + \omega_{\mathrm{cb}}^2, \qquad \omega_{\mathrm{cb}}^2 = a^2 + \frac{D}{4a}, \tag{4.29}$$

so that

$$\omega_{\mathrm{cb}} = a\sqrt{1 + \frac{D}{4a^3}}. \tag{4.30}$$

For the right-moving branch, one finds the complex turning point from the first integral as

$$z_{\mathrm{T}} \;=\; 2a\,\arccos\!\left(-1 - \frac{D}{2a^3}\right) \;=\; 2a\pi \;\pm\; 2ai\,\operatorname{arcosh}\!\left(1 + \frac{D}{2a^3}\right), \tag{4.31}$$

using $\arccos(-1-\xi) = \pi \pm i\,\operatorname{arcosh}(1+\xi)$. Multivaluedness encodes the two complex-conjugate

sheets relevant to the phase $\pm i\pi$.

4.3.1 Exact analytic solution for the stochastic complex bounce

A convenient representation of the complex bounce is

$$z_{\rm cl}(t) = 2a\pi \;\pm\; 4a\,\arctan\!\left(i\,\cosh(\omega_{\rm cb}t)\,\sqrt{\frac{D}{D+4a^3}}\right), \tag{4.32}$$

which follows from $1+\cosh(2x) = 2\cosh^2 x$ and the identity $\arctan\sqrt{X} = \frac{1}{2}\arccos\!\left(\frac{1-X}{1+X}\right)$. Equivalently,

$$z_{\rm cl}(t) = 2a\pi \;\pm\; 4a\,\arctan\!\left(\frac{i}{2\omega_{\rm cb}}\sqrt{\frac{D}{a}}\,\cosh(\omega_{\rm cb}t)\right), \tag{4.33}$$

since $\dfrac{1}{2\omega_{\rm cb}}\sqrt{\dfrac{D}{a}} = \sqrt{\dfrac{D}{D+4a^3}}$. To display the $[\mathcal{I}\bar{\mathcal{I}}]$ structure, rewrite (4.33) in exponential form and use the arctan addition law,

$$z_{\rm cl}(t) = 2a\pi \;\pm\; 4a\,\arctan\!\left(\frac{i}{4\omega_{\rm cb}}\sqrt{\frac{D}{a}}\left[e^{\omega_{\rm cb}t} + e^{-\omega_{\rm cb}t}\right]\right). \tag{4.34}$$

Introduce a (complex) separation $\mu_{\rm cb}$ by shifting $t \mapsto t \pm \mu_{\rm cb}$ and demand the representation as a difference of two elementary kinks:

$$z_{\rm cl}(t) = 2a\pi \;\pm\; 4a\Big[\arctan\!\big(e^{\omega_{\rm cb}(t+\mu_{\rm cb})}\big) - \arctan\!\big(e^{\omega_{\rm cb}(t-\mu_{\rm cb})}\big)\Big]. \tag{4.35}$$

Matching (4.34) and (4.35) gives

$$\frac{1}{1-e^{2\omega_{\rm cb}\mu_{\rm cb}}} = \frac{i}{4\omega_{\rm cb}}\sqrt{\frac{D}{a}}\;e^{-\omega_{\rm cb}\mu_{\rm cb}}, \tag{4.36}$$

whose exact solution is

$$\mu_{\rm cb} = \frac{1}{\omega_{\rm cb}} \operatorname{arsinh}\Big(i\,2\omega_{\rm cb}\sqrt{\frac{a}{D}}\Big) = \frac{i}{\omega_{\rm cb}} \arcsin\Big(2\omega_{\rm cb}\sqrt{\frac{a}{D}}\Big), \tag{4.37}$$

using $\operatorname{arsinh}(iz) = i \arcsin z$. For $D \to 0$,

$$\mu_{\rm cb} = \frac{1}{2a}\Big[\log\Big(\frac{16a^3}{D}\Big) \pm i\pi\Big] + \frac{D}{16a^4}\Big[1 \mp i\pi - \log\Big(\frac{16a^3}{D}\Big)\Big] + \frac{D^2}{512a^7}\Big[-7 \pm 6i\pi + 6\log\Big(\frac{16a^3}{D}\Big)\Big] + \mathcal{O}(D^3), \tag{4.38}$$

i.e., $2\mu_{\rm cb} \simeq \frac{1}{a}\big[\log\big(\frac{16a^3}{D}\big) \pm i\pi\big]$. The imaginary part $\operatorname{Im}\mu_{\rm cb} = \pm\pi/(2a) + \mathcal{O}(D)$ encodes the $\pm i\pi$ phase. At the special value, the trajectory crosses a branch and becomes discontinuous on the real axis (the "$\theta = \pi$" singular case); otherwise, the real-time profile is continuous, with a steep but finite transition. (4.35) agrees with Dunne *et al.* in (201) of [13], and a clear discussion on the singularity in the solution is given in Section 6.5 of [13].

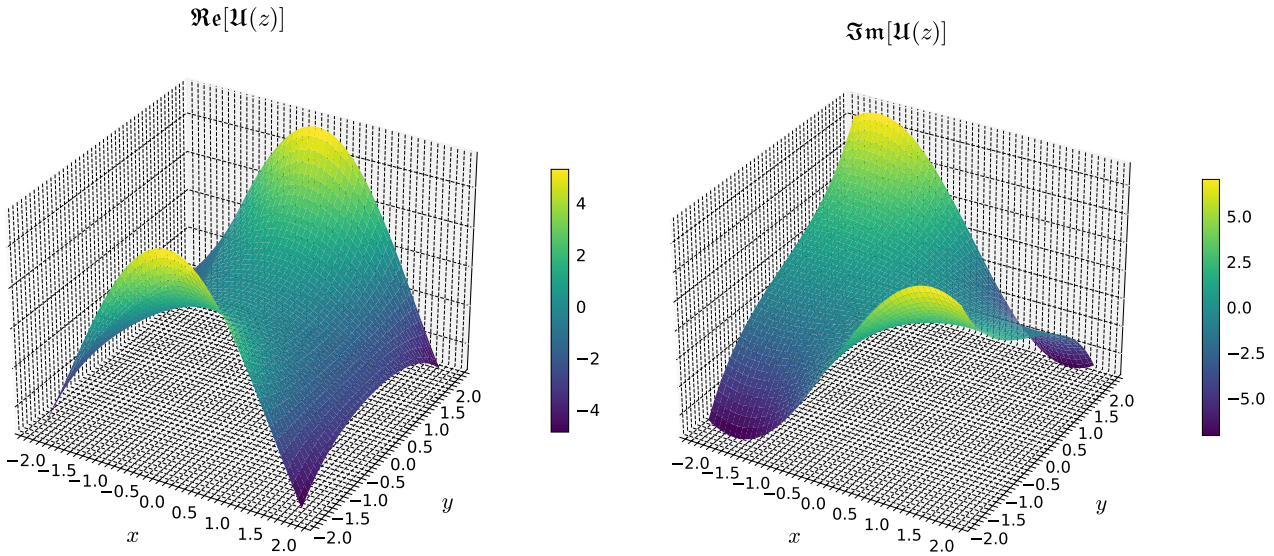

(a) Re $\mathfrak{U}(z)$. (b) Im $\mathfrak{U}(z)$.

Figure 4.6: Holomorphic Itô effective potential over $[-2,2] \times [-2,2] \subset \mathbb{C}$. Lighter regions are higher; darker regions are deeper wells.

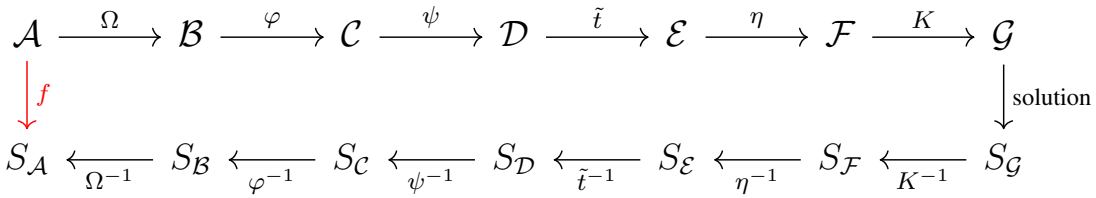

Figure 4.7: *Transformations leading to* (4.32)–(4.35)*;* $\Omega = \cos(z/2a)$, $\varphi = \Omega - 1$, $\psi = 1/\varphi$, $\tilde{t} = 2\omega_{\rm cb}t$, $\eta = \mu - \mu_D$, $K = 2\eta/r + 1$ *with* $\mu_D = -(2 + \frac{D}{2a^3})^{-1}$ *and* $r = \frac{D}{8a\,\omega_{\rm cb}^2}$.

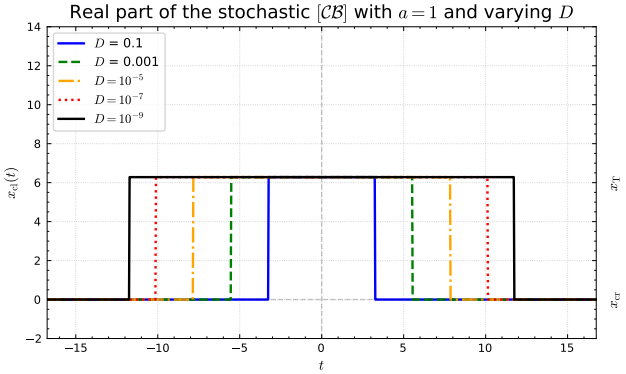

(a) Re $z_{\rm cl}(t)$ for varying D.

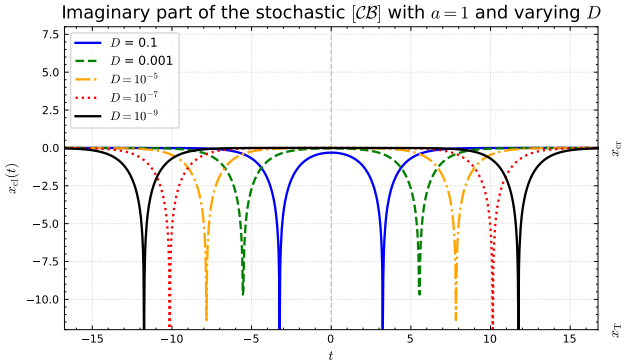

(b) Im $z_{\rm cl}(t)$ for varying D.

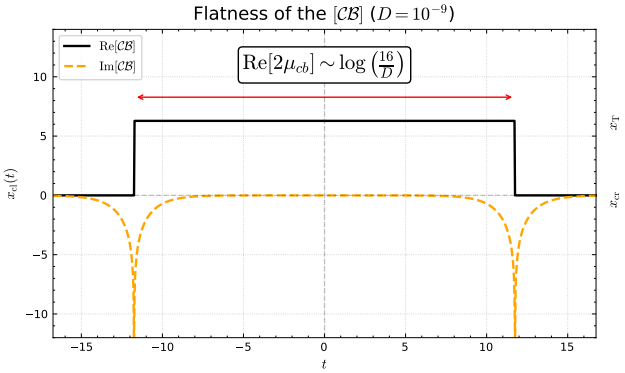

(c) Re $z_{\rm cl}(t)$ at fixed D.

Figure 4.8: Plots of the exact complex bounce solution, $z_{\rm cl}$, in the sine–Gordon effective potential for $a = 1$.

4.3.2 The stochastic complex bounce action

The action evaluated on the complex bounce is

$$\mathcal{S}[z] = -H\mathcal{T} + 4\int_{z_{\rm cr}}^{z_{\rm T}} \mathrm{d}z\, \sqrt{2aD\Big(1-\cos\frac{z}{2a}\Big) + 4a^4\Big(1-\cos^2\frac{z}{2a}\Big)}\,. \tag{4.39}$$

By substitution, this integrates to the closed form

$$\mathcal{S}[z] = -H\mathcal{T} + 32a^3\sqrt{1+\frac{D}{4a^3}} + 4D\,\log\left(\frac{1+\sqrt{1+\frac{D}{4a^3}}}{1-\sqrt{1+\frac{D}{4a^3}}}\right). \tag{4.40}$$

The stochastic complex bounce asymptotics read as

$$\mathcal{S}[z] = 32a^3 + 4D \pm 4i\pi D + 4D\log\left(\frac{16a^3}{D}\right) + \frac{D^2}{4a^3} + \mathcal{O}(D^3). \tag{4.41}$$

The $\pm$ sign comes from the choice of the turning point. We will formalise this in the language of intersection coefficients shortly.

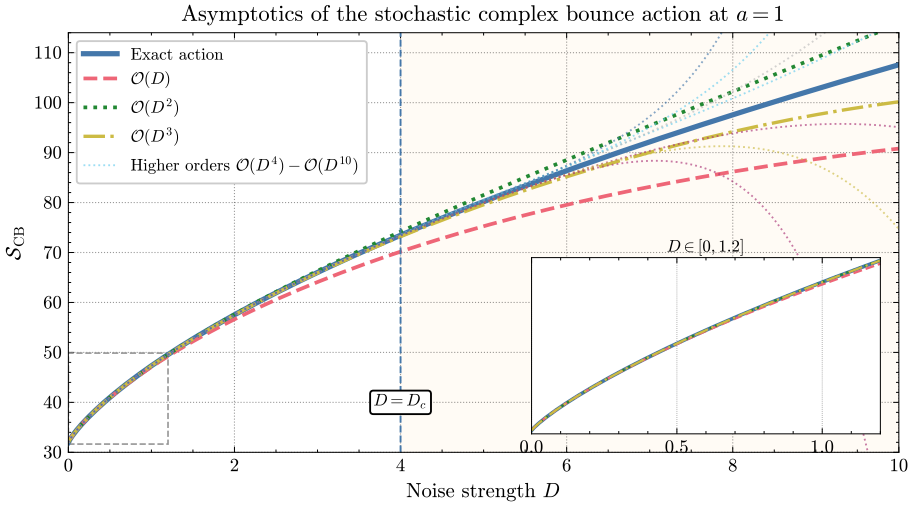

Figure 4.9: *Real part of the complex bounce action* $S_{\rm CB}(D) \equiv \mathrm{Re}\ \mathcal{S}[z_{\rm cl}]$ *at* $a = 1$ *vs. noise* D*. The solid curve is the exact closed form* (4.40) *with* $-H\mathcal{T}$ *removed and the log on its principal real branch (the* $\pm i\pi$ *discarded). Dashed/dotted: weak-noise truncations* $\mathcal{O}(D)$*,* $\mathcal{O}(D^2)$*,* $\mathcal{O}(D^3)$*, and* $\mathcal{O}(D^4)$*–*$\mathcal{O}(D^{10})$ *grouped. The vertical line marks* $D_c = 4a^3$*, beyond which the* real *bounce ceases to exist; the complex saddle persists.*

4.3.3 Stochastic complex bounce functional determinant

Using the master formula § 2.2, to leading order one finds the fluctuation determinant around the stochastic $[\mathcal{CB}]$ as

$$\lim_{\mathcal{T}\to\infty} \frac{1}{\langle \dot{z}_{\rm cl} \mid \dot{z}_{\rm cl} \rangle} \frac{\det{}' \hat{\mathcal{M}}}{\det \hat{\mathcal{M}}_0} = + \frac{D}{512\, a^8} \ + \ \text{higher-order terms}, \tag{4.42}$$

which is precisely $D \to -D$ in the $[\mathcal{RB}]$ determinant. This is strictly positive and has the same leading-order expansion as for the cubic $[\mathcal{CB}]$ in Chapter 3.

4.3.4 Recovery of the Kramers rate

The interaction potential can be derived from the ansatz

$$x^{\text{ansatz}}_{\mathcal{I}\bar{\mathcal{I}}}(t,\theta) = 4a\arctan\exp\left(\omega^{\text{ansatz}}_{\mathcal{I}\bar{\mathcal{I}}}\left(t+\frac{\theta}{2}\right)\right) - 4a\arctan\exp\left(\omega^{\text{ansatz}}_{\mathcal{I}\bar{\mathcal{I}}}\left(t-\frac{\theta}{2}\right)\right) + 2a\pi. \quad (4.43)$$

The interaction potential is attractive, so there is a complex critical point that matches the leading-order expansion of μ_{cb},

$$\mathcal{V}_-(\theta) = -64\,a^3\exp(-\omega_{cb}\theta) + 4D\,\omega_{cb}\,\theta, \quad (4.44)$$

where we have matched $\omega^{\text{ansatz}}_{\mathcal{I}\bar{\mathcal{I}}} = \omega_{cb}$. In this case, the thimble is just the real axis shifted by $\pm\frac{i\pi}{\omega_{cb}}$, that is,

$$\mathcal{J}_\theta = \mathbb{R} \pm i\,\frac{\pi}{\omega_{cb}}. \quad (4.45)$$

So, the $\mathrm{e}/\sqrt{2\pi}$ correction factor is needed to resolve the thimble computation. This is equivalent to setting $\mathcal{B} = 1$ in (3.8). Now, we shall compute the rate for a particle starting at the origin:

$$P(0,+\mathcal{T}/2 \mid 0,-\mathcal{T}/2) \;\approx\; \frac{1}{\sqrt{4\pi D}}\left[\frac{\det'\hat{\mathcal{M}}}{\det\hat{\mathcal{M}}_0}\right]^{-\frac{1}{2}}\exp\Big(-\mathcal{S}'[z]/(4D)\Big)\,\mathcal{T}, \quad (4.46)$$

where $\mathcal{S}'$ denotes $\mathcal{S}_{cb}$ with the energy term $-H\mathcal{T}$ omitted. The intersection coefficients follow identically to the cubic case (3.168), and we have the same dual-thimble shape as in (3.163), which means we find the rate as

$$-|\Gamma_{cb}|\mathcal{T} = -\frac{a}{2\pi}\exp(-\Delta V/D)\mathcal{T}. \quad (4.47)$$

Therefore, Kramers' rate has been recovered using the PL framework and stochastic $[\mathcal{CB}]$. Since the periodic potential on $\mathbb{R}$ admits no normalisable equilibrium density, one has to study $[\mathcal{I}\bar{\mathcal{I}}]$ configurations. On these sectors, complexification provides a systematic contour prescription via Picard–Lefschetz theory.

4.4 Instanton-instanton-type event

In the periodic sine–Gordon landscape, there is, in addition to the real and complex bounces, another classical path that contributes and lies on a real contour: an instanton-instanton-type $[\mathcal{I}\mathcal{I}]$ trajectory. We consider a particle on the highest Itô-effective energy level, $H = 2aD$, that moves from one maximum of the Itô effective potential to the next, crossing a single intermediate barrier. Disregarding any overall shifts by $4a\pi$, the path is

$$0 \;\longrightarrow\; 2a\pi \;\longrightarrow\; 4a\pi,$$

with $x(-\mathcal{T}/2) = 0$, $x(0) = 2a\pi$, and $x(+\mathcal{T}/2) = 4a\pi$. The first integral for the motion reads

$$\left(\frac{\mathrm{d}x}{\mathrm{d}t}\right)^2 = 4a^4\Big(1-\cos\frac{x}{2a}\Big)\Big[\,1+\cos\frac{x}{2a}+\frac{D}{2a^3}\,\Big], \tag{4.48}$$

and integrating by quadrature gives

$$t = \int_0^t 1\mathrm{d}t' = \int_{x_{\mathrm{T}}}^{x} \frac{\mathrm{d}x'}{\sqrt{4a^4\Big(1-\cos\frac{x'}{2a}\Big)\Big[\,1+\cos\frac{x'}{2a}+\frac{D}{2a^3}\,\Big]}}. \tag{4.49}$$

Expanding about the critical point $x_{\mathrm{cr}} = 0$, the fluctuation operator is

$$\hat{\mathcal{M}} = -\frac{\mathrm{d}^2}{\mathrm{d}t^2} - \frac{1}{2}\,\mathfrak{U}''(x_{\mathrm{cr}}) = -\frac{\mathrm{d}^2}{\mathrm{d}t^2} + a^2 + \frac{D}{4a}, \tag{4.50}$$

so the frequency is

$$\omega_{\mathcal{I}\mathcal{I}} = a\sqrt{1+\frac{D}{4a^3}}. \tag{4.51}$$

4.4.1 Exact analytic solution for the instanton-instanton-type event

Solving (4.48) by transformations (cf. Fig. 4.10) and inverting yield the exact classical trajectory solution,

$$x_{\rm cl}(t) = 2a\pi + 4a\,\arctan\!\left(\frac{1}{2\omega_{\mathcal{II}}}\sqrt{\frac{D}{a}}\,\sinh(\omega_{\mathcal{II}}t)\right) \;=\; 2a\pi + 4a\,\arctan\!\left(\sqrt{\frac{D}{4a^3+D}}\,\sinh(\omega_{\mathcal{II}}t)\right), \tag{4.52}$$

which satisfies $x_{\rm cl}(-\infty)=0$, $x_{\rm cl}(0)=2a\pi$, $x_{\rm cl}(+\infty)=4a\pi$. To display the composite nature, use the arctangent addition law to write

$$x_{\rm cl}(t) = 2a\pi + 4a\Big[\arctan\!\big(e^{\omega_{\mathcal{II}}(t+\mu_{\mathcal{II}})}\big) - \arctan\!\big(e^{-\omega_{\mathcal{II}}(t-\mu_{\mathcal{II}})}\big)\Big], \tag{4.53}$$

which is a sum of two instantons separated by $\mu_{\mathcal{II}}$. The matching of (4.52)–(4.53) gives

$$\mu_{\mathcal{II}} = \frac{1}{\omega_{\mathcal{II}}}\,\operatorname{arcosh}\sqrt{\frac{4a^3+D}{D}}, \tag{4.54}$$

so $\mu_{\mathcal{II}}\in\mathbb{R}$ for all $D>0$. Using $\arctan X-\arctan Y=\arctan\!\big(\frac{X-Y}{1+XY}\big)$ with $X=e^{\omega_{\mathcal{II}}(t+\mu_{\mathcal{II}})}$, $Y=e^{\omega_{\mathcal{II}}(-t+\mu_{\mathcal{II}})}$ shows that $\arctan\big(\operatorname{sech}(\omega_{\mathcal{II}}\mu_{\mathcal{II}})\,\sinh(\omega_{\mathcal{II}}t)\big)$ is reproduced exactly, with $\operatorname{sech}(\omega_{\mathcal{II}}\mu_{\mathcal{II}})=\sqrt{D/(4a^3+D)}$. (4.53) is consistent with the "real bion" solution given by Dunne *et al.* in (193) of [13].

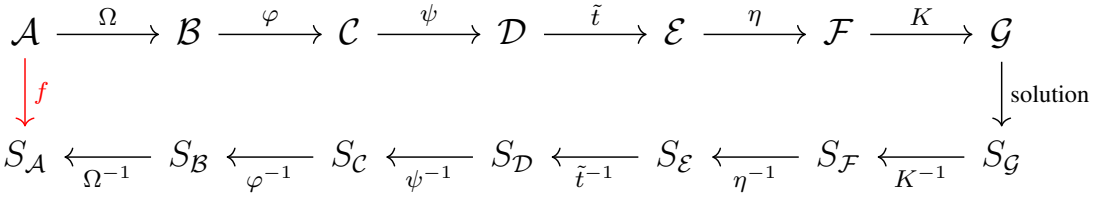

Figure 4.10: *Transformations used to obtain* (4.52)–(4.53). *One convenient chain of transformations is:* $\Omega=\cos(x/2a)$, $\varphi=\Omega-1$, $\psi=1/\varphi$, $\tilde{t}=2\omega_{\mathcal{II}}t$, $\eta=\mu-\mu_D$, $K=2\eta/r-1$ *with* $r=D/(8a\,\omega_{\mathcal{II}}^2)$. *Equivalent choices lead to the same closed form* (4.52).

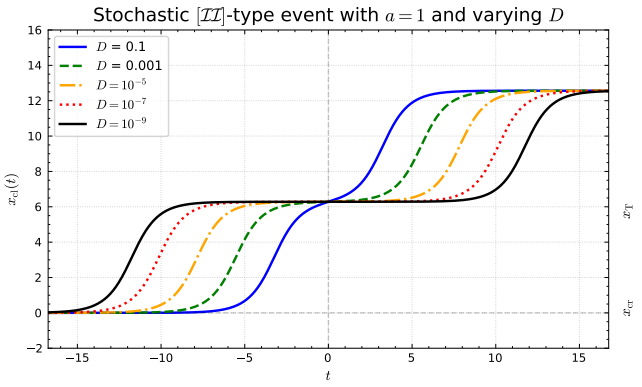

(a) Portrait of the stochastic $[\mathcal{II}]$ path for varying D.

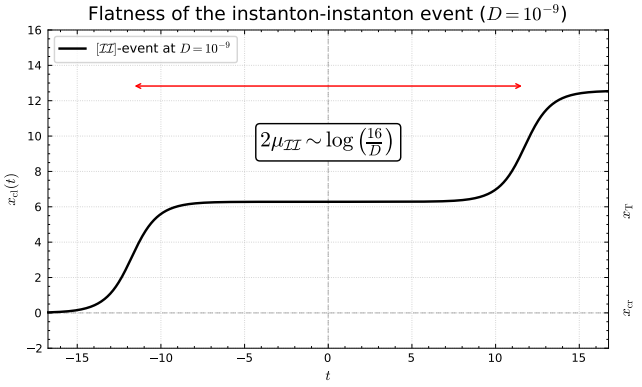

(b) Time evolution at $D = 10^{-6}$ (with $a = 1$).

Figure 4.11: Analytical solution of the $[\mathcal{II}]$-event.

4.4.2 Instanton-instanton-type event action

The action can be written as the line integral

$$\mathcal{S}[x] = -H\mathcal{T} + 4\int_0^{2a\pi} \mathrm{d}x \sqrt{4a^4\Big(1-\cos\frac{x}{2a}\Big)\Big[1+\cos\frac{x}{2a}+\frac{D}{2a^3}\Big]}\,, \tag{4.55}$$

which evaluates to the closed form,

$$\mathcal{S}[x] = -H\mathcal{T} + 32a^3\sqrt{1+\frac{D}{4a^3}} + 4D\,\log\left(\frac{\sqrt{1+\frac{D}{4a^3}}+1}{\sqrt{1+\frac{D}{4a^3}}-1}\right). \tag{4.56}$$

This is purely real for $D > 0$. The asymptotics read:

$$\mathcal{S}[x] = 32a^3 + 4D + 4D\log\left(\frac{16a^3}{D}\right) + \frac{D^2}{4a^3} + \mathcal{O}(D^3). \tag{4.57}$$

4.4.3 Instanton-instanton-type event functional determinant

The fluctuation determinant is positive. In our normalisation,

$$\lim_{\mathcal{T}\to\infty} \frac{1}{\langle \dot{x}_{\rm cl} \mid \dot{x}_{\rm cl}\rangle} \frac{\det' \hat{\mathcal{M}}}{\det \hat{\mathcal{M}}_0} = + \frac{D}{512\, a^8} + \text{ higher-order terms}, \tag{4.58}$$

in contrast to the real bounce case, and agreeing with the complex bounce case. Thus, there is no unstable direction to account for. Kramers' rate can also be derived from such a configuration, and the thimble integration can be performed exactly. For the $[\mathcal{I}\bar{\mathcal{I}}]$ sector, the relevant Lefschetz thimble is shifted off the real axis, so the quasi-zero mode must be integrated on a complex contour. In the $[\mathcal{I}\mathcal{I}]$ sector, the thimble coincides with $\mathbb{R}$; nevertheless, the quasi-zero mode integral is non-Gaussian and must be treated exactly. We now verify this by completing the computation.

4.4.4 Recovery of the Kramers rate

The interaction potential can be derived from the ansatz

$$x^{\text{ansatz}}_{\mathcal{I}\mathcal{I}}(t,\theta) = 4a \arctan\exp\left(\omega^{\text{ansatz}}_{\mathcal{I}\mathcal{I}}\left(t+\frac{\theta}{2}\right)\right) + 4a\arctan\exp\left(\omega^{\text{ansatz}}_{\mathcal{I}\mathcal{I}}\left(t-\frac{\theta}{2}\right)\right) - 2a\pi, \tag{4.59}$$

the interaction potential changes sign so that a real critical point exists,

$$\mathcal{V}_+(\theta) = +64\, a^3 \exp(-\omega_{\mathcal{I}\mathcal{I}}\theta) + 4D\,\omega_{\mathcal{I}\mathcal{I}}\,\theta, \tag{4.60}$$

where we have matched $\omega^{\text{ansatz}}_{\mathcal{I}\mathcal{I}} = \omega_{\mathcal{I}\mathcal{I}}$. In this case, the thimble is just the real axis,

$$\mathcal{J}_\theta = \mathbb{R}, \tag{4.61}$$

and so the $\mathrm{e}/\sqrt{2\pi}$ error factor is needed. The dual thimble is similar to (3.163) but with no shifts of π appearing in the expression,

$$x(y) = \frac{1}{\omega_{\mathcal{I}\mathcal{I}}} \log\left(\frac{16a^3}{D}\,\frac{\sin(\omega_{\mathcal{I}\mathcal{I}}y)}{\omega_{\mathcal{I}\mathcal{I}}y}\right), \tag{4.62}$$

which intersects $\mathbb{R}$ once at $\theta_* = (1/\omega_{\mathcal{I}\mathcal{I}})\log(16a^3/D)$ with positive orientation, hence the intersection coefficient is $+1$ and the PL decomposition is trivial. Collecting the remaining ingredients,

$$P(4a\pi, +\mathcal{T}/2 \mid 0, -\mathcal{T}/2) \;\approx\; \frac{1}{\sqrt{4\pi D}}\left[\frac{\det{}'\,\hat{\mathcal{M}}}{\det\hat{\mathcal{M}}_0}\right]^{-\frac{1}{2}} \exp\Big(-\mathcal{S}'_{\mathcal{I}\mathcal{I}}[x]/(4D)\Big)\,\mathcal{T}, \tag{4.63}$$

where $\mathcal{S}'_{\mathcal{I}\mathcal{I}}$ denotes $\mathcal{S}_{\mathcal{I}\mathcal{I}}$ with the energy term $-H\mathcal{T}$ omitted. Then, we find the rate as

$$\Gamma_{\mathcal{I}\mathcal{I}} = \frac{a}{2\pi}\exp(-\Delta V/D). \tag{4.64}$$

Our analysis is conducted entirely within the stochastic regime; however, the resulting classical mechanics shares a structural similarity with the results reported by Dunne *et al.* in Section 6 of [13], which pertain to the quantum field theory (QFT) framework. In particular, the effective potential in our setting is tilted as a direct consequence of the discretisation scheme applied in the stochastic context. Although the classical equations of motion derived in both cases are structurally analogous, the physical regimes and underlying mechanisms remain fundamentally different.

Chapter 5

Conclusion and Outlook

Chapter Summary

This chapter summarises the main contributions of the thesis, states a practical algorithm for computing escape rates and discusses further applications in non-equilibrium statistical mechanics

---

Summary of the main contributions

- **Itô variational calculus and the tilted saddle equation.** Using the Itô chain rule in the variational calculus yields an order-D tilt in the equations of motion,

$$\boxed{\ddot{x} \;=\; V'(x)\,V''(x) \;-\; D\,V'''(x)}$$

  reshaping the saddle geometry and making solutions explicitly D-dependent while leaving the Arrhenius factor unchanged.

- **Discovery of stochastic bounces.** Solving the Itô Euler–Lagrange equation reveals exact

two-instanton configurations—*stochastic real bounces* and *stochastic complex bounces*—as stochastic analogues of the real bounce and complex bion in QFT. At a critical noise level $D = D_c$ the real bounce disappears via a saddle-node bifurcation, whereas the complex bounce persists.

- **Complexification and thimble-based contour selection.** For instanton-instanton sectors $[\mathcal{I}\mathcal{I}]$ the undeformed real contour (real thimble) suffices but can be improved. For instanton-anti-instanton ($[\mathcal{I}\bar{\mathcal{I}}]$) sectors, we complexify the Onsager–Machlup path integral

$$P(x_1, +\mathcal{T}/2 \mid x_1, -\mathcal{T}/2) = \int_\gamma \mathcal{D}z \ \exp\left(-\frac{\mathcal{S}[z]}{4D}\right), \qquad \gamma \ := \ \text{Lefschetz thimble},$$

and work on the holomorphic landscape $\mathfrak{U}(z) = -\big(V'(z)\big)^2 + 2D\,V''(z)$. Although the original problem is real, the $[\mathcal{I}\bar{\mathcal{I}}]$ weak-noise asymptotics are governed by *complex* saddles.

- **Local product structure and clean factorisation.** Near each relevant saddle, the path integral measure admits a local product:

$$\text{Measure} \approx \text{EZM fibre} \ \times \ \mathrm{QZM\ line} \ \times \ \text{stable Gaussians},$$

yielding

$$P_\sigma \ \simeq \ \exp\left(-\frac{S_\sigma}{4D}\right) \underbrace{\mathrm{Vol(EZM)} \times \text{(Gaussian prefactor)}}_{\text{steepest descents + collective coordinates}} \times \underbrace{\int_{\mathcal{J}_\theta} \mathrm{d}\theta \ \exp\left(-\frac{S_{\mathrm{int}}(\theta)}{4D}\right)}_{\mathrm{QZM\ integral\ along\ the\ thimble}}.$$

This factorisation and choice of contour is enabled by the Picard–Lefschetz (PL) theory.

- **QZM contour and geometric sign (vs. Bogomolny–Zinn–Justin, BZJ).** Factorisation isolates the quasi-zero mode integral. For our $[\mathcal{I}\bar{\mathcal{I}}]$ case studies, the correct contour is $\mathcal{J}_\theta = \mathbb{R} \pm i\pi$; for $[\mathcal{I}\mathcal{I}]$ pairs, it is the full real line. Thus, both sectors extend beyond a positive half-line, and crucially, the $[\mathcal{I}\bar{\mathcal{I}}]$ sectors must be shifted off the real axis. This provides a geometric interpretation of the BZJ prescription. Any naive Gaussian approximation of the QZM (even after complexi-

fication) is uncontrolled due to the pseudo-flat direction and produces a spurious Stirling factor, which we identify and remove in general.

- **Non-zero energy and cancellation of divergences.** The tilt lifts bounces off zero energy, $H > 0$, producing a linear term $+H\,\mathcal{T}$ as $\mathcal{T} \to \infty$. We show that this divergence cancels against the normalisation of the path integral measure, always returning a finite result.

- **Fluctuation determinants and the correct overall sign.** We present a master formula for computing fluctuation determinants of stochastic bounces. Moreover, we find a relation linking Itô and Stratonovich prefactors (zero modes removed):

$$\lim_{\mathcal{T}\to\infty} \frac{1}{\langle \dot{x}_{\text{Itô}} \mid \dot{x}_{\text{Itô}} \rangle} \frac{\det{}' \hat{\mathcal{M}}_{\text{Itô}}}{\det \hat{\mathcal{M}}_0} \;=\; g(a)\, D \left[\lim_{\mathcal{T}\to\infty} \frac{1}{\langle \dot{x}_{\text{Strat}} \mid \dot{x}_{\text{Strat}} \rangle} \frac{\det{}' \hat{\mathcal{M}}_{\text{Strat}}}{\det \hat{\mathcal{M}}_0} \right]^2, \tag{5.1}$$

where the prime denotes removal of zero modes (and $g(a) > 0$ is model-dependent). For the stochastic complex bounce the determinant is positive and of order $\mathcal{O}(D)$; together with a multivalued action term $\pm 4\pi i D$ this yields an overall factor -1 and the physically correct transition sign. We demonstrate this explicitly in two case studies on a cubic and sine–Gordon potential.

- **Only two tilts reproduce Kramers exactly.** With a regulator ε interpolating discretisations, $\mathfrak{U}(x) = -(V')^2 + 2\varepsilon\, V''$, the escape rate takes the schematic form

$$\pm\big|\Gamma_\varepsilon\big|\,\mathcal{T} \;= \pm\, \frac{f(a)}{\pi} \Big(\frac{\varepsilon}{D}\Big)^{1-\varepsilon/D} \Gamma\Big(\frac{\varepsilon}{D}\Big)\, \exp\!\left(-\frac{\Delta V}{D}\right) \mathcal{T}.$$

Only the limits $\varepsilon \to 0$ (Stratonovich) and $\varepsilon \to D$ (Itô) reproduce Kramers at leading order. For clean contour selection and a geometric resolution of the QZM sign, we adopt the Itô framework.

5.1 Practical algorithm

This thesis presents an algorithmic procedure to recover Kramers' escape rate by analysing complex saddles of the stochastic path integral. The complexification and correct treatment of the QZM provide a systematic and rigorous approach to obtaining the correct formula while maintaining $D > 0$. From an applied perspective, the main insight is that $[\mathcal{I}\bar{\mathcal{I}}]$-type configurations must be addressed through complexification and tilting of the effective landscape. Notably, these two aspects are intrinsically linked: once the Itô discretisation is selected, it is necessary to consider complex trajectories. This requirement arises from the nature of the tilt term itself, and from the fact that real bounce trajectories in the tilted landscape originate at the barrier. This step is essential to reproduce the correct sign for Kramers' rate. In summary, the algorithm for $[\mathcal{I}\bar{\mathcal{I}}]$ configurations to derive the rate is as follows:

- Depending on the problem, it may be necessary to employ $[\mathcal{I}\bar{\mathcal{I}}]$-type configurations, i.e., non-confining potentials or those with no well-defined Boltzmann density.
- If $[\mathcal{I}\bar{\mathcal{I}}]$ configurations are required, select the Itô discretisation scheme and complexify the system. This entails studying Hamiltonian mechanics in a tilted, holomorphic potential.
- Derive all necessary results (numerical evaluation is acceptable for more complicated potentials): the action, extremising solution, and fluctuation determinant using the provided formulae.
- With an understanding of the underlying thimble geometry, assemble all components to obtain the rate, and multiply by the error factor arising from the Gaussian approximation to a non-Gaussian mode. The QZM can be isolated and its thimble integral evaluated exactly, or the general error formula given in § 3.8 may be used.

Thus, tilt, complexification, and error factor constitute the three key elements required to derive the escape rate without recourse to $D \to -D$ substitutions. These steps suffice to obtain the correct prefactor and a geometric resolution of phases, irrespective of the availability of closed-form expressions.

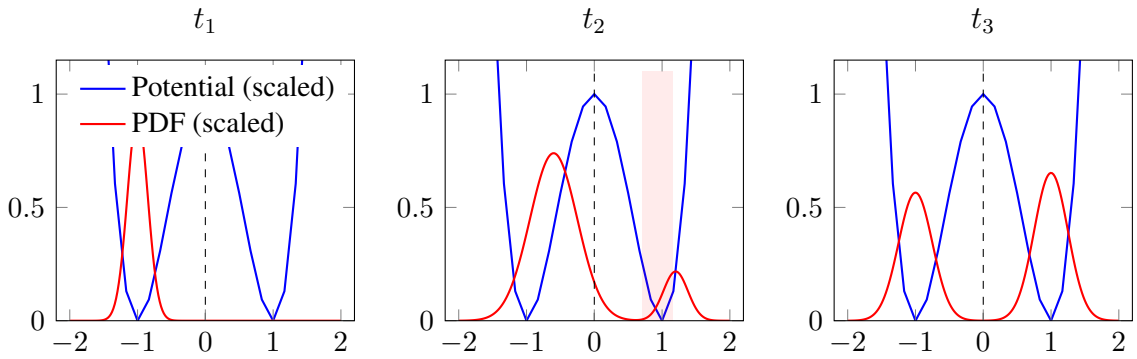

Figure 5.1: Qualitative evolution of the probability density during finite-time escape. Blue curves show the potential $V(x)$ (scaled) and red curves the probability density $\rho(x,t)$ (scaled), at three representative times $t_1 < t_2 < t_3$. At t_1 the density is localised near the left well and spreads under diffusion. At t_2 a secondary peak begins to form in the right well, creating a region where $\partial_x \rho > 0$, which implies $\partial_x S < 0$ and hence a dominant turning path approaching the target from the right. By t_3 the density has developed two well-separated peaks, approaching its long-time form.

5.2 Finite-time and non-equilibrium extensions

Throughout this thesis, we have operated under the assumption of infinite-time averaging for barrier crossing. The time interval was taken to be sufficiently large and ultimately infinite. The natural progression is to examine the role of complex saddles at finite observation times $\mathcal{T}$, when the density is still reorganising between the wells. For general $\mathcal{T}$, the density, initially concentrated as a delta spike near the left minimum, first shifts and broadens; at intermediate times, a secondary peak emerges in the right well and subsequently grows, asymptotically approaching the Boltzmann distribution as $\mathcal{T} \to \infty$. Non-equilibrium physics presents more challenges. Consider a general value of $\mathcal{T}$. As seen in Fig. 5.1, the initial delta function slides towards the local minimum and spreads (time t_1). After some time t_2 a small peak appears in the far well. This grows as the density flows over the barrier, asymptotically approaching the Boltzmann density as $\mathcal{T} \to \infty$.

When the second peak emerges, the system is far from equilibrium. At this stage, there exists a region of x in which the density is an increasing function of x (corresponding to the left slope of the nascent secondary peak). In this region, as $D \to 0$, the action must decrease with increasing x. This behaviour is only possible if the path reverses and approaches the final point from the right. In the Stratonovich

effective potential, such turning paths are prohibited—any extremal that crosses the barrier within finite time will diverge to infinity on the right. By contrast, for the Itô effective potential, turning solutions are permitted for sufficiently small H. This indicates that the Itô potential (and, by extension, general complexification) provides the appropriate framework for analysing finite-time non-equilibrium dynamics.

A new framework in quantum settings, called resurgence (see, for example, [11,48,53,55,72]), is being developed that provides a deeper analysis of the complex analysis at play and can be extended to more complicated multi-instanton structures. It is focused on the analytic continuation of path integrals. There is great interest in generating the full transseries (i.e., a full series representation containing perturbative and non-perturbative effects, logarithmic quasi-mode sectors and highly correlated expansion coefficients), and this framework is rooted in the idea of complex saddles and PL theory. The same complex skeleton may lie beneath the weak-noise asymptotics of the stochastic path integral. The key feature of resurgence is to make the hidden, non-perturbative physics visible; it would be an interesting task to begin to understand the role resurgence may play in the stochastic context. In particular, it could give meaning to the additional terms generated in the expansion and provide access to higher-order non-perturbative physics.

5.3 Universal phase of the complex bounce

In this thesis, we provide detailed calculations of the escape rate for the cubic and sine-Gordon potentials. In both cases for $[\mathcal{I}\bar{\mathcal{I}}]$-type trajectories, the action contained a $\exp(\pm i\pi) = -1$ factor that resolved the sign issue. We show, more generally, how this factor can arise through complex integration.

In the generic Itô case at small $D > 0$, the relevant turning points are complex. The associated complex saddle trajectories then contribute a universal imaginary phase to the action, which fixes the overall sign of the escape contribution. Our goal is to compute this imaginary piece generally using a contour formulation. The method is presented in a general form, though we shall use the cubic potential for

definiteness. It applies to polynomial V, and more generally to analytic V with sufficiently rapid growth at infinity for the residue-at-infinity argument to be justified. Throughout, we assume V is analytic and set

$$A(z) := V'(z), \qquad B(z) := H - 2D\,V''(z), \qquad P(z) := A(z)^2 + B(z), \qquad p(z) := \sqrt{P(z)}. \tag{5.2}$$

Let $z_{\mathrm{cr}} \in \mathbb{R}$ denote a critical point of the effective potential $\mathfrak{U}$ (not necessarily a strict critical point of V; for small D one has $z_{\mathrm{cr}} = z_0 + \mathcal{O}(D)$ if $V'(z_0) = 0$ and $V''(z_0) \neq 0$). Let $z_T^{\pm}$ be the two simple turning points (the simple zeros of $P(z)$) that bifurcate from z_{cr} for small D; for real-analytic V and real H, D they satisfy $z_T^- = \overline{z_T^+}$. We choose a branch cut γ joining z_T^- to z_T^+ and fix the boundary values so that on γ

$$p_-(z) \;=\; -\,p_+(z), \tag{5.3}$$

i.e., the square root flips sign across the cut. For one complex bounce, we define the open integral

$$I_{\mathrm{open}} \;:=\; \int_{z_{\mathrm{cr}}}^{z_T^+} p(z)\,\mathrm{d}z. \tag{5.4}$$

We also introduce the cut integral along the upper edge of the branch cut,

$$I_{\mathrm{cut}} \;:=\; \int_{z_T^-}^{z_T^+} p_+(z)\,\mathrm{d}z, \tag{5.5}$$

and the dog-bone contour integral,

$$I_{\mathrm{dog}} \;:=\; \oint_{\Gamma} p(z)\,\mathrm{d}z, \tag{5.6}$$

where Γ wraps once counter-clockwise around γ (down one edge, up the other). With these conventions,

$$I_{\mathrm{dog}} \;=\; 2\,I_{\mathrm{cut}}, \qquad I_{\mathrm{open}} - \overline{I_{\mathrm{open}}} \;=\; I_{\mathrm{cut}}, \tag{5.7}$$

and hence

$$\operatorname{Im} I_{\mathrm{open}} \;=\; \frac{1}{2\mathrm{i}}\,I_{\mathrm{cut}} \;=\; \frac{1}{4\mathrm{i}}\,I_{\mathrm{dog}}. \tag{5.8}$$

The contribution of a single complex bounce to the action is

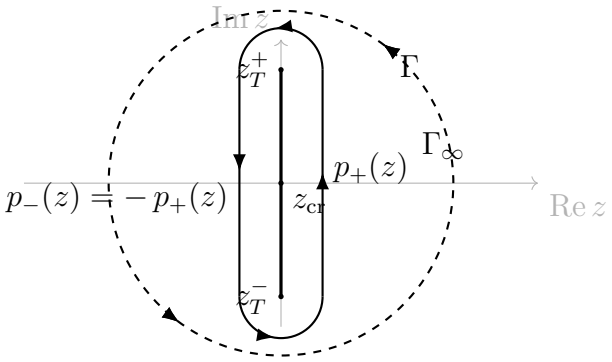

Figure 5.2: Dog-bone contour Γ wrapping the branch cut between the complex turning points $z_T^{\pm}$. Across the cut the WKB momentum flips sign, $p_-(z) = -p_+(z)$, so the closed contour integral $\oint_\Gamma p(z)\,\mathrm{d}z$ equals twice the single-edge cut integral. The dashed circle Γ_∞ indicates the blown-up contour used to evaluate $\oint_\Gamma p\,\mathrm{d}z$ via residues (including the residue at infinity).

$$S_{1\mathrm{b}} := 4\, I_{\mathrm{open}}. \tag{5.9}$$

Using (5.8), its imaginary part is

$$\mathrm{Im}\, S_{1\mathrm{b}} \;=\; 4\ \mathrm{Im}\, I_{\mathrm{open}} \;=\; \frac{2}{\mathrm{i}}\, I_{\mathrm{cut}} \;=\; \frac{1}{\mathrm{i}}\, I_{\mathrm{dog}}. \tag{5.10}$$

To compute I_{dog} we deform Γ away from the cut (optionally out to a large circle $|z| = R \to \infty$) and use the uniform binomial expansion. For a polynomial V of positive degree, $|A(z)| \to \infty$ while $B(z) = O(1) + O(z^{\deg V - 2})$ and $A(z)^2 \gg B(z)$. Hence, on $|z| = R$,

$$p(z) \;=\; A(z)\sqrt{1 + \frac{B(z)}{A(z)^2}} \;=\; A(z) \;+\; \frac{B(z)}{2A(z)} \;-\; \frac{B(z)^2}{8A(z)^3} \;+\; \cdots . \tag{5.11}$$

Define the meromorphic truncation

$$p_{\mathrm{mer}}(z) := A(z) \;+\; \frac{B(z)}{2A(z)} \;=\; V'(z) \;+\; \frac{H}{2}\frac{1}{V'(z)} \;-\; D\,\frac{V''(z)}{V'(z)}. \tag{5.12}$$

Then

$$I_{\rm dog} \;=\; \oint_{|z|=R} p(z)\,\mathrm{d}z \;=\; \oint_{|z|=R} p_{\rm mer}(z)\,\mathrm{d}z \;+\; \underbrace{\oint_{|z|=R} \sum_{n\geq 2} T_n(z)\,\mathrm{d}z}_{\text{higher-order terms}}, \tag{5.13}$$

where $T_n(z) = c_n\, B(z)^n / A(z)^{\,2n-1}$. If $\deg V = m \geq 2$, then $A(z) \sim z^{m-1}$, $V''(z) \sim z^{m-2}$, and

$$T_n(z) \;\sim\; \frac{z^{n(m-2)}}{z^{(m-1)(2n-1)}} = z^{-\,[1+m(n-1)]} \quad (|z| \to \infty). \tag{5.14}$$

Thus, $T_{n\geq 2}$ have no $1/z$ term at infinity, so $\mathrm{Res}_{z=\infty}\, T_{n\geq 2} = 0$. From now on,

$$I_{\rm dog} \;=\; \oint_{|z|=R} p_{\rm mer}(z)\,\mathrm{d}z. \tag{5.15}$$

With $A(z) = V'(z)$, we have a total derivative so that its Laurent series at infinity has no z^{-1} term. It immediately follows that $\oint A(z)\mathrm{d}z = 0$. For the next term,

$$\mathrm{Res}_{z=\infty} \frac{B(z)}{2A(z)} = -\sum_{z_k : A(z_k)=0} \mathrm{Res}_{z=z_k} \frac{B(z)}{2A(z)}, \tag{5.16}$$

where z_k denotes the simple poles of $1/V'(z)$. At a simple zero z_k, $A(z) = A'(z_k)(z-z_k) + \mathcal{O}(z-z_k)^2 \approx V''(z_k)(z-z_k)$ and $B(z)$ is analytic. Therefore,

$$\mathrm{Res}_{z=z_k} \frac{B(z)}{2A(z)} = \frac{B(z_k)}{2A'(z_k)} = \frac{H - 2DV''(z_k)}{2V''(z_k)}. \tag{5.17}$$

Hence, altogether we get

$$\oint_{\Gamma_\infty} p_{\rm mer}(z)\,dz = \frac{H}{2}\oint_{\Gamma_\infty} \frac{dz}{V'(z)} - D\oint_{\Gamma_\infty} \frac{V''(z)}{V'(z)}\,dz = 2\pi i\Big[\frac{H}{2}\sum \frac{1}{V''(z_k)} - DN\Big]. \tag{5.18}$$

where N is the number (with multiplicity/winding) of zeros of V' enclosed by Γ_∞.

Cubic check. For $V(x) = -\frac{1}{3}x^3 + a^2 x$, one has $V'(z) = -(z^2 - a^2)$, $V''(z) = -2z$. On the blown-up

contour enclosing both zeros $z_k = \pm a$,

$$\sum_k \frac{1}{V''(z_k)} \;=\; \frac{1}{-2a} \,+\, \frac{1}{+2a} \;=\; 0, \qquad N \;=\; 2, \tag{5.19}$$

so

$$I_{\rm dog} \;=\; -\,4\pi \mathrm{i}\, D. \tag{5.20}$$

Using (5.10), this gives

$$\mathrm{Im}\, S_{\rm 1b} \;=\; \frac{1}{\mathrm{i}}\, I_{\rm dog} \;=\; -\,4\pi D, \tag{5.21}$$

so the OM weight $e^{-S_{\rm 1b}/(4D)}$ carries the phase $e^{-\mathrm{i}\ \mathrm{Im}\, S_{\rm 1b}/(4D)} = e^{\mathrm{i}\pi} = -1$.

Appendix A

Steepest descent curves as we continue our parameter

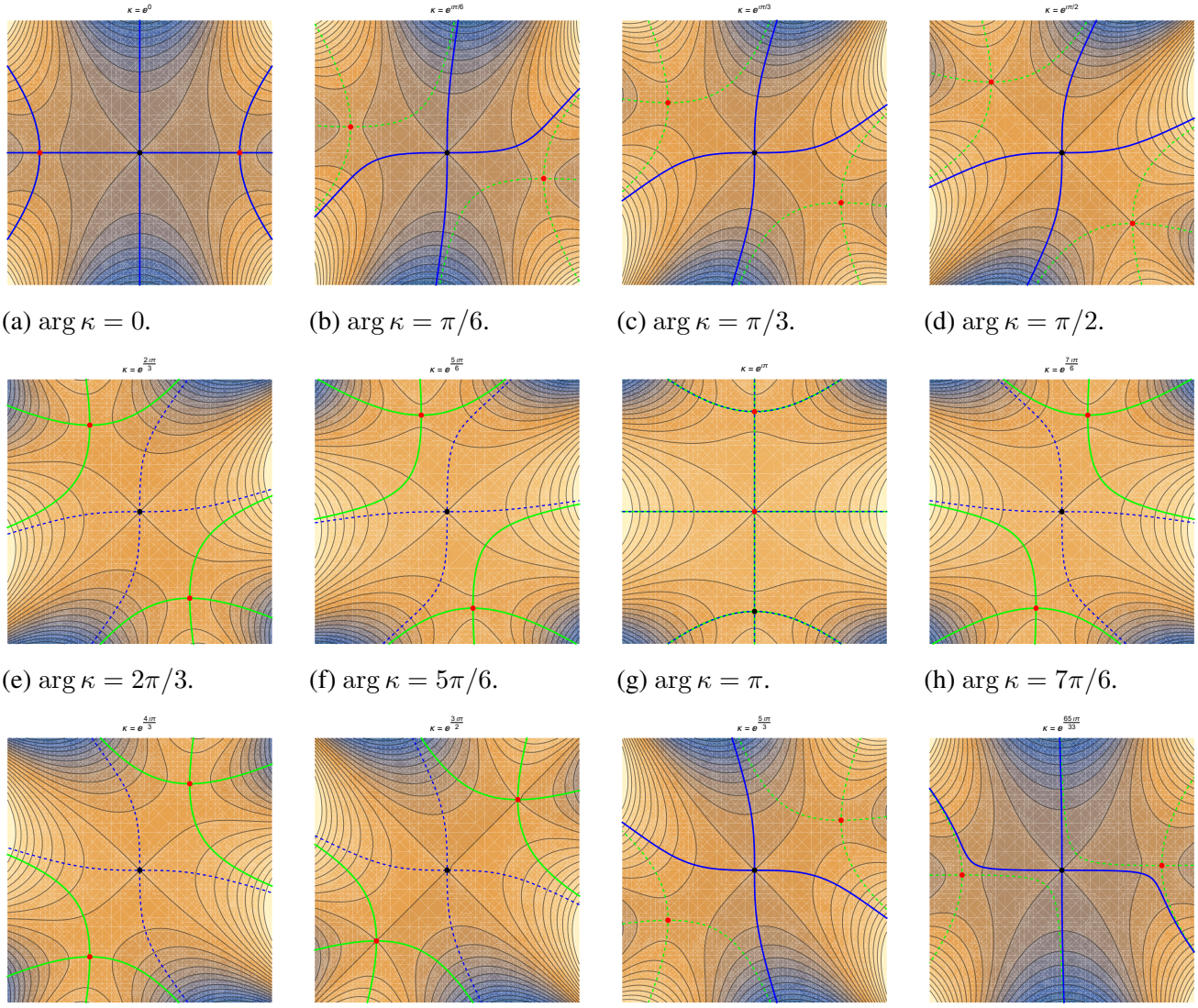

(a) $\arg \kappa = 0$. (b) $\arg \kappa = \pi/6$. (c) $\arg \kappa = \pi/3$. (d) $\arg \kappa = \pi/2$.

(e) $\arg \kappa = 2\pi/3$. (f) $\arg \kappa = 5\pi/6$. (g) $\arg \kappa = \pi$. (h) $\arg \kappa = 7\pi/6$.

(i) $\arg \kappa = 4\pi/3$. (j) $\arg \kappa = 3\pi/2$. (k) $\arg \kappa = 5\pi/3$. (l) $\arg \kappa = 65\pi/33$.

Figure A.1: One-dimensional steepest descent and steepest ascent curves (Lefschetz thimbles and dual thimbles) for the finite-dimensional model integral used to introduce the method of steepest descents in § 1.2.3 ($a = \kappa$) and to develop motivation for Picard–Lefschetz theory in § 3.6. Panels 1–12 correspond to the same integrand presented in § 1.2.3.1 under continuation of the complex parameter through the twelve arguments
$\arg \kappa \in \{0, \pi/6, \pi/3, \pi/2, 2\pi/3, 5\pi/6, \pi, 7\pi/6, 4\pi/3, 3\pi/2, 5\pi/3, 65\pi/33\}$ (in the ordering shown).

Appendix B

Global preliminaries

B.1 Gaussian noise PDF derivation

We briefly derive the continuum Gaussian noise weight used in (2.5). Let $[t_1, t_2]$ be partitioned into N equal subintervals of width Δ, so that $T := t_2 - t_1 = N\Delta$ and $t_k := t_1 + k\Delta$ for $k = 0, \ldots, N$. White noise $\xi(t)$ with covariance $\langle \xi(t)\, \xi(t') \rangle = 2D\, \delta(t - t')$ is rigorously handled via its *time-integrated* increments

$$\eta_k \;:=\; \int_{t_k}^{t_{k+1}} \xi(t)\, \mathrm{d}t, \qquad k = 0, \ldots, N-1. \tag{B.1}$$

These $\{\eta_k\}$ are independent, mean-zero Gaussians with variances

$$\langle \eta_k \eta_\ell \rangle \;=\; 2D\, \Delta\, \delta_{k\ell}. \tag{B.2}$$

Therefore, their joint density factorises:

$$P_N[\{\eta\}] \;=\; \prod_{k=0}^{N-1} \frac{1}{\sqrt{4\pi D\, \Delta}} \exp\!\left[-\frac{\eta_k^2}{4D\, \Delta} \right] \;=\; (4\pi D\, \Delta)^{-N/2} \exp\!\left[-\frac{1}{4D\, \Delta} \sum_{k=0}^{N-1} \eta_k^2 \right]. \tag{B.3}$$

To pass to the continuum form, note that $\eta_k = \int_{t_k}^{t_{k+1}} \xi(t)\,\mathrm{d}t \approx \xi(t_k)\,\Delta$ for small Δ, so

$$\frac{1}{\Delta}\sum_{k=0}^{N-1}\eta_k^2 \;\approx\; \sum_{k=0}^{N-1}\xi(t_k)^2\,\Delta \;\xrightarrow[\Delta\to 0]{}\; \int_{t_1}^{t_2}\xi(t)^2\,\mathrm{d}t,$$

i.e. the discrete quadratic form is a Riemann sum for $\int \xi^2$. Hence (B.3) becomes

$$P[\xi] \;\equiv\; \mathcal{N}_D\,\exp\!\left[-\frac{1}{4D}\int_{t_1}^{t_2}\xi(t)^2\,\mathrm{d}t\right], \qquad \mathcal{N}_D \;=\; \lim_{N\to\infty}(4\pi D\,\Delta)^{-N/2}, \tag{B.4}$$

which is the continuum Gaussian functional weight stated in (2.5). The prefactor $\mathcal{N}_D$ is the (divergent) product of one-dimensional Gaussian normalisations; in the main text it is absorbed into the definition of the free path measure (cf. $\mathcal{N}_D$ in Sec. 2.72).

Remark B.1.1 (Why use integrated noise increments?). Since white noise is the formal time derivative of a Wiener process, sampling "point values" $\xi(t_k)$ is not well-defined as ordinary random variables. The integrated increments $\eta_k = \int_{t_k}^{t_{k+1}} \xi\,\mathrm{d}t$ are bona fide Gaussians with variance $2D\Delta$, which makes (B.3) rigorous and leads cleanly to the continuum form (B.4).

B.2 Onsager–Machlup Jacobian derivation

We work on a time grid $t_k = t_1 + k\Delta$ for $k = 0, 1, \ldots, N$ with $t_2 - t_1 = N\Delta$. Define the path samples $x_k := x(t_k)$ and the integrated noise increments

$$\eta_k \;:=\; \int_{t_k}^{t_{k+1}} \xi(t)\;\mathrm{d}t, \qquad k = 0, \ldots, N-1, \tag{B.5}$$

so that $\eta_k \sim \mathcal{N}(0,\, 2D\,\Delta)$ are independent Gaussians. The λ-discretization of the overdamped Langevin equation

$$\dot{x} = F(x) + \xi(t) \tag{B.6}$$

reads

$$x_{k+1} - x_k \;=\; \Delta\big[(1-\lambda)F(x_k) + \lambda F(x_{k+1})\big] \;+\; \eta_k, \qquad k = 0, \dots, N-1. \tag{B.7}$$

For $\lambda = 0$ and $\lambda = \frac{1}{2}$ this reproduces the Itô and Stratonovich schemes, respectively. Given the fixed initial data x_0, (B.7) defines a one-to-one map

$$\{x_1, \dots, x_N\} \longleftrightarrow \{\eta_0, \dots, \eta_{N-1}\}, \qquad \eta_k \;=\; x_{k+1} - x_k - \Delta[(1-\lambda)F(x_k) + \lambda F(x_{k+1})]\,. \tag{B.8}$$

The Jacobian matrix J is

$$J_{k,m} \;:=\; \frac{\partial \eta_{k-1}}{\partial x_m}, \qquad k, m = 1, \dots, N, \tag{B.9}$$

(i.e. we pair the equation for η_{k-1} with the unknown x_k). Each η_{k-1} depends only on x_{k-1} and x_k, so J is *lower bidiagonal*:

$$\frac{\partial \eta_{k-1}}{\partial x_k} = \quad 1 \;-\; \lambda\,\Delta\,F'(x_k), \tag{B.10}$$

$$\frac{\partial \eta_{k-1}}{\partial x_{k-1}} = \; -1 \;-\; (1-\lambda)\,\Delta\,F'(x_{k-1}), \tag{B.11}$$

$$\frac{\partial \eta_{k-1}}{\partial x_m} = 0 \quad \text{otherwise.} \tag{B.12}$$

Thus

$$J \;=\; \begin{bmatrix} 1-\lambda\Delta F'(x_1) & 0 & 0 & \cdots \\ -1-(1-\lambda)\Delta F'(x_1) & 1-\lambda\Delta F'(x_2) & 0 & \cdots \\ 0 & -1-(1-\lambda)\Delta F'(x_2) & 1-\lambda\Delta F'(x_3) & \cdots \\ \vdots & \vdots & \vdots & \ddots \end{bmatrix}. \tag{B.13}$$

Being triangular, its determinant is the product of the diagonal entries:

$$\det J \;=\; \prod_{k=1}^{N} [\,1 - \lambda\,\Delta\,F'(x_k)\,]\,. \tag{B.14}$$

Taking logs and expanding $\log(1-z) = -z + O(z^2)$,

$$\log\det J \;=\; \sum_{k=1}^{N} \log\bigl(1 - \lambda\,\Delta\,F'(x_k)\bigr) \;=\; -\,\lambda\,\Delta \sum_{k=1}^{N} F'(x_k) \;+\; O(\Delta^2). \tag{B.15}$$

Hence, as $\Delta \to 0$ with $N\Delta = t_2 - t_1$,

$$\det J \;\longrightarrow\; \exp\!\left(-\lambda \int_{t_1}^{t_2} F'(x(t))\; \mathrm{d}t \right). \tag{B.16}$$

Two standard conventions follow immediately:

- **Itô ($\lambda = 0$):** $\det J \equiv 1$.
- **Stratonovich ($\lambda = \frac{1}{2}$):** with $F = -V'$ (conservative force),

$$\det J \;=\; \exp\!\left(\frac{1}{2} \int_{t_1}^{t_2} V''(x(t))\; \mathrm{d}t \right). \tag{B.17}$$

This is precisely the Onsager–Machlup Jacobian factor that multiplies the Gaussian weight of the noise in the path integral.

B.3 Interaction action for an instanton–instanton pair

Consider a metastable well at x_α, a barrier top at x_β with

$$V''(x_\beta) = -\omega_\beta, \qquad \omega_\beta := |V''(x_\beta)| > 0,$$

and a stable well at x_c (cf. Fig. 2.1). We construct a composite $[\mathcal{I}\mathcal{I}]$ path by gluing an uphill segment x_u (solving $\dot{x} = +V'(x)$) to a downhill segment x_d (solving $\dot{x} = -V'(x)$) across a short bridge centered

at time θ. Near x_β we use

$$V'(x) \;\simeq\; V''(x_\beta)\,(x - x_\beta) \;=\; -\omega_\beta\,(x - x_\beta),$$

so for the uphill flow $\dot{x} = +V'$ we have $\dot{x} \simeq -\omega_\beta(x - x_\beta)$ (velocity positive immediately to the left of the barrier), and for the downhill flow $\dot{x} = -V'$ we have $\dot{x} \simeq +\omega_\beta(x - x_\beta)$ (velocity positive immediately to the right).

Fix small $\delta x > 0$ and large $\delta\theta > 0$. Define the three pieces:

(i) Left/uphill tail x_i : $\quad x_i(\theta - \delta\theta) = x_\beta - \delta x, \qquad \dot{x}_i(\theta - \delta\theta) = +\omega_\beta\,\delta x,$

(ii) Short bridge x_j : $\quad x_j(\theta - \delta\theta) = x_\beta - \delta x, \qquad x_j(\theta + \delta\theta) = x_\beta + \delta x,$

(iii) Right/downhill tail x_k : $\quad x_k(\theta + \delta\theta) = x_\beta + \delta x, \qquad \dot{x}_k(\theta + \delta\theta) = +\omega_\beta\,\delta x.$

Here (i) and (iii) are the restrictions of the exact steepest descent solutions x_u and x_d to the linear region; (ii) will be the exact Euler–Lagrange solution that interpolates between the two sides.

On the bridge we solve the linearised E–L equation

$$\ddot{x} \;=\; V'(x)\,V''(x) \;\simeq\; \omega_\beta^2\,(x - x_\beta), \quad t \in [\theta - \delta\theta, \theta + \delta\theta],$$

with the two-point boundary data above. The unique solution is

$$x_j(t) \;=\; x_\beta + \delta x\,\frac{\sinh\big(\omega_\beta(t - \theta)\big)}{\sinh\big(\omega_\beta\delta\theta\big)}.$$

For the action density $L = \dot{x}^2 + [V'(x)]^2$ in the linear region we have

$$V'(x_j) \simeq -\omega_\beta(x_j - x_\beta), \qquad \dot{x}_j = \omega_\beta\delta x\,\frac{\cosh\big(\omega_\beta(t - \theta)\big)}{\sinh\big(\omega_\beta\delta\theta\big)}.$$

A short calculation yields

$$\mathcal{S}[x_j]_{\theta-\delta\theta}^{\theta+\delta\theta} = \int_{\theta-\delta\theta}^{\theta+\delta\theta} \left(\dot{x}_j^2 + \omega_\beta^2 (x_j - x_\beta)^2\right)\, \mathrm{d}t = 2\,\omega_\beta\,(\delta x)^2\,\coth\!\big(\omega_\beta \delta\theta\big). \tag{B.18}$$

The composite path is $x_{\rm cl} = x_i \cup x_j \cup x_k$, and we compare its action with the reference action of the pure uphill path x_u continued through the barrier region. Writing

$$\mathcal{S}[x_{\rm cl}] = \mathcal{S}[x_u]_{(-\infty,\theta-\delta\theta)} + \mathcal{S}[x_j]_{(\theta-\delta\theta,\theta+\delta\theta)} + \mathcal{S}[x_d]_{(\theta+\delta\theta,\infty)},$$

and adding and subtracting $\mathcal{S}[x_u]_{(\theta-\delta\theta,\infty)}$, we get

$$\mathcal{S}[x_{\rm cl}] = \mathcal{S}[x_u]_{(-\infty,\infty)} + \Big\{\mathcal{S}[x_j]_{(\theta-\delta\theta,\theta+\delta\theta)} - \mathcal{S}[x_u]_{(\theta-\delta\theta,\infty)} + \mathcal{S}[x_d]_{(\theta+\delta\theta,\infty)}\Big\}.$$

The last two terms form a *common tail* beyond the bridge: both the reference and the glued configuration evolve to the right well along steepest descent flow, so their far right contributions cancel in the difference.[1] Thus the *interaction action* is localized near the barrier and reads

$$\mathcal{S}_{\rm int}(\delta\theta, \delta x) \;=\; \mathcal{S}[x_j]_{\theta-\delta\theta}^{\theta+\delta\theta} - \mathcal{S}[x_u]_{\theta-\delta\theta}^{\infty}. \tag{B.19}$$

Along x_u we have $\dot{x}_u = +V'(x_u) \simeq -\omega_\beta(x_u - x_\beta)$, so $\dot{x}_u^2 = [V'(x_u)]^2 = \omega_\beta^2 (x_u - x_\beta)^2$. Near the barrier the uphill tail is $x_u(t) - x_\beta \simeq -\,\delta x\, e^{-\omega_\beta (t-(\theta-\delta\theta))}$. Therefore

$$\mathcal{S}[x_u]_{\theta-\delta\theta}^{\infty} = \int_{\theta-\delta\theta}^{\infty} \left(\dot{x}_u^2 + [V'(x_u)]^2\right)\, \mathrm{d}t = 2\,\omega_\beta^2 (\delta x)^2 \int_0^\infty e^{-2\omega_\beta \tau}\, d\tau = \omega_\beta\,(\delta x)^2. \tag{B.20}$$

Combining (B.18) and (B.20) in (B.19),

$$\mathcal{S}_{\rm int}(\delta\theta, \delta x) = 2\,\omega_\beta (\delta x)^2 \Big[\coth(\omega_\beta \delta\theta) - 1\Big] = 2\,\omega_\beta (\delta x)^2\, \frac{e^{-\omega_\beta \delta\theta}}{\sinh(\omega_\beta \delta\theta)}. \tag{B.21}$$

[1] Equivalently, one may truncate both paths at $\theta \pm \delta\theta$ and compare only the local replacement of the uphill tail by the bridge; the downhill evolution is identical in both and drops out.

Using the uphill relation at the bridge center,

$$\dot{x}_u(\theta) \;=\; \omega_\beta\, \delta x\, e^{-\omega_\beta \delta\theta},$$

we obtain for large separation $\omega_\beta \delta\theta \gg 1$ (so that $e^{-\omega_\beta\delta\theta}/\sinh(\omega_\beta\delta\theta) \to 2e^{-2\omega_\beta\delta\theta}$):

$$\mathcal{S}_{\text{int}} \;\xrightarrow{\delta\theta\to\infty}\; \frac{4}{\omega_\beta}\left[\dot{x}_u(\theta)\right]^2. \tag{B.22}$$

This is the form used in the main text. It matches the $\tau \to 0$ "no correlation" limit of McKane–Luckock [117] after accounting for our convention that the stochastic action is four times larger (see Chapter 2).

- The derivation is local: only the linearised barrier region enters $\mathcal{S}_{\text{int}}$. The precise duration $2\delta\theta$ drops out of the asymptotics through (B.22).
- The "downhill contributes nothing" statement in the main text means "the downhill *tail* cancels in the comparison": in going from the reference uphill continuation to the glued configuration, the only net change in action at leading order is the replacement of the uphill tail by the minimal bridge segment.

B.4 Stationarity, saddle points, and minima in the stochastic path integral

In the analysis of stochastic path integrals, particularly when studying semiclassical approximations via steepest descent (or Lefschetz thimble methods), it is crucial to understand the classification of stationary configurations. This appendix provides a precise mathematical and physical characterisation of the three canonical classes of stationary points: *global minima*, *local minima*, and *saddle points*, in the context of variational functionals defined over infinite-dimensional path spaces. These distinctions

underpin the interpretation of classical solutions and their corresponding fluctuation spectra in both quantum and stochastic formulations.

B.4.1 Stationarity and the First Variation

Let $S[x]$ denote the action functional. A path $x_{\text{cl}}(t)$ is said to be a *stationary point* of S if it satisfies the Euler–Lagrange equation:

$$\left.\frac{\delta S[x]}{\delta x(t)}\right|_{x=x_{\text{cl}}} = 0. \tag{B.23}$$

This is the condition that the *first variation* of the action vanishes. Such a path is an extremum of S, but its nature (minimum, maximum, saddle) is determined by the *second variation*.

B.4.2 Second Variation and Fluctuation Operator

The second variation defines the quadratic expansion of the action around $x_{\text{cl}}(t)$:

$$S[x] = S[x_{\text{cl}}] + \frac{1}{2}\int \mathrm{d}t_1 \int \mathrm{d}t_2 \; \eta(t_1)\hat{\mathcal{M}}(t_1,t_2)\eta(t_2) + \mathcal{O}(\eta^3), \tag{B.24}$$

where $\eta(t) = x(t) - x_{\text{cl}}(t)$ is the fluctuation and $\hat{\mathcal{M}}$ is the *fluctuation operator*, formally the Hessian of S:

$$\hat{\mathcal{M}}[t_1,t_2] = \left.\frac{\delta^2 S[x]}{\delta x(t_1)\delta x(t_2)}\right|_{x=x_{\text{cl}}}. \tag{B.25}$$

The spectral properties of $\hat{\mathcal{M}}$ determine the nature of $x_{\text{cl}}(t)$. In particular, we distinguish three canonical cases:

B.4.3 Classification of Stationary Points

(i) Global Minimum: A path x_{cl} is a global minimum of S if:

- It satisfies the Euler–Lagrange equation (stationarity).
- The second variation is *strictly positive* for all perturbations $\eta(t) \neq 0$ in the allowed function space:

$$\int \mathrm{d}t_1 \, \mathrm{d}t_2 \; \eta(t_1) \, \hat{\mathcal{M}}(t_1, t_2) \, \eta(t_2) > 0 \quad \forall \, \eta \neq 0. \tag{B.26}$$

- Moreover, $S[x_{\mathrm{cl}}] \leq S[x]$ for all admissible paths $x(t)$. This ensures *global minimality*.

(ii) Local Minimum: A path x_{cl} is a local minimum if the above positivity condition holds *only for sufficiently small* perturbations:

- The action increases under small deviations:

$$S[x_{\mathrm{cl}} + \varepsilon\eta] > S[x_{\mathrm{cl}}] \quad \text{for all } \eta, \text{ small } \varepsilon > 0. \tag{B.27}$$

- The fluctuation operator has *non-negative spectrum*:

$$\mathrm{Spec}(\hat{\mathcal{M}}) \subseteq [0, \infty), \quad \text{with zero modes removed or accounted for.} \tag{B.28}$$

Local minima are often metastable states in the path integral framework.

(iii) Saddle Point: A configuration x_{cl} is a saddle point if the second variation is *indefinite*, i.e., there exist directions η_+ and η_- in path space such that:

$$\int \mathrm{d}t_1 \, \mathrm{d}t_2 \; \eta_+(t_1) \, \hat{\mathcal{M}}[t_1, t_2] \, \eta_+(t_2) > 0, \quad \int \mathrm{d}t_1 \, \mathrm{d}t_2 \; \eta_-(t_1) \, \hat{\mathcal{M}}[t_1, t_2] \, \eta_-(t_2) < 0. \tag{B.29}$$

That is, S increases in some directions and decreases in others. This is precisely the case for the stochastic $[\mathcal{RB}]$ solution discussed in the main text: its fluctuation operator possesses a single negative eigenvalue (corresponding to an unstable mode), alongside a zero mode (associated with time-translation symmetry), and an infinite tower of positive modes.

Spectral Intuition: The number of negative eigenvalues of $\hat{\mathcal{M}}$ counts the number of unstable directions. Saddle points with one negative eigenvalue are generic in bounce-type solutions and lead to an imaginary contribution to the path integral under proper analytic continuation. This is consistent with their role in tunnelling or escape processes, where they mediate transitions between metastable states.

B.4.4 Path Integral Implications

In the semiclassical evaluation of path integrals, stationary configurations contribute leading-order terms via the saddle-point approximation. The classification above determines whether such contributions are suppressed, enhanced, or require special contour deformation (as in Lefschetz theory).

In particular:

- **Global minima** dominate zero-noise path integrals.
- **Local minima** yield real Gaussian contributions.
- **Saddle points** yield complex contributions and are essential in capturing non-perturbative effects.

Thus, the detailed structure of the fluctuation spectrum around a classical configuration is not merely technical: it is central to understanding the structure of perturbative vs. non-perturbative sectors, the role of negative modes.

Appendix C

Eigenvalue and eigenfunction analysis for the quasi-zero mode

This section benefited from conversations with Professor Steve Fitzgerald.

C.1 Analytic estimate of the QZM eigenvalue

We can use the real bounce results and continue $D \to -D$ to obtain the quasi-eigenvalue of the complex bounce. We study the following operator,

$$\mathcal{M}\, y(t) \;=\; \Big(-\frac{\mathrm{d}^2}{\mathrm{d}t^2} + \omega^2\, U(t) \Big)\, y(t) \;=\; \lambda\, y(t), \tag{C.1}$$

where U is a double Pöschl–Teller profile with the form

$$U(t) = 1 - \frac{3}{2}(S_+^2 + S_-^2), \tag{C.2}$$

where $S_\pm = \mathrm{sech}(\omega(t \pm t_0)/2)$. Introduce the rescaled variable $T = \omega t$ and $T_0 = \omega t_0$. Then

$$\frac{\mathrm{d}^2}{\mathrm{d}t^2} = \omega^2 \frac{\mathrm{d}^2}{\mathrm{d}T^2}, \qquad y''(t) = \omega^2\, y_{TT}(T), \qquad \lambda' = \frac{\lambda}{\omega^2}. \tag{C.3}$$

In T-coordinates, the operator is

$$\mathcal{M}'\, y \;=\; \Big(-\frac{\mathrm{d}^2}{\mathrm{d}T^2} + U(T) \Big)\, y \;=\; \lambda'\, y, \tag{C.4}$$

with the piecewise potential $\mathcal{M}' = \mathcal{M}_0 + \mathcal{M}_1$ where

$$\mathcal{M}_0 \;=\; \begin{cases} -\dfrac{\mathrm{d}^2}{\mathrm{d}T^2} + 1 - \dfrac{3}{2}\,\mathrm{sech}^2\big(\dfrac{T+T_0}{2}\big), & T < 0, \\[2ex] -\dfrac{\mathrm{d}^2}{\mathrm{d}T^2} + 1 - \dfrac{3}{2}\,\mathrm{sech}^2\big(\dfrac{T-T_0}{2}\big), & T > 0, \end{cases} \tag{C.5}$$

and

$$\mathcal{M}_1 \;=\; \begin{cases} -\dfrac{3}{2}\,\mathrm{sech}^2\big(\dfrac{T+T_0}{2}\big), & T < 0, \\[2ex] -\dfrac{3}{2}\,\mathrm{sech}^2\big(\dfrac{T-T_0}{2}\big), & T > 0. \end{cases} \tag{C.6}$$

This is continuous at $T = 0$. Define the (continuous) piecewise function,

$$y_0(T) \;=\; \begin{cases} \mathrm{sech}^2\big(\dfrac{T+T_0}{2}\big), & T < 0, \\[2ex] \mathrm{sech}^2\big(\dfrac{T-T_0}{2}\big), & T > 0. \end{cases} \tag{C.7}$$

which is the translation zero mode of each isolated Pöschl–Teller well. A direct check shows $\mathcal{M}_0 y_0 = 0$ away from $T = 0$ for the decoupled operator $\mathcal{M}_0$. The leading (small) eigenvalue of $\mathcal{M}'$ is well captured by the Rayleigh quotient with the trial state y_0:

$$\lambda' \;=\; \frac{\displaystyle\int_{-\infty}^{\infty} y_0\, \mathcal{M}_1 y_0\, \mathrm{d}T}{\displaystyle\int_{-\infty}^{\infty} y_0^2\, \mathrm{d}T} \;=\; -\frac{3}{2}\frac{I_1}{I_0}, \tag{C.8}$$

where

$$I_0 := \int_{-\infty}^{\infty} y_0^2 \, \mathrm{d}T, \qquad I_1 := 2\int_0^{\infty} \operatorname{sech}^4\!\Big(\frac{T-T_0}{2}\Big)\, \operatorname{sech}^2\!\Big(\frac{T+T_0}{2}\Big)\, \mathrm{d}T. \tag{C.9}$$

By evenness and change of variables $\tau = \frac{T-T_0}{2}$,

$$I_0 = 2\int_0^{\infty} \operatorname{sech}^4\!\Big(\frac{T-T_0}{2}\Big)\, \mathrm{d}T = 4\int_{-T_0/2}^{\infty} \operatorname{sech}^4\tau \, \mathrm{d}\tau.$$

Using $\int \operatorname{sech}^4\tau \, \mathrm{d}\tau = \tanh\tau - \frac{1}{3}\tanh^3\tau$ and setting $\mu := \tanh\big(\frac{T_0}{2}\big) \in (0,1)$, we obtain

$$I_0 = 4\Big[\tanh\tau - \frac{1}{3}\tanh^3\tau\Big]_{-T_0/2}^{\infty} = 4\Big(\frac{2}{3} + \mu - \frac{1}{3}\mu^3\Big). \tag{C.10}$$

A slightly more involved calculation for I_1 gives

$$I_1 = \frac{16\, e^{-2T_0}}{(1+\mu)^2}\left(\frac{1}{3} + \mu + \frac{1}{3}\mu^3\right), \qquad e^{-T_0} = \frac{1-\mu}{1+\mu}. \tag{C.11}$$

Using the large separation relation for T_0 (equivalently μ) and D obtained from the real bounce solution in Chapter 3, the factor $\exp(-2T_0)$ reduces to an $\mathcal{O}(D)$ contribution. Combining (C.8), (C.10) and (C.11) gives

$$\lambda = \omega^2\lambda' \approx -\frac{12D}{a}. \tag{C.12}$$

Taking $D \to -D$ gives the result.

Bibliography

[1] Gert Aarts, Lorenzo Bongiovanni, Erhard Seiler, and Dénes Sexty. Some remarks on Lefschetz thimbles and complex Langevin dynamics. *Journal of High Energy Physics*, 2014(10):159, 2014.

[2] Romain Allez and Laure Dumaz. Random matrices in non-confining potentials. *Journal of Statistical Physics*, 160:681–714, 2015.

[3] Alexander G. Anderson and Carl M. Bender. Complex Trajectories in a Classical Periodic Potential. *Journal of Physics A: Mathematical and Theoretical*, 45(45):455101, 2012.

[4] Hideaki Aoyama, Hisashi Kikuchi, Ikuo Okouchi, Masatoshi Sato, and Shinya Wada. Valleys in quantum mechanics. *Physics Letters B*, 424(1-2):93–100, 1998.

[5] Hideaki Aoyama, Hisashi Kikuchi, Ikuo Okouchi, Masatoshi Sato, and Shinya Wada. Valley views: instantons, large order behaviors, and supersymmetry. *Nuclear Physics B*, 553(3):644–710, 1999.

[6] V. I. Arnol'd. Characteristic class entering in quantization conditions. *Functional Analysis and Its Applications*, 1(1):1–13, 1967. Translated from *Funktsional'nyi Analiz i Ego Prilozheniya*, 1(1), 1–14 (1967).

[7] V. I. Arnol'd, S. M. Gusein-Zade, and A. N. Varchenko. *Singularities of Differentiable Maps, Volume 2: Monodromy and Asymptotics of Integrals*. Modern Birkhäuser Classics. Birkhäuser, Boston, MA, 2012.

[8] Serge Aubry and Pierre-Yves Le Daeron. The discrete Frenkel–Kontorova model and its extensions. I. Exact results for the ground-states. *Physica D: Nonlinear Phenomena*, 8:381–422, 1983.

[9] Léon Autonne. *Sur les matrices hypohermitiennes et sur les matrices unitaires*, volume 38 of *Annales de l'Université de Lyon. Nouvelle série I. Sciences, médecine*. A. Rey, Lyon, 1915.

[10] Steven G Avery and Burkhard UW Schwab. Noether's second theorem and Ward identities for gauge symmetries. *Journal of High Energy Physics*, 2016(2):1–31, 2016.

[11] Gökçe Basar, Gerald V Dunne, and Mithat Ünsal. Resurgence theory, ghost-instantons, and analytic continuation of path integrals. *Journal of High Energy Physics*, 2013(10):41, 2013.

[12] Alireza Behtash, Gerald V. Dunne, Thomas Schäfer, Tin Sulejmanpasic, and Mithat Ünsal. Complexified Path Integrals, Exact Saddles, and Supersymmetry. *Phys. Rev. Lett.*, 116(1):011601, 2016.

[13] Alireza Behtash, Gerald V. Dunne, Thomas Schäfer, Tin Sulejmanpasic, and Mithat Ünsal. Toward Picard–Lefschetz theory of path integrals, complex saddles and resurgence. *Annals of Mathematical Sciences and Applications*, 2(1):95–212, 2017.

[14] Alireza Behtash, Gerald V Dunne, Thomas Schäfer, Tin Sulejmanpasic, and Mithat Ünsal. Critical points at infinity, non-Gaussian saddles, and bions. *Journal of High Energy Physics*, 2018(6):68, 2018.

[15] Alireza Behtash, Erich Poppitz, Tin Sulejmanpasic, and Mithat Ünsal. The curious incident of multi-instantons and the necessity of Lefschetz thimbles. *Annals of Mathematical Sciences and Applications*, 2015.

[16] C. M. Bender and S. A. Orszag. *Advanced Mathematical Methods for Scientists and Engineers I: Asymptotic Methods and Perturbation Theory*. Springer, New York, 1999.

[17] Carl M. Bender, Joshua Feinberg, Daniel W. Hook, and David J. Weir. Chaotic Systems in Complex Phase Space. *Pramana — Journal of Physics*, 73(3):453–470, 2009.

[18] Carl M. Bender, Darryl D. Holm, and Daniel W. Hook. Complex Trajectories of a Simple Pendulum. *Journal of Physics A: Mathematical and Theoretical*, 40(3):F81–F89, 2007.

[19] Carl M. Bender and Daniel W. Hook. Complex Classical Motion in Potentials with Poles and Turning Points. *Studies in Applied Mathematics*, 133:318–336, 2014.

[20] Carl M. Bender, Daniel W. Hook, Peter N. Meisinger, and Qing-hai Wang. The Complex Correspondence Principle. *Physical Review Letters*, 104:061601, 2010.

[21] Nils Berglund. Kramers' law: Validity, derivations and generalisations. *Markov Processes and Related Fields*, 19(3):459–490, 2013.

[22] Lorenzo Bertini and Nicoletta Cancrini. The stochastic heat equation: Feynman-Kac formula and intermittence. *Journal of statistical Physics*, 78:1377–1401, 1995.

[23] Norman Bleistein and Richard A. Handelsman. *Asymptotic Expansions of Integrals*. Dover, 1986. Corrected reprint of the 1975 edition.

[24] E. B. Bogomolny. Calculation of instanton–anti-instanton contributions in quantum mechanics. *Phys. Lett. B*, 91(4):431–435, 1980.

[25] Frédéric Bouchet and Julien Reygner. Generalisation of the Eyring–Kramers law to non-gradient systems. *Annales Henri Poincaré*, 17(12):3499–3532, 2016.

[26] Anton Bovier and Frank den Hollander. *Metastability: A Potential-Theoretic Approach*. Springer, 2015.

[27] O. M. Braun and Yu. S. Kivshar. *The Frenkel–Kontorova Model: Concepts, Methods, and Applications*. Theoretical and Mathematical Physics. Springer, 2004.

[28] A. J. Bray, A. J. McKane, and T. J. Newman. Path integrals and non-Markov processes. II. Escape rates and stationary distributions in the weak-noise limit. *Phys. Rev. A*, 41(2):657, 1990.

[29] Robert Brown. A brief account of microscopical observations made in the months of June, July and August 1827, on the particles contained in the pollen of plants; and on the general existence of active molecules in organic and inorganic bodies. *Philosophical Magazine*, 4(21):161–173, 1828. Primary source on Brownian motion.

[30] Robert Brown. Additional remarks on active molecules. *Philosophical Magazine*, 6(33):161–166, 1829. Follow-up clarifications and further experiments.

[31] Angelika Bunse-Gerstner. Singular value decompositions of complex symmetric matrices. *Journal of Computational and Applied Mathematics*, 21(1):41–54, 1988.

[32] Bureau International des Poids et Mesures (BIPM) and National Institute of Standards and Technology (NIST). The International System of Units (SI), 2019 Edition. Technical Report NIST Special Publication 330, National Institute of Standards and Technology, 2019.

[33] Curtis G Callan Jr and Sidney Coleman. Fate of the false vacuum. II. First quantum corrections. *Physical Review D*, 16(6):1762, 1977.

[34] H. B. Callen and T. A. Welton. Irreversibility and Generalized Noise. *Physical Review*, 83:34–40, 1951.

[35] B Caroli, C Caroli, and B Roulet. Diffusion in a bistable potential: The functional integral approach. *Journal of Statistical Physics*, 26:83–111, 1981.

[36] S. Chandrasekhar. Stochastic Problems in Physics and Astronomy. *Reviews of Modern Physics*, 15:1–89, 1943.

[37] William T. Coffey, Yuri P. Kalmykov, and Joseph T. Waldron. *The Langevin Equation: With Applications to Stochastic Problems in Physics, Chemistry and Electrical Engineering*. World Scientific, 3 edition, 2012.

[38] Sidney Coleman. Fate of the false vacuum: Semiclassical theory. *Physical Review D*, 15(10):2929, 1977.

[39] Sidney Coleman. The uses of instantons. In *The whys of subnuclear physics*, pages 805–941. Springer, 1979.

[40] Fred Cooper, Avinash Khare, and Uday Sukhatme. Supersymmetry and quantum mechanics. *Physics Reports*, 251(5–6):267–385, 1995.

[41] Richard Courant. Variational Methods for the Solution of Problems of Equilibrium and Vibrations. *Bulletin of the American Mathematical Society*, 49(1):1–23, 1943.

[42] M. Cristoforetti, F. Di Renzo, and L. Scorzato (AuroraScience Collaboration). New approach to the sign problem in quantum field theories: Lefschetz thimble and the complex Langevin method. *Phys. Rev. D*, 86:074506, 2012.

[43] N. G. de Bruijn. *Asymptotic Methods in Analysis*. Dover Publications, Mineola, NY, 1981. Reprint of the 2nd ed., North-Holland, 1958.

[44] Pierre Del Moral. Feynman-kac formulae. In *Feynman-Kac Formulae: Genealogical and Interacting Particle Systems with Applications*, pages 47–93. Springer, 2004.

[45] Federica Devoto, Simone Devoto, Luca Di Luzio, and Giovanni Ridolfi. False vacuum decay: an introductory review. *Journal of Physics G: Nuclear and Particle Physics*, 49(10):103001, 2022.

[46] Paul AM Dirac. The lagrangian in quantum mechanics. In *Feynman's Thesis—A New Approach To Quantum Theory*, pages 111–119. World Scientific, 2005.

[47] Qian Dong, Guo-Hua Sun, Bing He, and Shi-Hai Dong. Semi-exact solutions of sextic potential plus a centrifugal term. *Journal of Mathematical Chemistry*, 58:2197–2203, 2020.

[48] Daniele Dorigoni and Philip Glass. Picard-Lefschetz decomposition and Cheshire Cat resurgence in 3D. *Journal of High Energy Physics*, 2019(12):1–40, 2019.

[49] J. J. Duistermaat. Oscillatory integrals, Lagrange immersions and unfolding of singularities. *Communications on Pure and Applied Mathematics*, 27(2):207–281, 1974.

[50] G. V. Dunne and M. Ünsal. Generating nonperturbative physics from perturbation theory. *Phys. Rev. D*, 89:041701(R), 2014.

[51] G. V. Dunne and M. Ünsal. Uniform WKB, multi-instantons, and resurgent trans-series. *Phys. Rev. D*, 89:105009, 2014.

[52] G. V. Dunne and M. Ünsal. WKB and Resurgence in the Mathieu Equation. *Phys. Rev. D*, 91:105006, 2015.

[53] Gerald Dunne. Resurgence and non-perturbative physics. *Lectures at CERN Winter School on Supergravity, Strings, and Gauge Theory*, 2014.

[54] Gerald V. Dunne. Functional determinants in quantum field theory. *Journal of Physics A: Mathematical and Theoretical*, 41(30):304006, 2008.

[55] Gerald V Dunne and Mithat Ünsal. Resurgence and trans-series in Quantum Field Theory. *Journal of high energy physics*, 2012(11):1–86, 2012.

[56] X. Durang, D. Panja, and M. Barma. Overdamped limit and inverse-friction expansion for Brownian motion in an inhomogeneous medium. *Physical Review E*, 91:062118, 2015.

[57] Weinan E, Weiqing Ren, and Eric Vanden-Eijnden. Minimum Action Method for the Study of Rare Events. *Communications on Pure and Applied Mathematics*, 57(5):637–656, 2004.

[58] Albert Einstein. Über die von der molekularkinetischen Theorie der Wärme geforderte Bewegung von in ruhenden Flüssigkeiten suspendierten Teilchen. *Annalen der Physik*, 322(8):549–560, 1905. English trans. in *Investigations on the Theory of the Brownian Movement* (1926/1956).

[59] Albert Einstein. *Investigations on the Theory of the Brownian Movement*. Dover Publications, New York, 1956. Reprint of Einstein's papers with commentary; original works 1905–1908.

[60] Matthias Ernzerhof. Taylor-series expansion of density functionals. *Physical Review A*, 50(6):4593, 1994.

[61] M. A. Escobar-Ruiz, E. Shuryak, and A. V. Turbiner. Quantum and thermal fluctuations in quantum mechanics and field theories from a new semiclassical approach. *Physical Review D*, 93:105039, 2016.

[62] Stewart N. Ethier and Thomas G. Kurtz. *Markov Processes: Characterization and Convergence*. Wiley, 1986.

[63] William Feller. The Parabolic Differential Equations and the Associated Semi-Groups of Transformations. *Annals of Mathematics*, 55(3):468–519, 1952.

[64] Richard P. Feynman. Space–Time Approach to Non-Relativistic Quantum Mechanics. *Reviews of Modern Physics*, 20:367–387, 1948.

[65] Richard P. Feynman, Albert R. Hibbs, and Daniel F. Styer. *Quantum Mechanics and Path Integrals: Emended Edition*. Dover, Mineola, NY, 2010.

[66] Siegmund Flügge. *Practical Quantum Mechanics*. Springer, 1999.

[67] Richard Forman. Functional determinants and geometry. *Physical Review A*, 35(10):3898–3905, 1987.

[68] Paul H Frampton. Consequences of vacuum instability in quantum field theory. *Physical Review D*, 15(10):2922, 1977.

[69] M. I. Freidlin and A. D. Wentzell. *Random Perturbations of Dynamical Systems*. Springer, 3 edition, 2012.

[70] H. Fujii, M. Honda, Y. Kikukawa, K. Nakayama, and T. Kanazawa. Path integral on Lefschetz thimbles: theory and application to the sign problem. *JHEP*, 2013(10):147, 2013.

[71] Toshiaki Fujimori, Syo Kamata, Tatsuhiro Misumi, Muneto Nitta, and Norisuke Sakai. Non-perturbative contributions from complexified solutions in $\mathbb{C}P^{N-1}$ models. *Physical Review D*, 94:105002, 2016.

[72] Toshiaki Fujimori, Syo Kamata, Tatsuhiro Misumi, Muneto Nitta, and Norisuke Sakai. All-order resurgence from complexified path integral in a quantum mechanical system with integrability. *Physical Review D*, 107(10):105011, 2023.

[73] Jean-François Le Gall. *Brownian Motion, Martingales, and Stochastic Calculus*, volume 274 of *Graduate Texts in Mathematics*. Springer, Cham, 2016.

[74] C. W. Gardiner. *Stochastic Methods: A Handbook for the Natural and Social Sciences*. Springer, Berlin, 4 edition, 2009.

[75] I. M. Gel'fand and A. M. Yaglom. Integration in functional spaces and its applications in quantum physics. *Journal of Mathematical Physics*, 1(1):48–69, 1960.

[76] J.-L. Gervais and B. Sakita. Extended systems in field theory and statistical mechanics. *Nuclear Physics B*, 34:632–639, 1971.

[77] I. V. Girsanov. On Transforming a Certain Class of Stochastic Processes by Absolutely Continuous Substitution of Measures. *Theory of Probability & Its Applications*, 5(3):285–301, 1960.

[78] Herbert Goldstein, Charles P. Poole, and John L. Safko. *Classical Mechanics*. Addison-Wesley, 3rd edition, 2002.

[79] R. Graham. Path-integral formulation of general diffusion processes. *Zeitschrift für Physik B*, 26:281–290, 1977.

[80] Melville S. Green. Markoff Random Processes and the Statistical Mechanics of Time-Dependent Phenomena. II. Irreversible Processes. *The Journal of Chemical Physics*, 22(3):398–413, 1954.

[81] David J Griffiths and Darrell F Schroeter. *Introduction to quantum mechanics*. Cambridge university press, 2018.

[82] Niels Grønbech-jensen and Sebastian Doniach. Long-time overdamped Langevin dynamics of molecular chains. *Journal of computational chemistry*, 15(9):997–1012, 1994.

[83] David J Gross, Malcolm J Perry, and Laurence G Yaffe. Instability of flat space at finite temperature. *Physical Review D*, 25(2):330, 1982.

[84] O. H. Hald and J. R. McLaughlin. Solution of inverse nodal problems. *Inverse Problems*, 5(3):307–347, 1989.

[85] Peter Hänggi, Peter Talkner, and Michal Borkovec. Reaction-rate theory: fifty years after kramers. *Reviews of Modern Physics*, 62(2):251–341, 1990.

[86] Peter Hänggi and Harry Thomas. Stochastic Processes: Time Evolution, Symmetries and Linear Response. *Physics Reports*, 88(4):207–319, 1982.

[87] Uwe Hassler. Ito's lemma. In *Stochastic Processes and Calculus: An Elementary Introduction with Applications*, pages 239–258. Springer, 2016.

[88] Roger A. Horn and Charles R. Johnson. *Matrix Analysis*. Cambridge University Press, Cambridge, 2 edition, 2012.

[89] S. Hottovy, G. Volpe, and J. Wehr. Smoluchowski–kramers approximation for a general class of stochastic differential equations with state-dependent friction. *Communications in Mathematical Physics*, 336:1259–1283, 2015.

[90] Kiyosi Itô. *On stochastic differential equations*. Number 4 in Memoirs of the American Mathematical Society. American Mathematical Society, Providence, RI, 1951.

[91] Claude Itzykson and Jean-Bernard Zuber. *Quantum Field Theory*. McGraw–Hill, 1980. Dover reprint (2006).

[92] Mark Kac. On distributions of certain Wiener functionals. *Transactions of the American Mathematical Society*, 65(1):1–13, 1949.

[93] Mark Kac. On some connections between probability theory and differential and integral equations. In *Proceedings of the Second Berkeley Symposium on Mathematical Statistics and Probability*, pages 189–215. University of California Press, Berkeley, 1951.

[94] Gopinath Kallianpur and Rajeeva L Karandikar. Girsanov's theorem. In *Introduction to Option Pricing Theory*, pages 95–101. Springer, 2000.

[95] Takuya Kanazawa and Yuya Tanizaki. Structure of Lefschetz thimbles in simple fermionic systems. *Journal of High Energy Physics*, 2015(3):1–36, 2015.

[96] Ioannis Karatzas and Steven E. Shreve. *Brownian Motion and Stochastic Calculus (2nd ed.)*, volume 113 of *Graduate Texts in Mathematics*. Springer, New York, 1991.

[97] A Kennedy, G Lazarides, and Qaisar Shafi. Decay of the false vacuum in the very early universe. *Physics Letters B*, 99(1):38–44, 1981.

[98] Klaus Kirsten and Alan J McKane. Functional determinants by contour integration methods. *Annals of Physics*, 308(2):502–527, 2003.

[99] Hagen Kleinert. *Path Integrals in Quantum Mechanics, Statistics, Polymer Physics, and Financial Markets*. World Scientific, 5th edition, 2009.

[100] A. Kolmogoroff. über die analytischen methoden in der wahrscheinlichkeitsrechnung. *Mathematische Annalen*, 104:415–458, 1931. In German; English title: "On the analytical methods in probability theory.".

[101] H. A. Kramers. Brownian motion in a field of force and the diffusion model of chemical reactions. *Physica*, 7(4):284–304, 1940.

[102] Hendrik Anthony Kramers. Wellenmechanik und halbzahlige Quantisierung. *Zeitschrift für Physik*, 39(10–11):828–840, 1926. [*English translation:* "Wave mechanics and half-integer quantization."].

[103] NV Krylov. On Ito's stochastic integral equations. *Theory of Probability & Its Applications*, 14(2):330–336, 1969.

[104] Ryogo Kubo. Statistical-Mechanical Theory of Irreversible Processes. I. General Theory and Simple Applications to Magnetic and Conduction Problems. *Journal of the Physical Society of Japan*, 12(6):570–586, 1957.

[105] Ryogo Kubo. The Fluctuation–Dissipation Theorem. *Reports on Progress in Physics*, 29(1):255–284, 1966.

[106] Hui-Hsiung Kuo. The Itô calculus and white noise theory: a brief survey toward general stochastic integration. *Communications on Stochastic Analysis*, 8(1):8, 2014.

[107] R. Kupferman, G. A. Pavliotis, and A. M. Stuart. Itô versus Stratonovich White-Noise Limits for Systems with Inertia and Colored Multiplicative Noise. *Physical Review E*, 70:036120, 2004.

[108] Steven P Lalley. Notes on the Itô Calculus, 2012.

[109] F. Langouche, D. Roekaerts, and E. Tirapegui. *Functional Integration and Semiclassical Expansions*. Springer, Dordrecht, 1982.

[110] A. W. C. Lau and T. C. Lubensky. State-dependent diffusion: Thermodynamic consistency and its path integral formulation. *Physical Review E*, 76:011123, 2007.

[111] Derek F Lawden. *Elliptic functions and applications*, volume 80. Springer Science & Business Media, 2013.

[112] Kimyeong Lee. Wormholes and Goldstone bosons. *Physical Review Letters*, 61(3):263, 1988.

[113] Anthony J Leggett. Some recent applications of instanton and related techniques in condensed-matter physics. *Progress of Theoretical Physics Supplement*, 80:10–18, 1984.

[114] Don S. Lemons and Anthony Gythiel. Paul Langevin's 1908 paper "On the Theory of Brownian Motion" ["Sur la théorie du mouvement brownien," C. R. Acad. Sci. (Paris) 146, 530–533

(1908)]. *American Journal of Physics*, 65(11):1079–1081, 1997. English translation and commentary; faithful to the 1908 French original.

[115] Chen Li. Exact analytical ground state solution of 1D H 2+ with soft Coulomb potential. *Journal of Mathematical Chemistry*, 60(1):184–194, 2022.

[116] Robert S. Liptser and Albert N. Shiryaev. *Statistics of Random Processes I: General Theory*. Applications of Mathematics. Springer, Berlin, 2nd edition, 2013.

[117] H. C. Luckock and A. J. McKane. Path integrals and non-Markov processes. III. Calculation of the escape-rate prefactor in the weak-noise limit. *Phys. Rev. A*, 42:1982–1996, Aug 1990.

[118] S. Machlup and L. Onsager. Fluctuations and irreversible processes. ii. *Physical Review*, 91(6):1512–1515, 1953.

[119] Ross A Maller, Gernot Müller, and Alex Szimayer. Ornstein–Uhlenbeck processes and extensions. In *Handbook of Financial Time Series*, pages 421–437. Springer, 2009.

[120] Nicholas Manton and Paul Sutcliffe. *Topological Solitons*. Cambridge University Press, 2004.

[121] Paul C. Martin, E. D. Siggia, and H. A. Rose. Statistical dynamics of classical systems. *Physical Review A*, 8(1):423–437, 1973.

[122] V. P. Maslov and M. V. Fedoriuk. *Semi-Classical Approximation in Quantum Mechanics*, volume 7 of *Mathematical Physics and Applied Mathematics*. D. Reidel Publishing Company, Dordrecht, 1981. Translated from the Russian by J. Niederle and J. Tolar; softcover reprint 2001 (Springer).

[123] AJ McKane, HC Luckock, and AJ Bray. Path integrals and non-Markov processes. I. General formalism. *Physical Review A*, 41(2):644, 1990.

[124] Alan McKane. *Vacuum instability in scalar field theories.* PhD thesis, University of Southampton, September 1978.

[125] Alan J McKane and Martin B Tarlie. Regularization of functional determinants using boundary perturbations. *Journal of Physics A: Mathematical and General*, 28(23):6931, 1995.

[126] Pedro B Melo, Pedro V Paraguassú, Eduardo S Nascimento, and Welles AM Morgado. Brownian Fluctuations of a non-confining potential. *Physica A: Statistical Mechanics and its Applications*, 650:129996, 2024.

[127] Patricia A Millard. Interacting instantons and quantum mechanical metastability. *Nuclear Physics B*, 297(2):412–428, 1988.

[128] Peter D. Miller. *Applied Asymptotic Analysis*, volume 75 of *Graduate Studies in Mathematics*. American Mathematical Society, Providence, RI, 2006.

[129] John Willard Milnor. *Morse theory*. Number 51 in Annals of Mathematics Studies. Princeton university press, 1963.

[130] Peter Mörters and Yuval Peres. *Brownian Motion*, volume 30 of *Cambridge Series in Statistical and Probabilistic Mathematics*. Cambridge University Press, Cambridge, 2010.

[131] D Mugnai and A Ranfagni. Instanton bounces as real physical processes. *Europhysics Letters*, 6(1):1, 1988.

[132] National Institute of Standards and Technology. NIST Digital Library of Mathematical Functions. NIST, 2025. Version 1.2.5; release date 2025-12-15.

[133] Bernt Øksendal. *Stochastic Differential Equations: An Introduction with Applications*. Springer, 6 edition, 2010.

[134] Frank W. J. Olver. *Asymptotics and Special Functions*. CRC Press, Boca Raton, 1997.

[135] Lars Onsager and S. Machlup. Fluctuations and irreversible processes. i. *Physical Review*, 91(6):1505–1512, 1953.

[136] Konrad Osterwalder and Robert Schrader. Axioms for Euclidean Green's Functions. *Communications in Mathematical Physics*, 31:83–112, 1973.

[137] Konrad Osterwalder and Robert Schrader. Axioms for Euclidean Green's Functions II. *Communications in Mathematical Physics*, 42:281–305, 1975.

[138] Richard B. Paris and David Kaminski. *Asymptotics and Mellin–Barnes Integrals*. Cambridge University Press, Cambridge, 2001.

[139] G. A. Pavliotis and A. M. Stuart. *Multiscale Methods: Averaging and Homogenization*. Springer, 2008.

[140] Grigorios A. Pavliotis. *Stochastic Processes and Applications: Diffusion Processes, the Fokker–Planck and Langevin Equations*, volume 60 of *Texts in Applied Mathematics*. Springer, 2014.

[141] Philip Pearle, Matthew Glasser, and Dean Nielson. What Brown saw and you can too. *American Journal of Physics*, 78(12):1278–1289, 2010. Modern, experimental–historical analysis of Brown's observations.

[142] Jean Perrin. Mouvement brownien et réalité moléculaire. *Journal de Physique Théorique et Appliquée*, 9:5–64, 1910. Eng. trans.: *Brownian Movement and Molecular Reality* (Taylor & Francis, 1910; Dover reprint).

[143] Frédéric Pham. Vanishing Homologies and the n-Variable Saddlepoint Method. *Astérisque*, 101–102:83–150, 1983.

[144] Max Planck. Über das Gesetz der Energieverteilung im Normalspektrum. *Annalen der Physik*, 309(3):553–563, 1901. English title: "On the Law of Distribution of Energy in the Normal Spectrum".

[145] Philip E. Protter. *Stochastic Integration and Differential Equations*. Springer, 2 edition, 2005.

[146] Wieslaw Pusz and S Lech Woronowicz. Functional calculus for sesquilinear forms and the purification map. *Reports on Mathematical Physics*, 8(2):159–170, 1975.

[147] G. Pöschl and E. Teller. Bemerkungen zur Quantenmechanik des anharmonischen Oszillators. *Zeitschrift für Physik*, 83:143–151, 1933.

[148] R. Rajaraman. *Solitons and Instantons: An Introduction to Solitons and Instantons in Quantum Field Theory*. North-Holland Personal Library. Elsevier North-Holland, Amsterdam, 1987.

[149] Sidney Redner. *A Guide to First-Passage Processes*. Cambridge University Press, 2001.

[150] Daniel Revuz and Marc Yor. *Continuous Martingales and Brownian Motion*, volume 293 of *Grundlehren der Mathematischen Wissenschaften*. Springer, Berlin, Heidelberg, 1999.

[151] H. Risken. *The Fokker–Planck Equation: Methods of Solution and Applications*. Springer, 2 edition, 1996.

[152] Walther Ritz. Über eine neue Methode zur Lösung gewisser Variationsprobleme der mathematischen Physik. *Journal für die reine und angewandte Mathematik*, 135:1–61, 1909. English translation: On a new method for the solution of certain variational problems of mathematical physics.

[153] L. C. G. Rogers and David Williams. *Diffusions, Markov Processes, and Martingales, Vol. 2: Itô Calculus*. Cambridge University Press, 2nd edition, 2000.

[154] J. M. Sancho, M. San Miguel, and D. Dürr. Adiabatic elimination for systems of Brownian particles with nonconstant damping coefficients. *Journal of Statistical Physics*, 28(2):291–305, 1982.

[155] Simo Särkkä and Arno Solin. *Applied Stochastic Differential Equations*. Institute of Mathematical Statistics Textbooks. Cambridge University Press, Cambridge, 2019.

[156] René L. Schilling and Lothar Partzsch. *Brownian Motion: An Introduction to Stochastic Processes*. De Gruyter, Berlin, Boston, 2014.

[157] Lawrence S. Schulman. *Techniques and Applications of Path Integration*. Wiley-VCH, 2005. Reprint of the 1981 edition.

[158] Zeev Schuss. *Theory and Applications of Stochastic Processes: An Analytical Approach*. Springer, 2010.

[159] Zachary Selk and Harsha Honnappa. The small-noise limit of the most likely element is the most likely element in the small-noise limit. *arXiv preprint arXiv:2209.04523*, 2022.

[160] James P Sethna and Stephen Kivelson. Photoinduced soliton pair production in polyacetylene: An instanton approach. *Physical Review B*, 26(6):3513, 1982.

[161] R. Shankar. *Principles of Quantum Mechanics*. Springer, New York, 2 edition, 1994.

[162] Edward V Shuryak. Toward the quantitative theory of the instanton liquid IV.: Tunneling in the double-well potential. *Nuclear Physics B*, 302(4):621–644, 1988.

[163] Barry Simon. *Functional Integration and Quantum Physics*. AMS Chelsea, Providence, RI, 2nd edition, 2005.

[164] Marian Smoluchowski. Zur kinetischen Theorie der Brownschen Molekularbewegung und der Suspensionen. *Annalen der Physik*, 326(14):756–780, 1906. On the Kinetic Theory of the Brownian Molecular Motion and of Suspensions, transl. R. Schmitz and R. Jones (University of Warsaw Press, 2017).

[165] Daniel W. Stroock and S. R. Srinivasa Varadhan. *Multidimensional Diffusion Processes*. Springer, 2006.

[166] Guo-Hua Sun, Chang-Yuan Chen, Hind Taud, C Yáñez-Márquez, and Shi-Hai Dong. Exact solutions of the 1D Schrödinger equation with the Mathieu potential. *Physics Letters A*, 384(19):126480, 2020.

[167] G. 't Hooft. Computation of the quantum effects due to a four-dimensional pseudoparticle. *Physical Review D*, 14(12):3432–3450, 1976. Erratum: Phys. Rev. D **18**, 2199 (1978), doi:10.1103/PhysRevD.18.2199.

[168] Teiji Takagi. On an algebraic problem related to an analytic theorem of Carathéodory and Fejér and on an allied theorem of Landau. *Japan Journal of Mathematics*, 1:83–93, 1925.

[169] Y. Tanizaki. Lefschetz-thimble techniques for path integral of zero-dimensional $O(n)$ sigma models. *JHEP*, 2014(07):097, 2014.

[170] Yuya Tanizaki and Takayuki Koike. Real-time Feynman path integral with Picard–Lefschetz theory and its applications to quantum tunneling. *Annals of Physics*, 351:250–274, 2014.

[171] Yuya Tanizaki, Hiromichi Nishimura, and Kouji Kashiwa. Evading the sign problem in the mean-field approximation through Lefschetz-thimble path integral. *Physical Review D*, 91(10):101701, 2015.

[172] G. E. Uhlenbeck and L. S. Ornstein. On the Theory of the Brownian Motion. *Physical Review*, 36:823–841, 1930.

[173] N. G. van Kampen. *Stochastic Processes in Physics and Chemistry*. Elsevier, 3 edition, 2007.

[174] NG Van Kampen. A soluble model for diffusion in a bistable potential. *Journal of Statistical Physics*, 17:71–88, 1977.

[175] V Varadarajan. Euler and his work on infinite series. *Bulletin of the American Mathematical Society*, 44(4):515–539, 2007.

[176] Vladislav Andreevič Vasil'ev. *Applied Picard-Lefschetz theory*. American Mathematical Soc., 2002.

[177] Alexander Vilenkin. Creation of universes from nothing. *Physics Letters B*, 117(1-2):25–28, 1982.

[178] Alexander Vilenkin. Birth of inflationary universes. *Physical Review D*, 27(12):2848, 1983.

[179] U Weiss, H Grabert, and S Linkwitz. Influence of friction and temperature on coherent quantum tunneling. *Journal of low temperature physics*, 68:213–244, 1987.

[180] Ulrich Weiss and Hermann Grabert. Quantum diffusion of a particle in a periodic potential with ohmic dissipation. *Physics Letters A*, 108(2):63–67, 1985.

[181] Gregor Wentzel. Eine Verallgemeinerung der Quantenbedingungen für die Zwecke der Wellenmechanik. *Zeitschrift für Physik*, 38(6–7):518–529, 1926. [*English translation:* "A generalization of the quantum conditions for the purposes of wave mechanics."].

[182] Horacio S Wio. *Path integrals for stochastic processes: An introduction*. World Scientific, 2013.

[183] Edward Witten. Dynamical breaking of supersymmetry. *Nuclear Physics B*, 188(3):513–554, 1981.

[184] Edward Witten. Analytic Continuation of Chern–Simons Theory. *arXiv:1001.2933 [hep-th]*, 2010.

[185] Roderick Wong. *Asymptotic Approximations of Integrals*, volume 34 of *Classics in Applied Mathematics*. SIAM, Philadelphia, 2001.

[186] Zhang Yun-Bo, Liang Jiu-Qing, and Pu Fu-Cho. Path integral calculation of quantum tunneling for cubic potential at finite temperature. *Acta Physica Sinica (Overseas Edition)*, 7(7):510, 1998.

[187] Anton Zettl. *Sturm–Liouville Theory*, volume 121 of *Mathematical Surveys and Monographs*. American Mathematical Society, Providence, RI, 2005.

[188] Jean Zinn-Justin. Multi-instanton contributions in quantum mechanics. *Nucl. Phys. B*, 192:125–173, 1981.

[189] Jean Zinn-Justin. *Quantum Field Theory and Critical Phenomena*. Oxford University Press, 4th edition, 2002. Quantum Field Theory and Critical Phenomena.

[190] Jean Zinn-Justin and Ulrich D. Jentschura. Multi-Instantons and Exact Results I: Conjectures, WKB Expansions, and Instanton Interactions. *Annals of Physics*, 313(1):197–267, 2004.